

LMU

MICHAEL BUSSMANN

**LASER-COOLED ION BEAMS AND
STRONGLY COUPLED PLASMAS FOR
PRECISION EXPERIMENTS**



DISSERTATION DER FAKULTÄT FÜR PHYSIK
DER
LUDWIG-MAXIMILIANS-UNIVERSITÄT MÜNCHEN

VORGELEGT VON MICHAEL BUSSMANN AUS BIELEFELD
MÜNCHEN, DEN 14.12.2007

1. **Gutachter:** Professor Dietrich Habs
2. **Gutachter:** Professor Gregor Morfill

Tag der mündlichen Prüfung: 17. März 2008

Für meine Familie – und für meine Freunde.

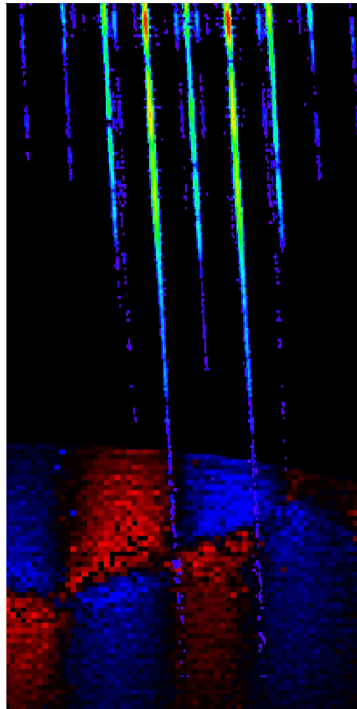
Back off, man, I'm a scientist!
Dr. P. Venkman in [1]

CONTENTS

| | |
|---|-----------|
| Abstract | 1 |
| Zusammenfassung | 3 |
| 1 Introduction | 7 |
| 1.1 Strong Coupling and Coulomb Crystallization | 7 |
| 1.2 Laser-Cooling and Precision Spectroscopy of Relativistic Ion Beams | 8 |
| 1.3 Stopping and Cooling Beams of Highly Charged Ions | 10 |
| 1.4 Outline of the Thesis | 11 |
| 2 Laser-Cooling and Precision Spectroscopy of Relativistic Ion Beams | 13 |
| 2.1 Applying Laser-Cooling to Ion Beams at Relativistic Energies . . | 13 |
| 2.2 Experimental Setup at the ESR at GSI | 13 |
| 2.2.1 The Experimental Storage Ring at GSI | 13 |
| 2.2.2 The Argon Ion Laser System | 15 |
| 2.2.3 Measuring the Relevant Beam Parameters | 16 |
| 2.3 Results | 17 |
| 2.3.1 Laser-Cooling of Relativistic Ion Beams | 17 |
| 2.3.2 Attaining a Small Ion Beam Momentum Spread | 19 |
| 2.3.3 Longitudinally Space-Charge Dominated Beams | 19 |
| 2.3.4 Three-Dimensional Cold Beams | 22 |
| 2.3.5 Ion Dynamics in the Bucket | 22 |
| 2.3.6 Precision VUV-Spectroscopy | 25 |
| 2.3.7 Increasing the Acceptance of the Laser Force | 26 |
| 3 Stopping and Cooling Beams of Highly Charged Ions | 31 |
| 3.1 In-trap Preparation of Highly Charged Ions for Precision Physics | 31 |
| 3.2 Numerical Methods | 31 |
| 3.2.1 Simulation Parameters | 32 |
| 3.2.2 Equation of Motion | 33 |
| 3.2.3 Simulation Methods | 34 |
| 3.3 Results | 35 |
| 3.3.1 Stopping Power and Stopping Times | 35 |
| 3.3.2 Plasma Response and Plasma Stability | 36 |
| 3.3.3 Energy Loss and Charge Exchange | 38 |
| 3.3.4 Recooling Conditions | 39 |

| | | |
|----------|---|------------|
| 4 | Collective Effects in Strongly Coupled OCPs | 41 |
| 4.1 | Collective Response, Correlations and Strong Coupling | 41 |
| 4.2 | Schottky Noise Spectra at Small Momentum Spread | 41 |
| 4.2.1 | Schottky Noise Spectra for Bunched Beams with Negligible Ion-Ion Interaction | 41 |
| 4.2.2 | Schottky Noise Power at Small Momentum Spread | 43 |
| 4.3 | Collective Plasma Response during Ion Stopping | 45 |
| 4.3.1 | Characteristic Lengths and Linear Response Theory | 46 |
| 4.3.2 | Collective Plasma Oscillations | 46 |
| 5 | Conclusion and Outlook | 53 |
| A | An Optical Nuclear Clock Transition for Fundamental Experiments | 57 |
| A.1 | Recent Experiments on the Isomeric First Excited State of ^{229}Th | 57 |
| A.2 | A Brilliant $^{229\text{m}}\text{Th}$ Decay Photon Source | 58 |
| A.3 | All-Optical Detection of the Decay of the Isomeric First Excited State of ^{229}Th | 59 |
| A.3.1 | Lens System | 60 |
| A.3.2 | Spectral Bandpass Filter | 62 |
| A.3.3 | Detector | 62 |
| A.4 | Laser Spectroscopy of Trapped $^{229\text{m}}\text{Th}^{3+}$ Ions | 64 |
| | Bibliography | 67 |
| | Publications by the Author | 87 |
| | Enclosed Publications | 91 |
| | Hyperfine Interactions 162(1) (2005) 181–188 | 93 |
| | AIP Conference Proceeding 821(1) (2006) 501–509 | 103 |
| | Journal of Physics: Conference Series 88 (2007) 012043 | 115 |
| | International Journal of Mass Spectrometry 251(2-3) (2006) 179–189 . | 123 |
| | European Physical Journal D 45(1) (2007) 129–132 | 137 |
| | Hyperfine Interactions 173(1-3) (2007) 27–34 | 143 |
| | Conference Presentations | 153 |
| | Poster Presentations | 153 |
| | Oral Presentations | 154 |
| | Curriculum Vitae | 157 |
| | Academic Education | 157 |
| | Practical Education | 158 |
| | Teaching Experience | 159 |
| | Danksagung | 161 |

ABSTRACT



This cumulative thesis summarizes experimental and theoretical results on cooling of ion beams using single-frequency, single-mode tabletop laser systems. It consists of two parts. One deals with experiments on laser-cooling of ion beams at relativistic energies, the other with simulations of stopping and sympathetic cooling of ions for precision in-trap experiments.

In the first part, experimental results are presented on laser-cooling of relativistic C^{3+} ion beams at a beam energy of 122 MeV/u, performed at the Experimental Storage Ring (*ESR*) at *GSI*. Two continuous-wave, frequency-stabilized, frequency-doubled argon ion laser systems are used to cool ion beams to longitudinal momentum spreads $\Delta p_{\parallel}/p_{\parallel} \approx 10^{-7}$ at ion beam currents below 10 μ A. Both ion beam and laser beam are brought in overlap in a section of the ring with the

laser beam counter-propagating to the ion beam. With moderate bunching of the beam at a bunching voltage of a few volts, the bucket force counteracting the laser force provides a velocity-dependent friction force.

Central to this cooling scheme is the relativistic Doppler-shift of the laboratory laser frequency to the rest frame of the ions. By changing the beam energy, the wavelength of the photons in the ion rest frame can be tuned to match the $2S_{1/2} \rightarrow 2P_{1/2}$ and $2S_{1/2} \rightarrow 2P_{3/2}$ transition wavelengths of 155.0705(39)(3) nm and 154.8127(39)(2) nm, respectively, selected for cooling the ions. This matching will be essential for laser-cooling at future storage rings, since it allows to address a multitude of ion species with a single laser system by selecting the proper ion charge state and ion beam energy.

The main results presented in this thesis include the first attainment of longitudinally space-charge dominated relativistic ion beams using pure laser-cooling. The momentum spreads observed are smaller than those of pure electron cooled beams by at least one order of magnitude. This reduction in momentum spread makes it possible to reach the regime of strong coupling of the ions at beam temperatures of a few kelvin. Furthermore, by increasing the coupling between the longitudinal and transverse degree of ion motion in the bucket, three-dimensional cold beams have been realized. Finally, precision measurements of the absolute

frequencies of the $2S_{1/2} \rightarrow 2P_{1/2}$ and $2S_{1/2} \rightarrow 2P_{3/2}$ transition have been performed, which challenge current theoretical estimates.

The results obtained in two measurement campaigns in 2004 and 2006 will serve as a valuable input for future laser-cooling experiments at higher beam energies at the future FAIR facility. With the beam energies accessible at FAIR, laser-cooling up to $^{238}\text{U}^{89+}$ and precision X-ray laser spectroscopy will be in reach by exploiting the relativistic Doppler-shift.

The second part lists theoretical results on stopping and sympathetic cooling of ions in a laser-cooled one-component plasma of singly charged ^{24}Mg ions, which are confined in a three-dimensional harmonic trap potential. This new cooling scheme will allow for in-trap preparation of unstable nuclei for precision experiments. The two main advantages of this scheme compared to other in-trap cooling schemes, especially for highly charged ions, are: First, the high charge state of the ions of interest can be maintained over the measuring time, since the expected rates for charge exchange processes are orders of magnitude smaller than the decay rate of the ions. Second, a very low final temperature of a few mK is in reach using sympathetic cooling, which allows for ultra-precise measurements.

The main focus lies on absolute mass-measurements to a relative precision of $\Delta m/m \approx 10^{-10}$ in the *MLLTRAP* Penning trap system using highly charged ions. Nevertheless, the cooling scheme can deliver ions of mK temperatures for a multitude of in-trap precision measurements, including experiments on the variation of the fine structure constant, tests of QED and laser-spectroscopy of nuclear transitions. One example for such a measurement is the first direct laser-spectroscopy of a nuclear transition in $^{229}\text{Th}^{3+}$ from the ground state to an isomeric state with a transition energy of about 7.6 eV.

Extensive parallel simulations computing the complete interaction of $N = 10^5$ ions in a realistic trap scenario have been performed using a newly developed simulation code, which intrinsically includes all effects of strong coupling between ions.

The energy loss of low-velocity ions in a macroscopic ensemble of laser-cooled ions is extracted from the simulation. At low ion energies of a few hundred meV the cooling force is found to be very efficient and cooling times on the order of ten to a hundred μs are realized. Furthermore, the complete evolution of the ion dynamics during the stopping process can be studied, showing that ion loss due to hard binary collisions can be neglected. Besides energy loss due to very few binary collisions, the energy lost by the ion during the passage through the laser-cooled ions is distributed over the complete plasma bulk. This important result implies that the plasma stays stable during the whole cooling process and no Coulomb explosion due to local disturbances of the plasma is observed in the simulation. It also shows that fast and efficient recooling is possible after the stopping process, using a single laser system at a fixed laser frequency.

Thus, the proposed cooling scheme will be feasible for cooling of rare highly charged ions with lifetimes below 100 ms.

ZUSAMMENFASSUNG

Diese kumulative Doktorarbeit ist eine Zusammenfassung experimenteller wie theoretischer Ergebnisse zum Kühlen von Ionenstrahlen mit Lasern. Die Arbeit umfasst zwei Teile, wovon der eine Laserkühlexperimente mit Ionenstrahlen relativistischer Energie behandelt, während der andere auf die Simulation von Stoppprozessen und sympathetischem Kühlen mit Ionen in Bezug auf Hochpräzisionsexperimente in Fallen eingeht.

Der erste Teil beinhaltet experimentelle Ergebnisse zum Laserkühlen von C^{3+} Ionenstrahlen mit einer relativistischen Strahlenergie von 122 MeV/u am Experimentellen Speicherring (ESR) an der GSI. Zur Ionenstrahlkühlung werden zwei frequenzstabilisierte, frequenzverdoppelte Dauerstrich-Argon-Ionen-Laser verwendet, um bei niedrigen Ionenströmen unterhalb von $10 \mu A$ die longitudinale Impulsbreite der Ionenstrahlen auf $\Delta p_{\parallel}/p_{\parallel} \approx 10^{-7}$ zu reduzieren. Der Laserstrahl wird mit dem Ionenstrahl in einer Sektion des Rings überlappt, wobei der Laserstrahl gegenläufig zum Ionenstrahl ist. Eine geringe longitudinale Dichtemodulation des Strahls, allgemein als *Bunching* bezeichnet, erzeugt bei einer Bunchspannung von wenigen Volt eine der Laserkühlkraft entgegenwirkende, geschwindigkeitsabhängige Reibungskraft, die so genannte *Bucketkraft*.

Ein wesentlicher Aspekt des vorgestellten Kühlschemas ist die relativistische Dopplerverschiebung der im Labor gemessenen Laserfrequenz bei Transformation in das Ruhesystem des Ionenstrahls. Mit Hilfe einer genauen Einstellung der Strahlenergie kann die Wellenlänge der Photonen im Ruhesystem der Ionen mit der Wellenlänge der $2S_{1/2} \rightarrow 2P_{1/2}$ und $2S_{1/2} \rightarrow 2P_{3/2}$ Übergänge von 155.0705(39)(3) nm beziehungsweise 154.8127(39)(2) nm in Übereinstimmung gebracht werden. Diese Übereinstimmung ist unabdingbar, um das Laserkühlen einer Vielzahl verschiedener Ionenspezies mit nur einem Lasersystem an zukünftigen Speicherringen zu ermöglichen. Hierzu ist eine geeignete Wahl des Ladungszustands der Ionen und der Ionenstrahlenergie ausreichend.

Als erstes der im Folgenden aufgeführten Hauptergebnisse der Doktorarbeit sei die Erzeugung longitudinal raumladungsdominierter, relativistischer Ionenstrahlen mit Hilfe der Laserkühlung angeführt. Die gemessenen Impulsbreiten sind hierbei um mindestens eine Größenordnung kleiner als im Fall reiner Elektronenkühlung. Durch diese Impulsbreitenreduktion wird das Regime starker Kopplung bei Strahltemperaturen von wenigen Kelvin erreicht. Dreidimensional kalte Strahlen werden erzeugt, indem man die Kopplung der transversalen Bewegungsfreiheitsgrade mit dem longitudinalen Bewegungsfreiheitsgrad innerhalb des *Bucket* erhöht. Im Rahmen der Experimente wurde schliesslich eine Präzisionsbestimmung der $2S_{1/2} \rightarrow 2P_{1/2}$ und $2S_{1/2} \rightarrow 2P_{3/2}$ Übergangswellenlängen vorgenommen, die eine Herausforderung an die Vorhersagegenauigkeit

derzeitiger theoretischer Modelle darstellt.

Die Ergebnisse, die während zweier Strahlzeiten in den Jahren 2004 und 2006 gesammelt wurden, liefern einen wertvollen Beitrag für zukünftige Laserkühllexperimente bei höheren Strahlenergien, wie sie an der Forschungsanlage FAIR zur Verfügung stehen werden. Mit den bei FAIR erreichbaren Strahlenergien wird es aufgrund der relativistischen Dopplerverschiebung der Laserfrequenz möglich sein, Laser im sichtbaren Wellenlängenbereich zur Kühlung von $^{238}\text{U}^{89+}$ Ionen und zur Spektroskopie im Röntgenbereich zu verwenden.

Der zweite Teil der Doktorarbeit besteht aus einer Auflistung theoretischer Ergebnisse zum Stoppen und sympathetischen Kühlen von Ionen in lasergekühlten Einkomponentenplasmen aus einfach geladenen $^{24}\text{Mg}^+$ Ionen, die in einer dreidimensionalen harmonischen Falle eingesperrt werden. Dies neue Kühlschema erlaubt es, instabile Kerne für Präzisionsexperimente innerhalb von Fallen zur Verfügung zu stellen. Im Vergleich zu anderen Kühlschemata hat das hier vorgestellte Schema zwei entscheidende Vorteile, insbesondere im Hinblick auf hochgeladene Ionen: Zum Ersten kann der hohe Ladungszustand des Ions während der Messzeit erhalten werden, da die für Umladungsprozesse erwarteten Raten um Größenordnungen geringer sind als die typischerweise zu erwartenden Zerfallsraten der Kerne. Zum Zweiten können mit Hilfe des sympathetischen Kühlens sehr niedrige Temperaturen von wenigen mK erreicht werden, die dann ultrapräzise Messungen erlauben.

Im Wesentlichen wird in dieser Doktorarbeit Bezug genommen auf die absolute Bestimmung der Massen hochgeladener Ionen mit Hilfe des *MLLTRAP* Penningfallensystems mit einer relativen Präzision besser als $\Delta m/m \approx 10^{-10}$. Darüber hinaus wird es mit Hilfe des vorgestellten Kühlschemas möglich sein, Ionen mit einer Temperatur von wenigen mK für eine Vielzahl von Präzisionsmessungen in Fallen zur Verfügung zu stellen, wie zum Beispiel der Bestimmung der zeitlichen Veränderung der Feinstrukturkonstante, Tests der Quantenelektrodynamik oder der Laserspektroskopie eines Kernübergangs von $^{229\text{m}}\text{Th}^{3+}$ vom Grundzustand in ein Isomer mit einer Übergangsenergie von 7.6 eV.

In umfangreichen parallelen Simulationen wurde die vollständige Wechselwirkung von $N = 10^5$ Ionen in einer realistischen Fallenumgebung berechnet. Die Simulation basiert auf einem neuentwickelten Programm, das sämtliche physikalischen Effekte der starken Kopplung zwischen Ionen intrinsisch berücksichtigt.

Der Energieverlust von Ionen geringer Geschwindigkeit in einem makroskopischen Ensemble lasergekühlter Ionen konnte mit Hilfe der Simulation bestimmt werden. Bei niedrigen Ionenenergien von wenigen hundert meV wird die Kühlkraft effizient genug, um Kühlzeiten von wenigen hundert μs zu erreichen. Weiterhin ist es möglich, die vollständige Entwicklung der Ionendynamik während des Stoppvorgangs zu studieren. Hierbei wurde herausgefunden, dass der Teilchenverlust aufgrund weniger harter Zweikörperstöße vernachlässigt werden kann. Sieht man von dem Energieverlust durch diese geringe Zahl harter Zweikörperstöße ab, so wird die Energie, die das Ion während seines Flugs durch das lasergekühlte Plasma verliert, über einen Grossteil des gesamten Plasmas

verteilt. Aufgrund dieses wichtigen Ergebnisses kann gezeigt werden, dass das Plasma während des gesamten Stoppvorgangs stabil bleibt und keine raumladungsbedingte schnelle Expansion zu erwarten ist. Ebenso belegt dieses Ergebnis, dass erneutes schnelles und effizientes Kühlen nach dem Stoppen des Ions mit einem einzigen Lasersystem fester Frequenz möglich ist. Die Ergebnisse zeigen, dass das hier vorgestellte Kühlschema es erlauben wird, seltene hochgeladene Ionen mit einer Lebensdauer unter 100 ms zu kühlen.

1. INTRODUCTION

This chapter briefly summarizes the main results of the present cumulative thesis on ion beam cooling and stopping using Doppler-free laser-cooling. Recently, ion beam cooling experiments at the model storage ring *PALLAS* ([2],[MB0302]), a circular Paul trap, have made possible the first experimental realization of Coulomb-crystallization of an ion beam [3, 4]. The scope of these experiments spans the vast range from trap-based physics, using ion ensembles or even single ions at rest confined in a table-top trap apparatus, to storage-ring-physics, using relativistic ion beams confined in a ring of several ten to hundred meters circumference.

The present thesis on the one hand extends the methods used at the *PALLAS* storage ring to storage rings typically found at accelerator labs¹, proving the feasibility of laser-cooling of relativistic ion beams. On the other hand, it opens new perspectives for stopping and cooling beams of ions and preparing the stopped ions for ultra-precise trap-based mass measurements and experiments on fundamental physics.

In this introduction, specific details are omitted to give a concise overview of the main results, preceded by a short introduction into the main concepts of laser-cooling of ions in traps and storage rings. The introduction closes with an orientation section that describes the outline of the thesis.

1.1 Strong Coupling and Coulomb Crystallization

With Doppler-free laser-cooling [5, 6] the final ion temperature T is limited by the minute photon recoil momentum ([5, 6],[MB0301]) to a few millikelvin [7, 8]. In the following, form, structure and dynamics of large ensembles of cold ions are discussed, with emphasis on the similarities between ion confinement in traps and storage rings.

Ensembles of like-sign ions are usually confined by electro-magnetic fields compensating the mutual repulsion due to the Coulomb force. The confinement is typically chosen to be harmonic in both the axial and radial direction, where the axial confining force is weaker than the radial and even zero if coasting ion beams in storage rings are considered. Such a situation can be found in Paul traps [9, 10], Penning traps [11–13] and, in the case of ion beams [14–17], in a storage ring.

If the inter-ion Coulomb energy E_{Coulomb} overcomes the thermal kinetic energy

¹In particular, the Experimental Storage Ring, *ESR*, at the Gesellschaft für Schwerionenforschung, *GSI*.

E_{th} of the ions, the plasma parameter [18, 19]

$$\Gamma_{\text{p}} = \frac{E_{\text{Coulomb}}}{E_{\text{th}}} \equiv \frac{1}{4\pi\epsilon_0} \frac{Q^2 e^2}{a_{\text{WS}} k_{\text{B}} T} \quad (1.1)$$

exceeds unity and the coupling between the ions becomes strong [20–24]. In the case of only one ionic species in one charge state the form of the harmonically confined one-component plasma [25, 26] resembles an ellipsoid [27, 28]. Both form and structure are completely determined by the charge Qe and mass m of the ions and the confining fields ([28, 29],[MB0303, MB0304, MB0401]). The one-component plasma of volume density n can undergo a phase transition to a Coulomb crystal [24, 30], an ordered state with an equal inter-ion spacing given by the Wigner-Seitz radius [9, 31–35]

$$a_{\text{WS}} = \left(\frac{3}{4\pi n} \right)^{1/3}. \quad (1.2)$$

Not only form and structure, but also the description of the dynamics of harmonically confined, strongly coupled ions is similar in both traps and storage rings [2, 18, 36–41]. In addition to the oscillation frequencies ω_{\perp} and ω_{\parallel} associated to the radial and axial harmonic potentials [28, 42], the plasma frequency [19]

$$\omega_{\text{p}} = \frac{2\pi}{\tau_{\text{p}}} = \sqrt{\frac{Q^2 e^2 n}{\epsilon_0 m}}, \quad (1.3)$$

defines the dominant time scale τ_{p} on which the plasma reacts to an outer disturbance, the so called plasma period.

In the regime of weak coupling at a plasma parameter below unity, the motion of the ions is determined by the ion temperature and the confining forces, while the inter-ionic forces can be neglected. If strong coupling is considered, long range correlations between the ions dominate the ion motion, resulting in nonlinear ion dynamics [23, 27, 43–48].

1.2 Laser-Cooling and Precision Spectroscopy of Relativistic Ion Beams

Laser-cooling of ion beams² has been demonstrated at the *TSR* in Heidelberg, at *ASTRID* in Aarhus, at the *PALLAS* storage ring in Munich and at the *ESR* in Darmstadt – and laser-cooling experiments are foreseen at the future *FAIR* facility [50] and at the *S-LSR* [51].

²The review [18] and the references found therein give a comprehensive overview of the present theoretical and experimental status. See also reference [49] for an overview on beam cooling techniques.

Experimental mile-stones of recent research include

- laser-cooling of bunched ion beams [52, 53],
- broadband [54] and "white-light" [55, 56] laser-cooling of ion beams,
- transverse laser-cooling of ion beams [57–59],
- extending laser-cooling to higher beam energies [60],
- the observation of ion ordering in the beam [61, 62],
- and the attainment of three-dimensional crystalline ion beams [3, 4].

Furthermore, electron cooling³ experiments have provided valuable insight into space-charge and beam ordering effects at low momentum spread and low ion currents [65–70]. These experiments were motivated by the observation of anomalous Schottky beam noise signals made at the *NAP-M* storage ring in Novosibirsk [71].

At relativistic energies, the strength of the laser-cooling force increases [MB0402] compared to typical laser-cooling experiments performed in the laboratory on ions at rest. This increase stems both from the relativistic Doppler-shift of the photon frequency from the laboratory frame to the rest frame of the ions and back, and the intrinsic properties of the Li-like and Na-like cooling transitions of the heavy ions subject to the laser force [MB0402]. At future storage rings, the Doppler-shift will allow for saturating the cooling transitions of heavy highly-charged ions up to $^{238}\text{U}^{89+}$ using a single laser system ([18],[MB0402]).

During two measurement campaigns in 2004 and 2006 at the *ESR* in Darmstadt,

- laser-cooling of relativistic bunched C^{3+} beams at 122 MeV/u could be demonstrated [MB0501],
- a longitudinal beam momentum spread at least one order of magnitude smaller than achievable by electron cooling could be attained [MB0601],
- the regime of space-charge dominated beams has been reached [MB0601],
- using moderate electron-cooling allowed to obtain three-dimensional cold beams [MB0601],
- strong coupling of ions in the bucket was observed [MB0501, MB0601],
- momentum-spread dependent changes in the longitudinal dynamics of cold bunched beams were compared to computer simulations [MB0704],
- precision VUV spectroscopy of the $2\text{S}_{1/2} \rightarrow 2\text{P}_{1/2}$ and the $2\text{S}_{1/2} \rightarrow 2\text{P}_{3/2}$ transition has been performed [MB0501] and

³For standard electron cooling theory see reference [63]. A more recent review with some remarks on ordering effects is available in reference [64].

- the momentum acceptance of the laser force was increased by using an additional scanning laser offset-locked to the frequency-locked cooling laser system [MB0704, MB0705].

A detailed discussion of these results can be found in part 2.

1.3 Stopping and Cooling Beams of Highly Charged Ions

Precision physics with cold trapped ions [72–78] requires the isolation, total positioning control over and manipulation of single ions, thus demanding a versatile cooling scheme. Unlike in storage rings, where many ion species can be addressed by laser-cooling at relativistic beam energies, only a few can be directly laser-cooled in traps, because at present the number of laser systems which can address the desired cooling frequencies is small.

Nevertheless, the Coulomb interaction between the directly laser-cooled ions and the ions of interest can provide for sympathetic cooling [79–88] of nearly any charged particle, ion or molecule, which can be trapped together with the laser-cooled ions [36–38, 89].

Sympathetic cooling of ions and molecules in traps forms the basis for a variety of experiments dedicated to fundamental physics. To name but one, laser spectroscopy of the $^{229\text{m}}\text{Th}^{3+}$ nuclear transition from the $J^\pi = \frac{5}{2}^+$ ground state to the $J^\pi = \frac{3}{2}^+$ isomeric state, will be discussed in appendix A. In spite of the multi-faceted physics of strongly coupled multi-species Coulomb crystals, in the following the focus will be on in-trap preparation of cooled highly charged ions, especially for ultra-precise mass measurements and fundamental physics. Currently, several trap systems dedicated to precision experiments with single ions⁴ are successfully operating, including *SHIPTRAP* [90], *CPT* [91], *SMILETRAP* [92], *ISOLTRAP* [93], *JYFLTRAP* [94], *LEBIT* [95] and *UW-PTMS* [96]. Furthermore, new trap systems are currently being built, namely *TITAN* [97], *HITRAP* [98] and *MLLTRAP* [MB0703]. The relative precision $\Delta m_{\text{HCl}}/m_{\text{HCl}}$ of in-trap mass measurements is determined by the measurement time τ_{m} , the magnetic field B and the number N_{m} of measurements with individual ions [73–75, 99]:

$$\frac{\Delta m_{\text{HCl}}}{m_{\text{HCl}}} \propto \frac{m_{\text{HCl}}}{\tau_{\text{m}} B N_{\text{m}}^{1/2}} \times \frac{1}{Q_{\text{HCl}}}. \quad (1.4)$$

If short-lived ions are considered, the most promising way to increase the precision is by increasing the charge state Q_{HCl} . For these ions, a relative precision of $\Delta m_{\text{HCl}}/m_{\text{HCl}} \approx 10^{-8} - 10^{-9}$ can be envisaged for $\tau_{\text{m}} < 100$ ms, while for stable ions the accuracy can be significantly extended – currently to a value of about 10^{-11} – using longer measurement times.

⁴This list only includes Penning traps dedicated to single-ion precision experiments. Thus, projects like *ATRAP*, *ATHENA/ALPHA*, *ASACUSA*, *LPCTRAP* and many others are not included in the list.

After charge breeding, typically performed in an Electron Beam Ion Source (*EBIS*) [100, 101] or via laser ionization [102, 103], the duration of the total process of ion transport, ion cooling, extraction into the precision trap and the mass measurement itself, must be of the same order of magnitude as the ion lifetime to achieve a reasonable number of consecutive measurements N_m . Following the extraction from the *EBIS*, the high charge state of the ions must be preserved until the end of the mass measurement. Furthermore, with the low rates expected for rare ions, the cooling scheme employed to match the ion beam momentum spread to the momentum acceptance of the precision trap system must be efficient enough to minimize losses of highly charged ions. Finally, it must also provide means of accumulation and controlled ejection of the ions into the measurement trap region.

Up to now, several cooling schemes have been successfully applied in precision mass measurement experiments. At low charge states, buffer gas cooling [8, 83, 104, 105] can be applied. At high charge states, however, it suffers from intolerable losses of highly charged ions due to charge exchange with the buffer gas. Resistive cooling [8, 83, 106, 107] on the other hand increases in efficiency for higher charge states, but requires a cold trap system and is essentially temperature limited to 4 K, which for ultra-precise measurements imposes a severe limitation. Most future trap systems currently favor in-trap electron cooling [19, 97, 98, 108, 109].

In this thesis, an alternative scheme of sympathetic cooling using laser-cooled ions instead of electrons is proposed. The advantages of this scheme are three-fold:

- First, ultra-low temperatures of the highly charged ions in the mK regime can be reached.
- Second, optical detection and manipulation of the ions by the combined force of the confining fields and the laser force gives precise position control over the ions.
- Third, even for high charge states virtually no loss of highly charged ions due to charge exchange is expected.

The results summarized in this thesis show that the proposed cooling scheme is efficient, fast and reliable enough to prepare highly charged ions for precision in-trap experiments.

1.4 Outline of the Thesis

This outline of the thesis aims to guide the reader through the thesis, briefly listing the content of each of the following five parts of the text.

The first is dedicated to direct laser-cooling of ion beams and to the discussion of future prospects of laser-cooling at ultra-relativistic energies. The second part is dedicated to the realistic simulation of in-trap preparation of highly charged ions

for precision experiments with regard to the *MLLTRAP* Penning-trap system. The third part is dedicated to collective effects in strongly coupled one-component plasmas.

The first two parts are subdivided in three sections. The first section lists the objectives of the experimental and theoretical investigations. It serves as a guide to the following sections. The second section includes all the relevant information on the experimental and theoretical background needed to understand the final third section. This third section discusses the main results of the thesis.

The discussion of yet unpublished data found in the third part revisits subjects already mentioned in the previous two parts and thus this part is restricted to an analysis of the relevant results.

Each of these parts must be understood as a brief summary of the detailed analysis found in the corresponding publications. They are intended to provide the reader with an overview of the most important aspects of the thesis and should thus be only read in combination with the publications enclosed.

The thesis is concluded by a short summary and outlook part and an appendix on experiments currently being built, which are related to the work presented here.

2. LASER-COOLING AND PRECISION SPECTROSCOPY OF RELATIVISTIC ION BEAMS

2.1 Applying Laser-Cooling to Ion Beams at Relativistic Energies

With the first experimental realization of crystalline ion beams at the table-top storage ring *PALLAS* [2–4, 17], searching for ordering effects in ion beams at large-scale storage rings is the next natural step. Only if the regime of strong coupling [23, 24] can be reached, long-range ordering of ions can occur. This requires low ion beam temperatures at moderate to high ion beam densities. Former large-scale storage ring experiments searching for beam ordering were finally limited by the ion density at which a sudden drop in the beam momentum spread was observed [65–71].

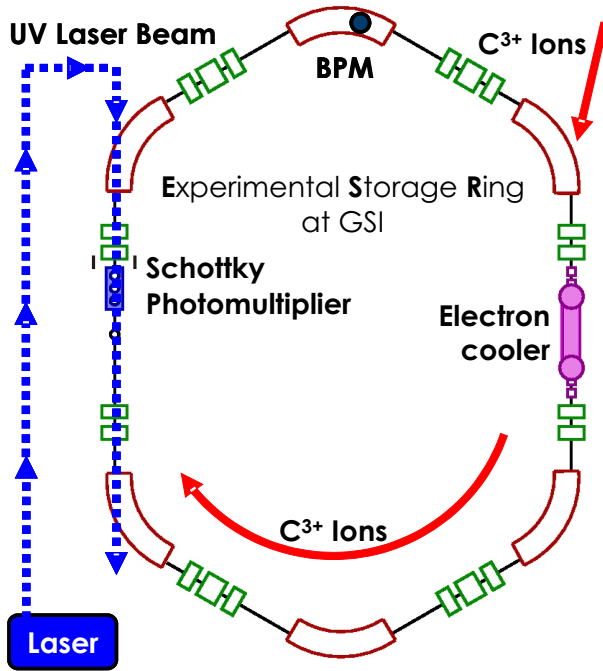
In contrast to these experiments, with direct laser-cooling of moderately bunched beams, longitudinally space-charge dominated beams can be attained at usually ten times higher ion beam currents [MB0601]. At these currents, the density of the ions confined in the center of the bucket pseudo-potential is high enough to enter the strong coupling regime at a momentum spread of about $\Delta p_{\parallel}/p_{\parallel} < 10^{-7}$ [MB0501, MB0601].

Following this part is a short overview of the experimental setup used for laser-cooling at the Experimental Storage Ring located at *GSI*, concluded by a summary of the results.

2.2 Experimental Setup at the ESR at GSI

2.2.1 The Experimental Storage Ring at GSI

The *ESR* storage ring (see Fig. 2.1) has a circumference of about 108 m and a twofold periodicity (see Tab. 2.1). The periodicity is the total number of individual focusing cells constituting the storage ring. In comparison to the *ESR*, the periodicity of the *PALLAS* storage ring is about 900, resulting in a very smooth storage ring lattice. A small periodicity imposes a severe limitation for observing a crystallization of the beam [18, 32] due to increased heating rates. In the experiments at *ESR*, multiply charged C^{3+} ions are used instead of the singly charged $^{24}Mg^{+}$ ions stored in *PALLAS*.



| <i>ESR</i> | |
|---------------------------------|---------------|
| Circumference | 108.36 m |
| Periodicity | 2 |
| Betatron tune | 2.3 |
| Slip factor | 0.607 |
| <i>Beam</i> | |
| Energy | 1.47 GeV |
| Relativistic β, γ | 0.47, 1.13 |
| Revolution freq. | 1.295 MHz |
| Lifetime | 450 s, 270 s |
| <i>Ion</i> | |
| Species | C^{3+} |
| $2S_{1/2} \rightarrow 2P_{1/2}$ | 155.07 nm |
| $2S_{1/2} \rightarrow 2P_{3/2}$ | 154.81 nm |
| <i>Laser</i> | |
| Laser source | cw Ar^+ |
| SHG | type II |
| Wave length | 257.34 nm |
| Power | 40-100 mW |
| Waist | 20-30 μm |

Left: Figure 2.1: Schematic view of the Experimental Storage Ring at *GSI*. The ions enter the ring revolving clockwise, while the laser beam enters the ring, counter-propagating to the ion beam, after about 60 m of transport in air. The overlap region is about 25 m long, the photomultiplier is placed in the drift tube region outside the vacuum. Also marked are the position of the beam profile monitor (BPM), the electron cooler and the pickup electrode (Schottky). **Right:** Table 2.1: Experimental parameters of the ion beam, laser system and cooling transition for the *ESR* measurement campaigns in 2004 and 2006.

For ions with multiple charge state the inter-ion Coulomb force increases quadratic with the charge state number, thus with the triply-charged C^{3+} ions used for laser-cooling, the ion interaction strength can be increased ninefold compared to *PALLAS*. The beam energy of the ions is chosen to be 122 MeV per nucleon, resulting in a relativistic γ -factor of 1.13, with the ions circulating the ring at 47 % of the speed of light at a revolution frequency of 1.295 MHz.

Moderate bunching of a few volts is applied to counteract the laser force. The bunching frequency f_b is set to a harmonic h of the revolution frequency f_{rev} . Bunching is performed at the 5th, 10th and 20th harmonic of the revolution frequency, providing a longitudinal density modulation of the ion beam. Its effect can be described by introducing a harmonic pseudo-potential, the *bucket*, in which the ions perform *synchrotron oscillations*, a periodic variation of the

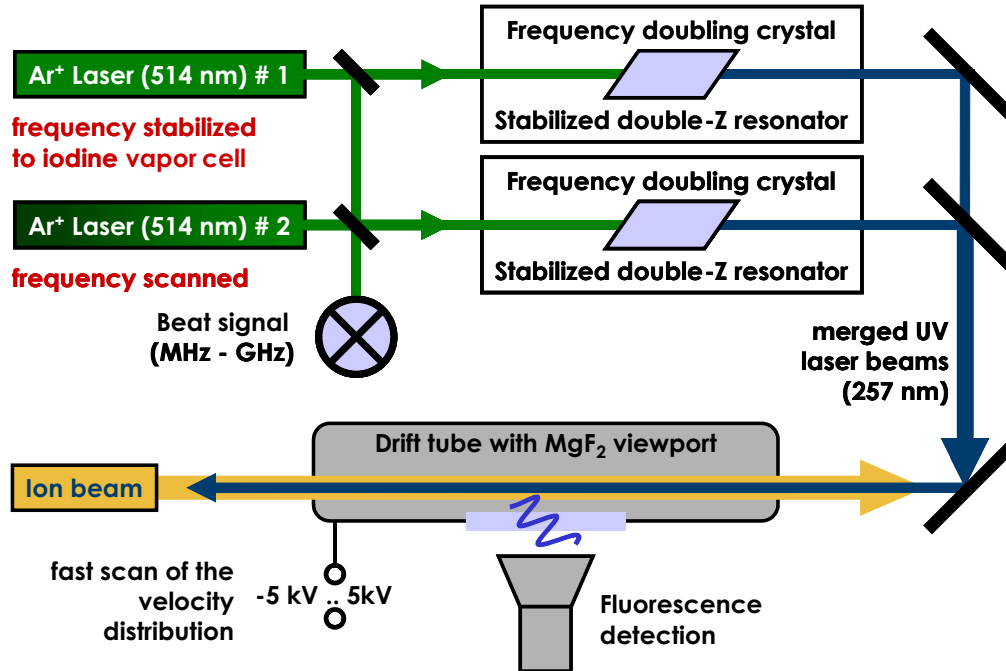


Figure 2.2: Schematic view of the laser system used in the second measurement campaign in 2006. Two argon ion laser systems are connected via a frequency-offset lock. Their relative detuning is measured by the beat signal of the merged laser beams. Both beams are merged into one and transported over a distance of about sixty meters in air, where the laser beam enters the ring. The fluorescence light of the ions is detected by a photomultiplier placed outside the vacuum. A fast voltage ramp of -5 kV to 5 kV can be applied to the drift tube section to realize an all-optical measurement of the longitudinal momentum distribution of the ion beam.

individual ion velocity along the beam axis. This variation is recorded by the Schottky pickup electrode.

In the first measurement campaign in 2004, excellent vacuum conditions were provided, resulting in a beam lifetime of 450 s to 470 s. In the second campaign in 2006, almost the same conditions could be provided and beam lifetimes of about 250 s were attained.

2.2.2 The Argon Ion Laser System

A continuous-wave argon ion laser system¹, frequency-stabilized using the absorption signal measured in an iodine vapor cell [111, 112], is frequency-doubled in an actively stabilized double-Z resonator² of the Hänsch-Couillaud type [114] with a quality factor of about 50 to 100. Second-harmonic generation of type

¹Coherent Innova 200, single-mode, single frequency operational mode [110]

²50 mm resonator focal length, coating provided by Laseroptik [113]

II in a beta-barium borate (BBO) crystal³ [117] produces laser light at a wavelength of about 257 nm at a power of up to 100 mW and a laser beam waist between 20 μm to 30 μm .

In the second measurement campaign in 2006, this laser system was complemented by a second argon ion laser system and a second resonator for frequency-doubling (the complete setup is found in Fig. 2.2). The second laser-system is modified in such a way that a tilt can be applied to the in-resonator etalon. This tilt both shifts the frequency of the laser light and reduces the light intensity. To compensate for the intensity reduction, the length of the laser resonator is actively adapted using a fast piezo-stack fixed to the mirror which couples out the laser light. By applying a voltage to the piezo-stack, the resonator length can be controlled, ultimately keeping the light intensity constant.

By using an offset-frequency locking scheme [111, 118], the frequency of the second laser beam can be actively detuned relatively to the first laser system. This detuning is determined measuring the beat signal of the two lasers with a 20 GHz photo-frequency counter⁴. The total gain range of an argon ion laser is about 8 GHz, but only a limited part of this range can be scanned without experiencing mode-hopping. If the etalon is tilted too far from its original position, the TEM₀₀ mode required for efficient frequency-doubling is replaced by a higher-order mode which better matches the resonating conditions, thus disabling the locking scheme. Still, a free scanning range of up to 1 GHz can be attained⁵. This scanning range is equivalent to about five to ten percent of the initial momentum spread of the ion beam and means about two orders of magnitude increase in the acceptance of the laser force.

With this setup, the small momentum acceptance of the laser force can be expanded to better match the initial longitudinal momentum spread of the ion beam. For this to happen, both laser beams are merged and transported over a distance of about 60 m, entering the ring counter-propagating to the ion beam. Both laser beam and ion beam are brought in overlap in a straight ring section of about 25 m length. For this, the laser beam is shadowed by the edges of the horizontal and vertical ion beam scrapers, which determine the ion beam position. Then, the intensity of the photomultiplier signal is optimized, measuring the fluorescence signal about 10 m away from the laser entrance window. This process is repeated several times until the beam overlap is optimized.

2.2.3 Measuring the Relevant Beam Parameters

Several detection systems exist at the *ESR* to measure all relevant beam parameters. The ion beam current monitor can be used to measure the lifetime of the beam without any cooling applied. This lifetime is mainly limited by the amount of residual gas in the ring. Fortunately, rest gas pressures down to 10^{-13} mbar were reached in 2004 and 2006, allowing for long beam lifetimes between 270 s

³Döhner Elektrooptik [115], Crystals of Siberia [116], 8 mm and 10 mm length, respectively

⁴New Focus NFI-1437-M 25 GHz photo detector [119]

⁵in the UV after frequency-doubling

and 450 s. After injection, the typical ion current is around $100 \mu\text{A}$. The current monitor works reliable for ion currents above $20 \mu\text{A}$. By measuring the beam lifetime precisely, an extrapolation to low ion currents of a few μA is possible, as described in reference [MB0501] reprinted on page 93.

The width of the beam can be determined using a beam profile monitor. The *ESR* beam profile monitor is limited to beam currents above about $2 \mu\text{A}$. For bunched beams, the pickup monitor, which measures the charge induced by the ions revolving in the ring, is used to determine the length of the bunch. Here, the resolution is limited by the length of the pickup electrode to about 0.35 m. Finally, the Schottky noise signal [120] induced on the pickup electrode can be recorded. A fast Fourier transformation of the temporal variation of the pickup signal gives a frequency spectrum $S_{\text{Schottky}}(\Delta f_{\text{b}})$ of the ion synchrotron oscillations [41, 121] in the bucket. With this information, the longitudinal momentum spread

$$\frac{\Delta p_{\parallel}}{p_{\parallel}} = \frac{1}{\eta} \frac{|\Delta f_{\text{b}}|}{f_{\text{b}}} \quad (2.1)$$

of the ions – related to the width of the frequency spectrum via the slip factor η [18] – can be measured to a precision of about 2×10^{-6} (for details on the exact derivation of the momentum spread see [18] and [MB0704]).

In addition to these detection systems an optical detection of the fluorescence signal via a photomultiplier tube, placed outside the vacuum, is installed in the drift tube section of the ring. With this photomultiplier a small part of the fluorescence photons can be detected, while the signal strength is mainly limited by the small solid angle visible to the photo cathode. By applying an additional fast voltage scan to the drift tube, thus probing the fluorescence light intensity for different velocity classes of ions [18, 54], an upper limit to the longitudinal momentum spread can be determined to $\Delta p_{\parallel}/p_{\parallel} < 10^{-7}$ [MB0501, MB0601], thereby increasing the resolution of the momentum measurement at least tenfold.

2.3 Results

2.3.1 Laser-Cooling of Relativistic Ion Beams

The Lorentz-transformation of the laser wavelength $\lambda_{\text{l,lab}}/2 = 257.34 \text{ nm}$ from the laboratory frame to the rest frame of the ions is

$$\lambda_{\text{l,rest}} = \frac{\lambda_{\text{l,lab}}/2}{\gamma(1 + \beta)} \approx \frac{257.34 \text{ nm}}{1.13 \times (1 + 0.47)} \approx 155 \text{ nm}, \quad (2.2)$$

where total overlap of the ion beam with the laser beam is assumed. By carefully tuning the ion energy, both the $2S_{1/2} \rightarrow 2P_{1/2}$ and $2S_{1/2} \rightarrow 2P_{3/2}$ can be saturated for laser-cooling [MB0501], proving the feasibility of laser-cooling at truly relativistic beam energies.

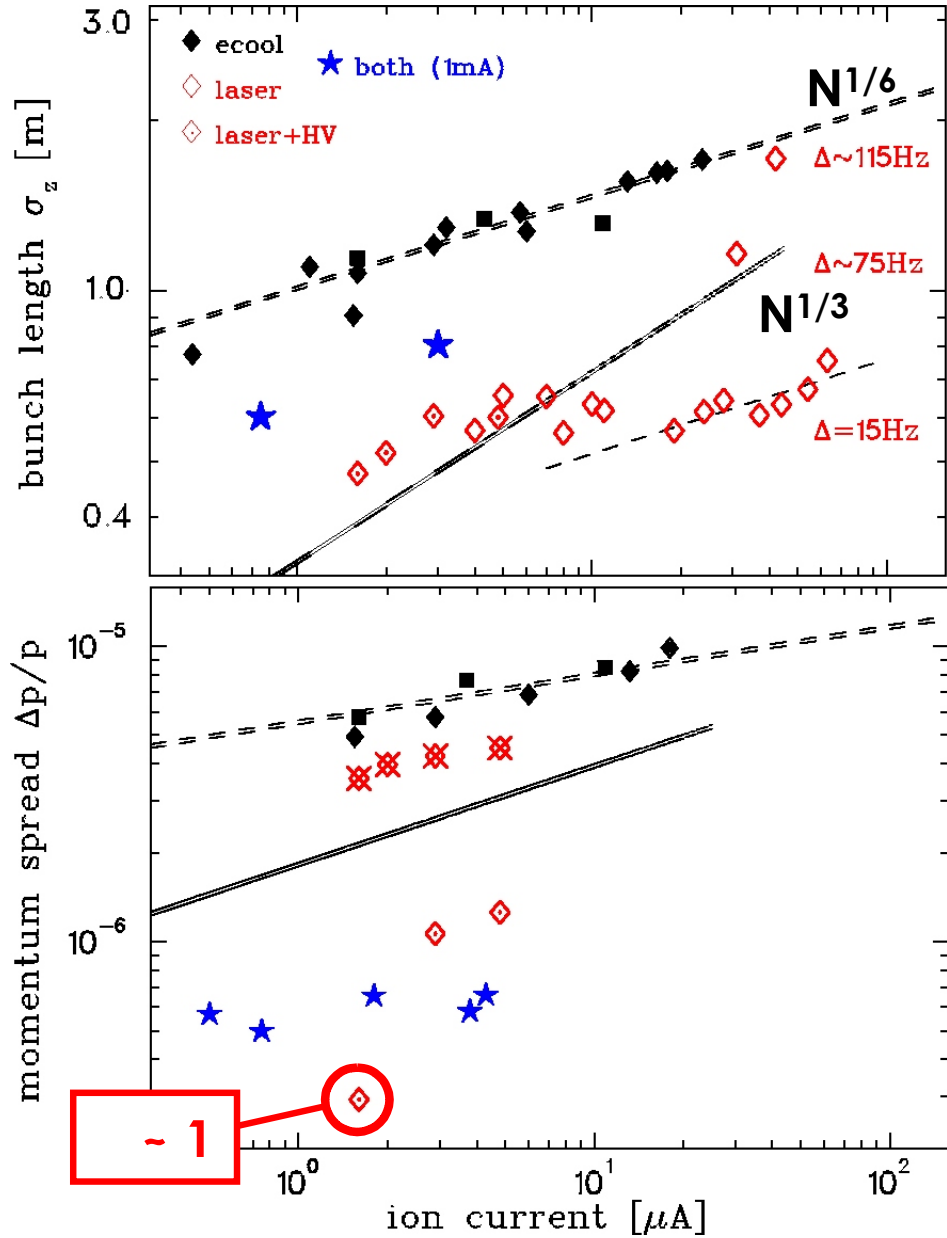


Figure 2.3: **Upper part:** Bunch length measured by the pickup electrode. **Lower part:** Longitudinal momentum spread extracted from the Schottky noise spectrum. Filled symbols mark data obtained for pure electron cooling at various electron currents. Open symbols indicate purely laser-cooled ion beams at various detuning of the laser frequency relative to the transition frequency of ions resting in the bucket. Dotted symbols stand for purely laser-cooled beams with a fast voltage ramp applied to the drift tube section. Blue stars mark those measurements where moderate electron cooling at an electron current of 1 mA was switched on for a few seconds at the beginning of the measurement, followed by a long period of pure laser-cooling. The dashed lines indicate the $N^{1/6}$ scaling of the bunch length expected for intra-beam scattering dominated beams, where N denotes the number of particles in the beam. The solid lines indicate the $N^{1/3}$ scaling expected for space-charge dominated beams. The corresponding scaling of the momentum spread is also indicated. See text for more details.

2.3.2 Attaining a Small Ion Beam Momentum Spread

Fig. 2.3 shows values for momentum spread and bunch length of purely laser-cooled moderately bunched ion beams measured at a fixed laser frequency, which are compared to the values obtained for pure electron cooling. The filled black symbols refer to purely electron-cooled beams at an electron current of 50 mA and 250 mA, respectively. No dependence of both bunch length and momentum spread on the electron current is observed. The open red symbols refer to purely laser-cooled ion beams. The crossed out rhombic symbols in the lower part of Fig. 2.3 mark those beams for which the momentum spread is extracted from the Schottky noise spectrum as explained in Fig. 2.6. These values for the momentum spread have to be compared to the values deduced from the fluorescence signal of the beam as described in part 2.2.3. The fluorescence measurement provides a momentum resolution which is at least ten times better than that of the Schottky signal. Following this comparison, it is evident that the longitudinal momentum spread of the laser-cooled ion beams is smaller than the value derived from the resolution-limited Schottky noise measurement.

With pure laser-cooling, longitudinal momentum spreads on the order of $\Delta p_{\parallel}/p_{\parallel} < 10^{-6}$ at ion currents below $10 \mu\text{A}$ are observed, while for electron cooled beams only momentum spreads larger by about one order of magnitude can be attained. For the latter case, the electron cooling current is usually set to 50 mA or 250 mA, respectively, while for those beams which are cooled by combined laser- and electron cooling as described below, the electron current is set to 1 mA. In order to distinguish purely space-charge dominated beams from intra-beam scattering dominated beams, the lines in the upper part of Fig. 2.3 indicate the different scaling of the bunch length with the number N of ions in the beam expected for the two scenarios [18, 122]. At moderate to low ion currents, the bunch length of the laser-cooled ion beams clearly follows the space-charge scaling [MB0303, MB0304], while for ion currents above $10 \mu\text{A}$ – meaning higher ion densities – the laser force can no longer compensate the heating due to close encounters of the ions and the scaling follows the trend expected for intra-beam scattering [122].

2.3.3 Longitudinally Space-Charge Dominated Beams

The results of the last section already indicate that space-charge dominated beams have been attained by pure laser-cooling. More evidence for this is presented in this section. When the ion beam reaches the space-charge dominated regime, the length of the ion bunch in the bucket is solely determined by the mutual Coulomb repulsion of the ions and the strength of the confining three-dimensional potential⁶.

⁶See [MB0303, MB0304] for a detailed discussion on the bunch length of very elongated, bunched crystalline ion beams. These publications address yet unexplained discrepancies found between theoretical estimates of the bunch length of space-charge dominated beams [27, 123–125] and bunch length measurements performed at the storage ring *PALLAS*, which are smaller than the theoretical predictions by a factor of two.

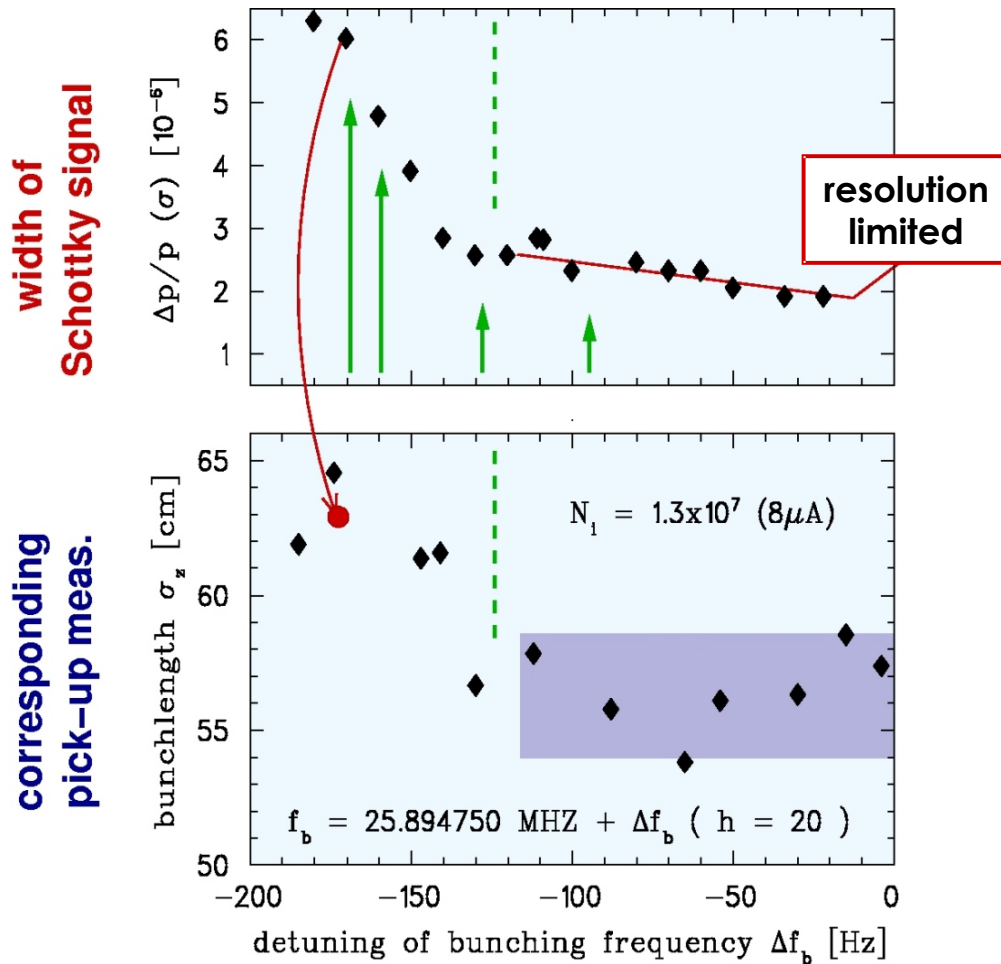


Figure 2.4: **Upper part:** Momentum spread of an ion beam at a constant ion current of $8 \mu\text{A}$ versus the detuning of the laser frequency.

Lower part: Corresponding bunch length. At a detuning of about -125 Hz, marked by the green dashed line, the resolution of the Schottky noise spectrum is reached and only an upper limit to the momentum spread can be deduced. At the same detuning frequency, the bunch length stays constant if the absolute detuning is further reduced, as indicated by the shaded area underlying the data points. The red circle data point depicts the bunch length calculated from the corresponding momentum spread, as indicated by the red arrow. The green arrows mark consecutive times at which a detailed analysis of the Schottky noise spectrum has been performed (see page 22 and Fig. 2.6 for details).

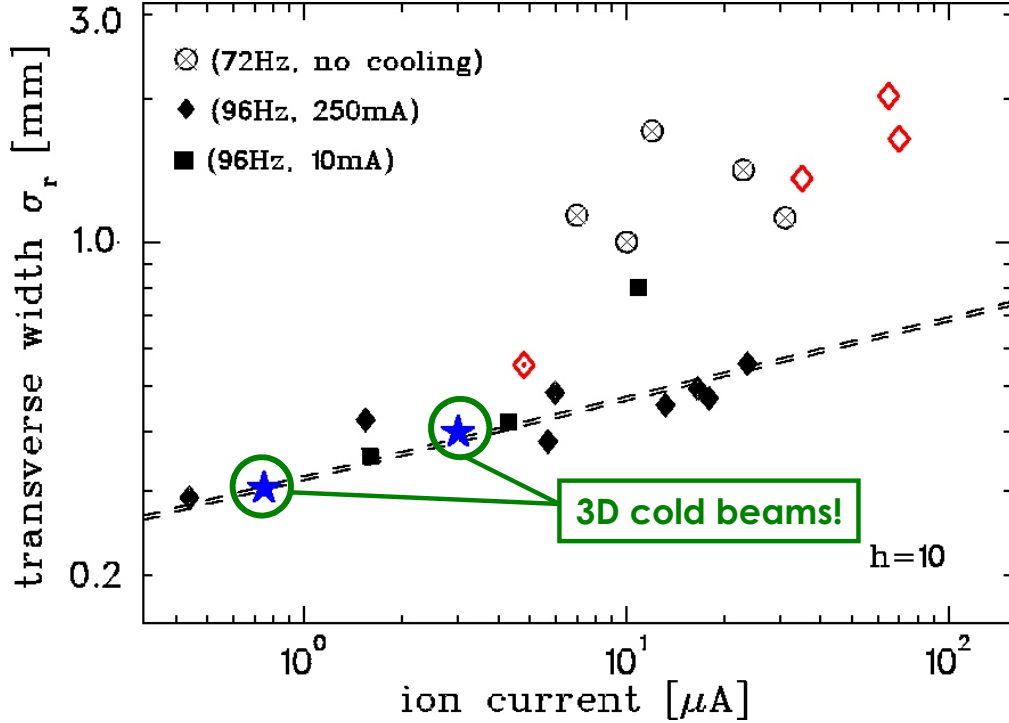


Figure 2.5: Beam widths of purely electron-cooled ion beams, purely laser-cooled ion beams and laser-cooled ion beams with additional moderate electron cooling applied. The symbol classification follows that of Fig. 2.3. The dashed line indicates the scaling of the beam width for intra-beam scattering dominated beams with the ion number N . The legend lists data points by the corresponding synchrotron frequency and electron cooler current. The blue stars refer to two beams also found in Fig. 2.3, which are examples of three-dimensional cold beams.

This means that, for a given ion current, the axial ion density stays constant and becomes (almost) independent of the momentum spread of the beam. If no ions are lost from the bucket, the bunch length thus stays constant for decreasing momentum spread.

In order to reduce the total momentum spread of the ion bunch, the initial broad momentum spread of the ions was matched to the small momentum acceptance of the laser force by continuously changing the bunching frequency. Thereby, the difference between the laser frequency and the transition frequency of the ions resting in the bucket center is continuously reduced, as discussed in detail in [MB0704] and parts 2.3.5 and 4.2.2.

With this cooling scheme the momentum spread of all ions confined in the bucket can be reduced to values reaching the resolution of the Schottky noise measurement. This is shown in Fig. 2.4. Here, momentum spread and bunch length

are measured for decreasing absolute detuning of the laser frequency. The figure clearly shows the constancy of the bunch length expected for a space-charge dominated bunched beam.

2.3.4 Three-Dimensional Cold Beams

As already indicated by the blue stars in Fig. 2.3, some beams were moderately electron cooled at an electron current of 1 mA in addition to the laser-cooling. The electron cooler was switched on for a few seconds, while for the rest of the beam lifetime only laser-cooling was applied.

The additional electron beam brought in overlap with the ion beam increases the charge density in the overlap region, thereby increasing the coupling between all charged particles. Thus, the coupling of the transverse ion motion to the longitudinal ion motion is enhanced due to the Coulomb interaction between the charged particles in the overlap region. Once both degrees of motion are coupled, the electron cooler can be switched off and only laser-cooling must be applied.

For two beams marked in Fig. 2.3 by blue stars, the corresponding beam width is found in 2.5. The measured beam width is equal to the values reached by continuous electron cooling with two orders of magnitude higher electron current.

2.3.5 Ion Dynamics in the Bucket

One open question raised by the experimental results summarized in this thesis is: How do the (longitudinal) ion dynamics in the bucket change when the beam becomes space-charge dominated? While the fluorescence detection increases the precision of the momentum spread measurement tenfold, this detection scheme could be used only in few cases due to insufficient photon counting rates⁷. Thus, most of the information on ion dynamics must be deduced from the Schottky noise spectra, which are limited in resolution.

Complementary to the experimental enhancements discussed in the outlook, part 5, a first attempt to simulate the ion dynamics has been made [MB0704]. The results are presented in Fig. 2.6. The black curves present measured Schottky noise spectra for various values of the detuning Δf_b , while the green curves present the corresponding simulation data. Both data sets exhibit pronounced peaks of incoherent sidebands distributed symmetrically around the central carrier signal peak. The momentum spread of the bunch is determined by the spread of these incoherent sidebands [MB0601], which can be deduced from the width of the sideband envelope as shown in the bottom-most part of Fig. 2.6. With decreasing detuning Δf_b , the momentum spread of the bunch is reduced and the sidebands vanish.

The simulation treats the ions in the bucket as non-interacting individual particles performing synchrotron oscillations in the bucket pseudo-potential. This simple model assumption is valid only for emittance-dominated beams. In this

⁷These rates will hopefully increase in future experiments. See part 5 for details.

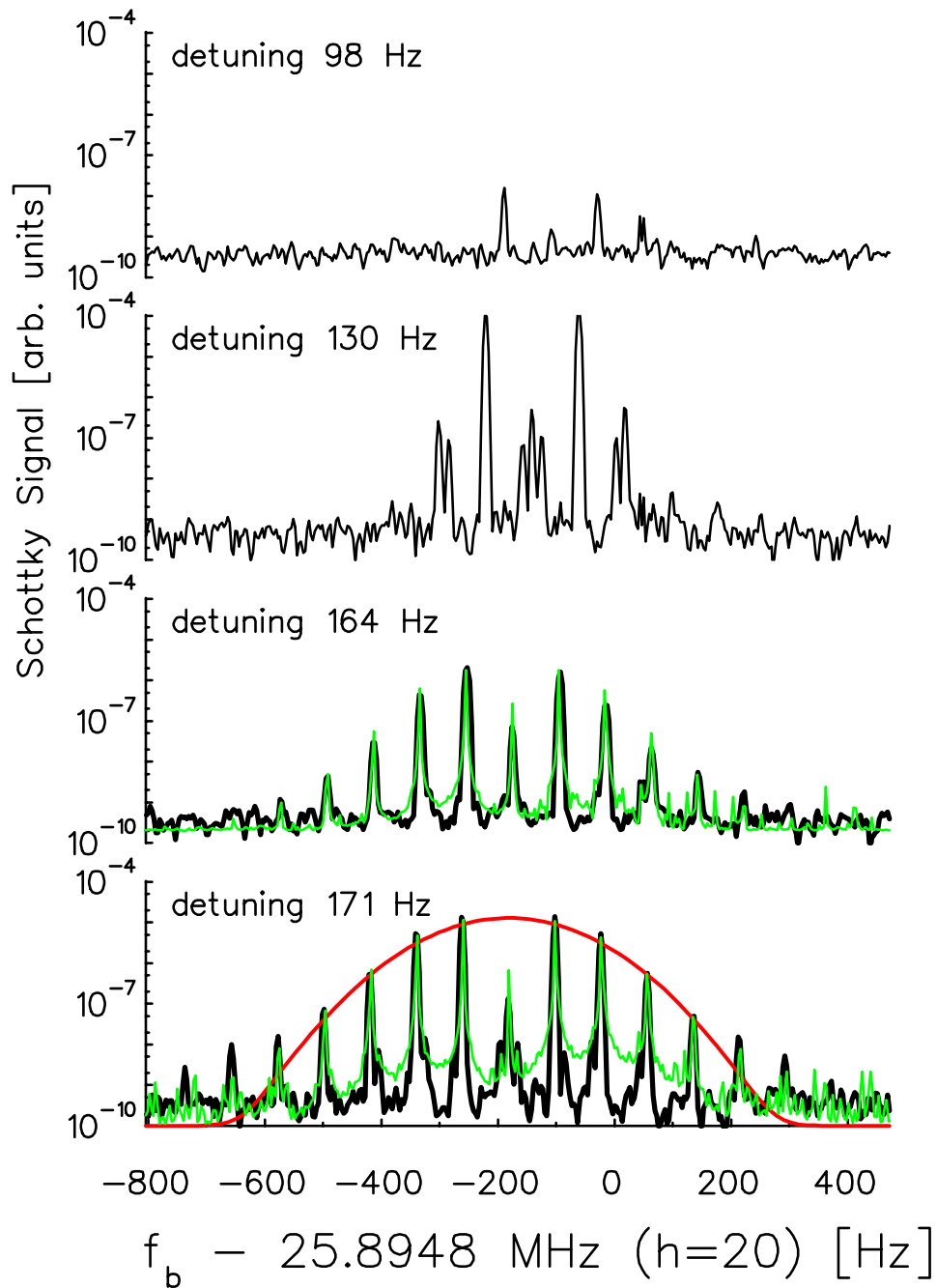


Figure 2.6: Schottky noise spectra (black curves) measured at various detuning values as indicated in the plots. These spectra correspond to the data points marked by green arrows in Fig. 2.4. The data was taken at the 20th harmonic of the revolution frequency. In the bottom-most plot the red Gaussian curve indicates the fitted momentum spread as shown in the upper part of Fig. 2.4, while the green curves show the simulation data.

case, heating due to intra-beam scattering and laser cooling are in equilibrium and the beam can be described by an ensemble of weakly coupled ions of constant temperature.

Typically, it is assumed that the barycenter of the ion bunch rests in the minimum of the bucket potential, resulting in a carrier signal amplitude proportional to the number of ions in the bunch [121, 126]. However, the experimental data suggests a reduction of the carrier peak amplitude compared to the amplitude of the incoherent sidebands, which is not caused by ion loss [MB0601, MB0704]. The simulation data plotted in green is obtained adding a collective oscillation of the ion bunch in the bucket potential to the individual ion motion. In the simulation, the longitudinal momentum spread of the ions is set to the experimental value deduced from the width of the sideband envelope and each ion is given a certain kinetic energy, assuming a Maxwellian distribution of the ion momenta. Similarly, the amplitude of the collective bunch oscillation is found to be solely determined by the detuning Δf_b of the laser frequency, which sets an upper bound to the beam momentum spread as discussed in [MB0704]. Superimposing the thermal motion of the ions with the collective bunch oscillation, the reduction of the carrier signal predicted by theory [120, 121, 126] and deduced from the simulation is in good agreement with the experimental data, as seen in Fig. 2.6. The collective oscillation is attributed to the stepwise change of the bunching frequency necessary for the cooling scheme employed [MB0704], which introduces a displacement of the bucket center in momentum space relative to the mean ion bunch momentum, causing the ions to oscillate in phase.

Compared to the experimental data, the continuous background of the simulation data is higher. It can be reduced by increasing the number of particles in the simulation, which is orders of magnitude smaller than for the experimental data⁸. The background is caused by the Fast-Fourier-Transform algorithm which computes the Schottky noise spectra from the individual ion motion. At low particle number, the algorithm produces randomly distributed spectral values which emerge as a Gaussian-distributed background of numerical noise. Since the contribution of these numerical artifacts is at least one to two orders smaller than the Schottky signal itself, no attempt was made to further reduce the background by increasing the simulated particle number.

While the two lower spectra in Fig. 2.6 relate to the intra-beam scattering regime, the two upper spectra relate to the space-charge dominated regime, as indicated by the green arrows in Fig. 2.4. No model has yet been able to fully explain the Schottky noise spectra observed for space-charge dominated beams. The simple model presented here clearly fails at the transition to this regime. It predicts a raise in the carrier signal strength [MB0704], while a reduction of the total Schottky signal strength by orders of magnitude is observed⁹.

A raise in the carrier signal intensity is expected for weakly coupled, non-

⁸Due to limited computation time, the number of simulated particles was kept small to only resemble the main characteristics of the spectra.

⁹Please note that no ions are lost from bucket. All ions instead reside in the bucket center.

interacting particles, because the reduction of the absolute frequency detuning damps the oscillation amplitude of the collective bunch oscillation as explained in part 4.2.1. Instead, the vanishing carrier signal clearly hints to ion dynamics beyond the simple approach outlined above. The reduction of the carrier signal intensity is attributed to the influence of the mutual interaction of the ions which can no longer be neglected for space-charge dominated beams. Unfortunately, no conclusive results from the fluorescence signal measurement could be obtained due to unexpected low rates, and thus no direct measurement of the true beam momentum spread or ion-ion correlations could be observed.

An experimental investigation of the beam dynamics at very low momentum spread is therefore foreseen for the next beam time at the *ESR*¹⁰, which will be accompanied by time-consuming simulations of the ion dynamics in the bucket, this time taking into account the complete ion-ion interaction¹¹.

2.3.6 Precision VUV-Spectroscopy

The reduction of the beam momentum spread allows to saturate the cooling transition of a large number of ions with a single laser system. The small momentum acceptance of the laser force, which is limited by the natural line width $\Gamma_{\text{trans}} \approx 2\pi \times 6.7$ MHz of the cooling transition, becomes important if laser spectroscopy of ion beams is considered.

The bandwidth of the laser line of about 1.2 GHz determines the relative energy spread of those ions which emit fluorescence light observable in the laboratory frame.

In the experiment, the beam energy has been determined indirectly using the well-known acceleration voltage of the *ESR* electron cooler. This voltage is calibrated to an absolute accuracy of the order of one volt, which results in a relative accuracy of 10^{-4} . Since the laser wavelength

$$\lambda_{\text{l,lab}}/2 = 514.6734664 \text{ nm}/2 \quad (2.3)$$

is known to a relative accuracy of better than 10^{-9} [112], the accuracy of the transition frequency ω_0 measurement solely depends on the accurate determination of the relativistic gamma factor γ as

$$\frac{\Delta\omega_0}{\omega_0} = \frac{1}{\beta} \frac{\Delta\gamma}{\gamma}. \quad (2.4)$$

Different to the experiments mentioned so far, in this measurement a coasting ion beam is used. Both the laser frequency and the mean energy of the electron cooled ion beam are brought in overlap observing the online Schottky noise spectrum of the ion beam¹², as described in reference [MB0501] reprinted on

¹⁰probably taking place in 2008

¹¹A newly developed parallel simulation code capable of performing this computational intensive task is introduced in part 3.2 of this thesis.

¹²In this special case the relative resolution of the Schottky spectrum is limited by the digitizing resolution of the online analysis, which is about 10^{-5} .

| | $\lambda_0(2S_{1/2} \rightarrow 2P_{1/2})$ [nm] | $\lambda_0(2S_{1/2} \rightarrow 2P_{3/2})$ [nm] |
|-----------------------------|---|---|
| Edlén (1983) [127] | 155.077 | 154.820 |
| Kim et al. (1991) [128] | 155.060 | 154.804 |
| Johnson et al. (1996) [129] | 155.078 | 154.819 |
| Tupitsyn et al. (2003) | 155.0739(26) | 154.8173(53) |
| priv. comm. [2004] | | |
| Schramm et al. (2005) | 155.0705(39)(3) | 154.8127(39)(2) |
| [MB0501] | | |

Table 2.2: Absolute wavelengths for the $2S_{1/2} \rightarrow 2P_{1/2}$ and $2S_{1/2} \rightarrow 2P_{3/2}$ transition in C^{3+} published by other groups as compared to the measurements performed at *ESR* presented in this thesis.

page 93. In order to compensate for the shift of the ion beam energy induced by the space-charge of the electron cooler beam, the overlap is restored by adjusting the electron cooler voltage at every time the electron cooler current is reduced. The final value of the electron cooler voltage is then determined by extrapolating to zero electron current. The final results listed in Tab. 2.2 obtained for the $2S_{1/2} \rightarrow 2P_{1/2}$ and $2S_{1/2} \rightarrow 2P_{3/2}$ transition in C^{3+} agree well within one standard deviation with previous theoretical calculations [127–129] and measurements [127].

In the experiment presented here, a direct measurement of the wavelength of the fluorescence photons, which lies in the deep VUV regime, has not been undertaken due to the lack of a suitable, precise detector. In future storage rings at highly relativistic beam energies, the emitted fluorescence photons will be visible as a strongly forward-boosted X-ray emission¹³. A direct measurement of the fluorescence light frequency in the laboratory frame will then allow to precisely determine the beam energy from the fixed laser frequency as discussed in reference [MB0402].

2.3.7 Increasing the Acceptance of the Laser Force

In order to replace the stepwise detuning of the bunching frequency by a directly detunable laser system, a second laser system complementing the fixed-frequency cooling laser was introduced in the 2006 beam time to better match the laser force acceptance to the ion beam momentum spread, see Fig. 2.2 on page 15.

¹³see [130] for an overview of X-ray spectroscopy using laser-cooled ion beams at the future FAIR facility

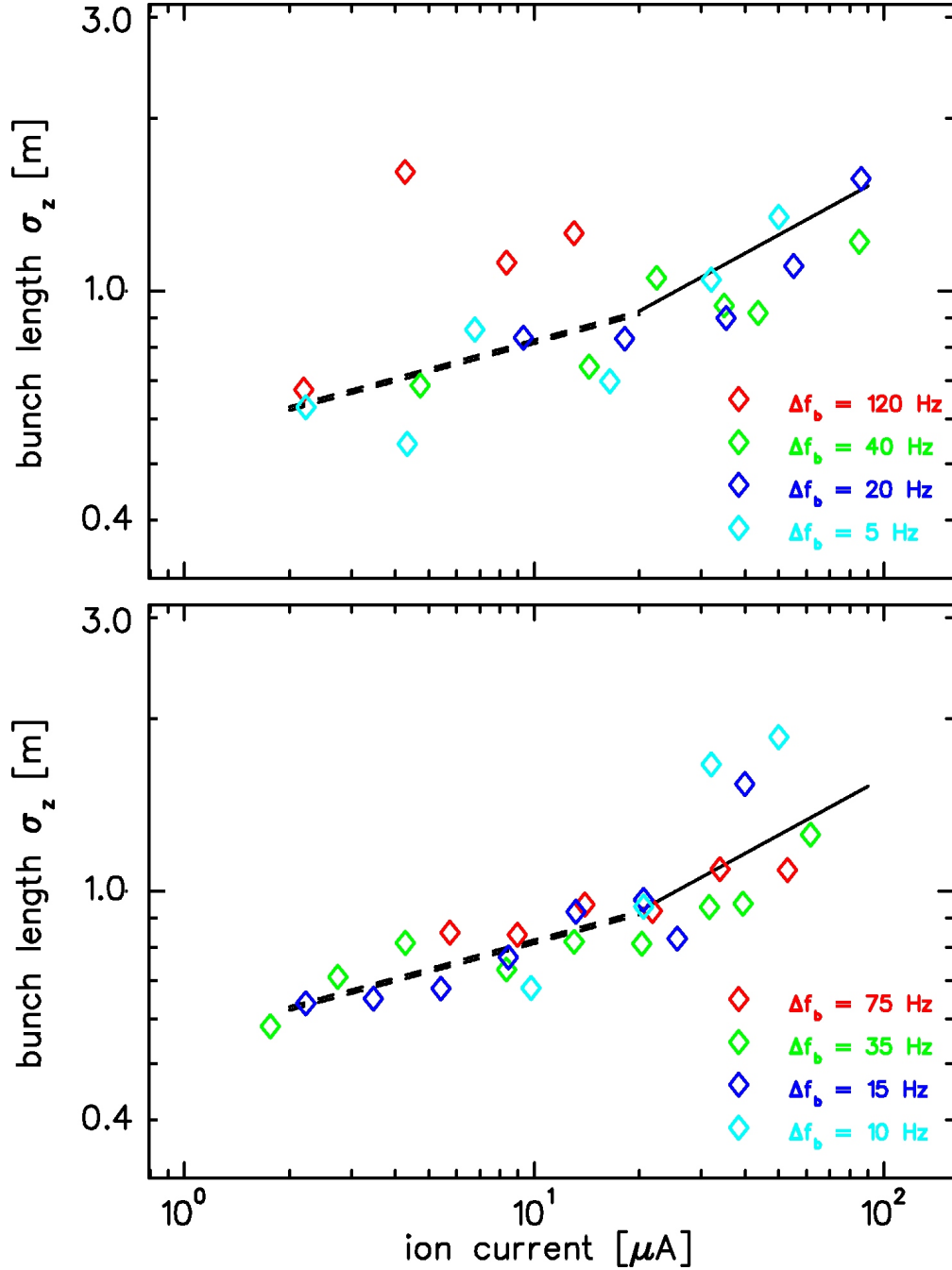


Figure 2.7: **Upper Part:** Four sets of bunch length measurements at various detuning values Δf_b of the bunching frequency relative to the laser frequency. These measurements were performed using a single, fixed-frequency laser system. **Lower Part:** In addition to the fixed-frequency laser system, a second scanning laser is introduced ($2\Delta f_{l,\text{lab}} = 400$ MHz) to increase the acceptance of the laser force as explained in the text. The black lines indicate the scaling of the bunch length with the ion current expected for space-charge (dashed) and, respectively, intra-beam scattering (solid) dominated beams, similar to Fig. 2.3 and are solely meant to guide the eye.

As discussed in part 2.2.2, an argon ion laser system is modified to address a scan range of maximum $2\Delta f_{1,\text{lab}} = 1$ GHz in the UV, giving a momentum acceptance of the laser force of

$$\frac{\Delta p_{\text{accept},l}}{p_{\text{accept},l}} = 2\gamma \frac{2\Delta f_{1,\text{lab}}}{2f_{1,\text{lab}}} = 2\gamma \frac{\lambda_{1,\text{lab}} \Delta f_{1,\text{lab}}}{c} \approx 2 \times 10^{-6}, \quad (2.5)$$

which is about a tenth of the total bucket momentum acceptance and of the same size as the momentum resolution of the Schottky noise measurement. This simple way to calculate the acceptance is only valid for a frequency scan fast enough to counteract intra-beam scattering. Unfortunately, the typical scanning time which allowed for stable scanning was on the order of some hundred milliseconds, and thus much longer than the plasma period τ_p of the ion beam. Even with a smaller detuning range of about $2\Delta f_{1,\text{lab}} = 400$ MHz in the UV, heating of the beam due to intra-beam scattering can be reduced. For this detuning range, Fig. 2.7 shows a comparison of two bunch length measurements. The color-coded data point sets refer to measurements of the bunch length at various detuning values Δf_b of the bucket frequency relative to the fixed frequency of the first laser. In the upper part of Fig. 2.7 one finds measurements for which only one laser at a fixed frequency was used for cooling. In the lower part, those measurements including a second, scanning laser system are shown. The dashed and solid lines, which indicate the scaling of the bunch length with the ion current for space-charge dominated (dashed) and intra-beam scattering dominated beams (solid), respectively, are meant to guide the eye. The position of the transition between the two regimes was set to the approximate ion current value at which the transition was observed in Fig. 2.3.

While for the first set of data points the bunch length measurements scatter over a large range and by a factor of almost ten, in the second set using an additional scanning laser reduces the deviations of the data points from the expected scaling. Such bunch length fluctuations can be induced by intra-beam scattering, which heats up a part of the beam. Hot ions can escape the acceptance of the fixed-frequency laser and are no longer cooled by its laser force. When this happens, the equilibrium of laser cooling and heating due to intra-beam scattering is no longer maintained and the beam consists of a hot and a cold part. The beam becomes unstable, resulting in fluctuations of the bunch length.

The laser force of the scanning laser counteracts these fluctuations and the bunch length at low ion currents smoothly follows the scaling for space-charge dominated beams. This becomes most evident at large detuning Δf_b , for which the single laser system is not sufficient to reach the space-charge dominated regime at all and the bunch length is drastically increased, as indicated by the red symbols in the upper part of Fig. 2.7.

It has to be pointed out that the second laser does not increase the overall strength of the laser force, but only its acceptance range, since the detuning between the two laser frequencies is usually so large that different velocity classes of ions are cooled by the two laser forces, and the cooling transition is already saturated when only one laser is used. Thus, the transition from the intra-beam

scattering to the space-charge dominated regime is assumed to occur at almost the same ion current, regardless of the number of laser systems.

At high currents, an increase in the bunch length is observed when using the combination of a fixed-frequency laser and a scanning laser at small detuning Δf_b . This increase can be attributed to the influence of the scanning laser, which at small detuning accidentally leads to a heating of the ions due to the increase in the photon scattering rate. Such an additional heating effect becomes important if the laser frequency is close to the cooling transition frequency [MB0301] in the ion rest frame. While the frequency of the first laser is fixed by the detuning Δf_b , the frequency of the scanning laser can fall below this value, increasing the photon scattering rate. At large ion currents – meaning large ion densities – this small additional heating can lead to a sudden increase of the intra-beam scattering rate and thus of the bunch length, which can no longer be compensated by the combined laser forces.

3. STOPPING AND COOLING BEAMS OF HIGHLY CHARGED IONS

3.1 In-trap Preparation of Highly Charged Ions for Precision Physics

Delivering cold highly-charged ions for precision in-trap measurements is currently investigated by several groups in the world ([92, 95, 97, 98],[MB0703]). It is a vital prerequisite to increase the precision of current mass measurements. Typically, charge breeding in an *EBIS* or direct laser ionization deliver ions in a high charge state. While charge breeding in an *EBIS* is currently the choice for very high charge states, laser ionization allows for the production of pure beams of ions of only a single charge state. The typical energy spread of an ion beam after charge breeding of some hundred eV [131] does not match the energy acceptance of a few eV to meV of the precision Penning trap system in which the ion mass is measured. Thus, additional cooling is required, especially for precision experiments investigating fundamental physical effects.

To test the feasibility of the cooling scheme proposed in this thesis, extensive computer simulations of the complete interaction dynamics of $N = 10^5$ ions in a three-dimensional harmonic potential have been performed. For this, a massive-parallel code has been developed, which can compute the complete stopping dynamics of the ion assuming realistic experimental conditions.

The results of such a realistic simulation can be directly applied to plan the experimental setup necessary for stopping and sympathetic cooling of highly charged ions, which is foreseen for the *MLLTRAP* system [MB0703, MB0706]. The subject is introduced by summarizing the numerical methods which have entered in the simulation, succeeded by a summary of the simulation results.

3.2 Numerical Methods

In the following two sections the numerical methods used in the simulation code are summarized. A more elaborate summary of these methods can be found in [MB0604].

First, the choice of simulation parameters is discussed, with emphasis on the choice for the initial kinetic energy of the ion of interest. Next, the equation of motion is introduced, followed by a section on the numerical aspects relevant for the integration of the equation of motions.

| <i>Confining Potential Properties</i> | | |
|---|----------------------|-----------------------|
| integration time $\Delta\tau_{\text{step}}$ [s] | 10 ⁻⁹ | |
| | lower plasma density | higher plasma density |
| Φ_{\perp} [V/m ²] | 2.5×10^5 | 3.5×10^5 |
| Φ_{\parallel} [V/m ²] | 2.5×10^3 | 3.5×10^3 |
| <i>One-component Plasma Properties</i> | | |
| Number N of Mg ⁺ ions | 10 ⁵ | |
| $A_{\text{Mg}}, Q_{\text{Mg}}$ | 24, 1 | |
| T_{Mg} [K] | 10 ⁻³ | |
| <i>Highly Charged Ion Properties</i> | | |
| Number of highly charged ions | 1 | |
| A_{HCI} | 100 | |
| Q_{HCI} | 10, 20, 30, 40 | |
| $E_{\text{kin,HCI}}$ [meV] | 100, 200, 300, 400 | |

Table 3.1: Complete list of simulation input parameters.

3.2.1 Simulation Parameters

The stopping dynamics for a single, highly charged ion are computed for several initial kinetic energies and charge states of the ion of interest, using a newly-developed, massive-parallel, object-oriented molecular dynamics simulation code. The initial temperature of the laser-cooled one-component plasma of $N = 10^5$ $^{24}\text{Mg}^+$ ions¹ is set to 1 mK. At this temperature, the $^{24}\text{Mg}^+$ ions are strongly coupled, exhibiting a long-range order [24, 33, 35]. In the three-dimensional harmonic potential in which the ions are confined their shape resembles that of a prolate ellipsoid [28, 42].

This ellipsoid displays a characteristic structure of concentric shells [33] as can be seen in Fig. 3.2 on page 37. At the beginning of each simulation, the highly charged ion is placed on the trap axis near the brim of the ellipsoid with its direction of flight along the ellipsoid’s axis. Two scenarios differing in plasma density, $n_{\text{Mg}} = 3.02 \times 10^{13} \text{ m}^{-3}$ and $n_{\text{Mg}} = 4.23 \times 10^{13} \text{ m}^{-3}$, respectively, are computed. All simulation input parameters are listed in Tab. 3.1.

The choice for the low initial kinetic energy of the highly charged ions is motivated by the fact that the energy loss $dE_{\text{kin,HCI}}$ per path length ds increases if the relative velocity between the highly charged ion and the constituent ions of

¹The reader should be aware of the fact that, up to now, typical molecular dynamics codes, which compute the complete particle-particle interaction without using any approximation in the computation of the interaction, cannot deal with more than 10^3 to 10^4 particles. Previously, such high particle numbers could only be achieved by approximating the Coulomb interaction, e.g. by Ewald summation [132–136], Particle-Mesh methods [133, 134, 137] or tree-based Multipole methods [133, 134, 138].

the one-component plasma decreases [19]. At higher ion energies – the typical ion energy spread after charge breeding is about 100 eV [131] – the stopping power decreases as $1/E_{\text{kin,HCI}}$. For the *MLLTRAP* setup [MB0703, MB0706] it is foreseen to match the energy spread by building a linear segmented radio-frequency quadrupole trap, in which the highly charged ions are stored in one part of the trap and then leak into the cooling section where the laser-cooled ions are stored (for details see [MB0602]).

In contrast to the final experimental setup, where laser-cooling will be applied continuously, the laser-cooling force is deliberately set to zero in the simulation. Without the influence of the laser force, the stopping dynamics can be directly studied. Such a study has the advantage that the heating dynamics caused by the energy loss of the highly charged ion can be separated from the cooling dynamics observed for an arbitrarily chosen laser force strength. With the knowledge gained by restricting the simulation to the stopping dynamics, the best cooling parameters for efficient and fast recooling of the one-component plasma can be chosen afterwards [MB0701].

3.2.2 Equation of Motion

Central to the simulation is an efficient integration of the equation of motion

$$\begin{aligned} m_i \frac{d^2 \vec{r}_i}{dt^2} &= \vec{F}_{\text{ion-ion}} + \vec{F}_{\text{trap}} + \vec{F}_{\text{cool}} \\ &= \left(\sum_{j \neq i}^{N+1} \frac{q_i q_j}{4\pi\epsilon_0 |\vec{r}_i - \vec{r}_j|^3} (\vec{r}_i - \vec{r}_j) \right) - q_i \vec{\Phi}_{\text{trap}}(t) \vec{r}_i + \vec{F}_{\text{cool}} \left(\frac{d\vec{r}_i}{dt}, t \right). \end{aligned} \quad (3.1)$$

As already pointed out, the laser force, \vec{F}_{cool} , has been deliberately set to zero. The typically time-dependent trapping potential is approximated by its pseudo-potential description, thus neglecting possible heating due to the fast-changing radio-frequency Paul trap field [18]. Essentially, a simple three-dimensional harmonic potential is chosen, where the axial confinement strength Φ_{\parallel} is two orders of magnitude weaker than the radial confinement strength Φ_{\perp} . Instead of restricting the potential to include certain mass-dependencies of the confining potential which depend on the trap geometry [18, 36, 38], the trapping force is simply chosen as

$$\vec{F}_{\text{trap}} = -q_i \vec{\Phi}_{\text{trap}}(t) \vec{r}_i = -q_i (\Phi_{\perp}, \Phi_{\perp}, \Phi_{\parallel}) \begin{pmatrix} x_i \\ y_i \\ z_i \end{pmatrix}. \quad (3.2)$$

Here, $\vec{r}_i = (x_i, y_i, z_i)$ marks the position of particle i , while q_i denotes its charge. For a given radio-frequency Paul trap setup, the strength of the trapping potential is proportional to the charge over mass ratio of the trapped ion. Trapping of two ion species in a single trap is only possible if the stability criterion

$$0 \leq q_{\text{RFQ}} \ll 1, \quad q_{\text{RFQ}} \propto \frac{Q e}{m} \quad (3.3)$$

is fulfilled for both ions species, where the dimensionless stability-parameter q_{RFQ} [18] is essentially given by the ratio of the full potential energy to the full kinetic energy of the particle motion in the Paul trap potential. The highly charged ions are thus more strongly confined than the singly charged $^{24}\text{Mg}^+$ ions. This difference in confinement strength, however, only plays a role if the final equilibrium positions of all ions are considered, but can be neglected if only the stopping process is investigated.

3.2.3 Simulation Methods

Two issues are important for the numerical integration of the equation of motion. First, the integration algorithm should conserve energy over the complete simulation period, without the need to couple the ion ensemble to an artificial temperature bath². Second, a large number of force calculations in one integration step should be avoided by the algorithm. This stems from the fact, that the computational effort for calculating the inter-ion force, $\vec{F}_{\text{ion-ion}}$, scales quadratically with the number N of ions.

Several integration algorithms have been tested on both criteria. These include the common Runge-Kutta algorithms (implicit and explicit), Predictor-Corrector algorithms and Verlet algorithms [139, 140, 142–145]. Usually, each of these algorithms chooses a compromise between integration precision and number of force computations. For a given integration time step $\Delta\tau_{\text{step}}$, increasing the precision helps to better fulfill energy conservation, while an increase in force calculations lengthens the computation time of one integration step.

After testing the different algorithms, the simple, yet effective Velocity-Verlet algorithm [142] was chosen. This simple algorithm is time-reversal, which results in good energy conservation³. It only needs two calculations of the force in one time step, yet the precision of the algorithm scales to the fourth power of the integration step size compared to the simple Euler one-step algorithm, for which the precision scales only linearly in step size.

The choice of the proper time step determines the overall precision of the simulation⁴. The time step must be decreased for increasing interaction strength and thus for increasing charge state of the ions. Furthermore, it must be decreased if the kinetic energy of the ion or the volume density of the plasma are increased. Even for the most unfavorable combination of these parameters ($E_{\text{kin,HCI}} = 400 \text{ meV}$, $Q_{\text{HCI}} = 40$, $n_{\text{Mg}} = 4.23 \times 10^{13} \text{ m}^{-3}$), the smallest time step required for energy conservation [137] is 4 ns [MB0604] and thus bigger than the chosen time step by a factor of four.

Parallelizing the integration algorithm is vital for achieving meaningful results in

²This commonly used technique resets the total energy of the ensemble to its initial value after a certain number of integration steps to 'simulate' energy conservation [139–141].

³Remember that energy conservation stems from the temporal symmetry of the equation of motion [146]. Many higher-order algorithms, especially the often favored Predictor-Corrector schemes, are not symmetric under time reversal.

⁴An elaborate discussion on choosing the right integration time step can be found in reference [137] (see also [MB0604])

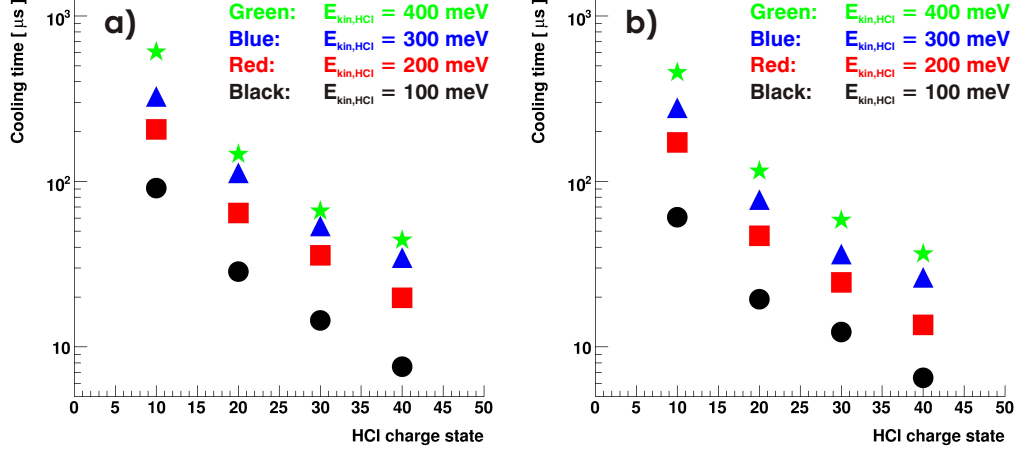


Figure 3.1: **a)** Stopping times versus ion charge state derived from the energy loss due to collective plasma response for various initial kinetic energies of the highly charged ion. Plasma density $n_{\text{Mg}} = 3.02 \times 10^{13} \text{ m}^{-3}$
b) Like a), $n_{\text{Mg}} = 4.23 \times 10^{13} \text{ m}^{-3}$

a reasonable amount of time. Again, several parallel patterns were implemented [147, 148]. For each computer system, a parallel pattern must be chosen which balances the communication of the computation nodes and the time for node-based computations. For the Leibniz Rechenzentrum cluster, the best choice is the simple checker-board algorithm [148], which was used for all the simulation runs presented in this thesis.

3.3 Results

3.3.1 Stopping Power and Stopping Times

Before presenting the simulation results on stopping times, the extraction of the stopping power from the simulation must be discussed. In a molecular dynamics simulation, the statistics on rare events during the stopping is sparse, especially if a variety of parameter-combinations has to be considered. The small number of rare close binary encounters observed during one simulation run (typically a few ten events) dominates the statistical uncertainty estimated for the stopping power. Nevertheless, by dividing the stopping power into two parts as

$$\frac{dE_{\text{kin,HCI}}}{ds} = \left. \frac{dE_{\text{kin,HCI}}}{ds} \right|_{\text{binary collisions}} + \left. \frac{dE_{\text{kin,HCI}}}{ds} \right|_{\text{collective response}}, \quad (3.4)$$

one can deduce a lower bound to the stopping power by neglecting the energy loss due to hard binary collisions of the highly charged ion with a single $^{24}\text{Mg}^+$ ion, taking only the energy loss due to collective response of the laser-cooled one-component plasma into account⁵.

⁵The extraction of stopping times from the simulation is covered in [MB0602].

The stopping times presented in Fig. 3.1 thus present an upper bound to the stopping time expected in the real experiment⁶. Nonetheless, from the few data on close binary collisions available, one can estimate that the energy loss due to these collisions is of the same order of magnitude as the energy loss due to the collective response of the laser-cooled ions [MB0602].

This estimate agrees with the prediction derived from linear stopping theory [19], which is valid at large velocities of the highly charged ion relative to the $^{24}\text{Mg}^+$ ions⁷, an assumption well founded during almost the complete stopping process.

As pointed out in part 3.2.1, the initial kinetic energies chosen for the highly charged ion in the simulation are smaller than those expected in the experiment and thus the stopping power must be either scaled to higher energies⁸, or the initial kinetic energy must be better matched for efficient cooling using a suitable trap system as explained in [MB0602]. Such a match should finally allow to reduce the stopping times for efficient cooling of unstable ions.

3.3.2 Plasma Response and Plasma Stability

Linear stopping theory can predict the order of magnitude of the stopping times expected for the presented cooling scheme. Furthermore, it can provide information on the final temperature of the plasma after equilibration.

However, it cannot describe the complete dynamics of the stopping process. Such a description must include issues such as loss of laser-cooled ions due to hard binary collisions, heating of the plasma during the stopping process and efficient recooling conditions. To cover the complete dynamics of the stopping theory, recently several attempts have been made to derive a realistic dielectric response function of the strongly-coupled one-component plasma [19, 27, 43–45, 150–153]. However, such an ansatz neglects simple effects such as close binary encounters, because it concentrates on the collective plasma response instead.

Here, realistic simulations can be of great importance, since they naturally include all possible dynamic effects, which altogether originate from the simple Coulomb interaction of all particles involved.

Fig. 3.2 shows four views of the same stopping process. In part a), the spatial image depicts the laser cooled plasma by displaying a slice through the center of the ellipsoid⁹. The path of the highly charged ion (black circle) is marked by

⁶The scaling of the stopping power with the charge state is weaker than expected from linear stopping theory. Similar effects have been observed for electron-cooled ion beams in storage rings [149] and are attributed to an enhanced screening of the ion charge [19, 149] in strongly coupled one-component plasmas.

⁷To be more precise, it is valid if the classical collision parameter is small compared to the adiabatic screening length [19].

⁸The standard $1/E_{\text{kin,HCI}}$ scaling can be applied since at high initial energies the stopping power is well described by linear stopping theory. See also [MB0602] for a comparison of the stopping power derived from simulation with the stopping power derived from linear response theory.

⁹The coordinate system defines X and Y as the radial coordinates and Z as the axial coordinate.

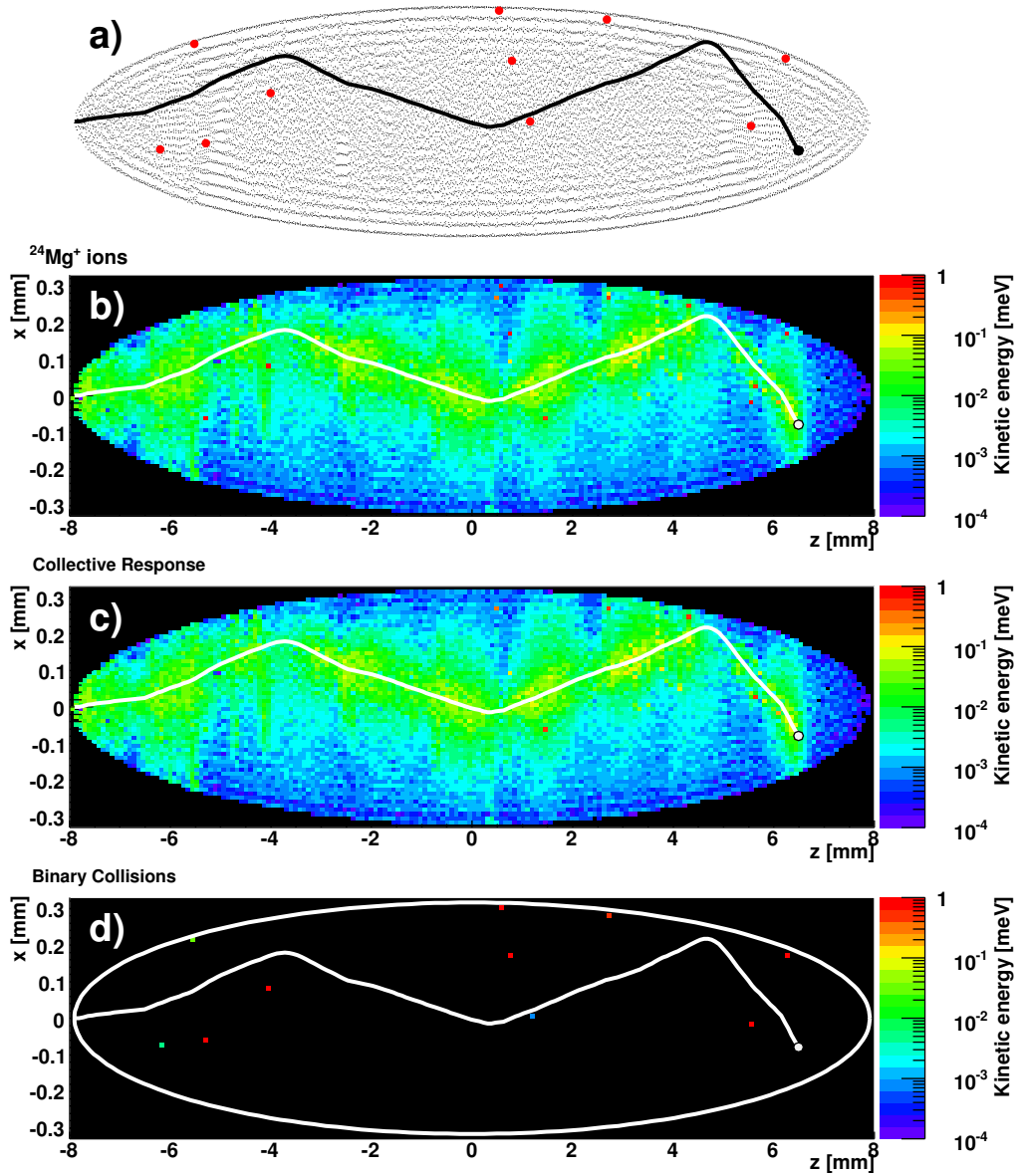


Figure 3.2: **a)** Real space image of the Coulomb crystal and the trajectory (black line) of the highly charged ion (black circle, $E_{\text{kin,HCI}} = 400$ meV, $Q_{\text{HCI}} = 20$) after $18 \mu\text{s}$ flight time. Only a vertical slice through the Coulomb crystal is displayed to reveal the shell structure. The red circles mark those $^{24}\text{Mg}^+$ ions knocked out of the lattice, thereby acquiring a kinetic energy of more than 1 meV. **b)** Histogram plot of the kinetic energy of all $^{24}\text{Mg}^+$ ions ($n_{\text{Mg}} = 3.02 \times 10^{13} \text{ m}^{-3}$). The kinetic energy is color-coded and displayed logarithmically. The values are integrated in the Y-direction. **c)** Like b), taking only those ions into account which did not take part in close binary collisions and thus never acquired a kinetic energy greater 1 meV. This histogram shows the collective plasma response to the ion stopping. **d)** Like b), taking only those ions into account which did take part in close binary collisions and thus have reached a kinetic energy of 1 meV or greater during the stopping (marked by red circles in a)).

the black line. The same path can be found in parts b) to d). Part b) shows a logarithmic, color-coded distribution of the kinetic energy of all $^{24}\text{Mg}^+$ ions, integrated in the Y-direction, while part c) shows only those ions that never acquire a kinetic energy greater 1 meV during the stopping process. Opposite to c), part d) shows only those ions which at least once acquire a kinetic energy greater 1 meV during the stopping process. The former ions are those which take part in the collective response of the plasma, while the latter originate from the very few hard binary collisions with the highly charged ion¹⁰. Those ions which are kicked out of the crystalline lattice are either lost from the cooling region or are subsequently recooled by sympathetic cooling in the Coulomb crystal. One can find three such cases in Fig. 3.2 d), indicated by those three histogram bins which are colored green and light blue, respectively. These bins mark ions which have been subject to a close binary collision but have lost energy due to sympathetic cooling afterwards.

Looking at Fig. 3.2 c), it becomes obvious that much of the kinetic energy lost by the highly charged ion is distributed over the whole plasma bulk.

As discussed in this and the previous part, the response of the plasma to the impact of the highly charged ion is collective in the way, that about half of the energy lost during the stopping is transferred to nearly all laser-cooled ions and that ion loss due to few close binary encounters is negligible ([MB0602] and [MB0604].).

This result is of great importance for the experimental realization of the cooling scheme. It implies that the one-component plasma stays stable during the stopping process and that no reloading of $^{24}\text{Mg}^+$ is necessary after stopping, thus providing a reusable stopping medium.

3.3.3 Energy Loss and Charge Exchange

Experimental data on charge exchange processes at small relative velocities is sparse. This is mainly caused by the need to confine and cool the ions of interest together in a trap. Therefore, the charge exchange rate expected for the presented stopping scheme can only be estimated from theoretical models.

The simulation itself does not yet include charge exchange processes. Moreover, all interaction processes other than Coulomb collisions, for example excitation and collisional ionization [154, 155], are not taken into account. While most of these processes add to the overall energy loss, two- and three-body charge exchange can significantly decrease the efficiency of the stopping scheme.

The theoretical estimates on the charge exchange rate have to be compared to experimental data published by other groups on either charge exchange of highly charged ions with neutral gas atoms at eV center-of-mass collision energies [155–160], or charge exchange between multiply charged ions at keV center-of-mass collision energies [161–163]. This experimental data and a simple estimate of the two-body charge exchange rate [164] already show that the expected rates

¹⁰The choice for the correct energy cutoff value is discussed in [MB0602].

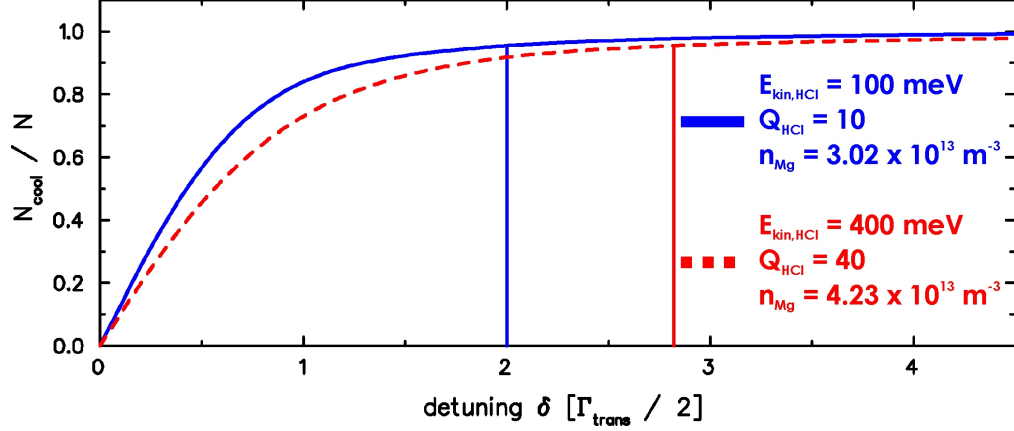


Figure 3.3: Number N_{cool} of ions in the acceptance range of the laser force over the total ion number N versus the detuning δ in units of the natural line width Γ_{trans} of the cooling transition. The two lines indicate the detuning value at which 95.4 % of the ions are in the acceptance range.

for these processes are orders of magnitude lower than the typical cooling rate [MB0602, MB0701]. Thus, a reduction in efficiency due to charge exchange processes is not expected in the experiment.

3.3.4 Recooling Conditions

Besides the plasma stability, the recooling conditions are of great importance for the realization of the cooling scheme. The momentum acceptance of the laser force

$$\vec{F}_1(\vec{v}_{\text{Mg}}) = \frac{S (\Gamma_{\text{trans}}/2)^3}{(\delta - \vec{v}_{\text{Mg}} \cdot \vec{k}_1)^2 + (\Gamma_{\text{trans}}/2)^2(1 + S)} \hbar \vec{k}_1 \quad (3.5)$$

is, for a given saturation parameter S , limited by the natural line width Γ_{trans} of the cooling transition, which for $^{24}\text{Mg}^+$ ions amounts to $2\pi \times 42.7$ MHz [18]. Mainly those ions with velocities

$$|\vec{v}_{\text{Mg}}| < \frac{\delta}{|\vec{k}_1|} \quad (3.6)$$

are addressed by the laser force. Here, δ denotes the detuning of the laser relative to the transition frequency, while $|\vec{k}_1| = 2\pi/\lambda_1$ denotes the wave vector. In the case of $^{24}\text{Mg}^+$, the transition wavelength λ_1 is approximately 280 nm.

To saturate the cooling transition of a single ion ($S \equiv 1$), the laser intensity must reach [6]

$$I_S = \frac{\pi \hbar c}{3} \times \frac{\Gamma_{\text{trans}}}{\lambda_1^3} \approx 2.54 \frac{\text{kW}}{\text{m}^2}, \quad (3.7)$$

which for a 100 μm focal diameter requires a laser power of 25 μW . At saturation, the maximum laser force is then [6]

$$F_{1,\text{max}} = \frac{h}{4} \times \frac{\Gamma_{\text{trans}}}{\lambda_1} \approx 1 \frac{\text{meV}}{\text{mm}} \quad (3.8)$$

If the laser frequency has to be scanned (see part 2.3) to cool the $^{24}\text{Mg}^+$ ions after stopping in order to address all ions, the time for recooling all ions to mK temperature would exceed the typical lifetime of unstable nuclei.

Fortunately, as Fig. 3.3 [MB0701] shows, nearly all ions can be continuously cooled by the laser force without the need for altering the laser frequency. The detuning necessary to recool the ions is found to be small enough to reach the crystalline state of the plasma, considering typical heating rates expected for the trap setup [165, 166]. Following from this, one can estimate the recooling times for the $^{24}\text{Mg}^+$ to be of the same order than the stopping times¹¹ listed in part 3.3.1.

¹¹An accurate estimate of the recooling time must take into account the total heating rate due to the confining fields and residual gas in the final trap system [165, 166]. Their values strongly depend on the details of the experimental realization. Thus a robust value cannot be stated here.

4. COLLECTIVE EFFECTS IN STRONGLY COUPLED OCPs

4.1 Collective Response, Correlations and Strong Coupling

This part of the thesis complements the results on ion beam cooling discussed in the two previous chapters. Here, yet unpublished results are presented which relate to collective effects of strongly coupled ions. As pointed out in the introduction, the ion dynamics in a Paul trap and a storage ring can be described in a similar way. The dynamics of a bunch of ions revolving in a storage ring, observed in the rest frame of the ions, resembles the ion dynamics in the three-dimensional harmonic confining potential of a Paul trap.

Thus, in the following, two aspects of collective ion motion are discussed, one related to laser cooling of relativistic bunched ion beams, the other related to stopping and sympathetic cooling of highly charged ions in a harmonically confined laser-cooled one-component plasma. First, Schottky spectra of bunched ion beams are revisited and second, the collective plasma response to the passage of the highly charged ion is analyzed in detail.

4.2 Schottky Noise Spectra at Small Momentum Spread

In part 2.3.5 of this thesis the influence of space-charge on the synchrotron oscillations of the ions in the bucket is addressed by analyzing various Schottky noise spectra. In this part, these Schottky spectra are discussed with regard to correlated ion dynamics at small momentum spread.

4.2.1 Schottky Noise Spectra for Bunched Beams with Negligible Ion-Ion Interaction

In a bunched, emittance-dominated beam, ions perform longitudinal oscillations at the synchrotron frequency

$$f_{\text{syn}} = \sqrt{\frac{Qe h \eta U_b}{2\pi\gamma m C^2}} \approx 114 \text{ Hz}, \quad (4.1)$$

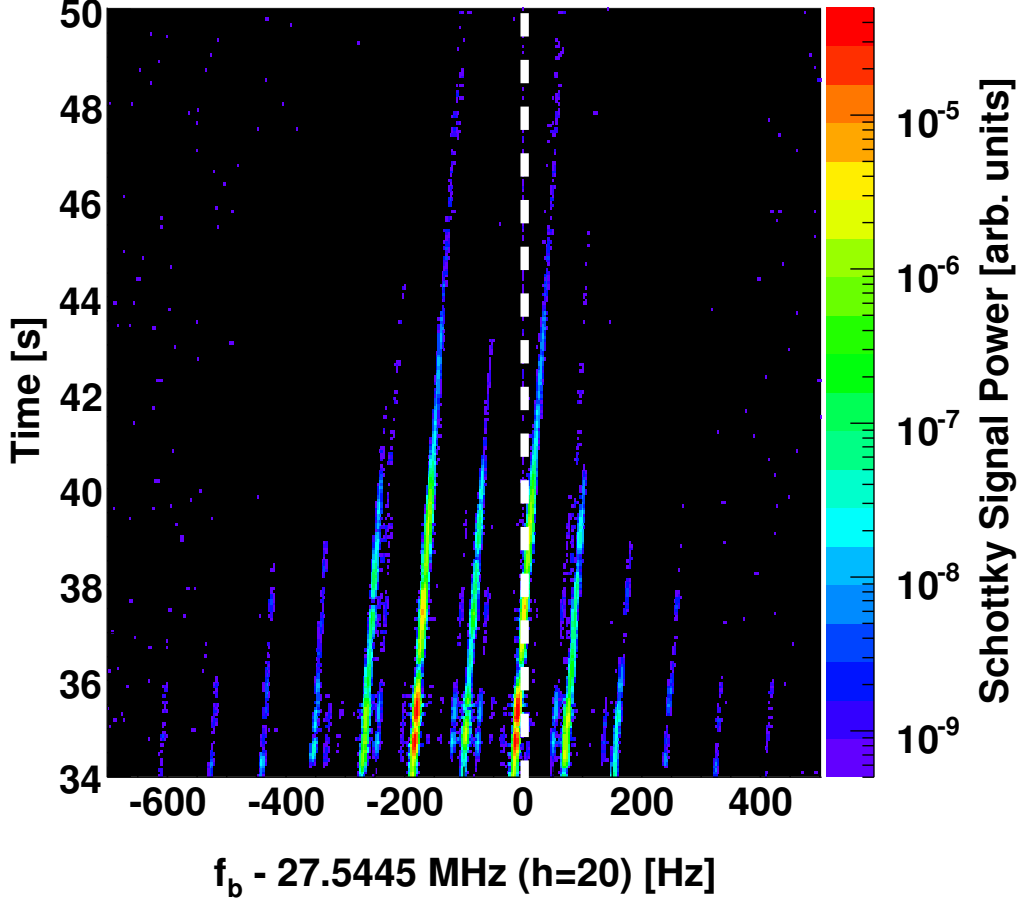


Figure 4.1: Color-coded Schottky noise spectrum measured for a C^{3+} ion beam at a beam energy of 1.47 GeV. The beam is bunched at the 20th harmonic of the revolution frequency. The ion current is $16 \mu\text{A}$. The bunch length varies between 1.01 m and 0.78 m, depending on the detuning. The bunch width is 5.26 mm. The intensity of the Schottky power signal is plotted logarithmically. The position of the laser frequency is indicated by the dashed white line. The bunching frequency f_b is scanned relatively to the fixed laser frequency, the Y-axis indicating the scanning time. The detuning is reduced during the scan, until the Schottky signal vanishes.

where $C \approx 108.36$ m is the storage ring circumference, $\eta \approx 0.607$ the slip factor [18], $U_b \approx 7.4$ V the bunching voltage, $h = 20$, $\gamma \approx 1.13$, $Q = +3$ and $m = 12$ u for $^{12}C^{3+}$. The charge of each individual ion j in a beam of N ions induces a periodic signal $S_j(t)$ on the pickup electrode. The total signal $S(t)$ at a given time t can be written in its spectral representation [120] as

$$S(t) = \sum_{j=1}^N S_j(t) = \sum_{j=1}^N \sum_{h=-\infty}^{+\infty} \sum_{m=-\infty}^{+\infty} A_{j,h,m} e^{-i\Omega_{j,h,m}t} e^{i\Phi_{j,h,m}} \quad (4.2)$$

separated in amplitudes $A_{j,h,m}$, frequencies $\Omega_{j,h,m}$ and phases $\Phi_{j,h,m}$ given by

$$A_{j,h,m} = \frac{q}{2\pi} J_m(h a_j), \quad (4.3)$$

$$\Omega_{j,h,m} = 2\pi (h f_{\text{rev}} + m f_{\text{syn}}), \quad (4.4)$$

$$\Phi_{j,h,m} = -h\phi_j + m\theta_P. \quad (4.5)$$

The phase depends on both the single-particle phase ϕ_j and the common localized azimuth angle θ_P , while the frequency depends on the harmonic h of the revolution frequency and the synchrotron frequency. Finally, the amplitude can be calculated from the single-particle oscillation amplitude a_j , which is weighed by the ordinary Bessel function of integer order m . The final spectrum is a symmetric distribution of incoherent sidebands around the carrier signal. The carrier signal is found at $h f_{\text{rev}}$, while the sidebands are located at each side of the carrier at harmonics m of the synchrotron frequency.

4.2.2 Schottky Noise Power at Small Momentum Spread

As shown in Fig. 4.1, the Schottky noise signal at each point t in time is given by a spectrum of lines with a spacing determined by the synchrotron frequency, distributed symmetrically around the carrier signal found at a harmonic of the revolution frequency, in accordance to Eq. 4.4.

In Fig. 4.1 the bunching frequency is scanned relatively to the laser frequency, as described in part 2.3.5. During the scan the detuning Δf_b between the bunching frequency and the laser frequency is gradually reduced while recording the Schottky noise signal [MB0705]. The momentum spread decreases, the sidebands vanish and the overall Schottky signal power drops rapidly. Finally, near the end of the scan, the Schottky signal vanishes entirely. As for the data set presented in Fig. 2.6, all the ions reside in the bucket center and no ion loss occurs. Nevertheless, the power of the signal induced by the ions on the pickup electrode is reduced by four to five orders of magnitude until it finally reaches the level of the background noise.

A multitude of Schottky spectra recorded during the *ESR* measurement campaigns in 2004 and 2006 exhibit similar characteristics. For some of these, the total Schottky power summed over all spectral lines at a given detuning is depicted in Fig 4.2, together with the longitudinal momentum spread deduced from the Schottky noise spectrum [MB0705].

Similar observations have been made for electron-cooled coasting ion beams at orders of magnitude lower ion currents [67–70], but until now, a Schottky signal reduction to this degree has not been published. This reduction still lacks a conclusive interpretation, although for coasting beams theoretical models attribute the vanishing Schottky signal to one-dimensional beam ordering [18, 68–70, 167–170]. An ordered beam induces a periodic signal on the pickup electrode, in

contrast to the purely random signal induced by a hot, intra-beam scattering dominated beam.

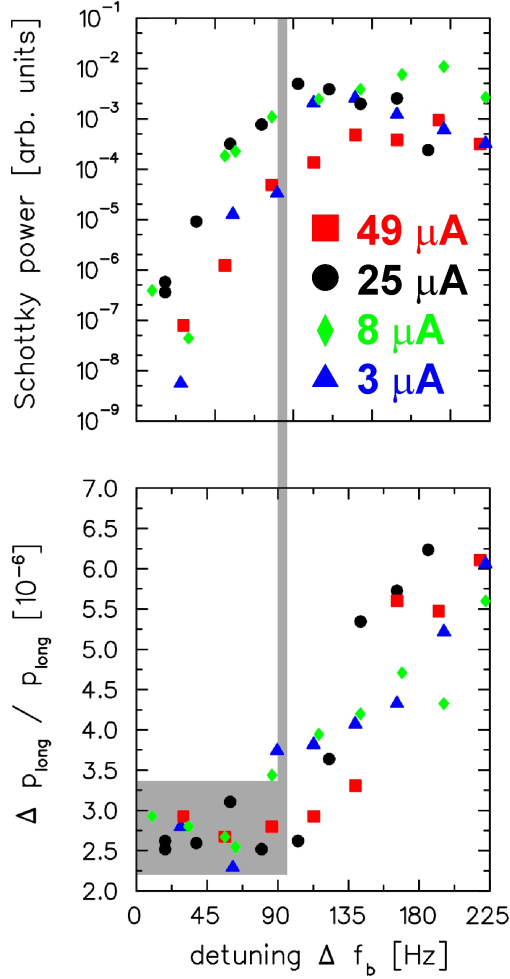


Figure 4.2: **Upper part:** Total Schottky signal power versus detuning of the bunching frequency. The Schottky power is summed over all frequency bands for a given value of the detuning Δf_b . A drop in the signal is seen at a certain detuning value, marked by the gray line, which is independent of the ion current. At this value, the Schottky measurement of the longitudinal momentum reaches its resolution limit. This reflects the transition shown in Fig. 4.1, where most of the incoherent sidebands vanish and only two sidebands and the carrier signal are visible.

Lower Part: Longitudinal momentum spread versus detuning of the bunching frequency. Again, a drastic reduction independent of the ion current is observed. The gray shading indicates the resolution limit of the Schottky momentum measurement.

The periodicity of this signal is determined by the mean ion distance in the ordered beam and would, for a coasting beam, ultimately lead to a dramatic decrease of the Schottky power signal [67].

For a bunched beam, however, both the coherent modulation of the beam charge density due to bunching and due to possible microscopic ordering in the beam must be taken into account [120]. The Schottky spectrum induced by bunches of uncorrelated ions, Eq. 4.2, cannot explain the drop in the Schottky power signal. Thus, future experiments are foreseen to look for correlations between the ions which can lead to coherent ion motion.

As can be clearly seen from Fig. 4.2, possible correlations cannot be resolved in the Schottky noise signal. An upgrade of the experimental setup will hopefully allow to increase the measurement precision by at least a factor of ten and to detect periodic variations in the fluorescence signal of the beam caused by beam

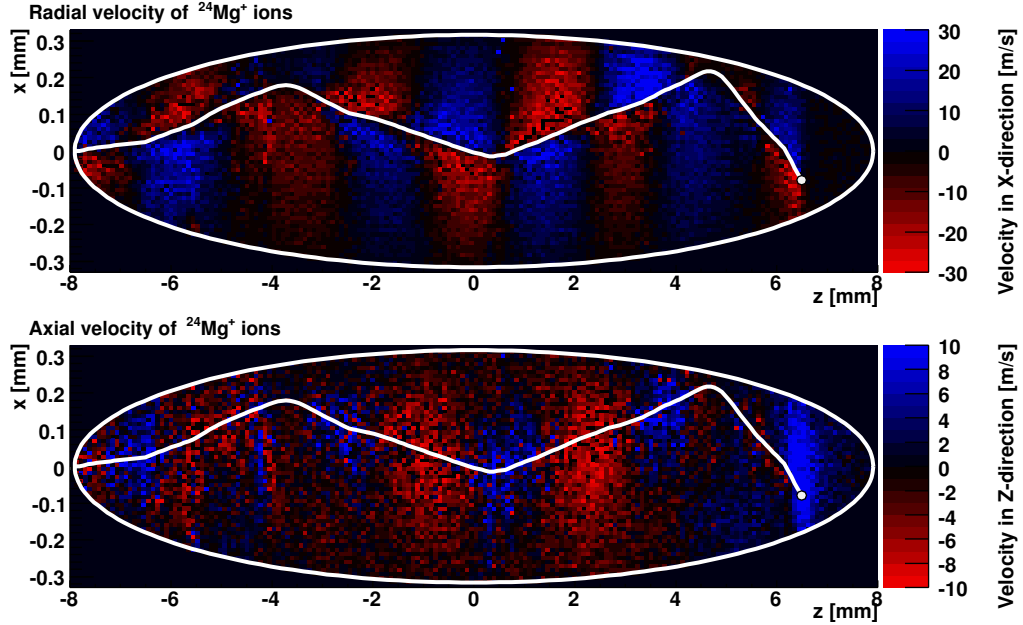


Figure 4.3: **Upper part:** Same data set as in Fig. 3.2. Velocity of the $^{24}\text{Mg}^+$ ions in X-direction. Negative velocity values are shown in red, positive values in blue. A clear transverse oscillation pattern following the ion trajectory is visible. **Lower Part:** Velocity of the $^{24}\text{Mg}^+$ ions in Z-direction, color-coding similar to the upper part. A complex oscillation pattern behind the ion emerges, while the heating of the plasma in front of the ion gradually decreases with distance from the ion.

ordering. Further details will be discussed in the outlook of this thesis.

4.3 Collective Plasma Response during Ion Stopping

In part 3.3.2 of this thesis, the collective response of a strongly coupled one-component plasma to the passage of a single highly charged ion is discussed. One central result of this discussion, the distribution of the energy lost by the ion over the whole plasma bulk, is shown in Fig. 3.2. In this part, the dynamics of the energy transfer from the highly charged ion, in the following also called the *projectile*, to the laser-cooled ions are analyzed. For this analysis, the data set from Fig. 3.2 is presented focusing on the collective plasma dynamics rather than on the stopping itself. Thus, in Fig. 4.3, the (signed) velocity of the ions instead of the kinetic energy is depicted.

While a clear transverse oscillation pattern can be seen in the upper part of Fig. 4.3, the lower part shows a more complex longitudinal oscillation pattern. In the following, the analysis of these oscillation patterns will be preceded by a short discussion on characteristic plasma lengths and the applicability of linear response theory.

4.3.1 Characteristic Lengths and Linear Response Theory

When the highly charged ion passes through the one-component plasma of $^{24}\text{Mg}^+$ ions at a velocity v_{rel} relative to the plasma ions, the Coulomb repulsion between the projectile and the plasma ions can be treated as a local disturbance of the electric field. The influence of the highly charged ion on the plasma can only reach as far as the adiabatic screening length [19]

$$\lambda_{\text{ad}} = \frac{v_{\text{rel}}}{\omega_p} \xrightarrow{v_{\text{rel}} \rightarrow v_{\text{th}}} \lambda_D = \sqrt{\frac{\epsilon_0 k_b T}{Q_{\text{Mg}}^2 e^2 n_{\text{Mg}}}}, \quad (4.6)$$

which for the relative velocity approaching the thermal velocity v_{th} becomes equal to the well-known Debye shielding length. A local polarization of the plasma ions shields the Coulomb field of the projectile ion on a scale defined by λ_{ad} . Thus, those ions at distances larger than the adiabatic screening length do not react directly to the Coulomb force of the highly charged ion. A second important parameter is the minimum impact parameter [19]

$$b_{\text{min}} = \frac{Q_1 Q_2 e^2}{4\pi\epsilon_0 \mu_{\text{red}} v_{\text{rel}}^2} = \frac{Q_{\text{Mg}} Q_{\text{HCl}} e^2}{4\pi\epsilon_0 \mu_{\text{red}} v_{\text{rel}}^2}, \quad (4.7)$$

which defines the impact parameter of two particles of charge states Q_1 and Q_2 and reduced mass μ_{red} at a scattering angle of ninety degrees.

The applicability of linear response theory to the coupled system of the single highly charged ion and the laser cooled ions can be determined by the ratio $b_{\text{min}}/\lambda_{\text{ad}}$. If this ratio exceeds unity, the coupling between the ion of interest and the plasma ions becomes strong and the plasma response non-linear [19]. The dependence of the adiabatic screening length and the minimum impact parameter on the kinetic energy of the projectile are shown in Fig. 4.4 a) for all combinations of the simulation parameters. For comparison, the mean inter-ion spacing given by the Wigner-Seitz radius is also plotted.

At large projectile energies the adiabatic screening length is on the order of a millimeter, about the radial diameter of the plasma ellipsoid. At smaller projectile energies, all characteristic lengths become comparable in size, and linear response theory can no longer describe the ion dynamics. When the minimum impact parameter exceeds the inter-ion spacing, hard binary collisions are no longer observed and the energy loss is determined solely by collective plasma response [MB0602].

4.3.2 Collective Plasma Oscillations

The dominant oscillation frequency related to the oscillation patterns depicted in Fig. 4.3 is the plasma frequency [42, 150, 171], see Fig. 4.4 b)-c). In this figure, the average radial and axial velocity of an ensemble of ions versus simulation time is plotted. The ion ensemble is defined as the set of those ions which are confined in a cube of $50 \mu\text{m}$ side length positioned close to the ion's

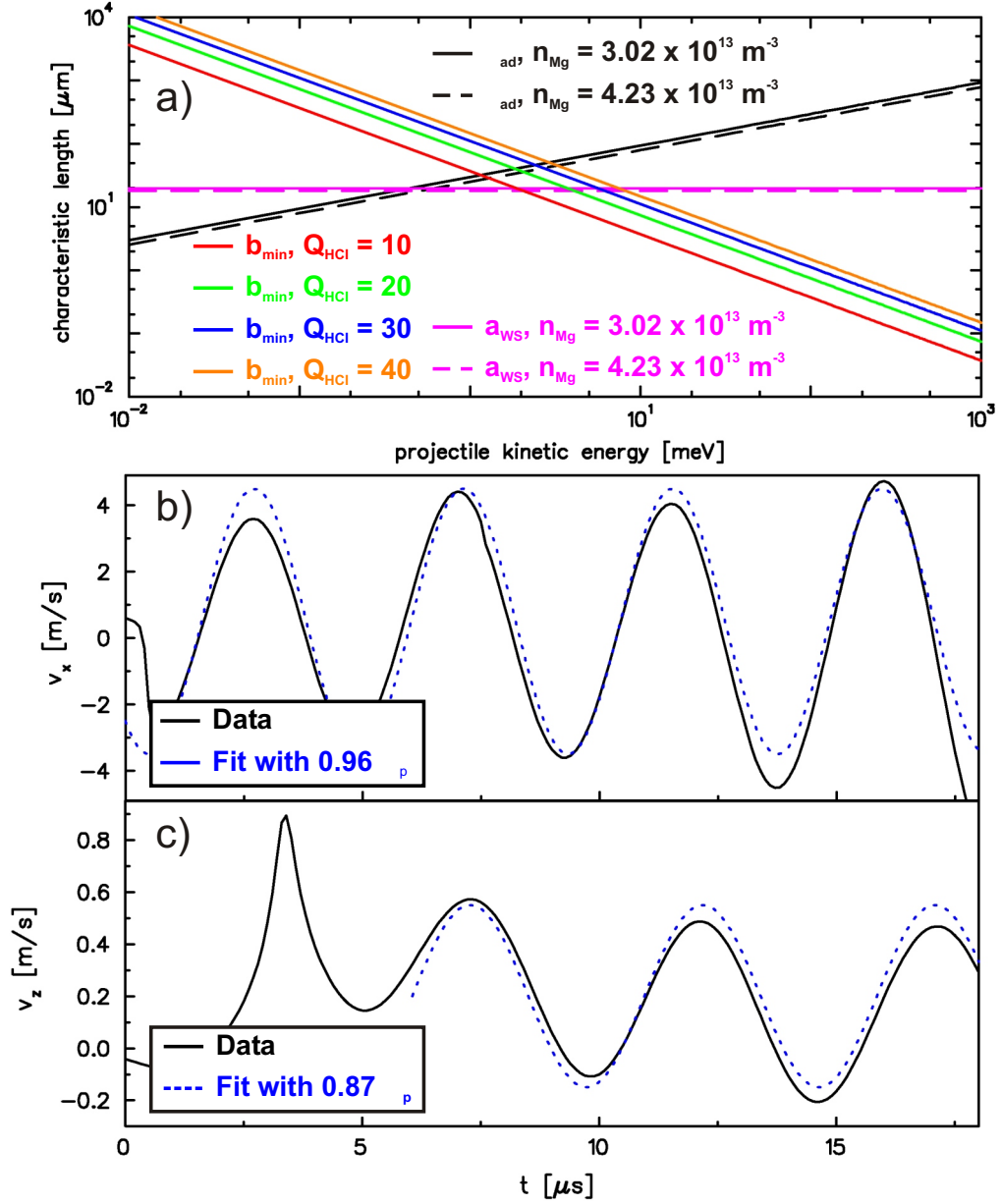


Figure 4.4: a) Characteristic lengths versus kinetic energy of the projectile. Linear response theory is no longer applicable if the characteristic lengths become comparable in size, see text for details.

b) Temporal evolution of the average radial velocity in X-direction of a small ensemble of $^{24}\text{Mg}^+$ plasma ions. The ensemble is located near the entrance point of the projectile into the plasma ellipsoid. The simulation data (black) is compared to a fit curve (blue). The plasma frequency ω_p is derived from the plasma charge density, see Eq. 1.3.

c) As in b), but for the axial velocity component in Z-direction. An initial delta-pulse-like shock induced by the supersonic projectile is followed by an ion oscillation at ω_p .

path of flight. By selecting the center position of the cube, every part of the plasma can be probed. For the two data sets presented in Fig. 4.4 b)-c), the center position was set to $(x, y, z) = (+0.05 \text{ mm}, +0.05 \text{ mm}, -7.5 \text{ mm})$ and $(+0.05 \text{ mm}, +0.05 \text{ mm}, -5 \text{ mm})$, respectively.

The local disturbance of the electric field induced by the highly charged ion causes the ions to oscillate in phase around their equilibrium position in the crystalline lattice [MB0602]. The amplitude of this oscillation is small, about one tenth of the inter-ion spacing, due to the small ion velocity and the short relaxation time τ_p . Thus, the oscillation patterns observed in Fig. 4.3 do not cause large density fluctuations of the plasma and the plasma response to the projectile can be treated as an elastic relaxation of the Coulomb crystal lattice¹. Looking closely at Fig. 4.4 b)-c), a 10 % difference between the oscillation frequency obtained by the data fit and the value obtained from Eq. 1.3 is observed. If the plasma frequency is derived from the external confining forces [18]

$$\omega_p^\dagger = \sqrt{2\Phi_\perp \frac{Q_{Mg}e}{m_{Mg}}}, \quad (4.8)$$

instead of using Eq. 1.3, a comparison with the fit values $\omega_{\text{fit},\perp}$ and $\omega_{\text{fit},\parallel}$ yields

$$\omega_p = 2\pi \times 0.236 \text{ MHz} \quad \omega_p^\dagger = 2\pi \times 0.226 \text{ MHz} \quad (4.9)$$

$$\omega_{\text{fit},\perp} = 0.96 \omega_p \quad \omega_{\text{fit},\parallel}^\dagger = 1.00 \omega_p^\dagger \quad (4.10)$$

$$\omega_{\text{fit},\perp} = 0.87 \omega_p \quad \omega_{\text{fit},\parallel}^\dagger = 0.91 \omega_p^\dagger. \quad (4.11)$$

The observed 10 % difference can thus be attributed to a poor determination of the ion density and other numerical errors.

Transverse Oscillations

During its passage through the Coulomb crystal, the plasma ions are pushed aside by the passing projectile ion. The transverse oscillation follows the path of the highly charged ion, forming a transverse wave. If linear response theory is applicable, the wavelength is given by

$$\lambda_\perp(z) = \frac{v_{\text{rel}}(z)}{\omega_p} = \lambda_{\text{ad}}. \quad (4.12)$$

One half of the wavelength is equal to the axial extent of that set of ions which are accelerated in a common direction during one half period of a plasma oscillation. This axial extent is equal to the maximum path length $v_{\text{rel}} \tau_p/2$ traveled by the projectile ion during this half period, after which the plasma relaxes, and the plasma ions reverse their direction of motion.

¹This assumption of course neglects hard binary collisions, in which plasma ions are kicked out of the Coulomb crystal lattice.

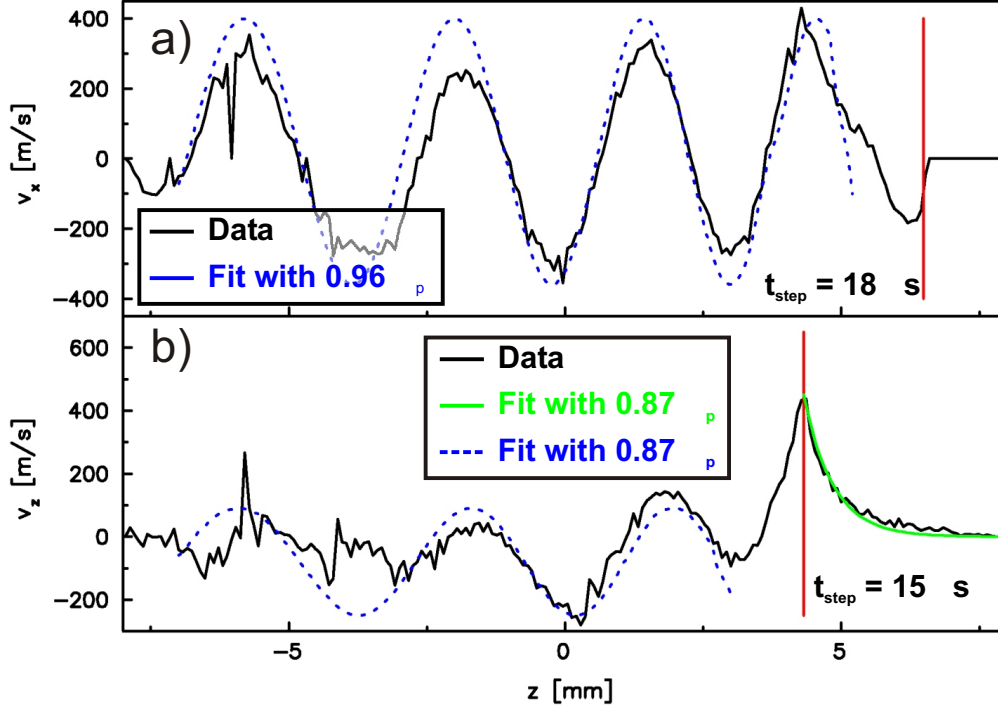


Figure 4.5: **a)** Sum of radial plasma ion velocities in X-direction (see text) versus the axial plasma ion position (black curve) 18 μ s after simulation start. The blue curve follows a sinusoidal fit using the wavelength given by Eq. 4.12. The free fit parameters are amplitude, phase and vertical displacement, while the wavelength is derived from the projectile velocities v_{rel} and the plasma frequency as described in the text. The vertical red line marks the position of the projectile ion.

b) Similar to a), but showing the sum of all axial plasma ion velocities. The green curve follows the exponential trend of adiabatic screening (Eq. 4.14), while the blue curve shows a wavelength fit based on Eq. 4.15.

This can be seen in Fig. 4.5 a), which shows the sum of the radial velocities of all ions located below the path of the projectile ion 18 μ s after it has entered the plasma. This sum velocity can also be obtained from the upper part of Fig. 4.3 by projecting all velocity values for those data points below the projectile trajectory onto the Z-axis. This summation yields a clear wave pattern along the Z-axis. Using Eq. 4.12, a sinusoidal fit curve (blue)

$$V_{\text{fit},\perp}(z) = V_0 \sin\left(\frac{z + z_0}{\lambda_{\perp}(z)}\right) + V_{\text{off}} \quad (4.13)$$

is plotted on top of the data (black). In this fit, the amplitude V_0 , longitudinal, z_0 , and vertical displacement, V_{off} , have been matched to fit the data curve, while the plasma frequency was taken from Fig. 4.4 b).

The adiabatic screening length itself was calculated for each Z-position in Fig. 4.5 a) by recording the local velocity v_{rel} of the projectile ion for each individual Z-position during the 18 μs simulation time. The position of the projectile ion corresponding to the current simulation time of 18 μs is marked by the red vertical line. Both the fitting curve and the data curve are found to be in good agreement.

Longitudinal Oscillations

The longitudinal oscillation essentially stems from the same mechanism, but in this case, the plasma dynamics are more complex. This complex pattern emerges, because the ion travels at a supersonic velocity in the one-component plasma, where the axial velocity of the projectile ion is greater than the longitudinal acoustic speed [171–173], which for all cases studied in this thesis is on the order of a few ten meters per second. Those plasma ions in front of the projectile ion are accelerated in Z-direction, until the highly charged ion overtakes the $^{24}\text{Mg}^+$ ions. As in the case of the transverse waves, after the projectile ion has passed, the plasma relaxes, performing longitudinal oscillations at the plasma frequency. Following standard plasma theory, the axial extent of the ensemble of those ions accelerated collectively by the Coulomb force of the highly charged ion is given by the adiabatic screening length. This can be seen in Fig. 4.5 b), in which the sum of all axial velocities 15 μs after simulation start is plotted. As before, this sum velocity can also be obtained by projecting the axial velocity values found in the lower part of Fig. 4.3 onto the Z-Axis. The green fit curve in the right part of Fig. 4.5 b) follows the exponential trend

$$V_{\text{fit,ad}}(z) = V_{0,\text{ad}} e^{-\frac{z-z_{\text{HCl}}}{\lambda_{\text{ad}}}}, \quad (4.14)$$

where z_{HCl} indicates the position of the highly charged ion, again marked by the red vertical line. In this fit, the only free parameter is the factor $V_{0,\text{ad}}$, which is set to the peak velocity value found at the intersection of the red line and the black data curve. As in the previous part, the adiabatic screening length was calculated using the plasma frequency value from Fig. 4.4 c) and the projectile ion velocity at the simulation time of 15 μs .

Computing the adiabatic screening length for all projectile ion velocities, the wavelength corresponding to each projectile ion position along the Z-axis is simply given by

$$\lambda_{\parallel}(z) = \lambda_{\text{ad}}(z). \quad (4.15)$$

The blue curve in Fig. 4.4 c) shows a sinusoidal fit, using Eq. 4.13 and replacing λ_{\perp} by λ_{\parallel} . Again, amplitude, phase and vertical displacement are chosen to match the black data curve, showing good agreement between the fit curve and the data curve.

In the field of complex (dusty) plasmas, there already exist a number of experimental and theoretical results on related phenomena [171, 173–180], which

exhibit similar behavior. For ionic one-component plasmas however, the literature is sparse, owing to the fact that there are few experimental results on the stopping dynamics, yet. As an interesting consequence of the results presented here, it might be possible to observe the stopping dynamics by measuring the intensity of the fluorescence light emitted by the $^{24}\text{Mg}^+$ ions, which depends on their velocity.

5. CONCLUSION AND OUTLOOK

The results presented in this thesis found the basis for unique experimental possibilities in the field of ultra-cold physics.

For the first time, laser-cooling of truly relativistic ion beams has been experimentally realized. It is shown that the broad momentum spread of the ion beam can be matched to the small momentum acceptance of the laser force. This matching triggered the attainment of space-charge dominated bunched beams using pure laser-cooling at high ion densities in the bucket. With additional moderate electron cooling, shortly applied at the beginning of the measurement, thereby increasing the coupling between the longitudinal and transverse motion of the ions, three-dimensional cold beams have been realized.

First applications of these ultra-cold beams include precision UV-spectroscopy of the cooling transitions. In the experiments performed at the *ESR*, the precision is mainly limited by the precise determination of the ion beam energy.

At future storage rings, namely *NESR*, *SIS100* and *SIS300* at the future *FAIR* facility, a vast range of ion species will become accessible for direct-laser cooling [50]. Using X-ray spectrometers to determine the Doppler-shifted energy of the fluorescence photons emitted by the ions at relativistic beam energies, a precise knowledge of the beam energy is no longer necessary. Instead, measuring the frequency of the laser beam and the fluorescence photons in the laboratory will determine the cooling transition frequency. The resolution of the measurement will then be mainly limited by the precision of the X-ray spectrometer [130].

In the near future, new measurement campaigns at the *ESR* are foreseen. New developments for these upcoming experiments will see an upgrade of the fluorescence detection, which will provide an increase in resolution for measuring the longitudinal momentum spread of the beam by orders of magnitude.

Here, two photomultipliers instead of one will be used to provide more control of the overlap of the laser beam with the ion beam. The photomultipliers will be put in vacuum near to the ion beam to minimize losses in fluorescence light by increasing the solid angle visible by the photomultiplier and reducing the photon loss due to absorption in air. This will increase the detection efficiency and will hopefully allow to study the fluorescence signal in detail. Studying the temporal distribution of the fluorescence photons might reveal correlations of the ions expected in the regime of strong coupling.

These advances in detection efficiency will be accompanied by using a pulsed laser system with pulse lengths in the ns domain at high repetition rate in combination with a single-mode, frequency locked continuous-wave laser system. With this combination of two laser systems, one can simultaneously cool both the initial broad momentum distribution of the ions and confine ions at low momentum spread, thereby significantly increasing the momentum acceptance of

the bucket force. With such a system, experiments on *tapered cooling* [181] and on increasing the coupling between the longitudinal and transverse degree of ion motion in the bucket are foreseen.

In the theoretical part of this thesis, a new cooling scheme for cooling highly charged ions sympathetically by laser-cooled ions in a linear radio-frequency quadrupole trap has been analyzed. The analysis shows that the proposed scheme is fast, very efficient and allows for unprecedented control over the highly-charged ions at mK temperatures. Compared to other cooling schemes such as buffer gas cooling, resistive cooling and electron cooling, no loss of ions due to charge exchange processes is expected. Furthermore, direct optical detection and manipulation of single ions allows to gain total control of the ions. This control will allow to separate and position single ions for precision in-trap measurements.

One open question concerns the extraction of the highly charged ions after cooling. During the cooling process, the ions of interest accumulate in the same trap region as the laser-cooled ions. At the point at which they are stopped in the plasma, they are strongly coupled with the laser-cooled ions. This strong coupling must be overcome to extract the ions from the cooling region. There are several possible ways to extract the ions, which rely on a combination of electrostatic forces and the laser force, which is only seen by the laser-cooled ions. Thus, an electrostatic extraction gradient could be counteracted by the laser force, keeping the laser-cooled ions in the trap region while extracting the ions of interest. Unfortunately, such an extraction scheme is not fast enough for rare ions. Nevertheless, several groups¹, which focus on sympathetic cooling of particles in traps, are investigating extraction schemes and the joint effort will hopefully see fast advances in this matter.

The highly charged ions delivered by the cooling RFQ will be extracted to the precision Penning-trap system *MLLTRAP* [MB0703, MB0706] where masses of both stable and unstable nuclei can be measured with unprecedented precision. In addition, direct measurements of the ion properties in the linear RFQ trap are possible.

While the experimental realization of the cooling scheme will be accompanied by measurements at the table-top storage ring *PALLAS* using a new, all-solid-state laser cooling system [182], new ideas of in-trap optical spectroscopy are currently studied.

One interesting experiment, which can be done using the planned trap setup, is the direct optical spectroscopy of the energy splitting of the ^{229}Th nuclear ground state doublet. For the first time, one would be able to directly pump a nuclear transition by purely optical means. Further details on this experiment are found in appendix A. Currently, precursory experiments enhancing the pre-

¹These include the group of Thomas Udem in Munich, the group of Tobias Schätz also in Munich, the group of Stephan Schiller in Düsseldorf, the group of Dieter Leibfried in Boulder and the group of Ferdinand Schmidt-Kahler in Ulm.

cision in frequency given by earlier measurements [183] are under way at our institute. The outcome of these experiments will serve as a valuable input to future laser-spectroscopy experiments which will be part of the *MAP* Cluster of Excellence initiative at our institute.

A. AN OPTICAL NUCLEAR CLOCK TRANSITION FOR FUNDAMENTAL EXPERIMENTS

A.1 Recent Experiments on the Isomeric First Excited State of ^{229}Th

Recently, the excitation energy of the isomeric first excited state of ^{229}Th has been measured to $7.6(\pm 0.5)$ eV [183] using cryogenic microcalorimeters. In units more common to laser physicists, the excitation energy can be transformed into a transition wavelength of $\lambda_{229\text{mTh}} = 163\left(\begin{smallmatrix} +11 \\ -10 \end{smallmatrix}\right)$ nm, a wavelength in the deep ultraviolet (UV). Both measurements [184] and theoretical estimates [183, 185, 186] suggest a half-life $t_{1/2}$ for the isomeric state of 3 to 5 hours, resulting in a natural line width of

$$\Gamma_{229\text{mTh}} = \frac{1}{\ln(2)t_{1/2}} \approx 2\pi \times 13 \mu\text{Hz} \cdots 2\pi \times 21 \mu\text{Hz}, \quad (\text{A.1})$$

leading to a minimum relative line width of

$$\frac{\Delta\omega_{229\text{mTh}}}{\omega_{229\text{mTh}}} = \frac{\Gamma_{229\text{mTh}} \lambda_{229\text{mTh}}}{2\pi c} \approx \frac{13 \mu\text{Hz} \cdot 163 \text{ nm}}{299792458 \text{ ms}^{-1}} \approx 7 \times 10^{-21} \quad (\text{A.2})$$

which is five to six orders of magnitude smaller than typical relative atomic line widths measured in experiments with single laser-cooled ions [187, 188].

Optical frequency and time standards allow for laboratory tests of fundamental physics [189, 190]. Compared to other time standards, an optical clock based on a nuclear transition has unique properties. First, the nuclear transition frequency is mainly determined by the strong interaction, while most other clock transition frequencies are determined by the electromagnetic interaction. This difference can be exploited in the search for variations of the fundamental coupling constants, especially of the fine structure constant and the coupling constant of the strong interaction [191]. Here, the precision to which the temporal variations can be detected might be greatly enhanced [192].

Second, the hyperfine interaction provides coupling of the atomic electron shell configuration and the nuclear electric and magnetic moments. This is of interest both when considering a single trapped $^{229\text{mTh}^{3+}}$ ion (see section A.3) or a crystalline solid like ThO_2 or ThF_4 . In the latter case, the transparent solid would allow for controlled experiments on the interplay between the crystalline lattice and the nuclear state [193].

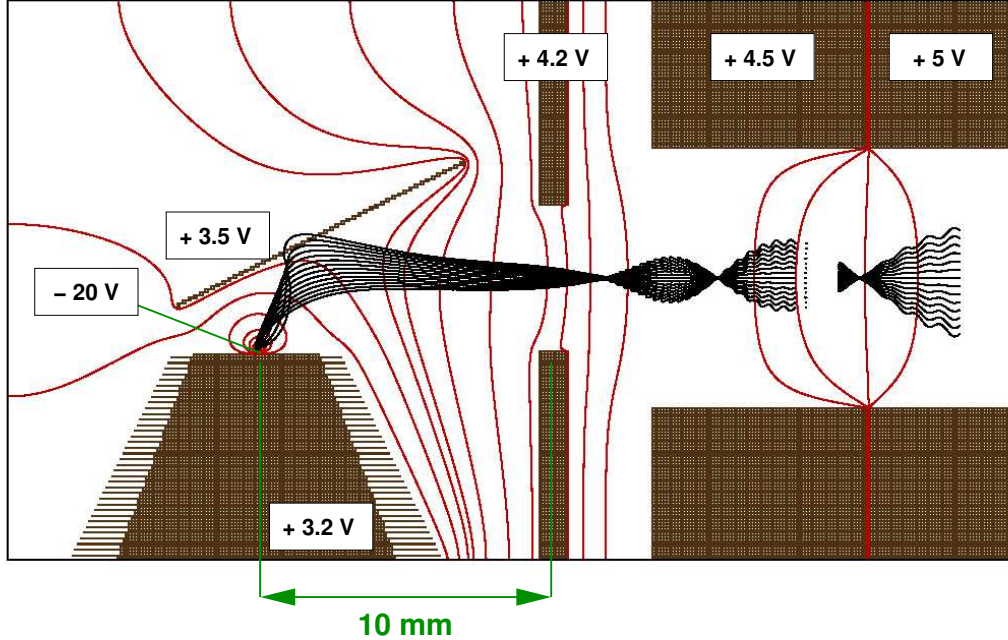


Figure A.1: Ions exit the ion guide (seen from right to left) and are deflected by a thin metal plate onto the tip of a small needle which is based on a large flat-top socket [194]. The voltages assigned to the different parts are given with respect to a common ground. The distance from the exit of the ion guide to the needle tip is 10 mm.

Third, unlike in most electronic transitions, the effect of external electric or magnetic fields on the nuclear transition is expected to be small [193]. This would allow for unprecedented possibilities when trapping single $^{229\text{m}}\text{Th}$ ions for precision spectroscopy using electromagnetic trapping fields. In the following, a new experiment is proposed which, if successful, would serve as a major step towards laser excitation of the $J^\pi = \frac{5}{2}^+ \rightarrow J^\pi = \frac{3}{2}^+$ nuclear ground state transition.

A.2 A Brilliant $^{229\text{m}}\text{Th}$ Decay Photon Source

In the deep ultra-violet range of the electromagnetic spectrum optics made from MgF_2 or CaF_2 are at hand with good imaging quality and transmission characteristics¹, see for example [195] and Fig. A.2 a). Furthermore, standard dielectric coating techniques are available for producing mirrors and filters in this region [113]. Finally, light detectors such as multi-channel plates and photomultipliers [196] exist which are sensitive in the desired wavelength range. With this at hand, it is currently planned at our institute to measure the aforementioned

¹This is mainly due to the demand imposed by the miniaturization in chip production, for which microlithography fluorine excimer lasers are used, which operate at a wavelength of 157 nm.

transition wavelength in an all-optical experiment, in which in contrast to previous experiments [183, 184, 197–199], ^{229}Th ions in the $J^\pi = \frac{3}{2}^+$ isomeric first excited state, which originate from the alpha-decay of a $^{233}\text{UF}_4$ source with a branching ratio of about 2 % [184], are collected in a gas stopping cell [105] and transported into a separate measurement chamber using a radio-frequency ion guide [200].

The $^{233}\text{UF}_4$ source is located about 60 mm from the entrance to the ion guide. The buffer-gas cell itself is filled with ^4He gas at a pressure of 40 mbar, which at $T = 25^\circ\text{C}$ results in a density of $n_{\text{He}} = 6.544\text{ gm}^{-3}$. Due to high electronic conversion² [202] and subsequent Auger electron cascades, the $^{229\text{m}}\text{Th}$ isomer is dominantly produced in high charge states. Charge exchange with buffer-gas atoms leads to a reduction of the high charge states to mainly singly- and doubly-charged $^{229\text{m}}\text{Th}$, although under ideal experimental conditions it might be possible to extract triply-charged $^{229\text{m}}\text{Th}$.

The $^{229\text{m}}\text{Th}$ ions pass through the radio-frequency ion guide and are extracted into a dedicated measurement vacuum chamber, where they are electrostatically guided to the tip of a needle, see Fig. A.1. The ions are collected on the tip of the needle, forming a micrometer-sized point-like source. Changes in the decay photon energy due to the trapping of the ions on the steel needle tip are expected to be negligible, providing a brilliant source of $^{229\text{m}}\text{Th}$ decay photons. The total time for extracting, guiding and depositing the ions on the needle tip is estimated to about 1 to 2 ms [194]. Fortunately, most of the ^{233}U decay products have half-lives shorter or comparable to the extraction time, while all of the decay products are short-lived compared to the $^{229\text{m}}\text{Th}$ first excited isomeric ground state.

To summarize, the setup described above provides a brilliant source of $^{229\text{m}}\text{Th}$ decay photons located inside a dedicated measurement vacuum chamber at a residual gas pressure on the order of 10^{-6} mbar to 10^{-7} mbar, well separated from other unwanted unstable nuclei produced in the decay of the ^{233}U . With this setup, almost all sources of background to the expected signal can be eliminated, especially photons originating from unwanted ^{233}U decay products, chemical target impurities and from the interaction of decay products with residual gas molecules [203–205].

A.3 All-Optical Detection of the Decay of the Isomeric First Excited State of ^{229}Th

The maximum activity of the $^{233}\text{UF}_4$ source of 4 kBq allowed under the current laboratory conditions limits the expected decay photon counting rate to a few Hz. These photons must be efficiently detected, requiring a detection scheme which

²For example, for the 29.192 keV energy level, which decays via a M1 transition to the $J^\pi = \frac{3}{2}^+$ first excited ground state with a probability of 1.8 %, one finds conversion coefficients $\alpha(\text{L}) = 112.7$ and $\alpha(\text{M}) = 27.1$ [201].

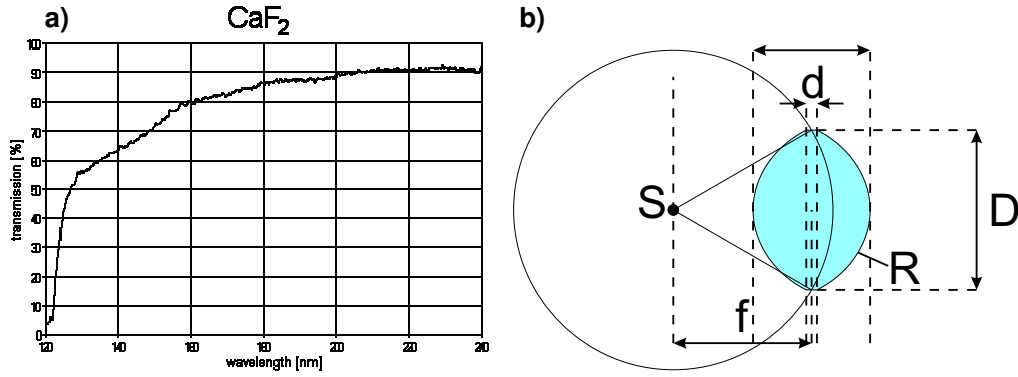


Figure A.2: **a)** Transmission in percent versus wavelength in nm for a two-surface optical element made of UV-grade CaF₂ (courtesy of Korth Kristalle GmbH [195]). The transmission of an optical element mainly depends on surface losses rather than transmission losses inside the material.

b) A lens of diameter D , radius R , lens thickness d and total thickness Δ is placed at a distance equal to its focal length f from the source S .

- allows to collect a large amount of the decay photons emitted by the source,
- can image these photons on a detector without intolerable intensity loss,
- can detect single photons at a low dark count rate.

The source emits photons homogeneously in all directions. To collect most of the emitted photons either the detector itself or an optical element which focuses the photons on the detector must cover a large solid angle around the source. While the first option can be ruled out because of the high cost of deep-UV detectors, the second option is more promising.

A.3.1 Lens System

The most efficient way to collect the decay photons would be to place the source in the focus of a parabolic mirror which is highly reflective in the deep UV. In the current setup, several reasons can be named which speak against using a parabolic mirror:

- Although dielectric high-reflectivity coatings exist for the desired wavelength range, they are typically limited in bandwidth to about 10 nm.
- For a strongly-focusing parabolic mirror, maintaining a desired surface roughness of the coated mirror of $\lambda/10$ or smaller is currently challenging for optics manufacturers.
- The substrate itself would be placed close to the exit of the ion guide, possibly affecting the guiding fields due to electrostatic charging of the mirror substrate.

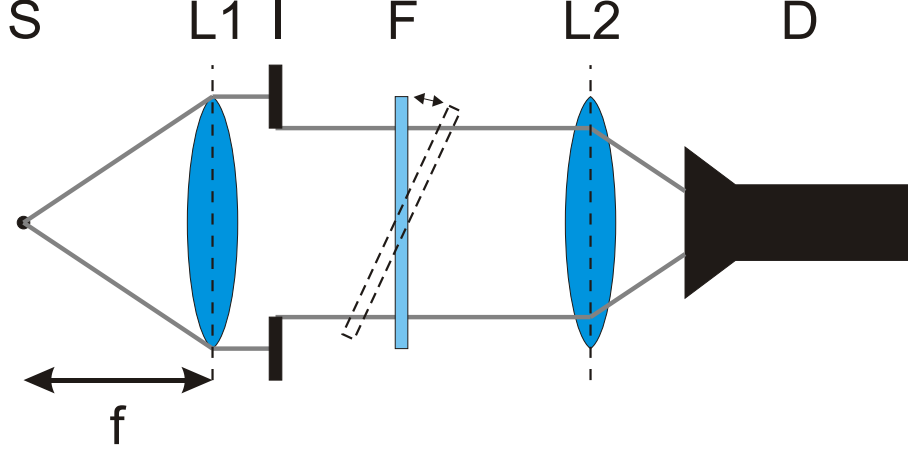


Figure A.3: Schematic setup for the optical detection of the decay photons emitted by the $^{229\text{m}}\text{Th}$ source **S**. The first lens, **L1**, is placed at a distance equal to its focal length f from the source. The light emitted by the source is parallelized. The spatial filter matches the source size to the effective diameter of the bandpass filter **F**, which is rotated between zero and 45 degrees to scan a wavelength range of about 10 nm. The second lens, **L2**, focuses the light on the detector **D**.

Thus, for the current setup it is foreseen to use a converging lens to focus a part of the decay photons on the detector. The lens parameters are the focal length f , the curvature radius R , the lens thickness d , the lens diameter D and the refractive index n which are connected by the lensmaker's equation [206]

$$\frac{1}{f} = (n - 1) \left(\frac{2}{R} + \frac{(n - 1) d}{nR^2} \right), \quad D \leq 2R, \quad (\text{A.3})$$

while the total lens thickness is $\Delta = d + 2R - \sqrt{4R^2 - D^2}$, see Fig. A.2 b). In order to collect a maximum number of photons, the distance between the source and the focal plane is set to the focal length. The fraction of photons collected by the lens is given by

$$g = \frac{1}{2} - \frac{f}{\sqrt{4f^2 + D^2}}. \quad (\text{A.4})$$

By increasing the lens diameter, this fraction can be increased, reaching a maximum *independent* of the focal length for $D \equiv 2R$. An increase in lens diameter leads to an increase in lens thickness. Fortunately, transmission loss is mainly caused by surface effects, especially by layers of dust and moisture, while transmission loss inside the crystalline lens material can be neglected. The surface-loss for a two-surface optical element is shown in Fig. A.2 a). Combining Eq. A.3 and A.4 and assuming $d \ll R$, $D \equiv 2R$ and $n \approx 1.54$ for CaF_2 at $\lambda_{229\text{mTh}} = 163$ nm, one finds $g \approx 0.16$ as the maximum fraction of all photons emitted by the source

which can be collected by a spherical lens. Although this result is independent of the focal length, it is nevertheless desirable to choose a shorter focal length, since this reduces both the lens thickness and the maximum lens diameter. The complete optical setup can be seen in Fig. A.3. It will be described in the following.

A.3.2 Spectral Bandpass Filter

The first lens, **L1**, is placed at a distance equal to its focal length from the source. After passing through the lens, the light emitted by the source is parallel. The key element to determine the wavelength is the bandpass filter **F**, see Fig. A.3 and A.4. It is transparent to light above a certain cutoff wavelength, while it blocks all light at smaller wavelengths. This cutoff wavelength can be altered by rotating the filter. A rotation of 45 degrees translates into a shift of the cutoff wavelength by about 10 nm to smaller wavelengths³.

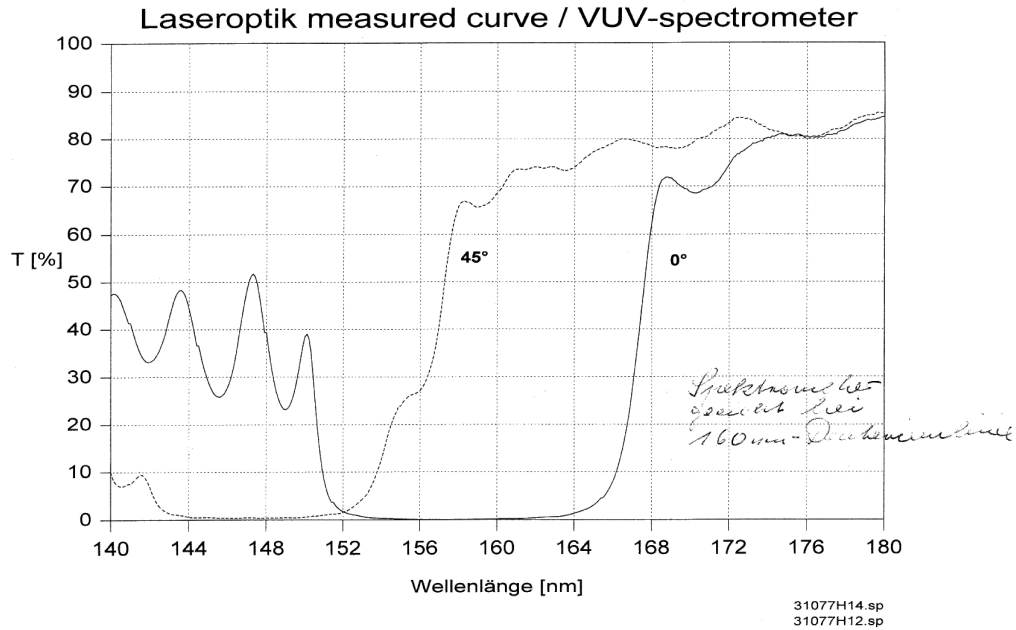
Two filter sets are available [113], see Fig. A.4, for which the transmission spectrum has been calibrated at the Laserzentrum Hannover to sub-nm accuracy using the 160 nm deuterium spectral line. Since the natural line width of the source spectral line is expected to be small, the convolution of the source spectral line with the transmission spectrum of the filter can be recorded for various rotation angles, effectively scanning the transmission curve with the source spectral line. Such a scan would allow to determine the wavelength of the source spectral line to at least the width of the step-like change in the transmission as shown in Fig. A.4. By prolonging the measurement time, the resolution of the wavelength determination can, in principle, be increased to match the resolution of the transmission curve.

A.3.3 Detector

The light transmitted through the filter is focused by the lens **L2** onto a low dark-count rate optical detector **D** sensitive in the deep UV. A low dark count rate is essential to maximize the signal-to-noise ratio for the low photon counting rates expected. For a first test a photomultiplier sensitive in the wavelength region between 110 nm and 230 nm [207] will be used to detect decay photons. Its dark count rate was measured by the manufacturer [196] to 2 counts/s at an optimum operating voltage of 3.5 kV. For further studies, a setup combining a Cs-coated multi-channel plate detector with a low-noise CCD-camera can provide much lower dark count rates. With this setup, it is foreseen to decrease the relative error on the wavelength to sub-nm accuracy.

³As can be seen in Fig. A.4, the slope of the transmission curve near the cutoff wavelength becomes flatter for larger angles of incident. In this case probing the transmission curve as described in the text can help to enhance the resolution.

31077H1: LP171nm/0-45°



01087H1: LP160nm/0-45°

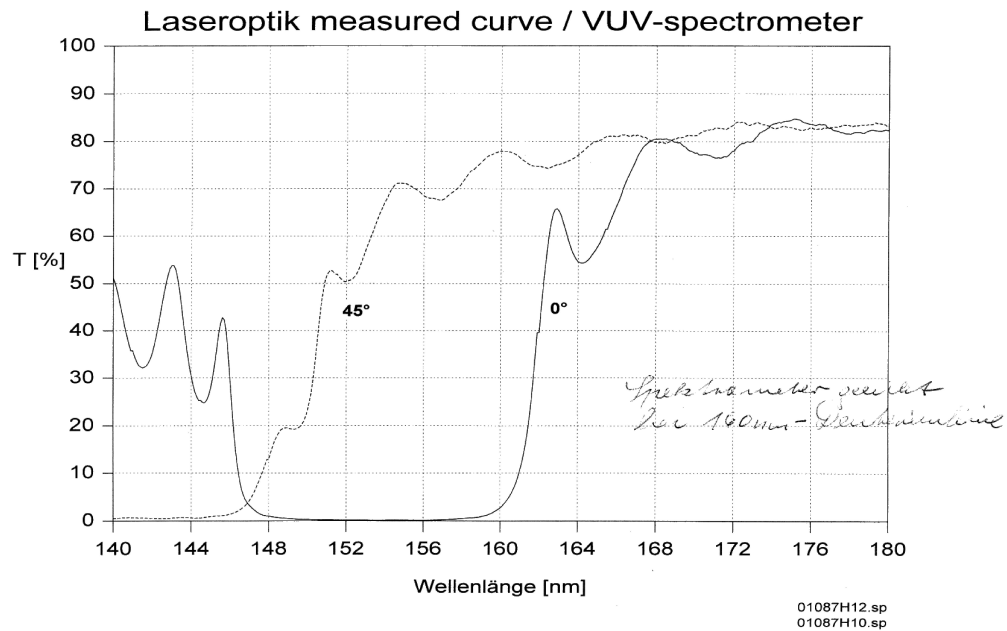


Figure A.4: Transmission spectra for two different sets of transmission band gap filters. Below a certain wavelength, the transmission T becomes negligible, while above this cutoff wavelength the transmission exceeds 80 %. The cutoff wavelength can be shifted to smaller wavelength values by changing the angle of incidence of the light emitted by the source. This requires the light emitted by the source to be parallel (courtesy of Laseroptik [113]).

| <i>Trap parameters</i> | <i>Value required for trapping $^{229\text{m}}\text{Th}^{3+}$</i> |
|---|--|
| aperture radius r_0 | 400 μm |
| trapping voltage amplitude U_{RF} | 850 V |
| trap radio frequency Ω_{RF} | $2\pi \times 29$ MHz |
| <i>Confinement parameters</i> | <i>Value derived from trap parameters</i> |
| secular trap frequency ω_{trap} | $2\pi \times 4.1$ MHz |
| stability parameter q | 0.41 |

Table A.1: Typical trap parameters for a linear Paul trap well-suited for direct laser cooling and spectroscopy of $^{229\text{m}}\text{Th}^{3+}$ [208].

A.4 Laser Spectroscopy of Trapped $^{229\text{m}}\text{Th}^{3+}$ Ions

The resonance cross-section for the optical excitation of the $^{229\text{m}}\text{Th}$ ground state transition by a light source with a line width $\Delta\omega_{\text{L}}$ scales like [209]

$$\sigma_{^{229\text{m}}\text{Th}} \propto \lambda_{^{229\text{m}}\text{Th}}^2 \frac{\Gamma_{^{229\text{m}}\text{Th}}}{\Delta\omega_{\text{L}}}, \quad (\text{A.5})$$

which is dominated by the ratio of the line width of the transition to the line width of the light source. Naively calculating the saturation intensity, Eq. 3.7 yields $I_{\text{S}} \approx 4 \text{ nWm}^{-2}$, which for a 100 μm focal diameter requires a laser power of only 123 *aW*. Today, coherent light sources exist with line widths close to the ideal millihertz regime determined by the phase diffusion of spontaneously emitted photons [210]. Following Eq. A.5, even with such a light source only about a fraction of 10^{-3} of the overall laser power will be used to saturate the transition. From this it is obvious that exciting the transition using a broadband light source would require very high total light intensity. Instead, using a narrow-band laser source requires much less intensity but a precise knowledge of the transition wavelength.

In this outlook an approach for laser spectroscopy of the $^{229\text{m}}\text{Th}$ ground state transition is discussed, which is based on trapped triply-charged $^{229\text{m}}\text{Th}$ ions. Recently, it was shown that $^{229\text{m}}\text{Th}^{3+}$ ions exhibit optical electronic transitions which allow for direct laser cooling [193, 211]. The atomic pumping scheme proposed in [193], see Fig. A.5, provides an indirect optical detection of the nuclear transition, because a change of the nuclear spin by \hbar changes the hyperfine splitting of the electronic transitions, causing a detectable detuning between the laser frequency and the cooling transition frequency. Using suitable laser systems, the nuclear ground state transition from the $J^\pi = \frac{5}{2}^+$ to the $J^\pi = \frac{3}{2}^+$ state can be detected by observing the fluorescence light of the electronic transitions, similar to the *optical shelving* technique [193, 212].

With laser cooling, one can control the temperature T of the $^{229\text{m}}\text{Th}^{3+}$ ions, thereby controlling the Doppler broadening [111] of the ground state transition

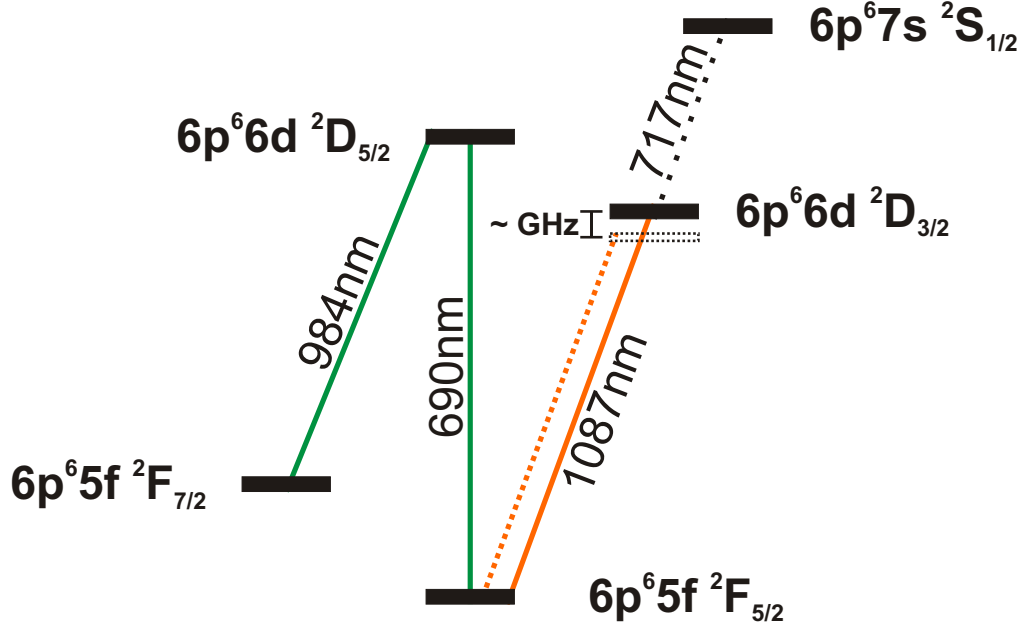


Figure A.5: Schematic view of the lowest electronic energy levels in $^{229\text{m}}\text{Th}^{3+}$ which are suitable for laser cooling. To avoid systematic shifts due to external fields, either the total electronic angular momentum J or the total atomic angular momentum F must be smaller than 1, while F has to be an integer. These requirements lead to two possible cooling schemes, either using a closed three-level Λ -system marked by the green lines or a closed two-level system marked by the orange line. The latter does not fulfill $J < 1$, but a metastable $7s^2S_{1/2}$ state is also available for cooling, marked by the dotted line, which is electric-dipole forbidden and has a lifetime on the order of one second. The laser wavelengths needed for cooling are given in nm. A change in nuclear spin by \hbar translates for a $7s$ electronic state to a change in hyperfine splitting of several GHz, as indicated for the two-level scheme, which can be easily detected via the fluorescence intensity. For further details please refer to Ref. [193].

spectral line

$$\frac{\Delta\omega_{\text{Doppler}}}{\omega_{229\text{mTh}}} = \sqrt{\frac{8k_{\text{B}}T \ln(2)}{m_{229\text{mTh}}c^2}}. \quad (\text{A.6})$$

This broadening of the spectral line can help to better match the small linewidth of the nuclear ground state transition to the laser line width⁴.

For measurements aiming for ultimate accuracy, cooling the $^{229\text{m}}\text{Th}^{3+}$ ions to their motional ground state is essential. This can hopefully be done either

⁴Please note that Doppler broadening is a statistical effect. It is based on the Doppler-effect which induces a velocity-dependent detuning of the transition frequency for a single ion. If the laser frequency and the Doppler-shifted transition frequency coincide, the transition is excited. For a large ensemble of ions at temperature T , such a coincidence becomes more likely.

directly by using a sideband cooling scheme [213, 214] or indirectly by sympathetic cooling [81]. In both cases, a steep linear Paul trap is required to reach the *Lamb-Dicke regime*, in which the spatial displacement of the ion due to the absorption of a single photon is small compared to the wavelength of the absorbed photon (this is equivalent to $\eta_{\text{LD}} \ll 1$, see Eq. A.7). In this case, the photon recoil momentum imposed on the laser-cooled ion does not excite an oscillation of the ion in the harmonic trap potential at the trap frequency ω_{trap} , but instead is taken up by the trap itself. Sideband cooling also requires the line width of the cooling transition to be much smaller than the secular frequency of the ion in the trap⁵.

When considering spectroscopy, the photon recoil momentum due to the excitation of the nuclear transition must also be taken into account. The Lamb-Dicke parameter [215] then amounts to

$$\eta_{\text{LD}} \equiv \frac{2\pi}{\lambda_{229\text{mTh}}} \sqrt{\frac{\hbar}{2m_{229\text{mTh}} \omega_{\text{trap}}}} \approx 0.09 \ll 1 \quad (\text{A.7})$$

for suitable trap parameters as listed in Tab. A.1, chosen in such a way that the excitation of the nuclear ground transition does not cause the ion to oscillate in the trap⁶.

Yet, no laser source at the desired wavelength exists. One limiting factor is the transmission properties of nonlinear crystals necessary for reaching very small wavelengths, for example by second-harmonic generation. The most promising nonlinear crystal material is LiB_3O_5 , normally referred to as *LBO*, which is transparent down to 160 nm [216]. Based on this nonlinear crystal, it is foreseen to build a laser source in the wavelength region of interest [217] at the Max-Planck-Institute for Quantum Optics (MPQ)⁷. With such a laser source, direct optical pumping of the transition is in reach.

In conclusion, trapping, cooling and laser spectroscopy of $^{229\text{m}}\text{Th}^{3+}$ is possible using known experimental techniques available at our institute and the Max-Planck-Institute for Quantum Optics. With these techniques at hand, an ultra-precise clock based on a nuclear ground state transition can be built which would serve as a tool for fundamental tests on the constancy of the fine structure constant and other aspects of fundamental physics [192].

⁵Up until now, there is no data available on the radiative lifetimes of the cooling transitions and thus sympathetic cooling using a well-known ion like $^{24}\text{Mg}^+$ might be more promising.

⁶Unfortunately, Doppler-free two-photon spectroscopy of the ground state transition is impossible due to the very small cross section for this process. Thus, one is left with using a strongly-confining trap potential.

⁷Recently, a frequency comb in the extreme UV has been realized at the MPQ operating at a repetition rate of 100 MHz [218]. At such a high repetition rate the mode-spacing is small enough to serve as a source for high-resolution spectroscopy in the extreme UV. Compared to a normal laser mode, the modes of a frequency comb have a much smaller line width, allowing to reach much higher accuracy in the proposed experiment.

BIBLIOGRAPHY

- [1] REITMAN I., AYKROYD D. AND RAMIS H. **Ghostbusters**. *Columbia Pictures*
<http://www.imdb.com/title/tt0087332/>
- [2] SCHÄTZ T., SCHRAMM U. AND HABS D. **Crystalline ion beams in Pallas**. *Proceedings of the Workshop on Ion Beam Cooling: Towards the Crystalline Beam, (Kyoto, Japan)* (2003) 74–90
<http://www.worldscibooks.com/physics/5159.html>
- [3] SCHÄTZ T., SCHRAMM U. AND HABS D. **Crystalline Ion Beams**. *Nature* **412(6848)** (2001) 717–720.
<http://dx.doi.org/10.1038/35089045>
- [4] SCHRAMM U., SCHÄTZ T. AND HABS D. **Bunched Crystalline Ion Beams**. *Physical Review Letters* **87(18)** (2001) 184801.
<http://dx.doi.org/10.1103/PhysRevLett.87.184801>
- [5] WINELAND D.J. AND ITANO W.M. **Laser cooling of atoms**. *Physical Review A* **20(4)** (1979) 1521–1540.
<http://dx.doi.org/10.1103/PhysRevA.20.1521>
- [6] METCALF H. AND VAN DER STRATEN P. *Laser Cooling and Trapping* (Springer Berlin Heidelberg New York, **2002**)
- [7] HANGST J.S., KRISTENSEN M., NIELSEN J.S., POULSEN O., SCHIFFER J.P. AND SHI P. **Laser cooling of a stored ion beam to 1 mK**. *Physical Review Letters* **67(10)** (1991) 1238–1241.
<http://dx.doi.org/10.1103/PhysRevLett.67.1238>
- [8] ITANO W., BERGQUIST J., BOLLINGER J. AND WINELAND D. **Cooling methods in ion traps**. *Physica Scripta* **1995(T59)** (1995) 106–120.
<http://dx.doi.org/10.1088/0031-8949/1995/T59/013>
- [9] BIRKL G., KASSNER S. AND WALTHER H. **Multiple-shell structures of laser-cooled Mg⁺ ions in a quadrupole storage ring**. *Nature* **357** (1992) 310–313.
<http://dx.doi.org/10.1038/357310a0>
- [10] DREWSSEN M., BRODERSEN C., HORNEKÆR L., HANGST J.S. AND SCHIFFER J.P. **Large Ion Crystals in a Linear Paul Trap**. *Physical Review Letters* **81(14)** (1998) 2878–2881.
<http://dx.doi.org/10.1103/PhysRevLett.81.2878>
- [11] BOLLINGER J., TAN J., ITANO W., WINELAND D. AND DUBIN D. **Nonneutral ion plasmas and crystals in Penning traps**. *Physica Scripta* **1995(T59)** (1995) 352–359.
<http://dx.doi.org/10.1088/0031-8949/1995/T59/048>
- [12] MITCHELL T.B., BOLLINGER J.J., DUBIN D.H., HUANG X.P., ITANO W.M. AND BAUGHMAN R.H. **Direct Observations of Structural Phase Transitions in Planar Crystallized Ion Plasmas**. *Science* **282(5392)** (1998) 1290–1293.
<http://dx.doi.org/10.1126/science.282.5392.1290>

- [13] ITANO W.M., BOLLINGER J.J., TAN J.N., JELENKOVIĆ B., HUANG X.P. AND WINELAND D.J. **Bragg Diffraction from Crystallized Ion Plasmas.** *Science* **279(5351)** (1998) 686–689.
<http://dx.doi.org/10.1126/science.279.5351.686>
- [14] HABS D. **Simple Treatment of Ordered Beams.** *GSI Report GSI-89-10* (1989) 43–63
- [15] WEI J., LI X.P. AND SESSLER A. **Crystalline Beams.** *AIP Conference Proceedings of the 6th Workshop on Advanced Accelerator Concepts, (Lake Geneva, Wisconsin (USA))* **335(1)** (1995) 224–244.
<http://dx.doi.org/10.1063/1.48243>
- [16] HABS D. AND GRIMM R. **Crystalline Ion Beams.** *Annual Review of Nuclear and Particle Science* **45** (1995) 391–428.
<http://dx.doi.org/10.1146/annurev.ns.45.120195.002135>
- [17] SCHRAMM U., SCHÄTZ T. AND HABS D. **Three-dimensional crystalline ion beams.** *Physical Review E* **66(3)** (2002) 036501.
<http://dx.doi.org/10.1103/PhysRevE.66.036501>
- [18] SCHRAMM U. AND HABS D. **Crystalline ion beams.** *Progress in Particle and Nuclear Physics* **53(2)** (2004) 583–677.
<http://dx.doi.org/10.1016/j.pnpnp.2004.03.002>
- [19] ZWICKNAGEL G., TOEPFFER C. AND REINHARD P.G. **Stopping of heavy ions in plasmas at strong coupling.** *Physics Reports* **309(3)** (1999) 117–208.
[http://dx.doi.org/10.1016/S0370-1573\(98\)00056-8](http://dx.doi.org/10.1016/S0370-1573(98)00056-8)
- [20] SINGWI K.S., TOSI M.P., LAND R.H. AND SJÖLANDER A. **Electron Correlations at Metallic Densities.** *Physical Review* **176(2)** (1968) 589–599.
<http://dx.doi.org/10.1103/PhysRev.176.589>
- [21] SINGWI K., SJÖLANDER A., TOSI M. AND LAND R. **Electron correlations at metallic densities - III.** *Solid State Communications* **7(20)** (1969) 1503–1505.
[http://dx.doi.org/10.1016/0038-1098\(69\)90030-1](http://dx.doi.org/10.1016/0038-1098(69)90030-1)
- [22] SINGWI K.S., SJÖLANDER A., TOSI M.P. AND LAND R.H. **Electron Correlations at Metallic Densities. IV.** *Physical Review B* **1(3)** (1970) 1044–1053.
<http://dx.doi.org/10.1103/PhysRevB.1.1044>
- [23] ICHIMARU S. **Strongly coupled plasmas: high-density classical plasmas and degenerate electron liquids.** *Reviews of Modern Physics* **54(4)** (1982) 1017–1059.
<http://dx.doi.org/10.1103/RevModPhys.54.1017>
- [24] DUBIN D.H.E. **Theory of structural phase transitions in a trapped Coulomb crystal.** *Physical Review Letters* **71(17)** (1993) 2753–2756.
<http://dx.doi.org/10.1103/PhysRevLett.71.2753>
- [25] HANSEN J. **Statistical Mechanics of Dense Ionized Matter. I. Equilibrium Properties of the Classical One-Component Plasma.** *Physical Review A* **8(6)** (1973) 3096–3109.
<http://dx.doi.org/10.1103/PhysRevA.8.3096>
- [26] O'NEIL T. **Plasmas with a single sign of charge (an overview).** *Physica Scripta* **1995(T59)** (1995) 341–351.
<http://dx.doi.org/10.1088/0031-8949/1995/T59/047>

- [27] DUBIN D. **Effect of correlations on the thermal equilibrium and normal modes of a non-neutral plasma.** *Physical Review E* **53(5)** (1996) 5268–5290.
<http://dx.doi.org/10.1103/PhysRevE.53.5268>
- [28] DUBIN D. AND O'NEIL T.M. **Trapped nonneutral plasmas, liquids, and crystals (the thermal equilibrium states).** *Reviews of Modern Physics* **71(1)** (1999) 87.
<http://dx.doi.org/10.1103/RevModPhys.71.87>
- [29] SCHIFFER J.P., DREWSSEN M., HANGST J.S. AND HORNEKAR L. **From the Cover: Temperature, ordering, and equilibrium with time-dependent confining forces.** *Proceedings of the National Academy of Sciences* **97(20)** (2000) 10697–10700.
<http://dx.doi.org/10.1073/pnas.190320397>
- [30] WALTHER H. **From a single ion to a mesoscopic system - crystallization of ions in Paul traps.** *Physica Scripta* **1995(T59)** (1995) 360–368.
<http://dx.doi.org/10.1088/0031-8949/1995/T59/049>
- [31] RAHMAN A. AND SCHIFFER J.P. **Structure of a One-Component Plasma in an External Field: A Molecular-Dynamics Study of Particle Arrangement in a Heavy-Ion Storage Ring.** *Physical Review Letters* **57(9)** (1986) 1133–1136.
<http://dx.doi.org/10.1103/PhysRevLett.57.1133>
- [32] SCHIFFER J.P. AND RAHMAN A. **Feasibility of a crystalline condensed state in cooled ion beams of a storage ring.** *Zeitschrift für Physik A* **331(1)** (1988) 71–74.
<http://dx.doi.org/10.1023/A:1012687402332>
- [33] HASSE R.W. AND SCHIFFER J.P. **The structure of the cylindrically confined Coulomb lattice.** *Annals of Physics* **203(2)** (1990) 419–448.
[http://dx.doi.org/10.1016/0003-4916\(90\)90177-P](http://dx.doi.org/10.1016/0003-4916(90)90177-P)
- [34] TAN J., BOLLINGER J.J., JELENKOVIC B. AND WINELAND D.J. **Long-Range Order in Laser-Cooled, Atomic-Ion Wigner Crystals Observed by Bragg Scattering.** *Physical Review Letters* **75(23)** (1995) 4198–4201.
<http://dx.doi.org/10.1103/PhysRevLett.75.4198>
- [35] SCHIFFER J. **Sparse Crystals.** *Science* **279(5351)** (1998) 675–676.
<http://dx.doi.org/10.1126/science.279.5351.675>
- [36] PAUL W. AND RAETHER M. **Das elektrische Massenfilter.** *Zeitschrift für Physik A* **140(3)** (1955) 262–273.
<http://dx.doi.org/10.1007/BF01328923>
- [37] DEHMELT H. **Radiofrequency Spectroscopy of Stored Ion I: Storage.** *Advances in Atomic and Molecular Physics* **3** (1967) 53–72
- [38] PAUL W. **Electromagnetic traps for charged and neutral particles.** *Reviews of Modern Physics* **62(3)** (1990) 531–540.
<http://dx.doi.org/10.1103/RevModPhys.62.531>
- [39] COURANT E., LIVINGSTON M. AND SNYDER H. **The Strong-Focusing Synchrotron—A New High Energy Accelerator.** *Physical Review* **88(5)** (1952) 1190–1196.
<http://dx.doi.org/10.1103/PhysRev.88.1190>

- [40] COURANT E.D. AND SNYDER H.S. **Theory of the alternating-gradient synchrotron.** *Annals of Physics* **3(1)** (1958) 1–48.
[http://dx.doi.org/10.1016/0003-4916\(58\)90012-5](http://dx.doi.org/10.1016/0003-4916(58)90012-5)
- [41] WIEDEMANN H. *Particle Accelerator Physics I* (Springer Berlin Heidelberg New York, **1999**)
- [42] DUBIN D.H.E. **Theory of electrostatic fluid modes in a cold spheroidal non-neutral plasma.** *Physical Review Letters* **66(16)** (1991) 2076–2079.
<http://dx.doi.org/10.1103/PhysRevLett.66.2076>
- [43] KALMAN G. AND GOLDEN K. **Response function and plasmon dispersion for strongly coupled Coulomb liquids.** *Physical Review A* **41(10)** (1990) 5516–5527.
<http://dx.doi.org/10.1103/PhysRevA.41.5516>
- [44] RYLYUK V.M. AND TKACHENKO I.M. **Dielectric tensor of strongly coupled plasmas.** *Physical Review A* **44(2)** (1991) 1287–1300.
<http://dx.doi.org/10.1103/PhysRevA.44.1287>
- [45] GOLDEN K., KALMAN G. AND WYNS P. **Dielectric tensor and shear-mode dispersion for strongly coupled Coulomb liquids: Three-dimensional one-component plasmas.** *Physical Review A* **46(6)** (1992) 3454–3462.
<http://dx.doi.org/10.1103/PhysRevA.46.3454>
- [46] AVILOV V.V. AND HOFMANN I. **Theory of longitudinal Schottky spectra of ordered ion beams in a storage ring.** *Physical Review E* **47(3)** (1993) 2019–2030.
<http://dx.doi.org/10.1103/PhysRevE.47.2019>
- [47] BLÜMEL R. **Nonlinear dynamics of trapped ions.** *Physica Scripta* **T59** (1995) 369–379.
<http://dx.doi.org/10.1088/0031-8949/1995/T59/050>
- [48] SEURER M., SPREITER Q. AND TOEPFFER C. **Limited heating rates in strongly coupled particle beams.** *Hyperfine Interactions* **99(1)** (1996) 253–258.
<http://dx.doi.org/10.1007/BF02274928>
- [49] MÖHL D. AND SESSLER A. **Beam cooling: principles and achievements.** *Nuclear Instruments and Methods in Physics Research Section A* **532(1-2)** (2004) 1–10.
<http://dx.doi.org/10.1016/j.nima.2004.06.102>
- [50] HABS D., SCHRAMM U., FRANZKE B., KLUGE J., KÜHL T., NOLDEN F., SCHÜTT P., STECK M., STÖHLKER T., GRIESER M., SAATHOF G., SCHWALM D. AND BACKE H. **Laser Cooling of Beams of Highly Charged Ions at SIS100/300.** *GSI Letter of Intent GSI-ESAC AP* (2004) 1–25
<http://www.gsi.de/documents/DOC-2004-Apr-50.html>
- [51] NODA A., FUJIMOTO S., IKEGAMI M., SHIRAI T., SOUDA H., TANABE M., TONGU H., NODA K., YAMADA S., SHIBUYA S., YAKEUCHI T., OKAMOTO H. AND GRIESER M. **Laser cooling for 3-D crystalline state at S-LSR.** *AIP Conference Proceeding of the International Workshop on Beam Cooling and Related Topics, COOL05 (Galena, Illinois (USA))* **821(1)** (2006) 491–500.
<http://dx.doi.org/10.1063/1.2190157>

- [52] HANGST J.S., NIELSEN J.S., POULSEN O., SHI P. AND SCHIFFER J.P. **Laser Cooling of a Bunched Beam in a Synchrotron Storage Ring.** *Physical Review Letters* **74(22)** (1995) 4432–4435.
<http://dx.doi.org/10.1103/PhysRevLett.74.4432>
- [53] EISENBARTH U., MUDRICH M., EIKE B., GRIESER M., GRIMM R., LUGER V., SCHÄTZ T., SCHRAMM U., SCHWALM D. AND WEIDEMÜLLER M. **Anomalous behaviour of laser cooled fast ion beams.** *Hyperfine Interactions* **127(1)** (2000) 223–235.
<http://dx.doi.org/10.1023/A:1012699719074>
- [54] WANNER B., GRIMM R., GRUBER A., HABS D., MIESNER H.J., NIELSEN J.S. AND SCHWALM D. **Rapid adiabatic passage in laser cooling of fast stored ion beams.** *Physical Review A* **58(3)** (1998) 2242–2251.
<http://dx.doi.org/10.1103/PhysRevA.58.2242>
- [55] ATUTOV S., BIANCALANA V., CALABRESE R., CLAUSER T., GRIMM R., GUIDI V., LAMANNA G., LAUER I., LENISA P., LUGER V., MARIOTTI E., MOI L. AND SCHRAMM U., STAGNO V., STÖSS EL M., TECCHIO L. AND VARIALE V. **First demonstration of “white-light” laser cooling of a stored ion beam.** *Hyperfine Interactions* **115(1)** (1998) 47–52.
<http://dx.doi.org/10.1023/A:1012680118088>
- [56] ATUTOV S.N., CALABRESE R., GRIMM R., GUIDI V., LAUER I., LENISA P., LUGER V., MARIOTTI E., MOI L., PETERS A., SCHRAMM U. AND STÖSSEL M. **“White-light” Laser Cooling of a Fast Stored Ion Beam.** *Physical Review Letters* **80(10)** (1998) 2129–2132.
<http://dx.doi.org/10.1103/PhysRevLett.80.2129>
- [57] MIESNER H.J., GRIMM R., GRIESER M., HABS D., SCHWALM D., WANNER B. AND WOLF A. **Efficient, Indirect Transverse Laser Cooling of a Fast Stored Ion Beam.** *Physical Review Letters* **77(4)** (1996) 623–626.
<http://dx.doi.org/10.1103/PhysRevLett.77.623>
- [58] MIESNER H.J., GRIESER M., GRIMM R., LAUER I., LUGER V., MERZ P., PETERS A., SCHRAMM U., SCHWALM D. AND STÖSSEL M. **Transverse laser cooling of a radio-frequency bunched ion beam in the storage ring TSR.** *Nuclear Instruments and Methods in Physics Research Section A* **383(2-3)** (1996) 634–636.
[http://dx.doi.org/10.1016/S0168-9002\(96\)00897-2](http://dx.doi.org/10.1016/S0168-9002(96)00897-2)
- [59] LAUER I., EISENBARTH U., GRIESER M., GRIMM R., LENISA P., LUGER V., SCHÄTZ T., SCHRAMM U., SCHWALM D. AND WEIDEMÜLLER M. **Transverse Laser Cooling of a Fast Stored Ion Beam through Dispersive Coupling.** *Physical Review Letters* **81(10)** (1998) 2052–2055.
<http://dx.doi.org/10.1103/PhysRevLett.81.2052>
- [60] SCHRÖDER S., KLEIN R., BOOS N., GERHARD M., GRIESER R., HUBER G., KARAFILLIDIS A., KRIEG M., SCHMIDT N., KÜHL T., NEUMANN R., BALKIN V., GRIESER M., HABS D., JAESCHKE E., KRÄMER D., KRISTENSEN M., MUSIC M., PETRICH W., SCHWALM D., SIGRAY P., STECK M., WANNER B. AND WOLF A. **First laser cooling of relativistic ions in a storage ring.** *Physical Review Letters* **64(24)** (1990) 2901–2904.
<http://dx.doi.org/10.1103/PhysRevLett.64.2901>

- [61] EISENBARTH U., EIKE B., GRIESER M., GRIMM R., LAUER I., LENISA P., LUGER V., MUDRICH M., SCHÄTZ T., SCHRAMM U., SCHWALM D. AND WEIDEMÜLLER M. **Laser cooling of fast stored ions in barrier buckets.** *Nuclear Instruments and Methods in Physics Research Section A* **441(1-2)** (2000) 209–218.
[http://dx.doi.org/10.1016/S0168-9002\(99\)01135-3](http://dx.doi.org/10.1016/S0168-9002(99)01135-3)
- [62] MADSEN N., BOWE P., NIELSEN J.S., SIEGFRIED L.E. AND HANGST J.S. **Low-Current, Vertical Blowup in a Stored Laser-Cooled Ion Beam.** *Physical Review Letters* **87(27)** (2001) 274801.
<http://dx.doi.org/10.1103/PhysRevLett.87.274801>
- [63] POTH H. **Electron cooling: Theory, experiment, application.** *Physics Reports* **196(3-4)** (1990) 135–297.
[http://dx.doi.org/10.1016/0370-1573\(90\)90040-9](http://dx.doi.org/10.1016/0370-1573(90)90040-9)
- [64] MESHKOV I. **Electron cooling – recent developments and trends.** *Nuclear Physics A* **626(1-2)** (1997) 459–471.
[http://dx.doi.org/10.1016/S0375-9474\(97\)00570-8](http://dx.doi.org/10.1016/S0375-9474(97)00570-8)
- [65] STECK M., BECKERT K., EICKHOFF H., FRANZKE B., NOLDEN F., REICH H., SCHLITT B. AND WINKLER T. **Anomalous Temperature Reduction of Electron-Cooled Heavy Ion Beams in the Storage Ring ESR.** *Physical Review Letters* **77(18)** (1996) 3803–3806.
<http://dx.doi.org/10.1103/PhysRevLett.77.3803>
- [66] STECK M., BECKERT K., EICKHOFF H., FRANZKE B., NOLDEN F., REICH H., SPÄDTKE P. AND WINKLER T. **Suppression of intrabeam scattering in cooled heavy ion beams.** *Hyperfine Interactions* **99(1)** (1996) 245–251.
<http://dx.doi.org/10.1007/BF02274927>
- [67] DANARED H., KÄLLBERG A., RENFELT K.G. AND SIMONSSON A. **Model and Observations of Schottky-Noise Suppression in a Cold Heavy-Ion Beam.** *Physical Review Letters* **88(17)** (2002) 174801.
<http://dx.doi.org/10.1103/PhysRevLett.88.174801>
- [68] DANARED H., KÄLLBERG A. AND SIMONSSON A. **One-dimensional ordering in coasting and bunched beams.** *Journal of Physics B* **36(5)** (2003) 1003–1010.
<http://dx.doi.org/10.1088/0953-4075/36/5/319>
- [69] NODA A., IKEGAMI M. AND SHIRAI T. **Approach to ordered structure of the beam at S-LSR.** *New Journal of Physics* **8(11)** (2006) 288.
<http://dx.doi.org/10.1088/1367-2630/8/11/288>
- [70] SHIRAI T., IKEGAMI M., FUJIMOTO S., SOUDA H., TANABE M., TONGU H., NODA A., NODA K., FUJIMOTO T., IWATA S., SHIBUYA S., SMIRNOV A., MESHKOV I., FADIL H. AND GRIESER M. **One-Dimensional Beam Ordering of Protons in a Storage Ring.** *Physical Review Letters* **98(20)** 204801.
<http://dx.doi.org/10.1103/PhysRevLett.98.204801>
- [71] DEMENT'EV E., DIKANSKII N., MEDVEDKO A.S.; PARKHOMCHUK V. AND PESTRIKOV D. **Measurement of the thermal noise of a proton beam in the NAP-M storage ring.** *Zhurnal Tekhnicheskoi Fiziki* **50(8)** (1980) 1717–1721
- [72] THOMPSON R.C. **Precision measurement aspects of ion traps.** *Measurement Science and Technology* **1(2)** (1990) 93–105.
<http://dx.doi.org/10.1088/0957-0233/1/2/001>

- [73] BOLLEN G. AND SCHWARZ S. **Penning trap mass measurements on rare isotopes – status and new developments.** *Journal of Physics B* **36(5)** (2003) 941–951.
<http://dx.doi.org/10.1088/0953-4075/36/5/313>
- [74] LUNNEY D., PEARSON J.M. AND THIBAUT C. **Recent trends in the determination of nuclear masses.** *Reviews of Modern Physics* **75(3)** (2003) 1021–1082.
<http://dx.doi.org/10.1103/RevModPhys.75.1021>
- [75] BLAUM K. **High-accuracy mass spectrometry with stored ions.** *Physics Reports* **425(1)** (2006) 1–78.
<http://dx.doi.org/10.1016/j.physrep.2005.10.011>
- [76] SCHEIDENBERGER C. **The contribution of precision mass measurements to nuclear physics.** *Nuclear Physics A* **751** (2005) 209–225.
<http://dx.doi.org/10.1016/j.nuclphysa.2005.02.006>
- [77] WERTH G. **Tests of quantum electrodynamics using ion traps.** *Hyperfine Interactions* **172(1)** (2006) 125–134.
<http://dx.doi.org/10.1007/s10751-007-9531-6>
- [78] SCHILLER S. **Hydrogenlike Highly Charged Ions for Tests of the Time Independence of Fundamental Constants.** *Physical Review Letters* **98(18)** 180801.
<http://dx.doi.org/10.1103/PhysRevLett.98.180801>
- [79] LARSON D.J., BERGQUIST J.C., BOLLINGER J.J., ITANO W.M. AND WINELAND D.J. **Sympathetic cooling of trapped ions: A laser-cooled two-species nonneutral ion plasma.** *Physical Review Letters* **57(1)** (1986) 70–73.
<http://dx.doi.org/10.1103/PhysRevLett.57.70>
- [80] BOWE P., HORNEKÆR L., BRODERSEN C., DREWSSEN M., HANGST J.S. AND SCHIFFER J.P. **Sympathetic Crystallization of Trapped Ions.** *Physical Review Letters* **82(10)** (1999) 2071–2074.
<http://dx.doi.org/10.1103/PhysRevLett.82.2071>
- [81] BARRETT M.D., DEMARCO B., SCHÄTZ T., MEYER V., LEIBFRIED D., BRITTON J., CHIAVERINI J., ITANO W.M., JELENKOVIĆ B., JOST J.D., LANGER C., ROSEN BAND T. AND WINELAND D.J. **Sympathetic cooling of ${}^9\text{Be}^+$ and ${}^{24}\text{Mg}^+$ for quantum logic.** *Physical Review A* **68(4)** (2003) 042302.
<http://dx.doi.org/10.1103/PhysRevA.68.042302>
- [82] DREWSSEN M., MORTENSEN A., MARTINUSSEN R., STAANUM P. AND SORENSEN J.L. **Nondestructive Identification of Cold and Extremely Localized Single Molecular Ions.** *Physical Review Letters* **93(24)** 243201.
<http://dx.doi.org/10.1103/PhysRevLett.93.243201>
- [83] MAJOR F., GHEORGE V. AND WERTH G. *Charged Particle Traps* (Springer Berlin Heidelberg New York, **2005**)
- [84] ROTH B., FROHLICH U. AND SCHILLER S. **Sympathetic Cooling of ${}^4\text{He}^+$ Ions in a Radio-Frequency Trap.** *Physical Review Letters* **94(5)** 053001.
<http://dx.doi.org/10.1103/PhysRevLett.94.053001>
- [85] TOLEIKIS S., MARUYAMA R., CHURCH D., SCHNEIDER D., FREEDMAN S., KOMINIS I. AND VETTER P. **RETrap - a cryogenic Penning ion trap system.** *Nuclear Instruments and Methods in Physics Research Section B* **235(1-4)** (2005)

479–481.

<http://dx.doi.org/10.1016/j.nimb.2005.03.228>

- [86] OSTENDORF A., ZHANG C.B., WILSON M.A., OFFENBERG D., ROTH B. AND SCHILLER S. **Sympathetic Cooling of Complex Molecular Ions to Millikelvin Temperatures.** *Physical Review Letters* **97(24)** 243005.
<http://dx.doi.org/10.1103/PhysRevLett.97.243005>
- [87] ROTH B., BLYTHE P. AND SCHILLER S. **Motional resonance coupling in cold multispecies Coulomb crystals.** *Physical Review A* **75(2)** 023402.
<http://dx.doi.org/10.1103/PhysRevA.75.023402>
- [88] KWAPIEŃ T., EICHMANN U. AND SANDNER W. **Sympathetic cooling of laser-produced doubly charged ions in a few-ion crystal.** *Physical Review A* **75(6)** 063418.
<http://dx.doi.org/10.1103/PhysRevA.75.063418>
- [89] DREWSSEN M. AND BRØNER A. **Harmonic linear Paul trap: Stability diagram and effective potentials.** *Physical Review A* **62(4)** (2000) 045401.
<http://dx.doi.org/10.1103/PhysRevA.62.045401>
- [90] BLOCK M., ACKERMANN D., BECK D., BLAUM K., BREITENFELDT M., CHAUDURI A., DOEMER A., ELISEEV S., HABS D., HEINZ S., HERFURTH F., HESSBERGER F.P., HOFMANN S., GEISSEL H., KLUGE H.J., KOLHINEN V., MARX G., NEUMAYR J.B., MUKHERJEE M., PETRICK M., PLASS W., QUINT W., RAHAMAN S., RAUTH C., RODRIGUEZ D., SCHEIDENBERGER C., SCHWEIKHARD L., SUHONEN M., THIROLF P.G., WANG Z. AND WEBER C. **The ion-trap facility SHIPTRAP - Status and perspectives.** *The European Physical Journal A* **25(s1)** (2005) s1.49–s1.50.
<http://dx.doi.org/10.1140/epjad/i2005-06-013-5>
- [91] SAVARD G., BUCHINGER F., CLARK J.A., CRAWFORD J.E., GULICK S., HARDY J.C., HECHT A.A., LEE J.K.P., LEVAND A.F., SCIELZO N.D., SHARMA H., SHARMA K.S., TANIHATA I., VILLARI A.C.C. AND WANG Y. **Q Value of the Superaligned Decay of ^{46}V and Its Influence on V_{ud} and the Unitarity of the Cabibbo-Kobayashi-Maskawa Matrix.** *Physical Review Letters* **95(10)** (2005) 102501.
<http://dx.doi.org/10.1103/PhysRevLett.95.102501>
- [92] NAGY S., FRITIOFF T., SUHONEN M., SCHUCH R., BLAUM K., BJÖRKHAGE M. AND BERGSTRÖM I. **New Mass Value for ^7Li .** *Physical Review Letters* **96(16)** 163004.
<http://dx.doi.org/10.1103/PhysRevLett.96.163004>
- [93] GUÉNAUT C., AUDI G., BECK D., BLAUM K., BOLLEN G., DELAHAYE P., HERFURTH F., KELLERBAUER A., KLUGE H.J., LIBERT J., LUNNEY D., SCHWARZ S., SCHWEIKHARD L. AND YAZIDJIAN C. **High-precision mass measurements of nickel, copper, and gallium isotopes and the purported shell closure at $N = 40$.** *Physical Review C* **75(4)** 044303.
<http://dx.doi.org/10.1103/PhysRevC.75.044303>
- [94] HAGER U., ELOMAA V.V., ERONEN T., HAKALA J., JOKINEN A., KANKAINEN A., RAHAMAN S., RINTA-ANTILA S., SAASTAMOINEN A., SONODA T. AND ÄYSTÖ J. **Precision mass measurements of neutron-rich Tc, Ru, Rh, and Pd isotopes.** *Physical Review C* **75(6)** 064302.
<http://dx.doi.org/10.1103/PhysRevC.75.064302>

- [95] RINGLE R., SUN T., BOLLEN G., DAVIES D., FACINA M., HUIKARI J., KWAN E., MORRISSEY D.J., PRINKE A., SAVORY J., SCHURY P., SCHWARZ S. AND SUMITHRARACHCHI C.S. **High-precision Penning trap mass measurements of $^{37,38}\text{Ca}$ and their contributions to conserved vector current and isobaric mass multiplet equation.** *Physical Review C* **75(5)** 055503.
<http://dx.doi.org/10.1103/PhysRevC.75.055503>
- [96] PINEGAR D., ZAFONTE S. AND VAN DYCK R. **Dynamical processes in complex plasmas.** *Hyperfine Interactions* **174(1)** (2007) 47–53.
<http://dx.doi.org/10.1007/s10751-007-9563-y>
- [97] DILLING J., BAARTMAN R., BRICAULT P., BRODEUR M., BLOMELEY L., BUCHINGER F., CRAWFORD J., CRESPO LOPEZ-URRUTIA J., DELHEIJ P., FROESE M., GWINNER G., KE Z., LEE J., MOORE R., RYJKOV V., SIKLER G., SMITH M., ULLRICH J. AND VAZ J. **Mass measurements on highly charged radioactive ions, a new approach to high precision with TITAN.** *International Journal of Mass Spectrometry* **251(2-3)** (2006) 198–203.
<http://dx.doi.org/10.1016/j.ijms.2006.01.044>
- [98] HERFURTH F., BEIER T., DAHL L., ELISEEV S., HEINZ S., KESTER O., KOZHUHAROV C., MAERO G. AND QUINT W. **Precision measurements with highly charged ions at rest: The HITRAP project at GSI.** *International Journal of Mass Spectrometry* **251(2-3)** (2006) 266–272.
<http://dx.doi.org/10.1016/j.ijms.2006.02.012>
- [99] MITTIG W., LEPINE-SZILY A. AND ORR N.A. **Mass Measurement far from Stability.** *Annual Review of Nuclear and Particle Science* **47(1)** (1997) 27–66.
<http://dx.doi.org/10.1146/annurev.nucl.47.1.27>
- [100] OLIVER KESTER F.W. AND BECKER R. **Charge breeding of stable and radioactive ion beams with EBIS/T devices.** *Journal of Physics: Conference Series* **2** (2004) 107–116.
<http://dx.doi.org/10.1088/1742-6596/2/1/014>
- [101] ALONSO J., BLAUM K., DJEKIC S., KLUGE H.J., QUINT W., SCHABINGER B., STAHL S., VERDU J., VOGEL M. AND WERTH G. **A miniature electron-beam ion source for in-trap creation of highly charged ions.** *Review of Scientific Instruments* **77(3)** 03A901.
<http://dx.doi.org/10.1063/1.2162857>
- [102] WIES K., GEPPERT C., BLAUM K., BRÜCK K., KLUGE H.J., SCHWARZ S. AND WENDT K. **Development Towards a Laser Ion Source Trap for the Production of Exotic Species.** *Hyperfine Interactions* **162(1)** (2005) 29–38.
<http://dx.doi.org/10.1007/s10751-005-9207-z>
- [103] ACHTZEHN T., LASSEN J., BRICAULT P., ALBERS D., COCOLIOS T., DOMBSKY M., HANEMAAYER V., LAVOIE J., LECESNE N., PEARSON M., PRIME E. AND WENDT K. **^{26}Al beam production by a solid state laser ion source at TRIUMF.** *Hyperfine Interactions* **174(1)** (2007) 27–32.
<http://dx.doi.org/10.1007/s10751-007-9560-1>
- [104] SAVARD G., BECKER S., BOLLEN G. AND KLUGE H.J., MOORE R.B., OTTO T., SCHWEIKHARD L. AND STOLZENBERG H. AND WIESS U. **A new cooling technique for heavy ions in a Penning trap.** *Physics Letters A* **158(5)** (1991) 247–252.
[http://dx.doi.org/10.1016/0375-9601\(91\)91008-2](http://dx.doi.org/10.1016/0375-9601(91)91008-2)

- [105] NEUMAYR J.B., THIROLF P.G., HABS D., HEINZ S., KOLHINEN V.S., SEWTZ M. AND SZERYPO J. **Performance of the MLL-IonCatcher.** *Review of Scientific Instruments* **77(6)** 065109.
<http://dx.doi.org/10.1063/1.2213154>
- [106] ROLSTON S. AND GABRIELSE G. **Cooling antiprotons in an ion trap.** *Hyperfine Interactions* **44(1)** (1989) 233–245.
<http://dx.doi.org/10.1007/BF02398673>
- [107] BRUNNER S., ENGEL T., SCHMITT A. AND WERTH G. **Determination of the helium-4 mass in a Penning trap.** *The European Physical Journal D* **15(2)** (2001) 181–188.
<http://dx.doi.org/10.1007/s100530170164>
- [108] GABRIELSE G., FEI X., OROZCO L.A., TJOELKER R.L., HAAS J., KALINOWSKY H., TRAINOR T.A. AND KELLS W. **Cooling and slowing of trapped antiprotons below 100 meV.** *Physical Review Letters* **63(13)** (1989) 1360–1363.
<http://dx.doi.org/10.1103/PhysRevLett.63.1360>
- [109] HALL D.S. AND GABRIELSE G. **Electron Cooling of Protons in a Nested Penning Trap.** *Physical Review Letters* **77(10)** (1996) 1962–1965.
<http://dx.doi.org/10.1103/PhysRevLett.77.1962>
- [110] **Coherent Inc., 5100 Patrick Henry Drive, Santa Clara, CA 95054 USA.**
<http://www.coherent.com>
- [111] DEMTRÖDER W. *Laser Spectroscopy: Basic Concepts and Instrumentation* (Springer Berlin Heidelberg New York, 2002)
- [112] SAATHOFF G., KARPUK S., EISENBARTH U., HUBER G., KROHN S., HORTA R.M.N., REINHARDT S., SCHWALM D., WOLF A. AND GWINNER G. **Improved Test of Time Dilation in Special Relativity.** *Physical Review Letters* **91(19)** (2003) 190403.
<http://dx.doi.org/10.1103/PhysRevLett.91.190403>
- [113] **Laseroptik, Gneisenaustrasse 14, D-30826 Garbsen, Germany.**
<http://www.laseroptik.de>
- [114] HÄNSCH T.W. AND COUILLAUD B. **Laser frequency stabilization by polarization spectroscopy of a reflecting reference cavity.** *Optics Communications* **35** (1980) 441–444.
[http://dx.doi.org/10.1016/0030-4018\(80\)90069-3](http://dx.doi.org/10.1016/0030-4018(80)90069-3)
- [115] **DÖHRER Elektrooptik GmbH, Ettlinger Strasse 5, D-76307 Karlsbad, Germany.**
<http://www.doehrer.com/>
- [116] **Crystals of Siberia Ltd., 43 Russkaya str., Novosibirsk 630058 Russia.**
<http://www.crystalsofsiberia.com>
- [117] BOYD G.D. AND KLEINMAN D.A. **Parametric Interaction of Focused Gaussian Light Beams.** *Journal of Applied Physics* **39(8)** (1968) 3597–3639.
<http://dx.doi.org/10.1063/1.1656831>
- [118] NÖRTERSCHÄUSER W., DAX A., EWALD G., KATAYAMA I., KIRCHNER R., KLUGE H.J., KÜHL T., SANCHEZ R., TANIHATA I., TOMASELLI M., WANG H. AND ZIMMERMANN C. **A setup for high-resolution isotope shift measurements on unstable lithium isotopes.** *Nuclear Instruments and Methods in*

- Physics Research Section B* **204** (2003) 644–648.
[http://dx.doi.org/10.1016/S0168-583X\(02\)02145-6](http://dx.doi.org/10.1016/S0168-583X(02)02145-6)
- [119] **New Focus Corporate Office, 2584 Junction Avenue, San Jose, CA 95134 USA.**
<http://www.newfocus.com>
- [120] CHATTOPADHYAY S. **Some Fundamental Aspects of Fluctuations and Coherence in Charged-Particle Beams in Storage Rings.** *CERN SPS* **84-11** (1984) 1–155
<http://cdsweb.cern.ch/record/155458>
- [121] BOUSSARD D. **Schottky Noise and Beam Transfer Function Diagnostics.** *CERN Accelerator School* **87-03(1)** (1987) 416–452.
<http://dx.doi.org/10.1103/PhysRevSTAB.8.034201>
- [122] STECK M. **Cooling of fast charged particle beams.** *Journal of the Optical Society of America B* **20(5)** (2003) 1016–1027
<http://josab.osa.org/abstract.cfm?id=71946>
- [123] ELLISON T.J.P., NAGAITSEV S.S., BALL M.S., CAUSSYN D.D., ELLISON M.J. AND HAMILTON B.J. **Attainment of space-charge dominated beams in a synchrotron.** *Physical Review Letters* **70(6)** (1993) 790–793.
<http://dx.doi.org/10.1103/PhysRevLett.70.790>
- [124] DUBIN D. **Minimum energy state of the one-dimensional Coulomb chain.** *Physical Review E* **55(4)** (1997) 4017–4028.
<http://dx.doi.org/10.1103/PhysRevE.55.4017>
- [125] JAMES D. **Quantum dynamics of cold trapped ions with application to quantum computation.** *Applied Physics B* **66(2)** (1998) 181–190.
<http://dx.doi.org/10.1007/s003400050373>
- [126] BOINE-FRANKENHEIM O. AND SHUKLA T. **Space charge effects in bunches for different rf wave forms.** *Physical Review Special Topics - Accelerators and Beams* **8(3)** (2005) 034201.
<http://dx.doi.org/10.1103/PhysRevSTAB.8.034201>
- [127] EDLÉN B. **Comparison of Theoretical and Experimental Level Values of the $n = 2$ Complex in Ions Isoelectronic with Li, Be, O and F.** *Physica Scripta* **28(1)** (1983) 51–67.
<http://dx.doi.org/10.1088/0031-8949/28/1/007>
- [128] KIM Y.K., BAIK D.H., INDELICATO P. AND DESCLAUX J.P. **Resonance transition energies of Li-, Na-, and Cu-like ions.** *Physical Review A* **44(1)** (1991) 148–166.
<http://dx.doi.org/10.1103/PhysRevA.44.148>
- [129] JOHNSON W.R., LIU Z.W. AND SAPIRSTEIN J. **Transition Rates for Lithium-like Ions, Sodium-like Ions, and Neutral Alkali-Metal Atoms.** *Atomic Data and Nuclear Data Tables* **64(2)** (1996) 279–300.
<http://dx.doi.org/10.1006/adnd.1996.0024>
- [130] BACKE H. **Precision spectroscopy at heavy ion ring accelerator SIS300.** *Hyperfine Interactions* **171(1)** (2006) 93–107.
<http://dx.doi.org/10.1007/s10751-007-9509-4>

- [131] KESTER O. *Entwicklung einer Elektronenstrahlionenquelle mit "schneller" Ionenextraktion zur Anwendung bei der Strahlentherapie mit leichten Ionen*. Ph.D. thesis, Johann-Wolfgang-Goethe Universität, Frankfurt (1995)
- [132] EWALD P.P. **Die Berechnung optischer und elektrostatischer Gitterpotentiale**. *Annalen der Physik* **369(3)** (1921) 253–287.
<http://dx.doi.org/10.1002/andp.19213690304>
- [133] ESSELINK K. **A comparison of algorithms for long-range interactions**. *Computer Physics Communications* **87(3)** (1995) 375–395.
[http://dx.doi.org/10.1016/0010-4655\(95\)00003-X](http://dx.doi.org/10.1016/0010-4655(95)00003-X)
- [134] POLLOCK E.L. AND GLOSLI J. **Comments on P3M, FMM, and the Ewald method for large periodic Coulombic systems**. *Computer Physics Communications* **95(2-3)** (1996) 93–110.
[http://dx.doi.org/10.1016/0010-4655\(96\)00043-4](http://dx.doi.org/10.1016/0010-4655(96)00043-4)
- [135] PORTO M. **Ewald summation of electrostatic interactions of systems with finite extent in two of three dimensions**. *Journal of Physics A* **33(35)** (2000) 6211–6218.
<http://dx.doi.org/10.1088/0305-4470/33/35/309>
- [136] LANGRIDGE D.J., HART J.F. AND CRAMPIN S. **Ewald summation technique for one-dimensional charge distributions**. *Computer Physics Communications* **134(1)** (2001) 78–85.
[http://dx.doi.org/10.1016/S0010-4655\(02\)00452-6](http://dx.doi.org/10.1016/S0010-4655(02)00452-6)
- [137] HOCKNEY R. AND EASTWOOD J. *Computer Simulation using Particles* (Adam Hilger, Bristol and Philadelphia, 1988)
- [138] BARNES J. AND HUT P. **A hierarchical $O(N \log N)$ force-calculation algorithm**. *Nature* **324(6096)** (1986) 446–449.
<http://dx.doi.org/10.1038/324446a0>
- [139] RAPAPORT D. *The Art of Molecular Dynamics Simulation* (Cambridge University Press, Cambridge UK, 1995)
- [140] SUTMANN G. **Classical Molecular Dynamics**. *NIC Series* **10** (2002) 1–46
<http://www.fz-juelich.de/nic-series/volume10/volume10.html>
- [141] WEDEKIND J., REGUERA D. AND STREY R. **Influence of thermostats and carrier gas on simulations of nucleation**. *The Journal of Chemical Physics* **127(6)** 064501.
<http://dx.doi.org/10.1063/1.2752154>
- [142] BEEMAN D. **Some multistep methods for use in molecular dynamics calculations**. *Journal of Computational Physics* **20(2)** (1976) 130–139.
[http://dx.doi.org/10.1016/0021-9991\(76\)90059-0](http://dx.doi.org/10.1016/0021-9991(76)90059-0)
- [143] ENGELN-MÜLLGES G. AND UHLIG F. *Numerical Algorithms with C* (Springer Berlin Heidelberg New York, 1996)
- [144] NOVIK K. AND COVENEY P. **Finite-difference methods for simulation models incorporating nonconservative forces**. *The Journal of Chemical Physics* **109(18)** (1998) 7667–7677.
<http://dx.doi.org/10.1063/1.477413>

- [145] BUTCHER J. *Numerical Methods for Ordinary Differential Equations* (John Wiley and Sons, Ltd., **2003**)
- [146] NOETHER E. **Invariante Variationsprobleme.** *Göttinger Nachrichten* **1918** (1918) 235–257
<http://resolver.sub.uni-goettingen.de/purl/?GDZPPN00250510X>
- [147] PLIMPTON S. **Fast Parallel Algorithms for Short-Range Molecular Dynamics.** *Journal of Computational Physics* **117(1)** (1995) 1–19.
<http://dx.doi.org/10.1006/jcph.1995.1039>
- [148] PLIMPTON S. AND HENDRICKSON B. **A new parallel method for molecular dynamics simulation of macromolecular systems.** *Journal of Computational Chemistry* **17(3)** (1996) 326–337.
[http://dx.doi.org/10.1002/\(SICI\)1096-987X\(199602\)17:3<326::AID-JCC7>3.0.CO;2-X](http://dx.doi.org/10.1002/(SICI)1096-987X(199602)17:3<326::AID-JCC7>3.0.CO;2-X)
- [149] WOLF A., ELLERT C., GRIESER M., HABS D., HOCHADEL B., REPNOW R. AND SCHWALM D. **Charge Dependence of the Electron Cooling Force for Heavy Ions.** *CERN* **94-03** (1994) 416–421
<http://cdsweb.cern.ch/record/398785>
- [150] HANSEN J.P., McDONALD I.R. AND POLLOCK E.L. **Statistical mechanics of dense ionized matter. III. Dynamical properties of the classical one-component plasma.** *Physical Review A* **11(3)** (1975) 1025–1039.
<http://dx.doi.org/10.1103/PhysRevA.11.1025>
- [151] KALMAN G. AND GENGA R. **High-frequency expansion of the plasma dielectric tensor.** *Physical Review A* **33(1)** (1986) 604–610.
<http://dx.doi.org/10.1103/PhysRevA.33.604>
- [152] DONKO Z., HARTMANN P. AND KALMAN G. **Molecular dynamics simulations of strongly coupled plasmas: Localization and microscopic dynamics.** *Physics of Plasmas* **10(5)** (2003) 1563–1568.
<http://dx.doi.org/10.1063/1.1560612>
- [153] KALMAN G., GOLDEN K., DONKO Z. AND HARTMANN P. **The quasilocalized charge approximation.** *Journal of Physics: Conference Series* **11** (2005) 254–267.
<http://dx.doi.org/10.1088/1742-6596/11/1/025>
- [154] CARLSON T., NESTOR JR. C., WASSERMAN N. AND MCDOWELL J. **Calculated ionization potentials for multiply charged ions.** *Atomic Data and Nuclear Data Tables* **2** (1970) 63–99.
[http://dx.doi.org/10.1016/S0092-640X\(70\)80005-5](http://dx.doi.org/10.1016/S0092-640X(70)80005-5)
- [155] CHURCH D.A. **Collision measurements and excited-level lifetime measurements on ions stored in Paul, Penning and Kingdon ion traps.** *Physics Reports* **228(5-6)** (1993) 253–358.
[http://dx.doi.org/10.1016/0370-1573\(93\)90030-H](http://dx.doi.org/10.1016/0370-1573(93)90030-H)
- [156] CEDERQUIST H., BIEDERMANN C., SELBERG N. AND HVELPLUND P. **Oscillations in mean capture Q values as functions of the projectile charge in slow $Xe^{q+} - He(25 \leq q \leq 44)$ collisions.** *Physical Review A* **51(3)** (1995) 2191–2198.
<http://dx.doi.org/10.1103/PhysRevA.51.2191>

- [157] BECK B.R., STEIGER J., WEINBERG G., CHURCH D.A., McDONALD J. AND SCHNEIDER D. **Measurement of Charge Exchange between H₂ and Low-Energy Ions with Charge States $35 \leq q \leq 80$.** *Physical Review Letters* **77(9)** (1996) 1735–1738.
<http://dx.doi.org/10.1103/PhysRevLett.77.1735>
- [158] SUZUKI K., OKUNO K. AND KOBAYASHI N. **Single- and multiple-charge changing cross sections in slow collisions of Ar^{q+} (q=4-9) with Ne.** *Physica Scripta* **T73** (1997) 172–174.
<http://dx.doi.org/10.1088/0031-8949/1997/T73/050>
- [159] OKUNO K., SAITOH H., SOEJIMA K., KRAVIS S.D. AND KOBAYASHI N. **Mini-EBIS report on electron capture in slow collisions of multiply charged ions with neutral targets.** *Physica Scripta* **T71** (1997) 140–146.
<http://dx.doi.org/10.1088/0031-8949/1997/T71/026>
- [160] ISHII K., OKUNO K. AND KOBAYASHI N. **Single- and Multiple-Charge Changing Cross Sections in Slow Collisions of Kr^{q+} (q=7-9) with Ne, N₂, O₂ and CO.** *Physica Scripta* **T80B** (1999) 176–178.
<http://dx.doi.org/10.1238/Physica.Topical.080a00176>
- [161] TRASSL R., BRÄUNING H., v. DIEMAR K., MELCHERT F., SALZBORN E. AND HOFMANN I. **Ion-ion charge-exchange collisions and applications.** *AIP Conference Proceedings of the Twelfth Topical Conference on Atomic Processes in Plasmas (Reno, Nevada(USA))* **547(1)** (2000) 157–166.
<http://dx.doi.org/10.1063/1.1361787>
- [162] MELCHERT F. AND SALZBORN E. **Charge-changing ion-ion collisions.** *AIP Conference Proceedings of the International Conference on The Physics of Electronic and Atomic Collisions, ICPEAC XXI (Sendai, Japan)* **500(1)** (2000) 478–494.
<http://dx.doi.org/10.1063/1.1302680>
- [163] DIEHL A., BRÄUNING H., TRASSL R., HATHIRAMANI D., THEISS A., KERN H., SALZBORN E. AND HOFMANN I. **Charge transfer and ionization in collisions between multiply charged noble gas ions.** *Journal of Physics B* **34(20)** (2001) 4073–4081.
<http://dx.doi.org/10.1088/0953-4075/34/20/317>
- [164] OLSON R.E. AND SALOP A. **Electron transfer between multicharged ions and neutral species.** *Physical Review A* **14(2)** (1976) 579–585.
<http://dx.doi.org/10.1103/PhysRevA.14.579>
- [165] TURCHETTE Q.A., KIELPINSKI, KING B.E., LEIBFRIED D., MEEKHOF D.M., MYATT C.J., ROWE M.A., SACKETT C.A., WOOD C.S., ITANO W.M., MONROE C. AND WINELAND D.J. **Heating of trapped ions from the quantum ground state.** *Physical Review A* **61(6)** (2000) 063418.
<http://dx.doi.org/10.1103/PhysRevA.61.063418>
- [166] EPSTEIN R.J., SEIDELIN S., LEIBFRIED D., WESENBERG J.H., BOLLINGER J.J., AMINI J.M., BLAKESTAD R.B., BRITTON J., HOME J.P., ITANO W.M., JOST J.D., KNILL E., LANGER C., OZERI R., SHIGA N. AND WINELAND D.J. **Simplified motional heating rate measurements of trapped ions.** *Physical Review A* **76(3)** (2007) 033411.
<http://dx.doi.org/10.1103/PhysRevA.76.033411>

- [167] PESTRIKOV D. **Schottky Spectra and Crystalline Beams.** *Nuclear Instruments and Methods in Physics Research Section A* **379(1)** (1996) 1–14.
[http://dx.doi.org/10.1016/0168-9002\(96\)00640-7](http://dx.doi.org/10.1016/0168-9002(96)00640-7)
- [168] HASSE R.W. **Theoretical Verification of Coulomb Order of Ions in a Storage Ring.** *Physical Review Letters* **83(17)** (1999) 3430–3433.
<http://dx.doi.org/10.1103/PhysRevLett.83.3430>
- [169] OKAMOTO H., YURI Y. AND OKABE K. **Oscillating Coulomb chain in a storage ring.** *Physical Review E* **67(4)** (2003) 046501.
<http://dx.doi.org/10.1103/PhysRevE.67.046501>
- [170] HASSE R.W. **Static Criteria for the Existence of Coulomb Strings in Storage Rings.** *Physical Review Letters* **90(20)** (2003) 204801.
<http://dx.doi.org/10.1103/PhysRevLett.90.204801>
- [171] FORTOV V., IVLEV A., KHRAPAK S., KHRAPAK A. AND MORFILL G. **Complex (dusty) plasmas: Current status, open issues, perspectives.** *Physics Reports* **421(1-2)** (2005) 1–103.
<http://dx.doi.org/10.1016/j.physrep.2005.08.007>
- [172] OHTA H. AND HAMAGUCHI S. **Wave Dispersion Relations in Yukawa Fluids.** *Physical Review Letters* **84(26)** (2000) 6026–6029.
<http://dx.doi.org/10.1103/PhysRevLett.84.6026>
- [173] WANG X., BHATTACHARJEE A. AND HU S. **Longitudinal and Transverse Waves in Yukawa Crystals.** *Physical Review Letters* **86(12)** (2001) 2569–2572.
<http://dx.doi.org/10.1103/PhysRevLett.86.2569>
- [174] NASIM M.H., MIRZA A., QAISAR M.S., MURTAZA G. AND SHUKLA P. **Energy loss of charged projectiles in dusty plasmas.** *Physics of Plasmas* **5(10)** (1998) 3581–3587.
<http://dx.doi.org/10.1063/1.873077>
- [175] NASIM M., MIRZA A., MURTAZA G. AND SHUKLA P. **Energy Loss of a Test Charge in Dusty Plasmas: Collective and Individual Particle Contributions.** *Physica Scripta* **59(5)** (1999) 379–388.
<http://dx.doi.org/10.1238/Physica.Regular.059a00379>
- [176] PIEL A. AND MELZER A. **Dynamical processes in complex plasmas.** *Plasma Physics and Controlled Fusion* **44(1)** (2002) R1–R26.
<http://dx.doi.org/10.1088/0741-3335/44/1/201>
- [177] PIEL A., HOMANN A., KLINDWORTH M., MELZER A., ZAFIU C., NOSENKO V. AND GOREE J. **Waves and oscillations in plasma crystals.** *Journal of Physics B* **36(3)** (2003) 533–543.
<http://dx.doi.org/10.1088/0953-4075/36/3/311>
- [178] BALLESTER D., FUENTES A. AND TKACHENKO I.M. **Fast-projectile stopping power of two-dimensional strongly correlated electron liquids.** *Europhysics Letters* **75(5)** (2006) 791–796.
<http://dx.doi.org/10.1209/epl/i2006-10169-6>
- [179] HOU L.J., MISKOVIC Z., JIANG K. AND WANG Y.N. **Energy Loss of a Charged Particle Moving over a 2D Strongly Coupled Dusty Plasma.** *Physical Review Letters* **96(25)** 255005.
<http://dx.doi.org/10.1103/PhysRevLett.96.255005>

- [180] JIANG K., HOU L., WANG Y. AND MISKOVIC Z. **Excitation of Mach cones and energy dissipation by charged particles moving over two-dimensional strongly coupled dusty plasmas.** *Physical Review E* **73(1)** (2006) 016404.
<http://dx.doi.org/10.1103/PhysRevE.73.016404>
- [181] OKAMOTO H. AND WEI J. **Theory of tapered cooling.** *Physical Review E* **58(3)** (1998) 3817–3825.
<http://dx.doi.org/10.1103/PhysRevE.58.3817>
- [182] FRIEDENAUER A., MARKERT F., SCHMITZ H., PETERSEN L., KAHRA S., HERMANN M., UDEM T., HÄNSCH T. AND SCHÄTZ T. **High power all solid state laser system near 280 nm.** *Applied Physics B* **84(3)** (2006) 371–373.
<http://dx.doi.org/10.1007/s00340-006-2274-2>
- [183] BECK B.R., BECKER J.A., BEIERSDORFER P., BROWN G.V., MOODY K.J., WILHELMI J.B., PORTER F.S., KILBOURNE C.A. AND KELLEY R.L. **Energy Splitting of the Ground-State Doublet in the Nucleus ^{229}Th .** *Physical Review Letters* **98(14)** (2007) 142501.
<http://dx.doi.org/10.1103/PhysRevLett.98.142501>
- [184] BROWNE E., NORMAN E.B., CANAAN R.D., GLASGOW D.C., KELLER J.M. AND YOUNG J.P. **Search for decay of the 3.5-eV level in ^{229}Th .** *Physical Review C* **64(1)** (2001) 014311.
<http://dx.doi.org/10.1103/PhysRevC.64.014311>
- [185] DYKHNE A. AND TKALYA E. **Matrix element of the anomalously low-energy (3.5 ± 0.5 eV) transition in ^{229}Th and the isomer lifetime.** *JETP Letters* **67(4)** (1998) 251–256.
<http://dx.doi.org/10.1134/1.567659>
- [186] TKALYA E.V., ZHERIKHIN A.N. AND ZHUDOV V.I. **Decay of the low-energy nuclear isomer $^{229}\text{Th}^m(3/2^+, 3.5 \pm 1.0$ eV) in solids (dielectrics and metals): A new scheme of experimental research.** *Physical Review C* **61(6)** (2000) 064308.
<http://dx.doi.org/10.1103/PhysRevC.61.064308>
- [187] BIZE S., DIDDAMS S.A., TANAKA U., TANNER C.E., OSKAY W.H., DRULLINGER R.E., PARKER T.E., HEAVNER T.P., JEFFERTS S.R., HOLLBERG L., ITANO W.M. AND BERGQUIST J.C. **Testing the Stability of Fundamental Constants with the $^{199}\text{Hg}^+$ Single-Ion Optical Clock.** *Physical Review Letters* **90(15)** (2003) 150802.
<http://dx.doi.org/10.1103/PhysRevLett.90.150802>
- [188] PEIK E., LIPPHARDT B., SCHNATZ H., SCHNEIDER T., TAMM C. AND KARSHENBOIM S.G. **Limit on the Present Temporal Variation of the Fine Structure Constant.** *Physical Review Letters* **93(17)** 170801.
<http://dx.doi.org/10.1103/PhysRevLett.93.170801>
- [189] DIDDAMS S.A., BERGQUIST J.C., JEFFERTS S.R. AND OATES C.W. **Standards of Time and Frequency at the Outset of the 21st Century.** *Science* **306(5700)** (2004) 1318–1324.
<http://dx.doi.org/10.1126/science.1102330>
- [190] KARSHENBOIM S.G. AND PEIK E. (eds.). *Astrophysics, Clocks and Fundamental Constants, Lecture Notes in Physics*, vol. 648 (Springer Berlin Heidelberg New York, 2004)

- [191] UZAN J.P. **The fundamental constants and their variation: observational and theoretical status.** *Reviews of Modern Physics* **75(2)** (2003) 403–455.
<http://dx.doi.org/10.1103/RevModPhys.75.403>
- [192] FLAMBAUM V.V. **Enhanced Effect of Temporal Variation of the Fine Structure Constant and the Strong Interaction in ^{229}Th .** *Physical Review Letters* **97(9)** 092502.
<http://dx.doi.org/10.1103/PhysRevLett.97.092502>
- [193] PEIK E. AND TAMM C. **Nuclear laser spectroscopy of the 3.5 eV transition in Th-229.** *Europhysics Letters* **61(2)** (2003) 181–186.
<http://dx.doi.org/10.1209/epl/i2003-00210-x>
- [194] NEUMAYR J. private communication (2007)
- [195] **Korth Kristalle GmbH, Am Jägersberg 3, D-24161 Altenholz, Germany.**
<http://www.korth.de>
- [196] **Sens-Tech Limited, Bury street, Ruislip, HA4 7TA, United Kingdom.**
<http://www.sens-tech.com>
- [197] HELMER R.G. AND REICH C.W. **An excited state of ^{229}Th at 3.5 eV.** *Physical Review C* **49(4)** (1994) 1845–1858.
<http://dx.doi.org/10.1103/PhysRevC.49.1845>
- [198] IRWIN G.M. AND KIM K.H. **Observation of Electromagnetic Radiation from Deexcitation of the ^{229}Th Isomer.** *Physical Review Letters* **79(6)** (1997) 990–993.
<http://dx.doi.org/10.1103/PhysRevLett.79.990>
- [199] RICHARDSON D.S., BENTON D.M., EVANS D.E., GRIFFITH J.A.R. AND TUNGATE G. **Ultraviolet Photon Emission Observed in the Search for the Decay of the ^{229}Th Isomer.** *Physical Review Letters* **80(15)** (1998) 3206–3208.
<http://dx.doi.org/10.1103/PhysRevLett.80.3206>
- [200] ELISEEV S., BLOCK M., CHAUDHURI A., DI Z., HABS D., HERFURTH F., KLUGE H.J., NEUMAYR J., PLASS W., RAUTH C., THIROLF P., VOROBYEV G. AND WANG Z. **Extraction efficiency and extraction time of the SHIPTRAP gas-filled stopping cell.** *Nuclear Instruments and Methods in Physics Research Section B* **258(2)** (2007) 479–484.
<http://dx.doi.org/10.1016/j.nimb.2007.01.291>
- [201] **Evaluated Nuclear Structure Data File (ENSDF), Database version of November 16, 2007.**
<http://www.nndc.bnl.gov/ensdf/>
- [202] BARCI V., ARDISSON G., BARCI-FUNEL G., WEISS B., EL SAMAD O. AND SHELINE R.K. **Nuclear structure of ^{229}Th from γ -ray spectroscopy study of ^{233}U α -particle decay.** *Physical Review C* **68(3)** (2003) 034329.
<http://dx.doi.org/10.1103/PhysRevC.68.034329>
- [203] UTTER S.B., BEIERSDORFER P., BARNES A., LOUGHEED R.W., CRESPO LÓPEZ-URRUTIA J.R., BECKER J.A. AND WEISS M.S. **Reexamination of the Optical Gamma Ray Decay in ^{229}Th .** *Physical Review Letters* **82(3)** (1999) 505–508.
<http://dx.doi.org/10.1103/PhysRevLett.82.505>

- [204] SHAW R.W., YOUNG J.P., COOPER S.P. AND WEBB O.F. **Spontaneous Ultraviolet Emission from $^{233}\text{Uranium}/^{229}\text{Thorium}$ Samples.** *Physical Review Letters* **82(6)** (1999) 1109–1111.
<http://dx.doi.org/10.1103/PhysRevLett.82.1109>
- [205] KÁLMÁN P. AND BÜKKI T. **Deexcitation of $^{229}\text{Th}^m$: Direct γ decay and electronic-bridge process.** *Physical Review C* **63(2)** (2001) 027601.
<http://dx.doi.org/10.1103/PhysRevC.63.027601>
- [206] HECHT E. *Optics*. 4th edn. (Addison-Wesley Longman, Amsterdam, **2003**)
- [207] **Photomultiplier 9403B, courtesy of Sens-Tech Limited, Bury street, Ruislip, HA4 7TA, United Kingdom.**
<http://www.electrontubes.com/pdf/9403B.pdf>
- [208] SCHÄTZ T. private communication (**2007**)
- [209] TKALYA E.V., VARLAMOV V.O., LOMONOSOV V.V. AND NIKULIN S.A. **Processes of the nuclear isomer $^{229m}\text{Th}(3/2+, 3.5 \pm 1.0 \text{ eV})$ resonant excitation by optical photons.** *Physica Scripta* **53(3)** (1996) 296–299.
<http://dx.doi.org/10.1088/0031-8949/53/3/003>
- [210] CUNDIFF S.T., YE J. AND HALL J.L. **Optical frequency synthesis based on mode-locked lasers.** *Review of Scientific Instruments* **72(10)** (2001) 3749–3771.
<http://dx.doi.org/10.1063/1.1400144>
- [211] KLINKENBERG P.F.A. **Spectral structure of trebly ionized thorium, Th IV.** *Physica B+C* **151(3)** (1988) 552–567.
[http://dx.doi.org/10.1016/0378-4363\(88\)90312-9](http://dx.doi.org/10.1016/0378-4363(88)90312-9)
- [212] WINELAND D.J., BERGQUIST J.C., ITANO W.M. AND DRULLINGER R.E. **Double-resonance and optical-pumping experiments on electromagnetically confined, laser-cooled ions.** *Optics Letters* **5(6)** (1980) 245–247
<http://www.opticsinfobase.org/abstract.cfm?URI=ol-5-6-245>
- [213] DIEDRICH F., BERGQUIST J.C., ITANO W.M. AND WINELAND D.J. **Laser Cooling to the Zero-Point Energy of Motion.** *Physical Review Letters* **62(4)** (1989) 403–406.
<http://dx.doi.org/10.1103/PhysRevLett.62.403>
- [214] MONROE C., MEEKHOF D.M., KING B.E., JEFFERTS S.R., ITANO W.M., WINELAND D.J. AND GOULD P. **Resolved-Sideband Raman Cooling of a Bound Atom to the 3D Zero-Point Energy.** *Physical Review Letters* **75(22)** (1995) 4011–4014.
<http://dx.doi.org/10.1103/PhysRevLett.75.4011>
- [215] STENHOLM S. **Dynamics of trapped particle cooling in the Lamb-Dicke limit.** *Journal of the Optical Society of America B* **2(11)** (1985) 1743
<http://josab.osa.org/abstract.cfm?URI=josab-2-11-1743>
- [216] **Properties of LBO, courtesy of DÖHRER Elektrooptik GmbH, Ettinger Strasse 5, D-76307 Karlsbad, Germany.**
http://www.doehrer.com/download_d/pdf/LBO.pdf
- [217] LIN J. AND KATO K. **Generation of deep-UV sources (160-250 nm) by frequency mixing in lithium-triborate crystal.** *Proceedings of SPIE, Nonlinear Optics, (Los Angeles, California (USA))* **1220(1)** (1990) 58–63.
<http://dx.doi.org/10.1117/12.18306>

- [218] GOHLE C., UDEM T., HERRMANN M., RAUSCHENBERGER J., HOLZWARTH R., SCHUESSLER H.A., KRAUSZ F. AND HÄNSCH T.W. **A frequency comb in the extreme ultraviolet.** *Nature* **436(7048)** (2005) 234–237.
<http://dx.doi.org/10.1038/nature03851>
- [219] TALKNER P., LUTZ E. AND HÄNGGI P. **Fluctuation theorems: Work is not an observable.** *Physical Review E* **75(5)** 050102.
<http://dx.doi.org/10.1103/PhysRevE.75.050102>

PUBLICATIONS BY THE AUTHOR

- [MB0201] SCHRAMM U., SCHÄTZ T., BUSSMANN M. AND HABS D. **The quest for crystalline ion beams.** *Plasma Physics and Controlled Fusion* **44(12B)** (2002) B375–B387.
<http://dx.doi.org/10.1088/0741-3335/44/12B/326>
- [MB0301] SCHRAMM U., SCHÄTZ T., BUSSMANN M. AND HABS D. **Cooling and heating of crystalline ion beams.** *Journal of Physics B* **36(3)** (2003) 561–571.
<http://dx.doi.org/10.1088/0953-4075/36/3/314>
- [MB0302] SCHÄTZ T., SCHRAMM U., BUSSMANN M. AND HABS D. **Crystallisation of ion beams in the rf quadrupole storage ring PALLAS.** *Applied Physics B* **76(2)** (2003) 183–190.
<http://dx.doi.org/10.1007/s00340-003-1110-1>
- [MB0303] BUSSMANN M., SCHRAMM U., SCHÄTZ T. AND HABS D. **Structural changes in bunched crystalline ion beams.** *Journal of Physics A* **36(22)** (2003) 6119–6127.
<http://dx.doi.org/10.1088/0305-4470/36/22/339>
- [MB0304] SCHRAMM U., SCHÄTZ T., BUSSMANN M. AND HABS D. **Spatial Compression of Bunched Crystalline Ion Beams.** *Physica Scripta* **2003(T104)** (2003) 189–195.
<http://dx.doi.org/10.1238/Physica.Topical.104a00189>
- [MB0305] SCHRAMM U., SCHÄTZ T., BUSSMANN M. AND HABS D. **Storage of Crystalline Beams.** *Proceedings of the 2003 Particle Accelerator Conference, PAC03 (Portland, Oregon (USA))* **1** (2003) 112–116.
<http://cern.ch/AccelConf/p03/PAPERS/TOAA004.PDF>
- [MB0401] SCHRAMM U., BUSSMANN M., SCHÄTZ T. AND HABS D. **Observations on Bunched Crystalline Ion Beams.** *Proceedings of the International Conference on Quantum Aspects Of Beam Physics 2003: The Joint 28th ICFE Advanced Beam Dynamics And Advanced & Novel Accelerators (Hiroshima, Japan)* (2004) 489–499
<http://www.worldscibooks.com/physics/5680.html>
- [MB0402] SCHRAMM U., BUSSMANN M. AND HABS D. **From laser cooling of non-relativistic to relativistic ion beams.** *Nuclear Instruments and Methods in Physics Research Section A* **532(1-2)** (2004) 348–356.
<http://dx.doi.org/10.1016/j.nima.2004.06.064>
- [MB0403] ROTH M., BLAZEVIC A., BRAMBRINK E., GEISSEL M., COWAN T., FUCHS J., KEMP A., RUHL H., AUDEBERT P., COBBLE J., FERNANDEZ J. HEGELICH M., LETZRING S., LEDINGHAM K., MCKENNA P., CLARKE R., NEELY D., KARSCH S., HABS D., SCHRAMM U., BUSSMANN M. AND J. S. **Laser-acceleration and Laser-cooling for Ion Beams.** *Proceedings of the 9th European Particle Accelerator Conference 2004, EPAC04*

(Lucerne, Switzerland) (2004) 54–58
<http://accelconf.web.cern.ch/AccelConf/e04/PAPERS/TUYACH01.PDF>

- [MB0501] SCHRAMM U., BUSSMANN M., HABS D., STECK M., KÜHL T., BECKERT K., BELLER P., FRANZKE B., NOLDEN F., SAATHOFF G., REINHARDT S. AND KARPUK S. **Laser Cooling and Spectroscopy of Relativistic C^{3+} Beams at the ESR.** *Hyperfine Interactions* **162(1)** (2005) 181–188.
<http://dx.doi.org/10.1007/s10751-005-9217-x>
- [MB0502] SCHRAMM U., BUSSMANN M., HABS D., KÜHL T., BELLER P., FRANZKE B., NOLDEN F., STECK M., SAATHOFF G., REINHARDT S. AND KARPUK S. **Laser-Spectroscopy of the 2s2S-2p2P transitions of relativistic Li-like carbon ions at the ESR.** *Proceedings of the 6th International Conference on Nuclear Physics at Storage Rings, STORI-2005 (Bonn, Germany)* **30** (2005) 324–327.
<http://hdl.handle.net/2128/574>
- [MB0503] SCHRAMM U., BUSSMANN M., HABS D., STECK M., KÜHL T., BECKERT K., BELLER P., FRANZKE B., NOLDEN F., SAATHOFF G., REINHARDT S. AND KARPUK S. **Laser Cooling of Relativistic Heavy Ion Beams.** *Proceedings of the 2005 Particle Accelerator Conference, PAC05 (Knoxville, Tennessee (USA))* (2005) 401–403
<http://cern.ch/AccelConf/p05/PAPERS/FOAD004.PDF>
- [MB0601] SCHRAMM U., BUSSMANN M., HABS D., KÜHL T., BELLER P., FRANZKE B., NOLDEN F., STECK M., SAATHOFF G., REINHARDT S. AND KARPUK S. **Combined Laser and Electron Cooling of Bunched C^{3+} Ion Beams at the Storage Ring ESR.** *AIP Conference Proceedings of the International Workshop on Beam Cooling and Related Topics, COOL05 (Galena, Illinois (USA))* **821(1)** (2006) 501–509.
<http://dx.doi.org/10.1063/1.2190157>
- [MB0602] BUSSMANN M., SCHRAMM U., HABS D., KOLHINEN V. AND SZERYPO J. **Stopping highly charged ions in a laser-cooled one component plasma of ions.** *International Journal of Mass Spectrometry* **251(2-3)** (2006) 179–189.
<http://dx.doi.org/10.1016/j.ijms.2006.01.042>
- [MB0603] SCHRAMM U., BUSSMANN M., HABS D., STECK M., KÜHL T., BECKERTS K., BELLER P., FRANZKE B., NOLDEN F., SAATHOFF G., REINHARDT S. AND KARPUK S. **Laser Cooling and Spectroscopy of Relativistic C^{3+} Beams at the ESR.** *Laser 2004* (2006) 181–188
http://dx.doi.org/10.1007/3-540-30926-8_22
- [MB0604] BUSSMANN M., SCHRAMM U. AND HABS D. **Simulating strongly coupled plasmas at low temperatures.** *AIP Conference Proceedings of the International Workshop on Non-Neutral Plasmas 2006, NNP06 (Aarhus, Denmark)* **862(1)** (2006) 221–231.
<http://dx.doi.org/10.1063/1.2387927>
- [MB0701] BUSSMANN M., SCHRAMM U. AND HABS D. **Preparing a laser cooled plasma for stopping highly charged ions.** *European Physical Journal D* **45(1)** (2007) 129–132.
<http://dx.doi.org/10.1140/epjd/e2007-00153-2>

- [MB0702] BUSSMANN M., SCHRAMM U. AND HABS D. **Simulating the stopping dynamics of highly charged ions in an ultra-cold, strongly coupled plasma.** *Hyperfine Interactions* **173(1-3)** (2007) 27–34.
<http://dx.doi.org/10.1007/s10751-007-9538-z>
- [MB0703] KOLHINEN V., BUSSMANN M., HABS D., NEUMAYR J., SCHRAMM U., SCHÜRMAN C., SZERYPO J., SEW TZ M. AND THIROLF P. **MLLTRAP: Penning trap facility for high precision measurements.** *Nuclear Instruments and Methods in Physics Research Section B* **266(19-20)** (2008) 4547–4550.
<http://dx.doi.org/10.1016/j.nimb.2008.05.100>
- [MB0704] BUSSMANN M., SCHRAMM U., HABS D., STECK M., KÜHL T., BECKERT K., BELLER P., FRANZKE B., NÖRTERS HÄUSER W., GEPPERT C., NOVOTNY C., KLUGE J., NOLDEN F., STÖHLKER T., KOZHUHAROV C., REINHARDT S., SAATHOFF G. AND KARPUK S. **The dynamics of bunched laser-cooled ion beams at relativistic energies.** *Journal of Physics: Conference Series* **88** (2007) 012043.
<http://dx.doi.org/10.1088/1742-6596/88/1/012043>
- [MB0705] BUSSMANN M., HABS D., SCHRAMM U., BECKERT K., BELLER P., FRANZKE B., KOZHUHAROV C., KÜHL T., NÖRTERS HÄUSER W., NOLDEN F., STECK M., KARPUK S., GEPPERT C., NOVOTNY C., SAATHOFF G. AND REINHARDT S. **Schottky Noise Signal and Momentum Spread for Laser-Cooled Bunched Ion Beams at Relativistic Energies.** *Proceedings of the Workshop on Beam Cooling and Related Topics, COOL07 (Bad Kreuznach, Germany)* **1** (2007) 226–229.
<http://accelconf.web.cern.ch/AccelConf/c107/PAPERS/FRM1C02.PDF>
- [MB0706] SZERYPO J., KOLHINEN V., BUSSMANN M., HABS D., NEUMAYR J., SCHÜRMAN C., SEW TZ M., THIROLF P. AND SCHRAMM U. **Penning trap progress in Munich.** *Acta Physica Polonica B* **39(2)** (2007) 471–476.
<http://th-www.if.uj.edu.pl/acta/vol39/abs/v39p0471.htm>
- [MLL02] BUSSMANN M., HABS D., SCHÄTZ T. AND SCHRAMM U. **Dynamics and Structural Properties of Crystalline Ion Beams.** *Maier-Leibnitz-Laboratory Annual Report* (2002) 63
http://www.bl.physik.uni-muenchen.de/bl_rep/jb2002/p63.ps
- [MLL0301] BUSSMANN M., HABS D., HORAK F. AND SCHRAMM U. **Structural and Temporal Analysis of Crystalline Ion Beams.** *Maier-Leibnitz-Laboratory Annual Report* (2003) 56
http://www.bl.physik.uni-muenchen.de/bl_rep/jb2003/p56.ps
- [MLL0302] SCHRAMM U., BUSSMANN M., HABS D., STECK M., STÖHLKER T., FRANZKE B., NOLDEN F. AND KÜHL T. **Laser Cooling of Stored Relativistic Heavy Ion Beams.** *Maier-Leibnitz-Laboratory Annual Report* (2003) 57
http://www.bl.physik.uni-muenchen.de/bl_rep/jb2003/p57.ps
- [MLL04] SCHRAMM U., BUSSMANN M., HABS D., STECK M., KÜHL T., BECKERT K., BELLER P., FRANZKE B., KLUGE H.J., NOLDEN F., STÖHLKER T., SAATHOFF G., REINHARDT S. AND KARPUK S. **Laser Cooling and**

Spectroscopy of Relativistic C^{3+} Beams at the ESR. *Maier-Leibnitz-Laboratory Annual Report* (2004) 56

http://www.bl.physik.uni-muenchen.de/bl_rep/jb2004/p056.ps

[MLL05] SCHRAMM U., BUSSMANN M., HABS D., STECK M., KÜHL T., BELLER P., FRANZKE B., NOLDEN F., SAATHOFF G., REINHARDT S. AND KARPUS S. **Combined Laser and Electron Cooling of Bunched C^{3+} Beams at the ESR.** *Maier-Leibnitz-Laboratory Annual Report* (2005) 46
http://www.bl.physik.uni-muenchen.de/bl_rep/jb2005/p046.pdf

[MLL06] BUSSMANN M., SCHRAMM U., KOLHINEN V., SZERYPO J., SEWTZ M., THIROLF P. AND HABS D. **Stopping Highly Charged Ions in a Laser-cooled Plasma.** *Maier-Leibnitz-Laboratory Annual Report* (2006) 55
http://www.bl.physik.uni-muenchen.de/bl_rep/jb2006/p055056.pdf

ENCLOSED PUBLICATIONS

This part encloses some of the publications relevant for the cumulative thesis. Some of the publications not enclosed contain a lot of redundant information which would increase the size of the cumulative thesis significantly without adding a proportional amount of new insights. Nevertheless, where additional results relevant for the thesis can only be found in a single publication, a citation of this publication is added.

Following is a short summary of the enclosed publications

- **Hyperfine Interactions 162(1) (2005) 181–188 93**
The first enclosed publication [MB0501] summarizes the main aspects of the laser-cooling experiments performed at the *ESR*. It especially includes a detailed analysis of the laser spectroscopy results obtained in the first measurement campaign in 2004.
- **AIP Conference Proceeding 821(1) (2006) 501–509 103**
The second publication [MB0601] summarizes the main results on space-charge dominated beams and three-dimensional cold beams. It presents a direct comparison of pure laser-cooling and combined laser- and electron cooling.
- **Journal of Physics: Conference Series 88 (2007) 012043 115**
The third publication [MB0704] deals with the dynamics of bunched ion beams at low momentum spread, comparing simulations of the ion dynamics with experimental data.
- **International Journal of Mass Spectrometry 251(2-3) (2006) 179–189 123**
The fourth publication [MB0602] is the most detailed publication of the first results on the stopping power of highly charged ions in a one-component plasma of laser-cooled ions.
- **European Physical Journal D 45(1) (2007) 129–132 137**
The fifth publication [MB0701] discusses in detail possible laser-cooling schemes for the final cooling trap setup.
- **Hyperfine Interactions 173(1-3) (2007) 27–34 143**
The sixth publication [MB0702] explains the technical aspects of the parallel simulation using realistic simulation assumptions.

SCHRAMM U., BUSSMANN M., HABS D., STECK M., KÜHL T., BECKERT K., BELLER P., FRANZKE B., NOLDEN F., SAATHOFF G., REINHARDT S. AND KARPUK S.

Laser Cooling and Spectroscopy of Relativistic C^{3+} Beams at the ESR.

Hyperfine Interactions **162(1)** (2005) 181–188

Springer Berlin Heidelberg New York

Reprinted with kind permission from Springer Science and Business Media.

License Number 1845950931344

Laser Cooling and Spectroscopy of Relativistic C^{3+} Beams at the ESR[★]

U. SCHRAMM^{1,*}, M. BUSSMANN¹, D. HABS¹, M. STECK², T. KÜHL²,
K. BECKERT², P. BELLER², B. FRANZKE², F. NOLDEN²,
G. SAATHOFF³, S. REINHARDT³, and S. KARPUK⁴

¹*Department für Physik, LMU München, D-85748 Garching, Germany;*
e-mail: uschramm@garching.physik.uni-muenchen.de

²*Gesellschaft für Schwerionenforschung (GSI), D- Darmstadt, Germany*

³*Max-Planck-Institut für Kernphysik, D-Heidelberg, Germany*

⁴*Institut für Physik, Universität Mainz, D-Mainz, Germany*

Abstract. We report on the first laser cooling of a bunched beam of multiply charged C^{3+} ions performed at the ESR (GSI) at a beam energy of $E = 1.47$ GeV. Moderate bunching provided a force counteracting the decelerating laser force of one counterpropagating laser beam. This versatile type of laser cooling lead to longitudinally space-charge dominated beams with an unprecedented momentum spread of $\Delta p/p \approx 10^{-7}$. Concerning the beam energy and charge state of the ion, the experiment depicts an important intermediate step from the established field of laser cooling of ion beams at low energies toward the unique laser cooling scheme proposed for relativistic beams of highly charged heavy ions at SIS 300 (FAIR).

Key Words: crystalline ion beams, laser cooling, Li-like heavy ions, storage rings.

1. Introduction

The cooling of stored heavy ion beams to high phase space densities is of general importance when low momentum spread is required for precision spectroscopy or high luminosity for collision experiments. Ultimately, cooling the thermal energy far below the mutual Coulomb energy of the ions leads to a phase transition – a crystallization of the ion beam [1] – into a regime where almost no further heating occurs and maximum brilliance is reached [2].

In the low energy regime this phase transition could recently be observed with laser-cooled $^{24}\text{Mg}^+$ ion beams [3–5]. However, as laser cooling relies on the repeated resonant scattering of photons, only a very limited number of ions can be accessed by this powerful cooling technique at existing storage rings, benchmarking and present activities being summarized in [2].

[★] Funded by the German BMBF under contract number 06ML183.

* Author for correspondence.

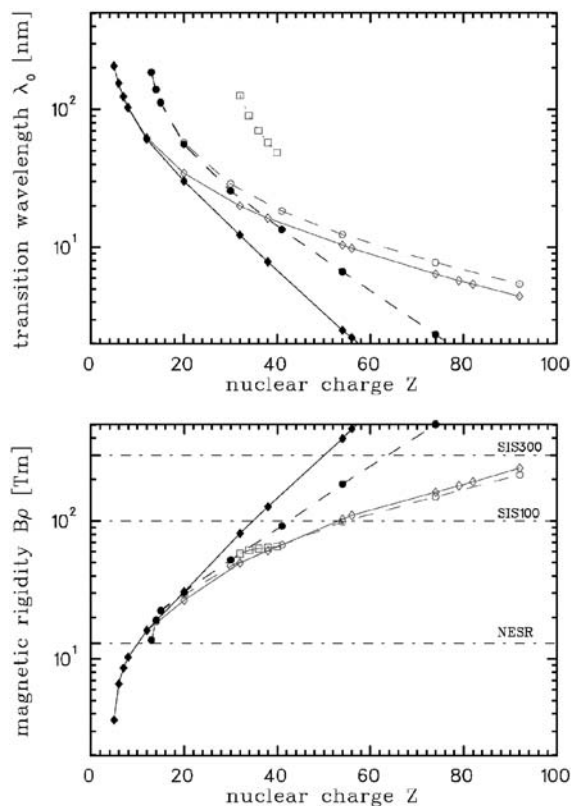


Figure 1. Left graph: Wavelength of the $nS_{1/2} - nP_{1/2}$ (black lines) and $nS_{1/2} - nP_{3/2}$ (grey lines) ground state transitions in the ion rest frame as a function of the nuclear charge [11]. The solid lines (rhombs, $n = 2$) refer to Li-like ions, the dashed lines (circles, $n = 3$) to Na-like and the dotted lines (squares, $n = 4$) to Cu-like ions. Right graph: Corresponding magnetic rigidity required for the storage of the ions at an energy Doppler shifting the transition wavelength to a laser wavelength of $\lambda_{uv} = 257$ nm. The horizontal lines denote the maximum rigidity of the FAIR storage rings.

At heavy ion storage rings like ESR (GSI), electron cooling has developed into a versatile tool for the cooling of highly charged ions independent from their internal atomic properties [6]. As the cooling force increases with the square of the ion charge, beam ordering effects of highly charged ions were observable with electron cooling at very low beam currents [7, 8], where competing heating mechanisms are reduced.

In the relativistic regime, that will be accessible at the future FAIR facility, the situation might be reversed. Electron cooling as the established tool in heavy ion storage rings cannot be readily applied any more. Yet, laser cooling, up to now only applied to beams of singly charged ions, seems promising. Due to the fast transition rates in highly charged ions and the relativistically increased momentum transfer in the photon scattering, the cooling force is predicted to

LASER COOLING AND SPECTROSCOPY OF RELATIVISTIC C^{3+} BEAMS AT THE ESR

principally increase with the third power of the ion energy [2, 9]. Moreover, ground-state transitions of all Li- and most Na-like heavy ions can be reached at FAIR when counterpropagating laser and ion beams are used as demonstrated in Figure 1 [10].

As an intermediate step between the laser cooling of highly relativistic heavy ion beams, anticipated at FAIR [10], and the known field of low energy beams [2], a test experiment was performed with a C^{3+} ion beam at a velocity of $\beta = 0.47$ at the ESR (GSI), of which first results will be presented.

2. Laser cooling of Li-like carbon ions

At the heavy ion storage ring ESR (GSI) laser cooling of Li-like C^{3+} ions becomes possible at a beam energy of 122 MeV/u ($\beta = 0.47$, $\gamma = 1.13$). At this energy the closed $2S_{1/2} - 2P_{3/2}$ transition ($\lambda_0 = 154.82$ nm, $\tau = 3.8$ ns [11]) is Doppler-shifted into resonance with the frequency doubled line of the Ar-ion laser ($\lambda_{laser}/2 = 257.34$ nm) when counterpropagating laser and ion beams are used. The decelerating laser force is counteracted by the restoring force of the bucket when the beam is bunched. This technique provides the momentum dependent friction force required for cooling [2] without the need of a copropagating laser beam.

In order not to challenge the laser force in this first experiment moderate bunching voltages of only few volts were applied at the 10th as well as at the 20th harmonic of the revolution frequency $f_{rev} = 1.295$ MHz. The bucket depth was determined by the measurement of the synchrotron frequency $f_{sync} \sim 100$ Hz ($h = 10$) and $f_{sync} \sim 170$ Hz ($h = 20$) and corresponds to a momentum acceptance of the order of $\Delta p/p \sim 2 \times 10^{-5}$ ($h = 10$). For an electron pre-cooled beam this momentum spread is reached for a total ion number of few 10^7 (few 10 μ A) limited by heating due to intra-beam scattering [2].

Bunched beam laser cooling relies on the damping of the single particle synchrotron motion by the strong but narrow-band resonant laser force. For a typical single-mode laser the width of the force is determined by the line-width of the transition of the ion used for the cooling and not by the width of the laser. It corresponds to $\Delta p/p \approx 5 \times 10^{-8}$. The width of the force is thus extremely mismatched to the initial momentum distribution, yet it principally allows cooling to similarly low momentum spreads. Two schemes are reported so far to resonantly interact with the full ion momentum distribution (see [2, 12]). For the first, invented at ASTRID (Aarhus) [13], the bunching frequency is continuously tuned from a starting frequency where the laser is resonant with ions just at the edge of the bucket to a final frequency close to the center of the bucket. This scheme is illustrated in Figure 2 and described in the caption. The final tuning has to be done carefully as crossing the center of the bucket leads to an equally strong driving of the synchrotron motion, visible in the lower half of Figure 2. The second scheme, invented at TSR [14, 15], relies on the repeated interaction

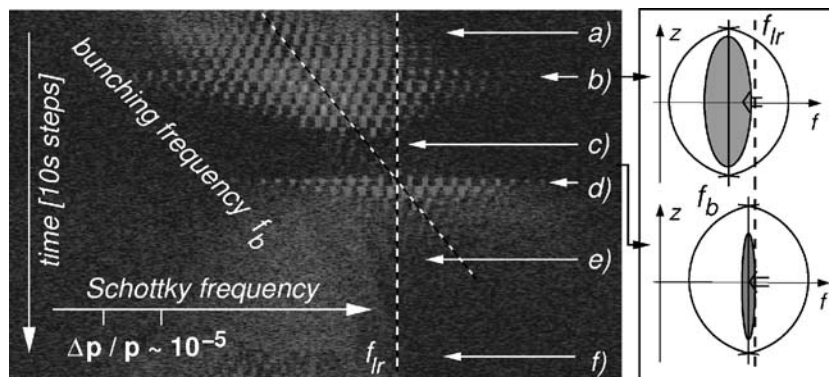


Figure 2. Schottky noise analysis (at the 47th harmonic) of a laser cooled bunched beam of C^{3+} ions with rising bunching frequency f_b (diagonal dashed line). The decelerating laser beam is operated at fixed frequency and resonant with ions of the same momentum class f_{lr} (vertical dashed line). The bunching frequency $f_b = hf_{rev} = 10 \times 1.295$ MHz is increased in steps of 10 Hz every 10 s. Starting at a low bunching frequency where ions close to the separatrix of the bucket come into resonance with the cooling laser beam, the ion beam is cooled into the bucket (a). Within the harmonic range, the number of synchrotron side bands increases (b and upper sketch) interpreted as a laser cooled bunched beam where individual ions perform synchrotron oscillations with $f_{sync} \sim 100$ Hz. From the synchrotron frequency (the side band spacing) a momentum acceptance of about $\Delta p/p \sim 2 \times 10^{-5}$ can be deduced that corresponds to the observed momentum spread (roughly the number of side bands). Closer to resonance ($f_b \rightarrow f_{lr}$) the side bands suddenly vanish (c) when the beam enters the space-charge dominated regime. When the laser beam comes into resonance with ions at the bucket center (d) the synchrotron motion is driven instead of damped. Ions are decelerated (e) out of the bucket until the cycle restarts (f).

of the ions circulating in the bucket with the laser tuned to optimum cooling close to the center of the bucket. Both schemes have been systematically studied at the ESR and detailed results will be published elsewhere.

In Figure 3a a complementary view of the first scheme is given. For decreasing detuning Δf_b and thus for increasing cooling strength for ions around the bucket center, the spatial width of the bunches, measured using capacitive pick-up devices, is shown. Following a continuous reduction of the bunch length, the length remains constant for $\Delta f_b < 100$ Hz. At the same detuning of about 100 Hz (corresponding to $\Delta p/p = 6 \times 10^{-6}$ for $h = 20$) the side bands in a Schottky noise spectrum similar to the one presented in Figure 2 abruptly vanish, interpreted above as the transition to a space-charge dominated regime. In this regime the length of the bucket does not depend on the momentum spread any more, being exactly the signature observed in the bunch length measurement depicted in Figure 3a. No ions are lost at this point although the Schottky-signal appears to be considerably weaker, as the integrated pick-up signal (not shown) remains constant. Furthermore, the measured bunch length can be reproduced under the assumption of space charge dominated bunches within 10% [16].

In the space-charge dominated regime, the momentum spread cannot be derived from the spatial distribution. However, laser cooling itself provides a

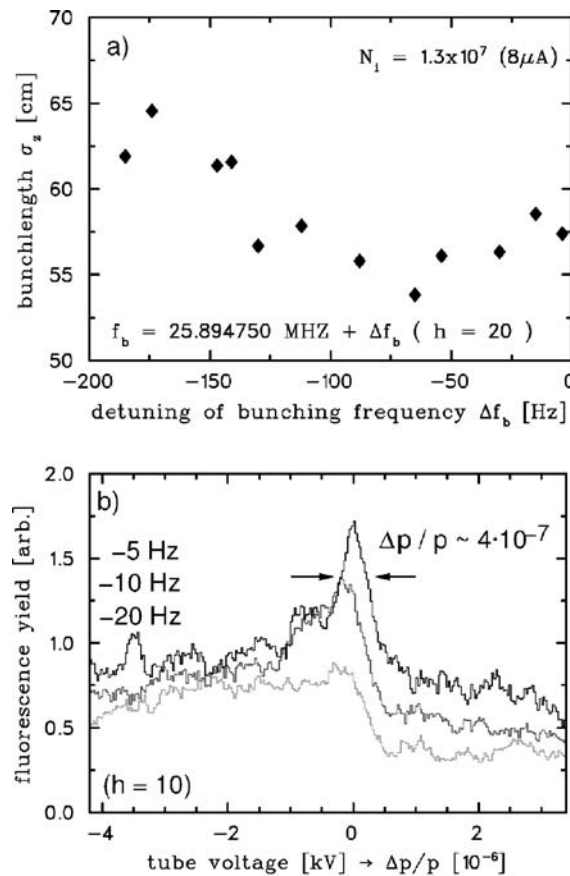
LASER COOLING AND SPECTROSCOPY OF RELATIVISTIC C^{3+} BEAMS AT THE ESR

Figure 3. (a) Bunch length of a laser-cooled beam as a function of the detuning Δf_b of the bucket center with respect to the laser resonance. At the detuning for which the side band structure vanishes in the corresponding Schottky spectrum ($\Delta f_b \sim 100$ Hz, here $h = 20$) the width of the bunch remains constant, indicating the space-charge dominated regime. (b) Momentum distribution of the laser cooled bunched beam ($h = 10$) close to minimum detuning. The momentum distribution is measured *via* the Doppler effect making use of a local change of the ion momentum inside a drift tube where the fluorescence is recorded, when the tube voltage is ramped.

unique diagnostic. Tuning the laser frequency over the Doppler-broadened line, the momentum distribution can be directly measured. In practice, the ion momentum is locally tuned by ramping a drift-tube. The result is depicted in Figure 3b. For a frequency detuning of only 5 Hz (corresponding to $\Delta p/p = 6 \times 10^{-7}$ at $h = 10$) a momentum spread of $\Delta p/p = 4 \times 10^{-7}$ is measured for a cold fraction of the beam. It is likely that part of the beam is about one order of magnitude hotter due to intra-beam scattering and subsequent re-circulating in the bucket, yet this beam represents the coldest measured in the ESR. For an ion number of about 1.5×10^6 it corresponds to a plasma parameter of $\Gamma \lesssim 1$.

Summarizing the complete experiment on laser cooling of Li-like carbon ions at 1.47 GeV, the full momentum acceptance of the test-bucket could be laser cooled without prior electron cooling. Yet, the transverse cooling of the injected beam only worked reasonably well after few seconds of electron pre-cooling. Otherwise, the motion in the different degrees of freedom seemed to have decoupled and the beam remained transversally hot. When cooled, the transverse profile was comparable to that of an electron cooled beam. Though, in principle, the laser cooling force exceeds the electron cooling force, electron cooling overrode laser cooling. This observation can be attributed to the extremely narrow bandwidth of the force and (in this special case) also to the insufficient laser intensity, as the transition could only be saturated by $\sim 10\%$.

For efficient laser cooling of the whole ion bunch, the width of the laser force has to be adapted at least to the momentum range that is given by intra-beam scattering, a problem well known from lower energy experiments [17, 18]. This is planned to be realized either by a second scanning laser system or by the use of a pulsed laser systems with pulse length of the order of few 100 ps to 1 ns in the near future.

3. Laser spectroscopy of Li-like carbon ions

As laser cooling of Li-like heavy ions relies on the resonant excitation of the $2S_{1/2} - 2P_{1/2}$ or the $2S_{1/2} - 2P_{3/2}$ transitions, the experiment incorporates the spectroscopy of these transitions. The Ar-ion laser can – in principle – be locked to a calibrated iodine line ($\lambda_{a3} = 514.6734664$ nm) with a relative precision of better than 10^{-9} [19]. However, due to the huge Doppler-effect $\omega_0 = \gamma(1 + \beta)\omega_{iv} \approx 1.66\omega_{iv}$ that enables the excitation of transitions in the deep UV or even X-ray range with near UV laser beams, the knowledge of the ion energy determines the accuracy of the spectroscopy in the rest-frame $\Delta\omega_0/\omega_0 = (1 - \beta^2)^{-1}\Delta\beta = \beta^{-1}\Delta\gamma/\gamma$ and thus a reliable method for the determination of the ion energy has to be found.

From the Schottky-noise spectra, like the one presented in Figure 2, the revolution frequency of a sufficiently cold ion beam can be deduced with comparative precision. However, as the length of the closed orbit depends on the individual setting of the storage ring lattice (usually known to 3×10^{-4} for the design orbit), this measurement does not translate into a beam energy of equivalent precision. At the ESR, where the beam can be electron-cooled, the determination of the acceleration voltage of the electron beam ($U_e \sim 67$ kV), calibrated with a relative precision of 10^{-4} and showing much less jitter, currently represents the method of choice. The spectroscopy measurement was performed in a way that, first, the position of the laser resonance was marked in the Schottky-spectrum for a coasting uncooled beam with a relative accuracy of $\sim 10^{-7}$. The laser wavelength was stabilized to the low-wavelength side of the

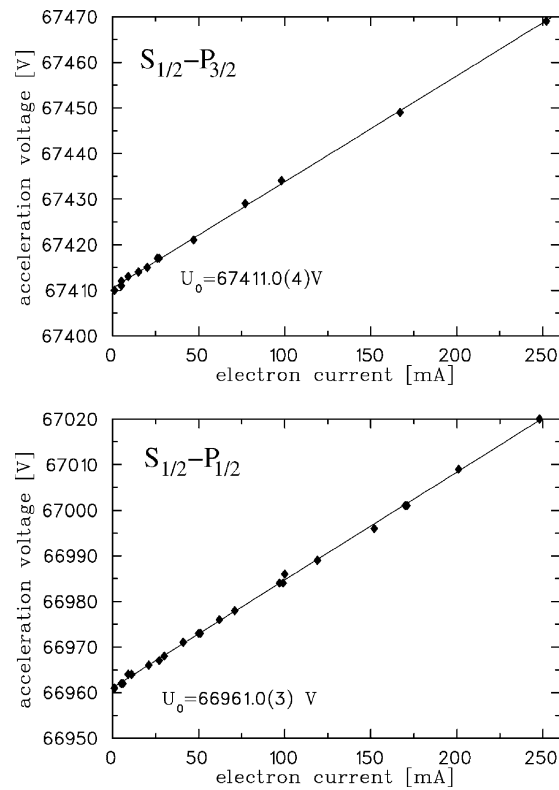
LASER COOLING AND SPECTROSCOPY OF RELATIVISTIC C^{3+} BEAMS AT THE ESR


Figure 4. Acceleration voltage of the electron cooler required to match the laser resonance as a function of the electron current.

Doppler-broadened iodine-line at $\lambda_{laser} = 514.6729(3)$ nm, the relative jitter was reduced to $\sim 5 \times 10^{-9}$. Then, electron cooling was activated and tuned to match the original position of the laser-resonance in the Schottky-spectrum to $\sim 10^{-5}$ (digitizing resolution). As the electron energy in the center of the beam, where the ion beam is positioned, is reduced by about 0.1% due to the space charge of the electron beam, the best way of eliminating this correction is to perform the above procedure for different electron currents and to extrapolate to zero current (Figure 4).

| | $\lambda(2S_{1/2} - 2P_{1/2})$ [nm] | $\lambda(2S_{1/2} - 2P_{3/2})$ [nm] |
|---|-------------------------------------|-------------------------------------|
| Kim <i>et al.</i> 1991 [20] | 155.060 | 154.804 |
| Johnson <i>et al.</i> 1996 [11] | 155.078 | 154.819 |
| Tupitsyn and Shabaev 2003, private communication [2004] | 155.0739(26) | 154.8173(53) |
| This work | 155.0705(39)(3) | 154.8127(39)(2) |
| Edlen <i>et al.</i> 1983 [21] | 155.077 | 154.820 |

From these electron energies eU_0 , matching the ion energies where the ions are in resonance with the laser light, the following transition wavelengths can be deduced, where the first error denotes the calibration accuracy of the power supply and the second the statistical error.

The present experimental results reach the same accuracy that is set by the actual theoretical work (Tupitsyn and Shabaev 2003, private communication [2004]) and are consistent within one standard deviation. Yet, for both lines the experiment yields slightly lower values and it seems likely that this is due to the absolute calibration of the acceleration voltage and thus a systematic effect.

Summarizing, already for this test experiment the same accuracy was reached that can be set by theory. With an improvement of the voltage calibration or measurements at different ion energies and laser wavelength on the same transition, theory could be readily challenged. At the ESR the method could be extended up to O^{5+} ions, while at FAIR, every element can be reached.

References

1. Schiffer J. P. and Kienle P., *Z. Phys. A* **321** (1985), 181.
2. Schramm U. and Habs D., *Progress in Particle and Nuclear Physics* **53** (2004), 583–677.
3. Schätz T., Schramm U. and Habs D., *Nature* (London) **412** (2001), 717.
4. Schramm U., Schätz T. and Habs D., *Phys. Rev. E* **66** (2002), 036501.
5. Schramm U. *et al.*, *Journal of Physics* **36** (2003), 561.
6. Steck M. *J. Opt. Soc. Am. B* **20** (2003), 1016.
7. Steck M. *et al.*, *J. Phys. B* **36**, 991 (2003) and *Phys. Rev. Lett.* **77** (1996), 3803.
8. Danared H. *et al.*, *J. Phys. B* **36** (2003), 1003.
9. Schramm U., Bussmann M. and Habs D., *Nucl. Instrum. Methods, A* **532** (2004), 348.
10. Schramm U. *et al.*, LoI #18 FAIR APPA–PAC (2004).
11. Johnson W. R. *et al.*, *At. Data Nucl. Data Tables* **64** (1996), 279.
12. Schramm U., Schätz T. and Habs D., *Phys. Rev. Lett.* **87** (2001), 184801.
13. Hangst J. S. *et al.*, *Phys. Rev. Lett.* **74** (1995), 4432.
14. Miesner H.-J. *et al.*, *Nucl. Instr. Meth.*, Letter to the Editor, **A 383** (1996), 634.
15. Eisenbarth U. *et al.*, *Nucl. Instrum. Methods, A* **441** (2000), 209.
16. Ellison T. J. P. *et al.*, *Phys. Rev. Lett.* **70** (1993), 790.
17. Wanner B. *et al.*, *Phys. Rev. A* **58** (1998), 2242.
18. Atutov S. N. *et al.*, *Phys. Rev. Lett.* **80** (1998), 2129.
19. Saathoff G. *et al.*, *Phys. Rev. Lett.* **91** (2003), 190403.
20. Kim Y.-K. *et al.*, *Phys. Rev. A* **44** (1991), 148.
21. Tupitsyn I. I. and Shabaev V. M., *priv. com.* (2004).
22. Edlen B., *Phys. Scripta* **28** (1983), 51.

SCHRAMM U., BUSSMANN M., HABS D., KÜHL T., BELLER P., FRANZKE B., NOLDEN F., STECK M., SAATHOFF G., REINHARDT S. AND KARPUK S.

Combined Laser and Electron Cooling of Bunched C³⁺ Ion Beams at the Storage Ring ESR.

AIP Conference Proceedings of the International Workshop on Beam Cooling and Related Topics, COOL05 (Galena, Illinois (USA)) **821(1)** (2006) 501–509

American Institute of Physics

Reused with permission from U. Schramm, in
Combined Laser and Electron Cooling of Bunched C³⁺ Ion Beams at the
Storage Ring ESR
Sergei Nagaitsev (ed)
Conference Proceeding 821, 501 (2006)
Copyright 2006, American Institute of Physics.
License Number 1777100757854

Combined Laser and Electron Cooling of Bunched C3+ Ion Beams at the Storage Ring ESR

U. Schramm[‡], M. Bussmann^{*}, D. Habs^{*}, T. Kühl[†], P. Beller[†], B. Franzke[†],
F. Nolden[†], M. Steck[†], G. Saathoff^{**}, S. Reinhardt^{**} and S. Karpuk[‡]

^{*}Department für Physik, LMU München, 85748 Garching, Germany

[†]Gesellschaft für Schwerionenforschung (GSI), Darmstadt, Germany

^{**}Max-Planck-Institut für Kernphysik, Heidelberg, Germany

[‡]Institut für Physik, Universität Mainz, Mainz, Germany

Abstract. We report on first laser cooling studies of bunched beams of triply charged carbon ions stored at an energy of 1.46 GeV at the ESR (GSI). Despite for the high beam energy and charge state laser cooling provided a reduction of the momentum spread of one order of magnitude in space-charge dominated bunches as compared to electron cooling. For ion currents exceeding $10\ \mu\text{A}$ intra-beam-scattering losses could not be compensated by the narrow band laser system presently in use. Yet, no unexpected problems occurred encouraging the envisaged extension of the laser cooling to highly relativistic beams. At ESR, especially the combination with modest electron cooling provided three-dimensionally cold beams in the plasma parameter range of unity, where ordering effects can be expected and a still unexplained signal reduction of the Schottky signal is observed.

Keywords: laser cooling, heavy ion beam cooling, storage rings, Coulomb ordering

PACS: 29.20.Dh, 41.75.-i, 42.50.Vk, 52.27.Gr

LASER COOLING OF STORED ION BEAMS

At heavy ion storage rings electron cooling represents the prominent technique for the reduction of the momentum spread as well as of the transverse emittance of stored ion beams until equilibrium with competing processes like intra-beam-scattering (IBS) is reached. Heating due to IBS increases with the phase space density of the beam implying that the equilibrium momentum spread for rf-bunched harmonically confined ion ensembles scales with the number of stored particles N as $N^{1/6}$. Thus, a further reduction of the momentum spread of an electron-cooled beam can be achieved by a reduction of the ion beam current or by the application of an additional cooling method increasing the cooling rate. Concerning the momentum spread, such an increase can be provided by laser cooling, relying on the resonant momentum transfer originating from the repeated scattering of photons out of a laser beam merged with the ion beam. Yet, the extremely steep momentum gradient of the laser force comes at the expense of a narrow momentum acceptance range, predominantly collinear action, and, at present machines, the limited number of ions with suitable optical transitions.

A strong motivation for the development of the laser cooling technique at the storage rings TSR in Heidelberg [1] and ASTRID in Aarhus [2] was the principle capability

¹ internet: www.ha.physik.uni-muenchen.de/uschramm/

of the method to reach ion beam temperatures, describing the energy spread in the co-moving frame, far below the mutual Coulomb energy of neighboring ions. In this regime a phase transition into a Coulomb-ordered or crystalline beam is expected [3]. Such a state is characterized by an almost complete vanishing of collision dominated heating mechanisms like IBS. Unfortunately, it turned out that this suppression of collisional heating also meant a reduction of the vital coupling between the transverse ion motion, experiencing little yet too much stochastic heating due to the randomness of the scattering process, and the longitudinal ion motion, directly laser cooled [4]. Thus, though techniques were developed that provide direct transverse laser cooling making use of storage ring dispersion[5], no stable crystalline beams could be observed in these two machines [4, 6], benchmarking and present activities being summarized in [7].

In the very low energy regime this phase transition could recently be demonstrated with laser-cooled $^{24}\text{Mg}^+$ ion beams in the rf quadrupole (RFQ) storage ring PALLAS [8] for coasting as well as for bunched beams [9]. The strong IBS heating of the cold beam could be overcome by first reducing the tune of the RFQ storage ring, which leads to a well-defined increase of the transverse beam size and thus to a reduced IBS rate, and increasing it again after the beam is longitudinally sufficiently cold. Here, the advantage of the RFQ is the adjustable tune whereas in conventional machines transverse heating might help [10]. In the crystalline regime transverse laser heating, as discussed for TSR and ASTRID was directly observed [11]. Yet, the online tuning capability of the focusing strength was sufficient for the compensation of the loss of indirect cooling by stronger transverse confinement, as again reviewed in [7].

At the heavy ion storage ring ESR (GSI) electron cooling of highly charged heavy ions has developed into a routine tool for the cooling of highly charged ions independent from their internal atomic properties [12]. As the cooling force (as well as the inter-ion coupling) roughly increases with the square of the ion charge, one dimensional beam ordering effects of highly charged ions were observable with electron cooling at extremely low beam currents [13, 14], where density dependent heating mechanisms become negligible.

Combining the experience from ESR, TSR and PALLAS the idea for the experiment presented in this paper is the demonstration of combined laser and electron cooling of C^{3+} ion beams. Laser cooling then should provide lowest momentum spread, electron cooling the transverse cooling and a larger momentum acceptance, and the relatively high charge state increases the ion-ion coupling.

BUNCHED BEAM (PURE) LASER COOLING AT THE ESR

At the ESR combined electron and laser cooling of C^{3+} ion beams can be performed at an energy of 122 MeV/u ($\beta = 0.47$, $\gamma = 1.13$). At this energy the closed optical $2S_{1/2} - 2P_{3/2}$ transition ($\lambda_0 = 154.82$ nm, $\tau = 3.8$ ns [15]) of the Li-like carbon ions is Doppler-shifted into resonance with the UV-laser line at $\lambda_{laser}/2 = 257.34$ nm [16] when counterpropagating laser and ion beams are used. The decelerating laser force is counteracted by the restoring force of a bucket when the beam is bunched. This established technique [17, 9, 7], sketched in the cartoons in Fig. 1, provides the momentum dependent friction force required for cooling without the need of a copropagating laser beam.

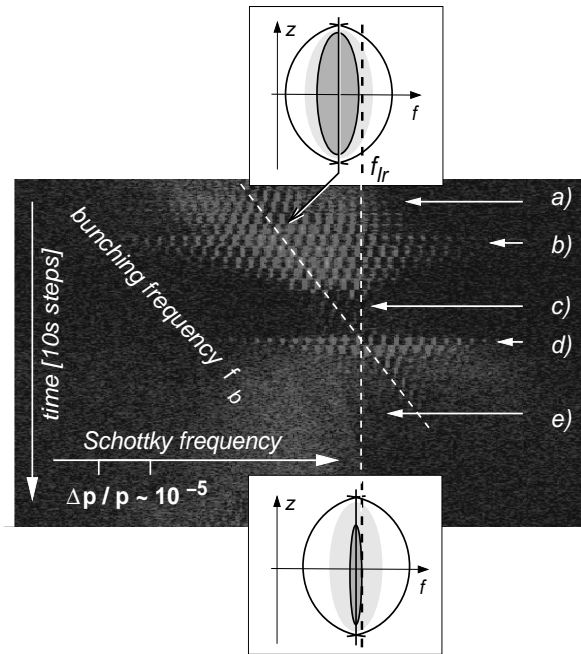


FIGURE 1. Schottky noise spectrum (47th harmonic, log. intensity coding) of a laser-cooled bunched C^{3+} beam recorded at scanning bunching frequency f_b (diagonal dashed line). The decelerating laser force is always resonant with ions at f_{lr} (vertical dashed line). For illustration $f_b = hf_{rev} = 10 \times 1.295 \text{ MHz}$ is increased in steps of 10 Hz every 10 s. Starting at a low bunching frequency ions close to the separatrix of the bucket come into resonance with the laser beam and are cooled into the bucket (a, and upper cartoon). Synchrotron sidebands appear (b), indicating a longitudinally laser-cooled bunch where the ions perform ‘incoherent’ synchrotron oscillations with $f_{sync} \sim 100 \text{ Hz}$. The initial envelope corresponds to the rms momentum acceptance of the bucket $\Delta p/p \sim 2 \times 10^{-5}$ and the cooling can be followed. Closer to resonance most sidebands vanish and the signal intensity decreases (c) when the beam enters the ‘space-charge dominated’ regime. Crossing the resonance (d) the synchrotron motion is driven instead of damped. Ions are decelerated (e) out of the bucket until the cycle restarts.

Moderate voltages for bunching of only few volts were applied at the 10th as well as at the 20th harmonic of the revolution frequency $f_{rev} = 1.295 \text{ MHz}$. The bucket depth was determined by the measurement of the synchrotron frequency $f_{sync} \sim 100 \text{ Hz}$ ($h = 10$) and $f_{sync} \sim 170 \text{ Hz}$ ($h = 20$) and corresponds to a momentum acceptance of the order of $\Delta p/p \sim 2 \times 10^{-5}$. For a purely electron-cooled beam this equilibrium momentum spread is reached for a total ion number of few 10^7 (few $10 \mu\text{A}$) [7]. The storage-time of the beam, electron pre-cooled for few seconds after injection, amounted to $\tau \sim 450 \text{ s}$, avoiding recombination losses in the electron cooler.

Bunched beam laser cooling, invented at ASTRID [17] now means damping of the synchrotron motion by the strong but narrow-band resonant laser force. For the cw-lasers used in the experiment [16], the band-width of the force is determined by the

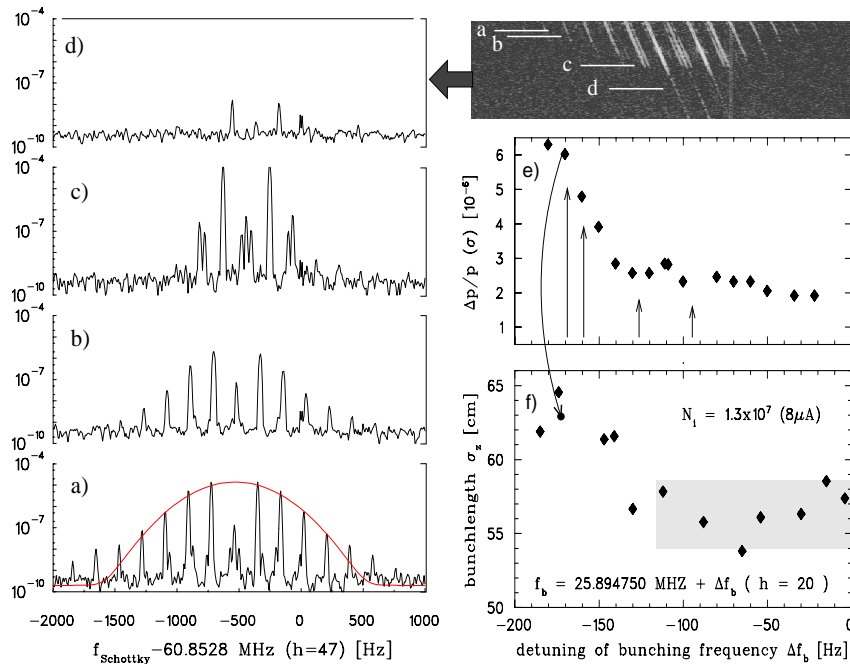


FIGURE 2. Left: Schottky-noise spectra corresponding to the detuning positions indicated in the upper right image with decreasing detuning from a) to d). The envelope in a) represents the Gaussian distribution used for the estimation of the momentum spread. Middle right: Momentum spread e) deduced from the width of the envelope of the 'incoherent' Schottky side-band spectrum as a function of the detuning Δf_b ($h = 20$). Arrows indicate the position of the spectra displayed in a)-d). Bottom right f): Bunch length (pick-up measurement) limited by the equilibrium length for constant ion density. The curved arrow indicates the correspondence between momentum spread and bunch length in the emittance (or IBS) dominated regime.

line-width of the transition corresponding to a momentum spread of $\Delta p/p \approx 5 \times 10^{-8}$. Two schemes exist to overcome this tremendous mismatch of the width of the cooling force and the initial momentum distribution besides the non-straightforward increase of the band-width of the force and, possibly, the additional application of momentum-matched electron cooling. In the first, the laser- or equally well the bunching-frequency is continuously tuned from a value where the laser is resonant with ions at the edge of the bucket to a final frequency close to its center [17]. Thereby, all ions are subsequently decelerated to the center of the bucket in momentum space and slightly shifted out of center in real space for the compensation of the decelerating laser force. However, note, that binary collisions may kick ions out of the narrow momentum acceptance range and a second broader distribution may form in the bucket. This scheme is illustrated in Fig. 1.

The development of the momentum distribution with continuously increasing cooling strength is depicted in Fig. 2e) as a function of the detuning Δf_b of the bucket center with respect to the laser resonance. The tuning rate is slow compared to the longitudinal

cooling rate so that the situation can be regarded as equilibrated. For large detuning the momentum spread can be deduced from the envelope of the ‘incoherent’ side-band spectrum [19] as indicated in Fig. 2a). The development of the spatial distribution, independently measured for a similar ion current using capacitive pick-up devices, is shown in Fig. 2f). Starting at large detuning, the momentum spread as well as the bunch length both decrease with increasing cooling strength or momentum compression of the bunch. For less detuning than -100Hz , corresponding to $\Delta p/p = 6 \times 10^{-6}$, the bunch length remains constant and can be reproduced under the assumption of longitudinally ‘space-charge dominated’ bunches [20] of constant linear density (gray area in the graph). Note, that the integrated pick-up signal and the beam current monitor do not show any unexpected ion losses at and beyond this point.

In the left Fig. 2 individual Schottky spectra that represent the different situations discussed above are shown in detail. The initial distributions (a,b) show a symmetric distribution of ‘incoherent’ synchrotron sidebands with reduced signal strength at the carrier. This reduction does not correspond to the Bessel-function description of the modulated spectrum for the given momentum spread [19] and might be attributed to prior laser heating. Close to the point where space-charge becomes dominant (c), presently unexplained satellites become observable on one side of the even side-bands at a frequency separation of $\sim 40\text{Hz}$. Well in the ‘space-charge dominated’ regime (d), identified by the behavior of the spatial distribution, most sidebands as well as the satellites have vanished, and the integrated signal intensity is unexpectedly reduced, leaving only the carrier and two distinct sidebands at the unaltered spacing of $f_{\text{sync}} = 188\text{Hz}$. Again, note, that the number of ions in the bunch remains constant.

In this regime the momentum spread cannot be derived from the envelope of the Schottky signal any more. However, laser cooling itself provides a unique diagnostic. Tuning the laser frequency across the Doppler-broadened transition, the momentum distribution can be directly observed via the laser fluorescence signal as described in [21].

COMBINED LASER AND ELECTRON COOLING

The second scheme for bunched beam laser cooling relies on the repeated interaction of the ions oscillating in the bucket with the laser beam tuned to optimum cooling slightly above to the center of the bucket. The advantage of this scheme, first used at TSR [18, 9], is that all momentum classes frequently interact with the laser beam, and that it is stationary so that electron and laser cooling can be easily synchronized. Systematic studies were performed at the ESR simultaneously recording the Schottky-spectra, the momentum dependent fluorescence signal [21], and the longitudinal and the transverse spatial profiles, for the latter using a residual gas ionization beam profile monitor close to its spatial resolution and at integration times of about a minute. For comparison continuous electron cooling was applied at different electron currents. Results are displayed in Figs. 3 and 4, filled symbols representing electron cooling and open ones laser cooling at fixed detuning for all the following graphs.

For continuous electron cooling of the C^{3+} beam, momentum matched to the center of the bucket, the momentum spread as well as the longitudinal and transverse spatial

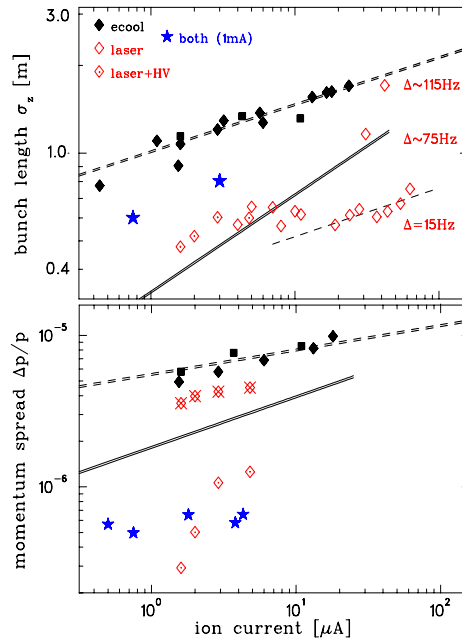


FIGURE 3. Upper graph: Spatial bunch length as a function of the ion current, measured with a current transformer. Filled symbols stand for electron cooling with different electron current, open ones for laser cooling at given detuning and stars for combined cooling, details consistently given in the legend of the following three graphs. The dashed lines indicate the $N^{1/6}$ scaling expected from IBS, the solid the equilibrium length for space charge dominated bunches ($\propto N^{1/3}$). Lower graph: Momentum spread deduced from the Schottky spectra for the electron-cooled case and only giving upper limits for the laser cooled one and deduced from the fluorescence scan (marked HV).

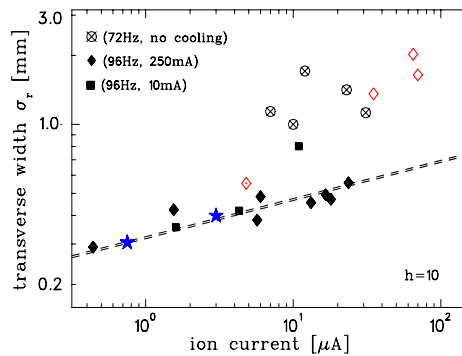


FIGURE 4. Transverse beam size as a function of the ion current for the beams presented in Fig. 3. A size of 0.4 mm corresponds to an rms emittance of $\epsilon = 4 \times 10^{-3} \pi$ mm mrad.

profiles are well in agreement with standard IBS theory ($\propto N^{1/6}$) and existing ESR data [12] and will serve as a reference for the laser cooling measurements. No dependence in equilibrium beam properties was observable on the electron beam current, varied between 10, 50 and 250 mA, however, for 10 mA transverse cooling became less effective at higher ion currents.

Regarding first the spatial bunch length for ion currents below $10\ \mu\text{A}$, laser cooling almost at resonance ($\Delta f_b = 15\ \text{Hz}$ corresponds to $\Delta p/p \sim 10^{-6}$ at $h = 10$) leads to a reduction of the length of a factor of two as compared to electron cooling. The solid line in the upper Fig. 3 depicts the absolute value for the equilibrium length for space-charge dominated bunches of corresponding ion number ($\propto N^{1/3}$) indicating that all ions in the bunch are efficiently laser-cooled. This seems to be different for higher ion currents. Starting from higher currents after injection, the decrease almost proportional to $N^{1/6}$ suggests that, as not enough phase space is available in the region defined by the laser detuning, a hot IBS dominated fraction of the beam exists that could not be resolved due to large noise-dominated base-line fluctuations in the pick-up measurement. Increasing the detuning in this situation and thereby opening momentum space for laser-cooled ions around the center of the bucket leads to an increase in the bunch length and in the integrated pick-up signal, corresponding to a larger number of laser-cooled ions. The same general behavior is observed when different rf voltages are applied (not shown).

Related to the bunch length, the momentum spread is shown in the lower Fig. 3. For the electron-cooled beams it is derived from the Schottky spectra. The solid line is meant to guide the eye indicating at which momentum spread space charge becomes relevant in the upper graph. Evidently, the true momentum spread measured via the laser fluorescence method decreases far beyond this limit into the few times 10^{-7} range, while the bunch length remains constant.

Regarding the little data recorded for the transverse beam profiles the laser-cooled beams above $10\ \mu\text{A}$ do not show any sign of transverse cooling, while for low currents, an onset might be visible. This completely changes when simultaneously electron cooling at an electron current of only 1 mA is applied (stars in the graphs). Though the momentum spread is slightly increased, the beam becomes transversally as cold as for strong electron cooling. Given the low momentum spread and the low emittance, the plasma parameter of these beams is of the order of unity.

SUMMARY AND FUTURE PERSPECTIVES

Summarizing the latter, this first combination of laser and electron cooling provided three-dimensionally cold beams of unprecedented momentum spread for ion currents below $10\ \mu\text{A}$. In the longitudinal degree-of-freedom, laser cooling lead to a reduction of a factor of two in the bunch length and of one order of magnitude in momentum spread as compared to the purely electron-cooled beam. Although only an upper limit of the transverse beam temperature can be given as for the case of electron cooling, stating a plasma parameter of about $\Gamma \gtrsim 1$ seems justified. As the interesting beam currents correspond to linear densities where one-dimensional ordering is possible, one might speculate about such effects being involved in the observation of the unexpected intensity drop of the Schottky signal, shown in Fig. 2d), yet, further experimental as well

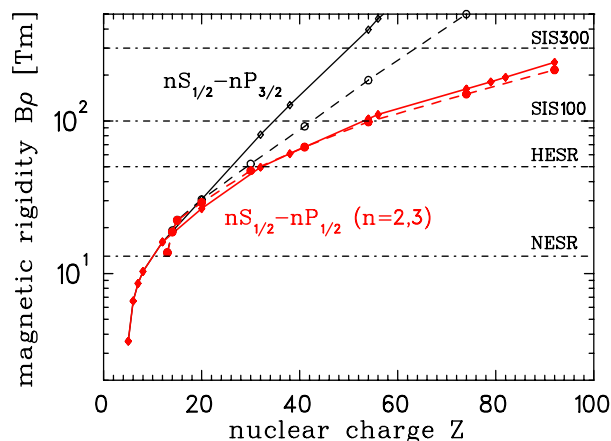


FIGURE 5. Magnetic rigidity required for the storage of ions at an energy where the transition wavelength of the ground state transitions of Li-like (solid lines, rhombs, $n = 2$) and Na-like ions (dashed lines, circles, $n = 3$) are Doppler-shifted into resonance with a counterpropagating laser beam of wavelength $\lambda_{uv} = 257$ nm.

as theoretical studies are mandatory.

Longitudinal cooling times were of the order of seconds and strongly dependent on the cooling scheme, especially when scanning is involved. Consequently, the introduction of an additional broad-band laser system should improve the cooling time. Besides the direct addressing of the whole initial momentum distribution, a broad-band system also has the advantage of efficiently recycling those ions into the cooling process that are lost out of resonance in an IBS event and thus also the control of higher currents should become possible. Ideally, the broad-band laser system can be realized by conventional pulsed laser systems with pulse length in the ns-range. At present, an additional scanning laser system is prepared for first tests instead of a true broad-band system.

The prominent drawback for the practical use of laser cooling as a general cooling method is the lack of suitable optical transitions in most ions of interest. This drawback, however, can be overcome in future heavy ion synchrotrons like the SIS 300 envisaged within FAIR, as the high magnetic rigidity of such machines allows for beam energies Doppler-shifting the ground state excitation of all Li-like heavy ions into an accessible laser frequency range [23], as shown in Fig. 4. Moreover, in this highly relativistic regime, where electron cooling cannot be readily applied any more, the laser force principally increases with the third power of the ion energy [7, 22]. On the one hand, this gain in efficiency is due to the relativistic Doppler-shift, increasing the momentum transfer while, on the other hand, optical transitions in the highly charged ions of interest become faster with the nuclear charge of the ion, for details see [7, 22]. Assuming that broad-band laser systems can be used, cooling times of the order of only few seconds seem possible at energies of $\gamma \sim 30$ for Li-like uranium ions, clearly warranting the further investigation of the method while, for an estimation of equilibrium temperatures, a profound analysis of the competing mechanisms is required.

ACKNOWLEDGMENTS

Work supported by the German BMBF (06ML183).

REFERENCES

1. S. Schröder, et al., Phys. Rev. Lett. **64**, 2901 (1990)
2. J.S. Hangst, et al., Phys. Rev. Lett **67**, 1238 (1991)
3. J.P. Schiffer and P. Kienle, Z. Phys. **A 321**, 181 (1985)
4. N. Madsen, et al., Phys. Rev. Lett. **87**, 274801 (2001)
5. I. Lauer, et al., Phys. Rev. Lett. **81**, 2052 (1998)
6. U. Eisenbarth, et al., Hyperfine Interactions **127**, 223 (2000)
7. U. Schramm, D. Habs, Progress in Particle and Nuclear Physics **53**, 583 (2004)
8. T. Schätz, et al., Nature (London) **412**, 717 (2001), U. Schramm, et al., Phys. Rev. **E 66**, 036501 (2002)
9. U. Schramm, et al., Phys. Rev. Lett. **87**, 184801 (2001)
10. A. Smirnov, et al., these proceedings (COOL05)
11. U. Schramm, et al., Journal of Physics **36**, 561 (2003)
12. M. Steck, J. Opt. Soc. Am. B **20**, 1016 (2003)
13. M. Steck, et al., J. Phys. B **36**, 991 (2003) and Phys. Rev. Lett. **77**, 3803 (1996)
14. H. Danared, et al., J. Phys. B **36**, 1003 (2003)
15. W.R. Johnson, et al., At. Data Nucl. Data Tab. **64**, 279 (1996)
16. U. Schramm, et al., Hyperfine Int. **115** (1998) 57
17. J.S. Hangst, et al., Phys. Rev. Lett. **74**, 4432 (1995)
18. H.-J. Miesner, et al., Nucl. Instr. Meth. **A 383**, 634 (1996)
19. D. Boussard, CAS, CERN-87/3, 416 (1987), O. Boine-Frankenheim, T. Shukla, Phys. Rev. ST AB **8** 034201 (2005)
20. T.J.P. Ellison et al., Phys. Rev. Lett. **70**, 790 (1993)
21. U. Schramm. et al., Proc. PAC 2005, Jacow, FOAD004 (2005)
22. U. Schramm, et al., Nucl. Instr. Meth. **A 532**, 348 (2004)
23. U. Schramm, et al., Lol#18 FAIR APPA–PAC (2004)

BUSSMANN M., SCHRAMM U., HABS D., STECK M., KÜHL T., BECKERT K., BELLER P., FRANZKE B., NÖRTERSCHÄUSER W., GEPPERT C., NOVOTNY C., KLUGE J., NOLDEN F., STÖHLKER T., KOZHUHAROV C., REINHARDT S., SAATHOFF G. AND KARPUK S.

The Dynamics of Bunched Laser-Cooled Ion Beams at Relativistic Energies.

Journal of Physics: Conference Series **88** (2007) 012043

IOP Publishing Limited

Reprinted with kind permission from IOP Publishing Limited. For further information please refer to <http://www.iop.org/EJ/journal/conf>.
License Number 29/8/07

The Dynamics of Bunched Laser-Cooled Ion Beams at Relativistic Energies

M Bussmann¹, U Schramm², D Habs¹, M Steck³, T Kühl³, K Beckert³, P Beller³, B Franzke³, W Nörtershäuser^{3,6}, C Geppert^{3,6}, C Novotny^{3,6}, J Kluge³, F Nolden³, T Stöhlker³, C Kozhuharov³, S Reinhardt⁴, G Saathoff⁵, S Karpuk⁶

¹ Ludwig-Maximilians Universität München, Am Coulombwall 1, D-85748 Garching, Germany

² Forschungszentrum Dresden-Rossendorf e.V., Bautzner Landstrasse 128, D-01328 Dresden, Germany

³ Gesellschaft für Schwerionenforschung mbH, Planckstrasse 1, D-64291 Darmstadt, Germany

⁴ Max-Planck-Institut für Kernphysik, Saupfercheckweg 1, D-69117 Heidelberg, Germany

⁵ Max-Planck-Institut für Quantenoptik, Hans-Kopfermann-Strasse 1, D-85748 Garching, Germany

⁶ Johannes-Gutenberg Universität Mainz, Staudingerweg 7, D-55128 Mainz, Germany

E-mail: michael.bussmann@physik.uni-muenchen.de

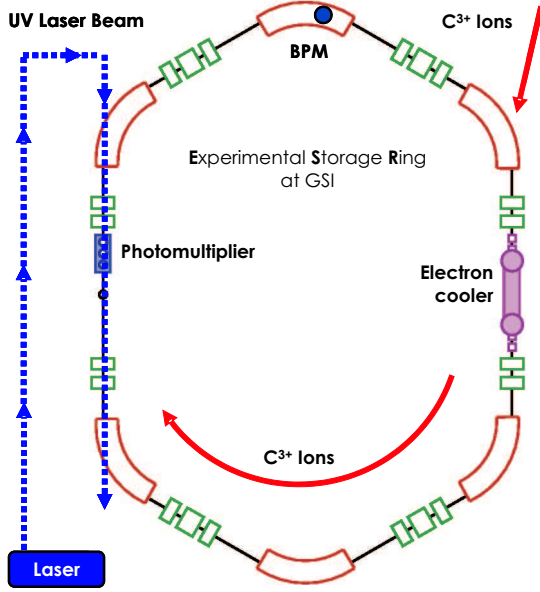
Abstract. We discuss the axial dynamics of laser-cooled relativistic C^{3+} ion beams at moderate bunching voltages. Schottky noise spectra measured at a beam energy of 122 MeV/u are compared to simulations of the axial beam dynamics. Ions confined in the bucket are addressed by the narrow-band force of a laser beam counter-propagating to the ion beam, while the laser frequency is detuned relatively to the cooling transition frequency in the rest frame of the bucket.

At large detuning comparable to the momentum acceptance of the bucket, the axial dynamics can be well explained by the secular motion of individual non-interacting ions. At small detuning, corresponding to a small axial momentum spread $\Delta p_{axial}/p_{axial} < 10^{-6}$ of the ions, the measured Schottky noise spectra can no longer be explained using an approach which neglects the ion-ion interaction. Instead, the model fails when the ion bunch enters the *space-charge dominated* regime, at which the mutual Coulomb-energy of the ions becomes comparable to the kinetic energy of the ions.

1. Introduction

Laser-cooling of bunched ion beams, as first demonstrated in the *ASTRID* storage ring [1], utilises the restoring force of the bucket to counteract the laser force. This cooling scheme does not require a laser beam co-propagating with the ion beam. Instead, only one laser beam counter-propagating to the ion beam is needed to provide a momentum-dependent friction force which damps the synchrotron oscillation of the ions in the bucket. While the ions oscillate in the bucket, those ions in resonance with the laser light are cooled by the combined forces of the bucket and the laser.

Before laser-cooling is applied, the momentum distribution of the bucket resembles the momentum acceptance of the bucket, which is approximately $\Delta p_{acc,b}/p_{acc,b} \approx 2 \times 10^{-5}$ in the experiment discussed here. The momentum acceptance of the laser force of about



| ESR Parameters | |
|---------------------------------------|-----------------------------------|
| Circumference | 108,36 m |
| Betatron tune | 2.3 |
| Slip factor | 0.607 |
| Ion Species | C ³⁺ |
| Beam Energy | 1.47 GeV |
| relativistic β, γ | 0.47, 1.13 |
| revolution frequency | 1.295 MHz |
| lifetime | 450 s |
| Laser Parameters | |
| Laser Source | Ar ⁺ ion laser |
| Operational Mode | cw, single mode, single frequency |
| Wave Length | 257.34 nm (SHG) |
| Power | 40-100 mW |
| Cooling Transitions [2] | |
| 2S _{1/2} → 2P _{1/2} | 155.07 nm |
| 2S _{1/2} → 2P _{3/2} | 155.81 nm |

Figure 1. *Left:* (color online) Schematic view of the *Experimental Storage Ring* ESR at GSI in Darmstadt. The C³⁺ ions circulate clockwise in the ring. The ion beam is overlapped with the counter-propagating laser beam in a straight section of the ring. The laser beam focus is placed at the position of the photomultiplier to maximize the fluorescence light intensity. *Right:* List of experimental parameters.

$\Delta p_{acc,1}/p_{acc,1} \approx 5 \times 10^{-8}$ does not match the initial momentum distribution of the hot ions. Two cooling schemes exist to overcome this mismatch, which both rely on detuning the laser frequency relative to the frequency of the cooling transition for ions at rest in the bucket center. This can be done either by scanning the laser frequency directly or by changing the bunching frequency and keeping the laser frequency fixed. The latter scheme provides a wider detuning range as is accessible with the laser system which was used in the experiment and will thus be the focus of this work. In the following, the experimental conditions will be briefly summarized, before the dynamics of the ions in the bucket and the corresponding beam characteristics will be discussed in detail.

2. Experimental Setup

Laser-cooling is provided using a continuous-wave, single mode, single frequency argon ion laser system. After doubling the laser frequency to $\lambda_{l,lab}/2 = 257.34$ nm, the laser beam is overlapped with the C³⁺ ion beam – see Fig. 1 for a schematic overview of the storage ring including a list of the most important experimental parameters. With the ion beam energy set to 1.47 GeV, the relativistic Doppler shift of the laser wave length from the laboratory frame to the ion rest frame [3] amounts to

$$\lambda_{l,rest} = \frac{\lambda_{l,lab}/2}{\gamma(1 + \beta)} \approx \frac{257.34 \text{ nm}}{1.13 \times (1 + 0.47)} \approx 155 \text{ nm}, \tag{1}$$

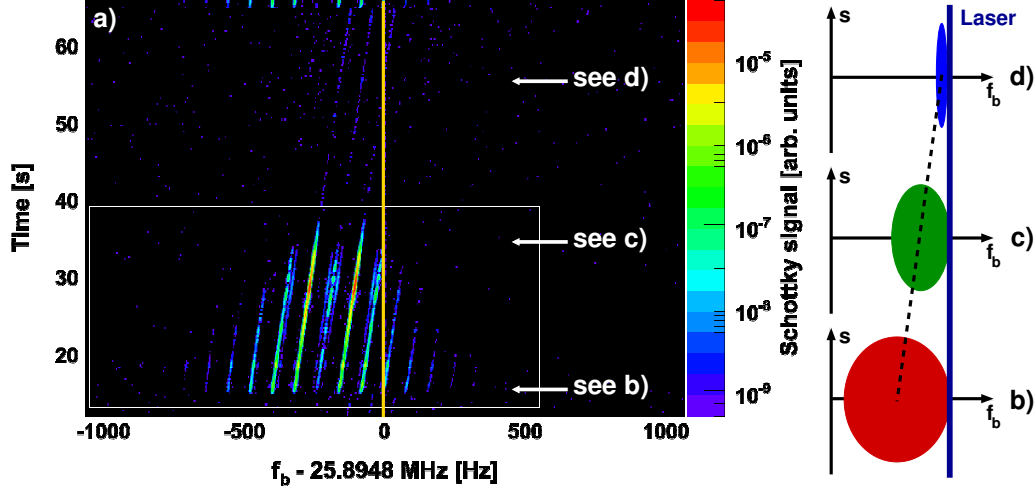


Figure 2. (color online) *a)* Schottky noise signal versus scanning time. The intensity is colour-coded. The white box encloses the part of the spectrum discussed in Fig. 3. The yellow line marks the (fixed) position of the laser frequency relative to the bunching frequency. *b)–d)* Schematic view of the ion bunch (ellipse) at three distinct values of the absolute detuning. The absolute detuning of the bunching frequency relative to the laser frequency decreases from Fig. b) to d) as indicated by the black dotted line. The position of the laser is marked by the solid blue line.

b) The laser is close to the separatrix. A number of sidebands can be seen which indicate the momentum spread of the beam.

c) The absolute detuning has been reduced, the ion bunch is now space-charge dominated.

d) The absolute detuning has almost reached its minimum value. No blowup of the beam due to intra beam scattering is observed.

assuming the orientation of the ion beam and the laser beam to be anti-parallel.

Compared to bunched beams typically provided in storage rings, the moderate bunching voltages of only a few volts resulted in weak axial confinement of the ions and thus in bunch lengths of about 1 m at ion currents on the order of $10 \mu\text{A}$. Measurements of the beam parameters were performed for various bunching frequencies $f_b = h \times f_{\text{rev}}$ subsequently set to the 5th, 10th and 20th harmonic h of the revolution frequency f_{rev} . Given a betatron tune of $Q = 2.3$ [4], the betatron frequency $f_{\text{beta}} = Q \times f_{\text{rev}} \approx 2.9785 \text{ MHz}$ is orders of magnitude larger than the synchrotron frequency of $f_{\text{sync}} \approx 188 \text{ Hz}$ measured for the 20th harmonic at a bunching voltage of about $U_b \approx 7 \text{ V}$. The bunch form thus resembles an ellipsoid elongated in the axial direction.

3. Detuning the bunching frequency relatively to the laser frequency

In the following we focus on a single series of Schottky signals recorded at a bunching frequency of $f_{b,0} \approx 20 \times f_{\text{rev}} \approx 25.894750 \text{ MHz}$, previously discussed in [5]. The sign of the bunching frequency detuning $\Delta f_b = f_b - f_{b,0}$ indicates whether the bucket force and the laser force are opposed to each other (negative Δf_b), thus providing a net cooling force, or if both point in the same direction (positive sign). When both the bucket force and the laser force point in the same direction, the ions are driven out of the bucket by the combined bunching and laser force. The change from negative to positive detuning Δf_b thus easily marks the bunching frequency

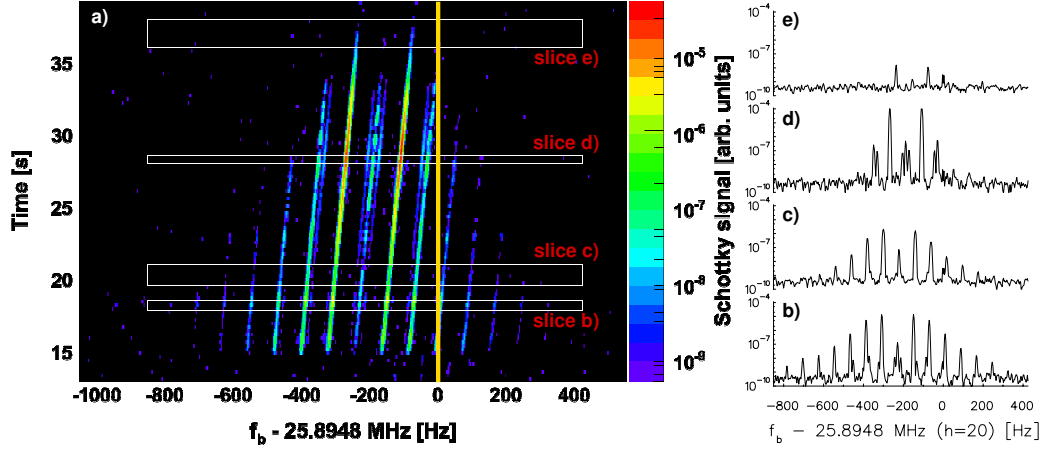


Figure 3. (color online) *a)* Schottky noise signal versus scanning time. This is a detailed view of the region marked by the white box in Fig. 2. The intensity is colour-coded. The white boxes indicate the slices shown in Part *b)*–*e)* of this figure. Again, the yellow line marks the (fixed) position of the laser frequency relative to the bunching frequency. *b)*–*e)* Slices selected from the time evolution of the Schottky signal. The absolute detuning of the bunching frequency relative to the laser frequency decreases from Fig. *b)* to *e)*. The amplitudes of the curves are normalized with respect to the time for which the slice is integrated.

$f_{b,0}$ at which those ions at rest in the bucket are in resonance with the laser frequency. The bunching frequency is detuned at a rate of 10 Hz per second, meaning that every second the bunching frequency is increased by 10 Hz in a single step. During the scan the laser frequency is kept at a fixed value. The scan of the bucket frequency starts with the laser frequency being near the brim of the separatrix, meaning that the relative detuning of the bucket frequency is of the same order as the relative momentum acceptance

$$\frac{\Delta p_{acc,b}}{p_{acc,b}} \approx 2 \times 10^{-5} \approx \frac{1}{\eta} \frac{|\Delta f_b|}{f_b} \quad (2)$$

of the bucket. Both are related by the slip factor η [4]. When the absolute detuning is reduced, subsequently ions with lower relative momentum come in resonance with the laser force and are thus cooled. The total axial momentum spread is therefore reduced during the scan of the bucket frequency. This cooling scheme relies on the cooling time being much faster than the time for the frequency scan (for an estimate of the cooling time see [3]). Furthermore, intra-beam scattering (IBS) can cause fast heating of the ions, which can lead to a sudden increase of the axial momentum that cannot be counteracted by a single, narrow-band laser. A schematic view of the cooling scheme is shown in Fig. 2. The total axial momentum spread of the beam is determined by the position of the laser frequency in momentum space, so that

$$\frac{\Delta p_{axial}}{p_{axial}} \lesssim \frac{1}{\eta} \frac{|\Delta f_b|}{f_b}, \quad (3)$$

as long as no strong heating due to IBS occurs.

4. A detailed discussion of Schottky noise spectra

Fig. 3 *a)* shows a colour-coded plot of the Schottky noise spectrum. The intensity of the Schottky signal is scaled logarithmically, the Y-axis shows the scanning time and the X-axis

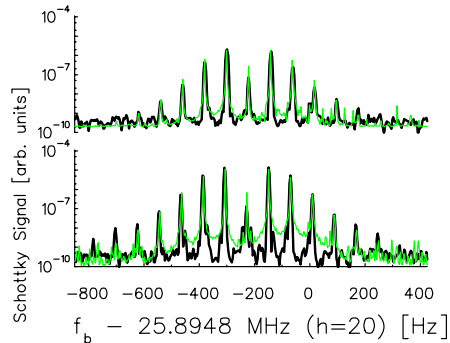


Figure 4. (color online) Slices taken from the Schottky noise spectrum as shown in Fig. 3 b) (lower part) and c) (upper part).

The black curves show the measured data while the green curves depict the simulation result. Spacing, total position and relative intensity of the carrier to the sidebands are well matched by the simulation. The increased pedestal can be attributed to the number of ions used in the simulation, which was about a factor 1000 smaller than in the measurement. The simulation data was scaled in intensity to match the measured curves.

the bunch frequency. The yellow line illustrates the fixed position of the laser frequency. Four slices marked b), c), d) and e) are selected from the time evolution of the Schottky spectrum as indicated by four white boxes.

With decreasing absolute detuning the momentum spread, corresponding to the number of side bands visible in the spectrum, decreases. In Fig. 3 b) the laser frequency is located near the brim of the separatrix, while in part c) the momentum spread is already significantly reduced. Part d) of Fig. 3 marks the transition from an axially emittance dominated beam to a space-charge dominated [6] beam. A detailed analysis of this transition is given in [5], indicating that the linear density of the bunch remains constant for smaller absolute detuning [7], while the axial momentum spread of the beam becomes smaller than the resolution of the Schottky pickup measurement. Finally, part e) of Fig. 3 shows a Schottky spectrum at small absolute detuning. In the following we will focus on two features of the time evolution of the spectra. First, the reduced intensity of the carrier signal compared to the intensity of the side bands. Second, the overall reduction of the intensity of the Schottky noise signal, which finally leads to an almost vanishing signal at small absolute detuning.

5. Axial dynamics of the laser-cooled ions in the bucket

In a simple, yet far reaching simulation of the axial dynamics of the laser-cooled ions in the bucket, we assume that the ions do not interact with each other, but instead can oscillate independently in a harmonic bucket potential. The detuning of the laser force is set according to the measured spectra shown in Fig. 3 b) and c). The axial momentum spread of the ions is precisely reproduced by setting $\Delta p_{\text{axial}}/p_{\text{axial}} \equiv |\Delta f_b|/(\eta f_b)$.

The reduction of the carrier intensity can be simulated by a collective axial oscillation of the ions in the bunch. The amplitude of this oscillation is bounded by the position of the laser force in the bucket well, meaning that the amplitude can be derived by equating the maximum potential energy of the ions with the energy difference given by the absolute detuning of the laser frequency relative to the bucket center.

The collective oscillation itself can be understood by looking closer at the experimental realization of the cooling scheme. Instead of continuously changing the bunching frequency, it has been changed stepwise, thus altering the position of the bucket in momentum space abruptly. We attribute the collective oscillation of the ions in the bucket to this abrupt change in the position of the bucket minimum. The only force counteracting the oscillation is the laser force, which rapidly damps all oscillation amplitudes exceeding the barrier defined by the position of the laser frequency relative to the bucket center.

Thus, assuming both the amplitude of the collective oscillation and the momentum spread of the ions are bounded by the absolute detuning, the Schottky noise spectra depicted in Fig. 3 b)

and c) are reproduced by the simulation, as can be seen in Fig. 4.

Besides the physical characteristics of the Schottky spectra, numerical artefacts due to the underlying Fast-Fourier-Transformation (FFT) algorithm are found both in simulation and experimental data. Namely, the amplitude of the satellite side bands, which appear in 3 d) next to the two regular first order side bands, could be both increased and decreased to zero depending on the number of revolutions of the beam used as an input for the FFT. They could thus be identified to have no physical significance.

6. Schottky noise spectra of space-charge dominated beams

This situation changes when $|\Delta f_b|$ is further reduced. While in the simulation the carrier signal increases drastically, the measurement shows an almost vanishing carrier signal and a further reduction of the first side bands.

In the simulation, the increase of the carrier signal is caused by the reduction of the collective oscillation amplitude. The simulated Schottky noise signal therefore becomes equal to the signal of a stationary ensemble of non-interacting ions resting in the bucket, for which the intensity of the carrier signal is proportional to the number of particles confined in the bucket [8].

The simulation can no longer be brought in accordance with the experimental data when the beam becomes space-charge dominated in the axial direction. In particular, it does not reproduce the decreasing signal strength of the Schottky signal. In the emittance-dominated regime, which is well described by the simulation, the ion dynamics can be modeled neglecting the Coulomb interaction of the ions, since the kinetic energy of the ions is much larger than the mutual Coulomb energy. However, in the space-charge dominated regime, the kinetic energy of the ions is reduced to values where it becomes comparable to the the mutual Coulomb energy [6]. The simulation model therefore has to fail.

7. Conclusion and Outlook

We have shown that a simple model of non-interacting, laser-cooled ions confined in a bucket can reproduce the Schottky noise spectra of emittance-dominated bunched ion beams. At the transition from the emittance-dominated regime to the space-charge dominated regime, the model fails. Currently, no convincing explanation for the observed evolution of the spectra in the space-charge dominated regime exists.

We are currently modifying the experimental setup to overcome the diagnostic limitation of the Schottky measurement and extend the precision of the momentum spread determination based on measuring the fluorescence intensity of the ions in the direct vicinity of the beam. These experimental modifications will be accompanied by a complete, realistic simulation of the ion dynamics in the bucket, which includes the Coulomb-interaction of the ions.

This work was supported by the German BMBF (06ML183).

References

- [1] Hangst J S, Nielsen J S, Poulsen O, Shi P and Schiffer J P 1995 *Phys. Rev. Lett.* **74** 4432–4435
- [2] Schramm U, Bussmann M, Habs D, Steck M, Kühl T, Beckert K, Beller P, Franzke B, Nolden F, Saathoff G, Reinhardt S and Karpuk S 2005 *Hyperfine Interactions* **162** 181–188
- [3] Schramm U, Bussmann M and Habs D 2004 *Nuclear Instruments and Methods in Physics Research Section A: Accelerators, Spectrometers, Detectors and Associated Equipment* **532** 348–356
- [4] Schramm U and Habs D 2004 *Progress in Particle and Nuclear Physics* **53** 583–677
- [5] Schramm U, Bussmann M, Habs D, Steck M, Kühl T, Beckert K Beller P, Franzke B, Nolden F, Saathoff G, Reinhardt S and Karpuk S 2005 *Proceedings of the 2005 Particle Accelerator Conference, PAC05* 401–403
- [6] Dubin D H E and O’Neil T M 1999 *Rev. Mod. Phys.* **71** 87
- [7] Ellison T J P, Nagaitsev S S, Ball M S, Caussyn D D, Ellison M J and Hamilton B J 1993 *Phys. Rev. Lett.* **70** 790–793
- [8] Boussard D 1987 *CERN Accelerator School* **87-03** 416–452

BUSSMANN M., SCHRAMM U., HABS D., KOLHINEN V. AND SZERYPO J.

Stopping highly charged ions in a laser-cooled one component plasma of ions.

International Journal of Mass Spectrometry **251(2-3)** (2006)
179–189

Elsevier Limited

Reprinted from

International Journal of Mass Spectrometry 251(2-3)

Bussmann M., Schramm U., Habs D., Kolhinen V. and Szerypo J.

Stopping highly charged ions in a laser-cooled one component plasma
of ions, 179–189, Copyright (2006)

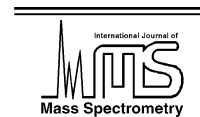
with permission from Elsevier.

License Number 1845960528880

Available online at www.sciencedirect.com

SCIENCE @ DIRECT®

International Journal of Mass Spectrometry 251 (2006) 179–189

www.elsevier.com/locate/ijms

Stopping highly charged ions in a laser-cooled one component plasma of $^{24}\text{Mg}^+$ ions

M. Bussmann*, U. Schramm, D. Habs, V.S. Kolhinen, J. Szerypo

Department für Physik Universität München, Am Coulombwall 1, D-85748 Garching, Germany

Received 7 October 2005; received in revised form 22 December 2005; accepted 19 January 2006

Available online 15 March 2006

Abstract

In-trap preparation of highly charged ions (HCIs) for precision mass measurements by cooling in a strongly coupled plasma of laser-cooled $^{24}\text{Mg}^+$ ions is investigated by molecular dynamics simulations. For HCIs electrostatically decelerated below 1 eV the simulation suggests stopping times of a few 10 μs for high charge states ($Q_{\text{HCI}} = 40$, $A_{\text{HCI}} = 100$). The deposited energy is found to be distributed almost over the entire crystalline plasma of $N = 10^5$ $^{24}\text{Mg}^+$ ions due to collective target response. Almost all $^{24}\text{Mg}^+$ ions stay within the acceptance range of the laser cooling force, thus allowing for the maintenance of the plasma conditions and efficient continuous cooling. Energy loss due to collective effects and hard binary collisions can be clearly distinguished, and can be of the same magnitude for the highest projectile charge states. While the former one can be described by the action of an effective stopping power, the latter is governed by large statistical fluctuations.

© 2006 Elsevier B.V. All rights reserved.

PACS: 21.10.Dr; 24.30.Gd; 25.85.Ge; 27.90.+b

Keywords: Simulation; Laser cooling; Penning trap; HCI; Radio frequency quadrupole

1. Introduction

At present buffer gas cooling [1,2], resistive cooling [3], or electron cooling [4] are standard techniques for the cooling of hot ions to the ambient temperature, which in principle can be applied to any ion species of interest. Laser cooling of ions in traps (see [5] and references therein) in comparison is limited to a small number of ion species, while mK temperatures can be reached in shorter cooling times. We discuss a cooling scheme that can reach temperatures almost as low as those reached by laser cooling, while not being restricted to a particular ion species using a cold plasma of laser-cooled ions, into which an ion of another species is injected and cooled. This scheme is known as *sympathetic* cooling.

Cooling of one ion species by another has been studied extensively in traps [6–9]. Here we focus on a method which aims for delivering cold, highly charged ions for precision nuclear mass measurements. A more precise determination of the fine

structure constant α for example, or a microscopic definition of the mass unit demand uncertainties of $\Delta m/m \approx 10^{-10}$ in the mass measurement of stable nuclei, while weak interaction studies (the unitarity of CKM matrix or a test of the CVC hypothesis) must be supplied with data on nuclei far from the region of stability measured with a relative precision better than $\Delta m/m \approx 10^{-8}$. In the latter case the typical lifetime of the unstable nuclei determines the maximum duration of the cooling process and the measurement. In combination with low production rates lifetimes below 100 ms demand fast and efficient cooling techniques.

For heavy nuclear masses the most precise measurements have been performed in Penning trap systems [10,11] and besides the now operating systems [12–16] there exists a variety of plans for future systems [17–20].

The measurement accuracy in a Penning trap can be expressed by

$$\frac{\Delta m}{m} \propto \frac{m}{t_{\text{RF}} B N_{\text{counts}}^{1/2}} \times \frac{1}{Q_{\text{HCI}}} \quad (1)$$

where t_{RF} is the measurement time, B the magnetic field, and N_{counts} is the number of measurements with individual ions.

* Corresponding author.

E-mail address: michael.bussmann@physik.uni-muenchen.de (M. Bussmann).

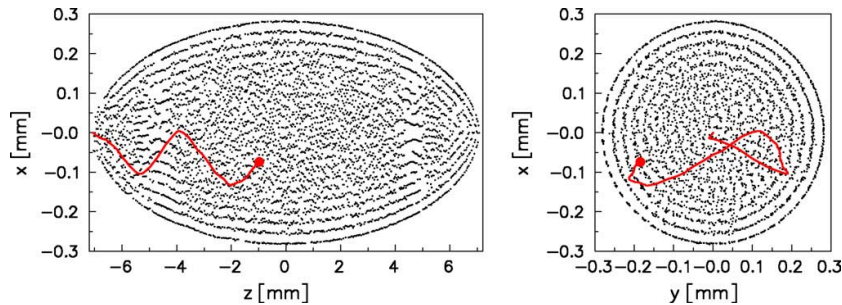


Fig. 1. Trajectory of the HCl through the crystalline plasma in side view (left), the ion having entered from the left, and front view (right). Plasma density: $n_{\text{Mg}} = 4.23 \times 10^{13} \text{ m}^{-3}$, initial energy: $E_{\text{kin,HCl}} = 300 \text{ meV}$, charge state: $Q_{\text{HCl}} = 30$, time: $t = 11.4 \mu\text{s}$. Only a slice through the symmetry plane of the crystal is displayed to reveal the crystalline structure.

While increasing the magnetic field is costly and limited in gain, and a significant increase of t_{RF} or N_{counts} might be impossible for radioactive nuclei, breeding ions to higher charge states Q_{HCl} can be readily applied and gives a considerable increase in precision. With highly charged ions relative accuracies of $\Delta m/m \approx 10^{-8} - 10^{-9}$ can be envisaged for $t_{\text{RF}} < 100 \text{ ms}$. So far the most advanced trap systems in the field, ISOLTRAP at CERN, working with singly charged radioactive ions, and SMILETRAP working with highly charged stable ions, have reached a residual systematic uncertainty of 8×10^{-9} [10] and $10^{-9} - 10^{-10}$ [11], respectively.

In this work we propose a new way of cooling highly charged radioactive ions after charge breeding, typically performed in an electron beam ion source (EBIS), using a combination of electrostatic deceleration of the HCIs and sympathetic cooling in a laser-cooled plasma.

The need for cooling the ions arises from both the ion transport as well as from the accuracy required for precision mass measurements, because the ion bunch suffers from an energy spread of some 10–100 eV, which does not fit the energy acceptance of a precision Penning trap.

Traditional buffer gas cooling in a radio frequency quadrupole (RFQ) cannot be applied to highly charged ions, since charge exchange between the buffer gas atoms and the highly charged ions at a gas pressure of the order of 10^{-1} mbar would result in recombination losses of the high charge states. Resistive cooling requires a cold trap environment and suffers from cooling times longer than the lifetime of short-lived nuclei. Electron or positron cooling is currently investigated (see for example [21]) and also seems promising for in-trap cooling of highly charged ions. The most prominent difference between the ion cooling scheme introduced here and electron cooling schemes is the use of a laser-cooled plasma of ions as a stopping medium instead of electrons cooled by synchrotron radiation. The HCl is injected into the cold one component plasma (OCP) stored in a harmonic potential (see Fig. 1 and the last section for details). The plasma provides a dense, low temperature cooling medium of heavy, charged particles, complementary to standard electron cooling. Demonstrating the feasibility of the stopping of highly charged ions in a laser-cooled OCP of ions requires

two demands to be fulfilled:

- (1) The HCl should be efficiently stopped in and later extracted from the plasma in a time short enough to allow for fast transport to a precision trap.
- (2) The energy deposited in the plasma should not destroy the cold plasma but should instead be distributed over the whole plasma to be quickly cooled by laser cooling.

2. Molecular dynamics simulation of the stopping process

In the following we will use the terms *projectile*, labeling those particles with a high initial energy, usually the HCl, and *target*, labeling the particles of the cooling medium, to distinguish between these two species. Generally the target temperature is kept at an almost constant value via an efficient cooling technique like laser cooling. The cooling rates depend on the strength of the mutual Coulomb-interaction and therefore increase with the square of the charge state of the projectile. Furthermore, the energy transfer is not limited to a finite range of relative projectile–target velocities, and a proper choice of target properties can maximize the heat transfer rate.

Our study focuses on the energy transfer from highly charged ions of some 100 meV initial kinetic energy to a crystalline ensemble of $N = 10^5 \text{ } ^{24}\text{Mg}^+$ ions confined in a three-dimensional harmonic potential (for a comprehensive list of the parameter region covered please refer to Table 1). The radial confinement Ψ_{radial} is strong compared to the longitudinal confinement Ψ_{long} . In this configuration, normally found in Paul traps or Penning traps the shape of the plasma resembles a prolate ellipsoid of width L_{radial} and length $L_{\text{long}} = \alpha L_{\text{radial}}$. When the mutual Coulomb-energy of the ions exceeds the kinetic energy at low temperatures, the plasma is strongly coupled, characterized by a plasma parameter $\Gamma = Q_{\text{r}}^2 e^2 / (4\pi\epsilon_0 a_{\text{WS}} k_{\text{B}} T_{\text{r}}) \geq 1$. For larger values of Γ coupling increases, and the plasma can undergo a phase transition to a crystalline state. In the Coulomb-crystal the ions are ordered in a regular pattern and can interact over a long range. The inter-ion spacing at a plasma density

Table 1
Parameters for the molecular dynamics simulation

| Integration time Δt_{step} (s) 10^{-9} | Lower plasma density | Higher plasma density |
|--|-----------------------|-----------------------|
| Common input parameters | | |
| Ψ_{radial} (V/m ²) | 2.5×10^5 | 3.5×10^5 |
| Ψ_{long} (V/m ²) | 2.5×10^3 | 3.5×10^3 |
| Plasma input parameters | | |
| Number of Mg ⁺ ions | | 10^5 |
| A_{Mg} , Q_{Mg} | | 24, 1 |
| T_{Mg} (K) | | 10^{-3} |
| Input parameters for the highly charged ion (HCI) | | |
| Number of highly charged ions | | 1 |
| A_{HCI} | | 100 |
| Q_{HCI} | | 10, 20, 30, 40 |
| $E_{\text{kin,HCI}}$ (meV) | | 100, 200, 300, 400 |
| Plasma properties derived from the simulation | | |
| L_{radial} (m) | 632×10^{-6} | 565×10^{-6} |
| L_{long} (m) | 15.8×10^{-3} | 14.1×10^{-3} |
| α | 25 | 25 |
| n_{Mg} (m ⁻³) | 3.02×10^{13} | 4.23×10^{13} |
| $a_{\text{WS}}(n_{\text{Mg}})$ (m) | 19.9×10^{-6} | 17.8×10^{-6} |
| ω_{p} ($2\pi \times$ MHz) | 1.482 | 1.754 |
| Γ_{Mg} | 814 | 911 |

n_t is given by the Wigner-Seitz radius $a_{\text{WS}} = (4\pi n_t/3)^{-1/3} = (3Q_t e / (8\pi\epsilon_0 \Psi_{\text{radial}}))^{1/3}$, thus defining a typical length scale of the system. In a strongly coupled plasma the response of the target to the projectile changes significantly compared to the case of a weakly coupled plasma [22], because long-range correlations between the ions are dominant.

In our discussion we frequently use the term *collective* response. It denotes the response of the plasma to the projectile if a major part of all target particles is involved, as, for example, in a plasma wake. In this sense a plasma response due to strong coupling of the target is a collective effect, but collective plasma response does not require strong coupling.

2.1. The simulation model

The creation of the crystalline plasma in a controlled manner is the prerequisite for the simulation. At the start, the $N = 10^5$ ion are placed randomly in the infinite simulation volume and are allowed to propagate freely in the harmonic potential while interacting with each other. Periods of free propagation alternate with periods of strong cooling, until the crystal structure is formed and the individual ion velocities are almost zero. At this point the ion velocities are reset according to the desired temperature, and the plasma is given enough time for equilibration (see Fig. 1 for an impression of the dimensions of the crystalline plasma).

The starting point of the simulation is defined by placing the highly charged ion near the brim of the plasma ellipsoid on the longitudinal symmetry axis of the crystal. The HCI is given an initial kinetic energy with only a velocity component along the longitudinal crystal axis. After a short period the projectile enters the plasma, experiencing subsequent deflections in its binary encounters with the target ions. Fig. 1 shows a typical case

of the projectile path through the crystalline plasma, while the vertical and longitudinal dimensions are not to scale to resolve the crystal order.

No laser cooling is included in the simulation, allowing for direct observation of the energy dissipation in the plasma and the development of the velocity distribution of the $^{24}\text{Mg}^+$ ions. Laser cooling can be safely omitted as long as the relative velocity v_{rel} can be replaced by the projectile velocity v_{p} . However if v_{p} approaches the thermal velocity v_{th} this approximation becomes invalid since the motion of the $^{24}\text{Mg}^+$ ions is strongly influenced by the laser.

In the simulation we concentrate on the energy loss due to the Coulomb-interaction of the projectile with the target ions and do not consider other means of energy loss like excitation, ionization and charge exchange [23–25]. Particularly, the ionization time in the two body charge exchange process $^{24}\text{Mg}^{1+} + ^{100}\text{X}^{40+} \rightarrow ^{24}\text{Mg}^{2+} + ^{100}\text{X}^{39+}$ can be estimated to several thousand seconds [26]. During the passage of the projectile the Coulomb-interaction of all particles with all particles is computed at each time step, thus including the interaction of target ions with both the projectile and other target ions. This imposes a huge amount of computing power, demanding a parallelization of the simulation.

2.2. Simulation techniques

Systems with a large number of charged particles N are usually treated in simulations using Ewald-summation, multipole expansion or related techniques [27]. These techniques approximate the mutual Coulomb-interaction by computing the Coulomb-force for only a subset of particles, describing the interaction with the remaining particles by a mean field approximation. The approximations are either based on a given symmetry of the system or neglect long-range interactions and are not suitable to simulate a particle traversing through a strongly coupled plasma ellipsoid. It is therefore necessary to explicitly compute the mutual Coulomb-interaction for all N particles in the system.

One can choose to simulate stopping via Coulomb-interaction using either molecular dynamics or Monte Carlo techniques. In the latter case only a small section of the entire stopping volume is regarded, and the total stopping power is calculated by statistically summing up the stopping power due to different particle configurations in this volume. The result gained from this summation generally gives a statistically well-defined mean value for the stopping power. However, this approach fails if the regarded volume and thus the computation time becomes too large, as it is the case here. Long-range interactions of the projectile with the target and correlations of the target ions due to strong coupling suggest to simulate the complete system rather than only a small volume.

Thus a molecular dynamics simulation of the stopping which computes the full $N \times N$ Coulomb-force terms for all particles was chosen in the studied case. Since the computational effort of this task grows by N^2 , efficient parallel algorithms [27,28] are used to simulate our model system of $N_{\text{Mg}} = 10^5$ $^{24}\text{Mg}^+$

particles. Still it remains mandatory to minimize the number of force calculations when integrating the equation of motion

$$m_i \frac{d^2 \vec{r}_i}{dt^2} = \left(\sum_{j \neq i}^N \frac{q_i q_j}{4\pi\epsilon_0 |\vec{r}_i - \vec{r}_j|^3} (\vec{r}_i - \vec{r}_j) \right) - q_i (\Psi_{\text{radial}} x_i, \Psi_{\text{radial}} y_i, \Psi_{\text{long}} z_i) \quad (2)$$

where m_i , q_i and $\vec{r}_i = (x_i, y_i, z_i)$ are the mass, charge and coordinate vector of the i th particle. This equation of motion is only valid for small relative velocities and is essentially non-relativistic.

To find the optimum balance between accuracy and computation time, we have tested several numerical integrating schemes, including single-step Runge-Kutta and multi-step predictor-corrector methods [27,29]. Most of these integrating schemes are not time reversible and therefore do not preserve energy, which is a vital constraint when simulating sympathetic cooling. The simple, yet effective, Velocity-Verlet [27] algorithm finally chosen requires only two force computations at an accuracy of $(\Delta\tau_{\text{step}})^4$ for an integration time step $\Delta\tau_{\text{step}} = 1$ ns and is energy conserving. The chosen time step satisfies the criterion $\Delta\tau_{\text{step}} \leq \Delta\tau_{\text{stable}} \equiv (16\pi^3\epsilon_0\mu b_{\text{min}}^3/(Q_t Q_p e^2))^{1/2}$ [30] for stable integration of collision kinematics at the minimum impact parameter b_{min} and for the simulation parameters discussed here we find at minimum $\Delta\tau_{\text{stable}} \approx 4$ ns. Thorough checks of the energy conservation in the system reveal that the simulation is numerically stable for the long simulation period of several thousand time steps, again proving that the integration time chosen is sufficiently small.

An important demand on simulating the mutual interaction of huge numbers of particles is parallelization of the computing algorithm. In this study each time step requires $2N^2 = 2 \times 10^{10}$ computations of the Coulomb-interaction – two for each particle pair, one at time t_0 and one at $t_0 + \Delta\tau_{\text{step}}$. To finish the simulation in a reasonable amount of time while gaining enough information on both the scaling behavior for important parameters as well as systematic errors, it was mandatory to use high end computing power. Fortunately, with the combined computational power of more than three teraflops of two computing clusters housed at our institute and the Leibniz Rechenzentrum, computational time could be lowered to several weeks. To acquire a realistic picture of the stopping dynamics, all particle positions and velocities at each time step were stored on disk for later analysis, and thus several terabyte of data storage were required.

2.3. Modeling the stopping process

Within the linear response model [22] two approaches modeling the target response to the projectile are considered, the binary collision model and the dielectric response model.

In the binary collision model, short-range projectile–target interactions are described by successive binary collisions between the projectile and a target ion. In the dielectric response model, long-range projectile–target interactions are described by the polarization of the plasma induced by the projectile. The

impact parameter b can be used to distinguish between these approaches. At small impact parameters the energy loss can be approximated by pure binary collisions, at large impact parameters it can be restricted to collective target response. A simple way of combining both approaches is by writing the energy loss dE_p per length ds as the sum of the contributions due to binary collisions and to collective effects as

$$\frac{dE_p}{ds} = \int_{b_{\text{min}}}^{b_{\text{trans}}} \frac{d^2 E_{\text{binary}}}{ds db} db + \int_{b_{\text{trans}}}^{b_{\text{max}}} \frac{dE_{\text{collective}}}{ds db} db, \quad (3)$$

choosing appropriate impact parameters b_{min} , b_{max} and b_{trans} . This choice strongly depends on the properties of projectile and target [22,32], as will be discussed later. The minimum impact parameter is determined by the maximum momentum transfer $b_{\text{min}} = Q_p Q_t e^2 / (4\pi\epsilon_0 \mu v_{\text{rel}}^2)$. Here Q_p and Q_t are the projectile, and target particle charge numbers and μ is their reduced mass. A common choice for the maximum impact parameter is the adiabatic screening length $b_{\text{max}} = \lambda_{\text{ad}} = v_{\text{rel}}/\omega_p$. Here v_{rel} is the mean relative velocity of projectile and target particles and ω_p is the plasma frequency of the target plasma [22]. In our case this length can be as long as several hundred micrometers and screening lengths of this size can be directly observed in the simulation. For a target plasma of temperature T_t and constituent mass m_t the relative velocity $v_{\text{rel}} = (v_{\text{th}}^2 + v_p^2)^{1/2}$ is defined by the thermal velocity of the target $v_{\text{th}} = (3k_B T_t/m_t)^{1/2}$ and the projectile velocity v_p .

If both the target–projectile and target–target coupling are weak, the energy loss can be written for $v_p \gg v_{\text{th}}$ as [22]

$$\frac{dE_p}{ds} = -\frac{Q_p^2 e^2}{4\pi\epsilon_0} \frac{\omega_p^2}{v_p^2} \int_{b_{\text{min}}}^{b_{\text{max}}} \frac{db}{b} = \frac{Q_p^2 e^2}{4\pi\epsilon_0} \frac{\omega_p^2}{v_p^2} \Lambda_C(E_p) \propto \frac{\Lambda_C}{E_p}, \quad (4)$$

introducing the Coulomb-logarithm $\Lambda_C \equiv \int_{b_{\text{min}}}^{b_{\text{max}}} \frac{db}{b} = \ln(b_{\text{max}}/b_{\text{min}})$ which depends on the kinetic energy of the projectile. The time scale for the response of a target plasma of density n_t to the projectile particle is given by the inverse $\tau_p \equiv \omega_p^{-1}$ of the plasma frequency $\omega_p = (Q_t^2 e^2 n_t / (\epsilon_0 m_t))^{1/2}$. On shorter time scales the target response to the projectile is less pronounced and screening due to target particles is suppressed.

At large projectile velocities compared to the thermal velocity of the target particles the energy loss shows the typical scaling $dE_p/ds \propto Q_p^2/E_p$. As the projectile approaches the thermal velocity the energy loss increases drastically, reaching its maximum for $v_p = v_{\text{th}}$. If compared to typical values for electron cooling – $T_{t,e} \approx 10^3$ K, $v_{\text{th},e} \approx 10^4$ m/s, $n_{t,e} \approx 3 \times 10^{13}$ m⁻³ [33] – the maximum energy loss in a laser-cooled one component plasma of ²⁴Mg⁺ ions ($v_{\text{th},\text{Mg}} \approx 1$ m/s, see Table 1) is roughly $(dE_{\text{Mg}}/ds)/(dE_e/ds) = m_e v_{\text{th},e}^2 / (m_{\text{Mg}} v_{\text{th},\text{Mg}}^2) \approx 10^3$, assuming similar Coulomb-logarithms and target densities.

In two ways the linear response model is challenged in the studied case. First, it is unable to describe the target response adequately, because it neglects long-range correlations between the constituents of the target. Second, it cannot fully describe the projectile's motion through the plasma, especially at small projectile velocities, since this is affected by the internal target

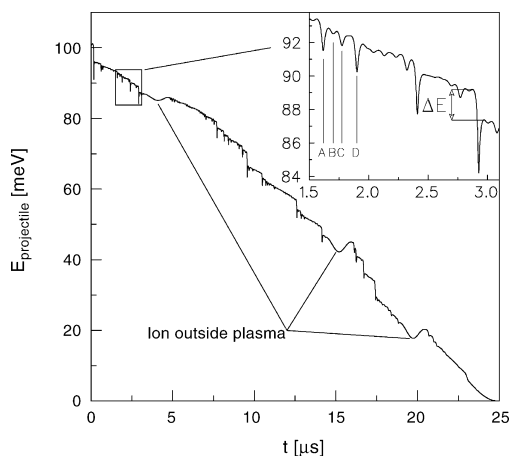


Fig. 2. Kinetic energy of a highly charged ion ($A_{\text{HCl}} = 100$, $Q_{\text{HCl}} = 10$) during the passage through the $^{24}\text{Mg}^+$ plasma ($\Gamma_{\text{Mg}} = 814$). The insert shows a hard collision with energy loss ΔE in detail and points A, B, C and D indicate successive hard collisions. In addition those times at which the highly charged ion is found outside of the plasma are indicated.

configuration. For a correct analysis of the stopping dynamics it is thus vital to use a molecular dynamics simulation which includes these effects.

Fig. 2 shows a typical example of the change in kinetic energy a highly charged ion experiences when passing through the $^{24}\text{Mg}^+$ crystal. While energy loss due to collective effects leads to a steady decrease in kinetic energy defining the slope of the energy curve, hard binary collisions are characterized by a rapid short-time decrease in the kinetic energy, followed by an equally fast acceleration phase. In the following we will try to analyze both energy loss processes. Due to the low statistics imposed by the huge simulation effort we focus on the energy loss due to collective response, for which we will present results on stopping times.

3. Results

3.1. Energy loss via hard binary collisions

Binary collisions are accurately resolved by the simulation, as seen, for example, at the points labeled A, B, C and D in Fig. 2. The time intervals are well explained by successive collisions of the projectile with velocity $v_{\text{HCl}} \approx 420$ m/s with target ions for an average spacing of $a_{\text{WS}} \approx 20$ μm . For a single collision the energy loss, denoted ΔE in Fig. 2, will be analyzed in the following. In a pure binary collision the total energy $E_{\text{sum}} = E_{\text{kin,HCl}} + E_{\text{kin,Mg}} + E_{\text{pot}}$ is conserved. When the highly charged ion approaches the resting $^{24}\text{Mg}^+$ the potential energy E_{pot} and the kinetic energy $E_{\text{kin,Mg}}$ of the $^{24}\text{Mg}^+$ increase. The potential energy and the acceleration of the $^{24}\text{Mg}^+$ reach their maxima at the point of closest approach, indicated by the vertical black line in Fig. 3. The fraction of the potential energy that is not converted into kinetic energy of the

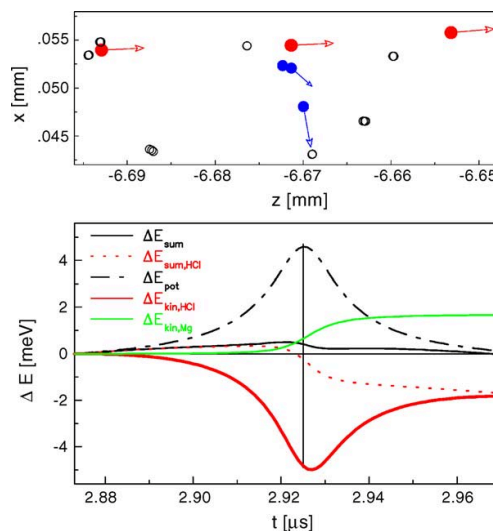


Fig. 3. The upper figure shows three stages of the binary collision denoted by the energy loss ΔE in Fig. 2. The three positions of the ions corresponding to the three stages of the collision are plotted together. Red dots: position of the highly charged ion at (from left to right) the beginning of the collision where the $^{24}\text{Mg}^+$ ion is still at rest, the moment of closest approach and the end of the collision, blue dots: position of its $^{24}\text{Mg}^+$ collision partner, black dots: $^{24}\text{Mg}^+$ ions in their vicinity. The arrows indicate the direction of flight as well as the velocity. The ion positions are shown in projection, thereby losing the depth information. Below: development of the total energy during the collision as described in the text. (For interpretation of the references to color in this figure legend, the reader is referred to the web version of the article.)

$^{24}\text{Mg}^+$ ion is regained by the passing highly charged ion after the impact.

In Fig. 3 the change in E_{sum} denoted by ΔE_{sum} is plotted from the onset of the collision to its end together with the changes in the kinetic energy of the highly charged ion and the $^{24}\text{Mg}^+$ ion, $\Delta E_{\text{kin,HCl}}$ and $\Delta E_{\text{kin,Mg}}$. Additionally the change ΔE_{pot} in potential energy and in the total energy of the highly charged ion, $\Delta E_{\text{sum,HCl}} = \Delta E_{\text{kin,HCl}} + \Delta E_{\text{pot}}$, are depicted.

Unlike in a free binary collision one finds $\Delta E_{\text{sum}} > 0$ during the collision. The positive excess can be identified with the binding energy of the $^{24}\text{Mg}^+$ ion in the crystal lattice. This example shows that the simulation, unlike a simple binary collision approach, is capable of providing insight in the full collision kinematics.

Since the mass of the highly charged ion m_{HCl} is comparable to the $^{24}\text{Mg}^+$ mass m_{Mg} and fluctuations in the projectile velocity are proportional to $(m_{\text{Mg}}/m_{\text{HCl}})^{1/2}$ [31], the energy loss in a single, close binary collision can become significantly large compared to the overall energy loss. Thus the summed stopping power of few such encounters can be substantial, although only a small number of $^{24}\text{Mg}^+$ ions experiences hard collisions with the HCl.

These results show that a correct treatment of the energy loss due to hard binary collisions demands a thorough statistical analysis of the fluctuations in the target velocity. With the data yet available, it is not possible to give a well based

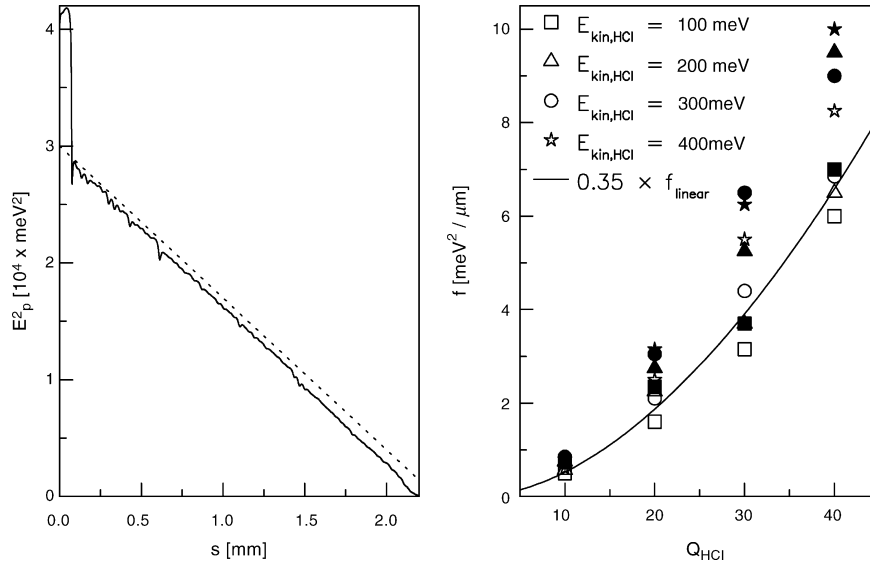


Fig. 4. Left: energy curve ($Q_{\text{HCl}} = 40$, $n_{\text{Mg}} = 3.02 \times 10^{13} \text{ m}^{-3}$) overlaid with a dashed line of slope $-2f$. Right: the slope f of the energy curve determined by the energy loss in collective scatterings is presented for various initial energies. The solid symbols correspond to $n_{\text{Mg}} = 4.23 \times 10^{13} \text{ m}^{-3}$, the open symbols to $n_{\text{Mg}} = 3.02 \times 10^{13} \text{ m}^{-3}$. The solid curve indicates the scaling $f_{\text{linear}} \propto Q_{\text{HCl}}^2$ predicted by linear response theory.

result for $d^2 E_{\text{binary}}/dsdb$. Fortunately, with the computational power available at the Leibniz Rechenzentrum, the statistics will be increased in the future. For increasing charge states the simulations suggest an increase in the contribution of hard binary collisions to the total energy loss, amounting to more than half of the energy loss due to collective response, see Fig. 8.

3.2. Energy loss via collective effects: stopping powers and cooling times

Collective effects can be distinguished from hard binary collisions by setting an upper limit to the kinetic energy carried away by a single $^{24}\text{Mg}^+$ ion, equivalent to a threshold impact parameter b_{trans} above which binary collisions are neglected (see [32] and Eq. (3)). Note, that not only those interactions included in the dielectric response model, but also long-range interactions due to correlations contribute to the energy loss.

Following Eq. (4) one finds $dE_p/ds = -f/E_p$, where f is the stopping power multiplied by the projectile energy. This simple approach neglects the weak energy dependence of the Coulomb-logarithm. In the linear response model the factor f can be expressed as

$$f_{\text{linear}} = \frac{Q_p^2 e^2 m_p \omega_p^2}{8\pi\epsilon_0} \times \Lambda_C \frac{v_p \gg v_{\text{rel}}}{m_p \gg m_t} \frac{Q_p^2 e^2 m_p \omega_p^2}{8\pi\epsilon_0} \times \ln \left(\frac{128^{1/2} \pi \epsilon_0}{Q_p Q_t e^2 m_p^{1/2} \omega_p} E_p^{3/2} \right). \quad (5)$$

Integration yields $E_p^2 = -2fs$. In the left part of Fig. 4 $E_{\text{kin,HCl}}^2$ is plotted versus the path length s denoting the distance the pro-

jectile has traveled through the target plasma. If only the overall slope of the energy curve is considered, neglecting the influence of the hard binary collisions, one can deduce an estimate for f as demonstrated by the dotted line. Hard binary collisions lead to steps in the energy curve, but do not alter the continuous slope significantly. This slope is determined by the continuous loss due to simultaneous interactions of the projectile with a large number of target ions, each taking away only a very small fraction of the energy. By fitting a straight line following this general slope, neglecting the large steps caused by hard binary collisions, one can estimate the energy loss due to collective effects. Due to low statistics and systematic errors in fitting a combined error of about 20% is assumed.

These values are plotted in the right part of Fig. 4 versus the projectile charge state. For the special case of $E_{\text{kin,HCl}} = 100 \text{ meV}$ and $n_{\text{Mg}} = 4.23 \times 10^{13} \text{ m}^{-3}$, corresponding to the solid square data points, the curve $0.35 \times f_{\text{linear}}$ is plotted as a fit to the data points. This suggests that the stopping power due to collective response amounts to about one third of the total stopping power predicted by linear response theory.

The scaling of the data with Q_{HCl} and $E_{\text{kin,HCl}}$ is compared to the scaling predicted by linear response theory. In Fig. 5 all data points are divided by the corresponding value for f_{linear} . Although the statistical basis of single runs in the simulation is weak, a trend can be observed: the scaling of the energy loss with the charge state of the highly charged ion is weaker than expected. We attribute this to enhanced screening as known from the case of electron cooling. No significant change in the energy dependence of the stopping power is found for $v_p \gg v_{\text{th}}$.

If the maximum impact parameter is chosen to be $b_{\text{max}} = \lambda_{\text{ad}}$, one can calculate a value for b_{trans} . Introducing the Coulomb-logarithm $\Lambda_r \equiv \ln(b_{\text{max}}/b_{\text{trans}})$ and the ratio $r \equiv f/f_{\text{linear}}$ one

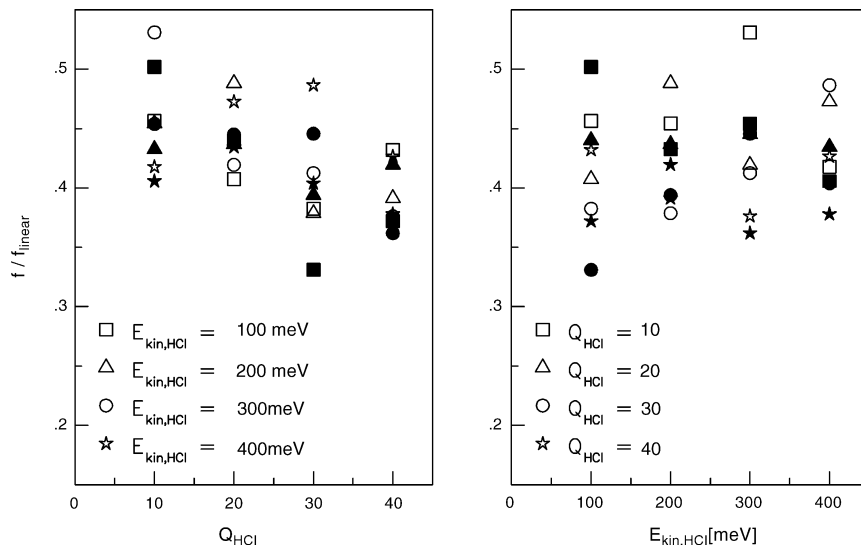


Fig. 5. Scaling of f with charge state (left) and initial kinetic energy (right). The solid symbols correspond to $n_{\text{Mg}} = 4.23 \times 10^{13} \text{ m}^{-3}$, the open symbols to $n_{\text{Mg}} = 3.02 \times 10^{13} \text{ m}^{-3}$. The values correspond to the data points found in Fig. 4.

finds $b_{\text{trans}} \equiv (b_{\text{max}}/b_{\text{min}})^{1-r} \times b_{\text{min}}$. With this we approximate f by $(Q_p^2 e^2 m_p \omega_p^2 / (8\pi\epsilon_0)) \times \Lambda_r$. For the case of $E_{\text{kin,HCl}} = 100$ meV, $n_{\text{Mg}} = 4.23 \times 10^{13} \text{ m}^{-3}$ and $Q_{\text{HCl}} = 40$ we find $b_{\text{trans}} = 0.64 \times a_{\text{WS}}$ with $r = 0.35$. Following Eq. (3) this would suggest that energy loss due to collective response can be found for impact parameters as low as $0.64 \times a_{\text{WS}}$. The energy transfer in a collision with impact parameter $0.64 \times a_{\text{WS}}$ would amount to $\Delta E = 2Q_p^2 Q_{\text{HCl}}^2 e^4 / ((4\pi\epsilon_0)^2 m_t b_{\text{trans}}^2 v_{\text{rel}}^2) \approx 1$ meV [32]. This indicates that linear response theory might be insufficient to give a full description of the stopping dynamics in the studied case.

Plotted in Fig. 6 is the stopping time $\tau_{\text{stop}} = (2m_p E_p^3)^{1/2} / f$ [31], which again only serves as an upper limit to the expected value. Stopping times of a few 10 μs are observed for the high charge states of interest.

A thorough theoretical treatment of the stopping due to collective target response must include further analysis of screening lengths, plasma oscillations and the influence of coupling. This can be achieved by a detailed analysis of the energy deposition in the plasma (see Fig. 7). Though such an analysis goes beyond the scope of this paper, some features of the projectile's passage through the crystal which are related to screening will be

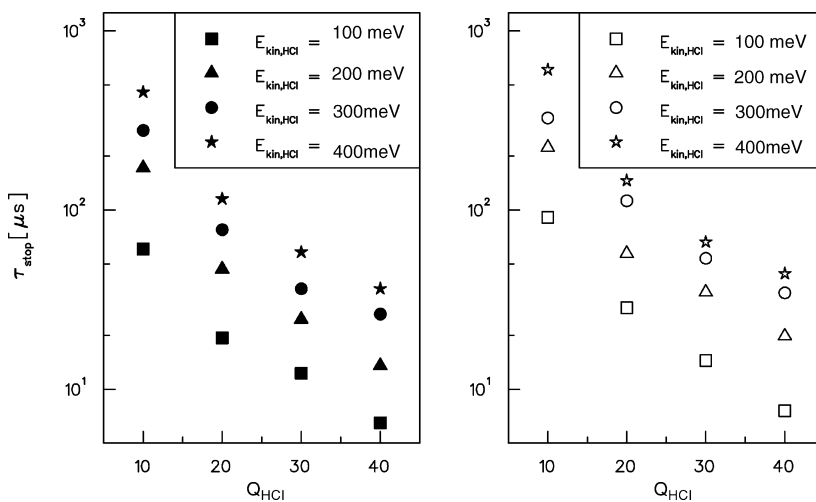


Fig. 6. Stopping times for various initial energies. The solid symbols correspond to $n_{\text{Mg}} = 4.23 \times 10^{13} \text{ m}^{-3}$, the open symbols to $n_{\text{Mg}} = 3.02 \times 10^{13} \text{ m}^{-3}$. The values correspond to the data points found in Fig. 4.

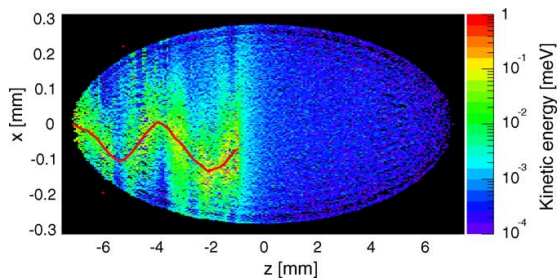


Fig. 7. Spatial distribution of the energy deposited by the HCI after passing through the $^{24}\text{Mg}^+$ plasma. The color encoded energy values result from a projection of the kinetic energy of the $^{24}\text{Mg}^+$ ions along the y -axis and are presented in a logarithmic scale. The trajectory of the HCI is shown in red. The corresponding simulation parameters are the same as in Fig. 1. (For interpretation of the references to color in this figure legend, the reader is referred to the web version of the article.)

discussed. From the spatial distribution of the deposited energy one can deduce an upper limit to the interaction radius which has to be taken into account when determining Δ_C . The energy deposition of the projectile in the plasma ranges as far as several hundred micrometers, proving the existence of long-range interactions of the projectile ion with the target ions. The propagation of the deposited energy is determined by the projectile velocity and at early stages of the projectile's passage through the target plasma one finds that the flow of energy in the plasma is slow compared to the projectile velocity. We attribute this to the long time τ_p it takes the plasma to react to the projectile.

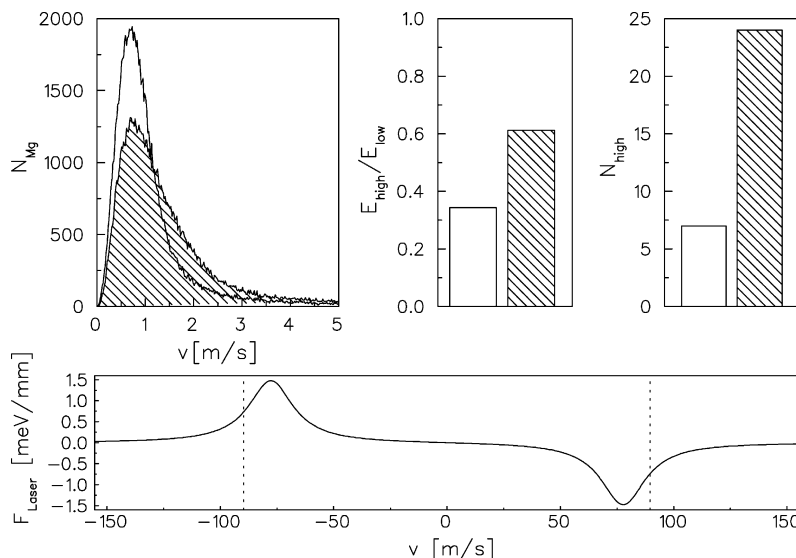


Fig. 8. Upper left: velocity distribution of the $^{24}\text{Mg}^+$ after the HCI has stopped ($n_{\text{Mg}} = 3.02 \times 10^{13} \text{ m}^{-3}$). Upper middle: ratio of the total kinetic energy E_{high} of all $^{24}\text{Mg}^+$ with $E_{\text{kin,Mg}} > 1 \text{ meV}$ and the total kinetic energy E_{low} of all $^{24}\text{Mg}^+$ with $E_{\text{kin,Mg}} < 1 \text{ meV}$. Upper right: number of ions with $E_{\text{kin,Mg}} > 1 \text{ meV}$. The hatched area corresponds to $Q_{\text{HCI}} = 40$, $E_{\text{kin,HCI}} = 400 \text{ meV}$, the other to $Q_{\text{HCI}} = 10$, $E_{\text{kin,HCI}} = 100 \text{ meV}$. Lower part: combined force of two counterpropagating laser beams as given in Eq. (6) ($\delta = 6.5 \times \Gamma_L$, $S = 3$, transition wavelength $\lambda_L = 2\pi/|k_L| = 280 \text{ nm}$, natural linewidth $\Gamma_L = 2\pi \times 42.7 \text{ MHz}$). The dashed lines at $v = \pm 90 \text{ m/s}$ correspond to an ion energy of $E_{\text{kin,Mg}} = 1 \text{ meV}$.

3.3. Plasma stability and laser cooling

In all simulated cases the crystalline plasma does not show signs of Coulomb-explosion. Although the energy deposition by the projectile is considerable, the crystalline structure is only locally disturbed. Even in the case of high initial projectile energy and charge state the structural damage remains local, because much of the projectile energy is deposited over the whole plasma volume. The energy loss due to collective effects thus counteracts the local destruction of the crystalline structure due to hard binary collisions and prevents a Coulomb-explosion of the target plasma.

Fast and efficient laser cooling of the target plasma demands that most of the target ions remain within the acceptance of the laser force

$$F_L(\vec{v}_{\text{Mg}}) = (\hbar/8) \times |\vec{k}_L| S \Gamma_L^3 / ((\delta - \vec{v}_{\text{Mg}} \cdot \vec{k}_L)^2 + (\Gamma_L/2)^2 (1 + S)) \quad (6)$$

of typically only few 10 m/s (some 100 μeV). Typically two counterpropagating laser beams with direction \vec{k}_L are applied for cooling, both at negative detuning δ as sketched in Fig. 8. The strength of the resulting laser force is determined by the saturation parameter S . Since a detuning of few Γ_L is needed to maintain a low plasma temperature, the velocity acceptance of the laser force is limited if the laser frequency is not scanned, a procedure that takes considerable time and should thus be avoided. The selection of an appropriate detuning value therefore depends on the velocity distribution of the target plasma after the projectile has deposited its initial energy in the plasma.

The upper left part of Fig. 8 shows two examples of the final velocity distribution of the plasma ions. For a detuning of $\delta = 6.5 \times \Gamma_L$ all $^{24}\text{Mg}^+$ ions with $E_{\text{kin,Mg}} < 1$ meV or $v_{\text{Mg}} = 90$ m/s are in the acceptance of the laser force. In the middle part the total kinetic energy of all $^{24}\text{Mg}^+$ ions with $E_{\text{kin,Mg}} > 1$ meV is set in relation to the total kinetic energy of those $^{24}\text{Mg}^+$ ions with $E_{\text{kin,Mg}} < 1$ meV. The total number of the ions with $E_{\text{kin,Mg}} > 1$ meV is negligibly small as can be seen in the upper right part of the figure. Nevertheless the amount of the total kinetic energy carried away by these hot ions is considerable. Further studies must show whether these ions are sympathetically cooled by the cold ions or if a sort of evaporative cooling can be applied.

4. Experimental realization of the cooling scheme

Inside an Electron Beam Ion Source (EBIS) atoms of interest for precision mass measurements undergo an ionization cascade in collisions with energetic electrons until the desired charge state is reached after few 10 ms. The resulting ion beam consists of an ensemble of ions of varying charge state and energy and can be characterized by an extraction time τ_{EBIS} after which 90% of the ions are extracted. To adjust the kinetic energy of the HCIs exiting the EBIS with an energy spread of some 10–100 eV to the level where ion cooling as described above is most efficient, we propose the use of a segmented linear radio frequency quadrupole (RFQ) system. In such a linear Paul trap ions are radially confined by a radio frequency quadrupole field of frequency Ω_{RF} if $0 < q \ll 0.9$. The stability parameter $q \approx \frac{1}{\Omega} \sqrt{8 \frac{Qe}{m}} \Psi_{\text{radial}}$ depends on the particle's charge to mass ratio Qe/m . By adjusting the strength and frequency of the radial confinement field, ions of different species and charge state can be trapped and cooled together [5].

A pulsed beam of HCIs coming from the EBIS is transferred into the RFQ. The pulse duration, the energy spread ΔE_{EBIS} and the desired efficiency determine the length L_{RFQ} of the RFQ.

Assuming a rectangular pulse shape one can introduce an injection efficiency p_{inj} determining the fraction of ions that are trapped in the RFQ and its length is then given by $L_{\text{RFQ}} =$

$\tau_{\text{EBIS}} p_{\text{inj}} (Q_{\text{HCl}} e \Delta E_{\text{EBIS}} / (2m_{\text{HCl}}))^{1/2}$. For the proposed cooling scheme shortening the RFQ results in shorter cooling times for the sacrifice of a decrease in injection efficiency. This decrease can be compensated if shorter pulses are achieved – for example by using fast extraction schemes [34]. Optimizing the overall duration and efficiency of both charge breeding and cooling for a specific ion of interest requires careful tuning of the EBIS ion beam parameters to the acceptance of the RFQ cooler.

During the cooling the ions in the RFQ are trapped in a potential well $U_{\text{RFQ}}(z)$ along the beam direction z by applying different voltages to the electrode segments (see Fig. 9). Opposite to the injection region of the RFQ the $^{24}\text{Mg}^+$ ions are laser-cooled in a potential well separated from the trapping region, while the HCl oscillate in the trapping region. When the trapping potential is raised those highly charged ions with sufficient energy to overcome the barrier separating the trapping region from the cooling region enter the laser-cooled $^{24}\text{Mg}^+$ plasma, which can be detected by a change in the fluorescence of the $^{24}\text{Mg}^+$ ions. By constantly rising the trapping potential, all highly charged ions can be successively cooled, stored and detected in the cooling region. For efficient cooling the difference in kinetic energy between the HCl and $^{24}\text{Mg}^+$ ions should be kept as small as possible (see Eq. (4)).

The overall storage period for all HCIs trapped depends on the length L_{RFQ} of the RFQ and the energy spread of the HCl beam. While the length of the RFQ determines the maximum time it requires for a highly charged ion to reach the cooling region, the energy spread determines the overall raise of the trapping potential with respect to the cooling region. The system can be optimized for either high efficiency or fast cooling, depending on the ion of interest. For rare short-lived ions, detected in the cooling region, the cycle could even be stopped for immediate transfer to the measurement trap. In this operation mode the time for the electrostatic deceleration can be kept small compared to the time needed for cooling and ejection of the HCl.

Those highly charged ions stopped in the plasma of laser-cooled $^{24}\text{Mg}^+$ reside in the cooling region and must be extracted to be transferred to the precision Penning trap. One method of extraction is to lower the potential at the RFQ exit leading to the precision Penning trap while holding back the $^{24}\text{Mg}^+$ ions by

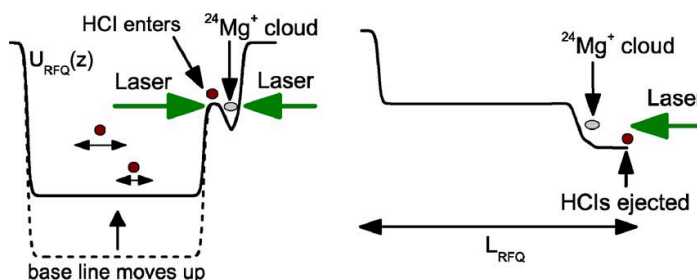


Fig. 9. Left: sketch of the longitudinal potential gradient during the cooling. The trap is divided in a long trapping section and a small cooling section where the $^{24}\text{Mg}^+$ ions are located. During the cooling the base line of the storing section potential is continuously raised. Right: potential configuration for the extraction of the HCIs. The laser force keeps the $^{24}\text{Mg}^+$ ions inside the trap while the HCIs are ejected.

the laser force. If the HCIs are positioned close to the edge of the plasma they travel along the potential gradient towards the RFQ exit while the counteracting laser force prevents the loss of the $^{24}\text{Mg}^+$ ions. The advantages of this extraction scheme are two-fold. First, no reloading of $^{24}\text{Mg}^+$ ions is necessary after the extraction of the cooled highly charged ions. Second, reheating of the cool ensemble of highly charged ions during extraction can be minimized by adjusting the potential gradient. Since the laser has to counteract the potential gradient to avoid a loss of plasma ions the potential gradient E_{extract} cannot be greater than some meV per mm. Fortunately the corresponding acceleration force $F_{\text{extract}} = Q_{\text{HCI}} e E_{\text{extract}}$ grows with the charge state. Still, extraction times of the ions might be constrained by shielding effects in the cold plasma and the small potential gradient. In the future we plan to simulate this extraction scheme.

5. Conclusion and outlook

We have shown that efficient stopping of low energy highly charged ions in a one component plasma of laser-cooled $^{24}\text{Mg}^+$ is possible, providing cooling times of a few 10 μs once the ion is prepared at sub-eV energies. Many important properties of the stopping process can be modeled using classical linear response theory. Nevertheless, the determination of absolute values for the stopping power requires a well-justified definition of the correct range of projectile–target interactions. This definition demands a separate treatment of energy loss due to hard collisions and collective effects. While the latter can be described by an effective energy loss the former can only be treated defining an average stopping power deduced from statistically summing the results of consecutive measurements. Fully understanding the complexities of the stopping process remains an open task which we plan to address in the future. This includes studies of the collective response of the crystalline plasma and a comparison with electron and positron cooling. Furthermore, recent results not included here suggest only a weak dependence of the stopping power on the strength of the target coupling, promising similar stopping power for moderately laser-cooled plasmas. To conclude, we believe that ion cooling can become an important tool in future precision mass experiments.

Acknowledgments

The authors want to thank Jürgen Kluge for many inspiring interactions, keeping atomic and laser physics stirring at GSI. M. Bussmann would furthermore like to thank M. Schubert (LS Habs) and R. Bader (LRZ) for their invaluable help with the computer clusters which were used in the simulation. This work was partially supported by Leibniz Rechenzentrum project UH351AE.

References

- [1] G. Savard, St. Becker, G. Bollen, H.-J. Kluge, R.B. Moore, Th. Otto, L. Schweikhard, H. Stolzenberg, U. Wiess, *Phys. Lett. A* 158 (1991) 247.
- [2] F. Herfurth, J. Dilling, A. Kellerbauer, G. Bollen, S. Henry, H.-J. Kluge, E. Lamour, D. Lunney, R.B. Moore, C. Scheidenberger, S. Schwarz, G. Sikler, J. Szerypo, *Nucl. Instrum. Methods Phys. Res., Sect. A* 469 (2001) 254.
- [3] H. Häffner, T. Beier, S. Djekić, N. Hermanspahn, H.-J. Kluge, W. Quint, S. Stahl, J. Verdú, T. Valenzuela, G. Werth, *Eur. Phys. J. D* 22 (2003) 163.
- [4] G. Gabrielse, X. Fei, L.A. Orozco, R.L. Tjoelker, J. Haas, H. Kalinowsky, T.A. Trainor, W. Kells, *Phys. Rev. Lett.* 63 (1989) 1360.
- [5] U. Schramm, D. Habs, *Prog. Part. Nucl. Phys.* 53 (2004) 583.
- [6] D.J. Larson, J.C. Bergquist, J.J. Bollinger, W.M. Itano, D.J. Wineland, *Phys. Rev. Lett.* 57 (1986) 70.
- [7] P. Bowe, L. Hornekar, C. Brodersen, M. Drewsen, J.S. Hangst, *Phys. Rev. Lett.* 82 (1999) 2071.
- [8] B. Roth, U. Fröhlich, S. Schiller, *Phys. Rev. Lett.* 94 (2005) 053001-1.
- [9] S. Toleikis, R. Maruyama, D.A. Church, D. Schneider, S.J. Freedman, I. Kominis, P.A. Vetter, *Nucl. Instrum. Methods Phys. Res., Sect. B* 235 (2005) 479.
- [10] A. Kellerbauer, K. Blaum, G. Bollen, F. Herfurth, H.-J. Kluge, M. Kuckein, E. Sauvan, C. Scheidenberger, L. Schweikhard, *Eur. Phys. J. D* 22 (2003) 53.
- [11] T. Fritioff, H. Bluhme, R. Schuch, I. Bergström, M. Björkhage, *Nucl. Phys. A* 723 (2003) 3.
- [12] I. Bergström, C. Carlberg, T. Fritioff, G. Douyset, J. Schönfelder, R. Schuch, *Nucl. Instrum. Methods Phys. Res., Sect. A* 487 (2002) 618.
- [13] G. Bollen, F. Ames, G. Audi, D. Beck, J. Dilling, O. Engels, S. Henry, F. Herfurth, A. Kellerbauer, H.-J. Kluge, A. Kohl, E. Lamour, D. Lunney, R.B. Moore, M. Oinonen, C. Scheidenberger, S. Schwarz, G. Sikler, J. Szerypo, C. Weber, The ISOLDE Collaboration, *Hyperfine Interact.* 132 (2001) 215.
- [14] G. Savard, R.C. Barber, C. Boudreau, F. Buchinger, J. Caggiano, J. Clark, J.E. Crawford, H. Fukutani, S. Gulick, J.C. Hardy, A. Heinz, J.K.P. Lee, R.B. Moore, K.S. Sharma, J. Schwartz, D. Seweryniaki, G.D. Sprouse, J. Vaz, *Hyperfine Interact.* 132 (2001) 223.
- [15] V.S. Kolhinen, S. Kopecky, T. Eronen, U. Hager, J. Hakala, J. Huikari, A. Jokinen, A. Nieminen, S. Rinta-Antila, J. Szerypo, J. Äystö, *Nucl. Instrum. Methods Phys. Res., Sect. A* 528 (2004) 776.
- [16] G. Marx, J. Dilling, H.-J. Kluge, M. Mukherjee, W. Quint, S. Rahaman, D. Rodriguez, G. Sikler, M. Tarisien, C. Weber, SHIPTRAP Collaboration, *Hyperfine Interact.* 146/147 (2003) 245.
- [17] J. Dilling, P. Bricault, M. Smith, H.-J. Kluge, The TITAN Collaboration, *Nucl. Instrum. Methods Phys. Res., Sect. B* 204 (2003) 492.
- [18] S. Schwarz, G. Bollen, D. Lawton, P. Lofy, D.J. Morrissey, J. Ottarson, R. Ringle, P. Schury, T. Sun, V. Varentsov, L. Weissman, *Nucl. Instrum. Methods Phys. Res., Sect. B* 204 (2003) 507.
- [19] W. Quint, J. Dilling, S. Djekić, H. Häffner, N. Hermanspahn, H.-J. Kluge, G. Marx, R. Moore, D. Rodriguez, J. Schönfelder, G. Sikler, T. Valenzuela, J. Verdú, C. Weber, G. Werth, *Hyperfine Interact.* 132 (2001) 457.
- [20] J. Szerypo, D. Habs, S. Heinz, J. Neumayr, P. Thierolf, A. Wilfert, F. Voit, *Nucl. Instrum. Methods Phys. Res., Sect. B* 204 (2003) 512.
- [21] K. Blaum, MATS Collaboration, MATS technical proposal (FAIR/NUSTAR LOI Identification No. 8, 2005).
- [22] G. Zwicknagel, C. Toepffer, P.-G. Reinhard, *Phys. Rep.* 309 (1999) 117.
- [23] With ionisation energies of $\Delta E(^{24}\text{Mg}^{1+} \rightarrow ^{24}\text{Mg}^{2+}) = 1.527\text{ eV}$ and $\Delta E(^{24}\text{Mg}^{2+} \rightarrow ^{24}\text{Mg}^{3+}) = 7.871\text{ eV}$ respectively ionisation and excitation can be safely neglected. See T.A. Carlson, C.W. Nestor Jr., N. Wasserman, J.D. McDowell, *At. Data Nucl. Data Tables* 2 (1970) 63.
- [24] H. Cederquist, C. Biedermann, N. Selberg, P. Hvelplund, *Phys. Rev. A: At., Mol., Opt. Phys.* 51 (1995) 2191.
- [25] B.R. Beck, J. Steiger, G. Weinberg, D.A. Church, J. McDonald, D. Schneider, *Phys. Rev. Lett.* 77 (1996) 1735.
- [26] R.E. Olson, A. Salop, *Phys. Rev. A: At., Mol., Opt. Phys.* 14 (1976) 579.
- [27] G. Sutmann, In: J. Grotendorst, D. Marx, M. Muramatsu (Ed.), *Quantum Simulations of Complex Many-Body Systems, NIC Series*, vol. 10, John von Neumann Institute for Computing, Jülich, 2002, p. 211.
- [28] S. Plimpton, B. Hendrickson, *J. Comput. Chem.* 17 (1996) 326.

- [29] G. Engeln-Müllges, F. Uhlig, *Numerical Algorithms* with C Springer, Berlin, Heidelberg and New York, 1996.
- [30] R.W. Hockney, J.W. Eastwood, *Computer Simulation using Particles*, Adam Hilger, Bristol and Philadelphia, 1988.
- [31] A.H. Sørensen, E. Bonderup, *Nucl. Instrum. Methods Phys. Res.* 215 (1983) 27.
- [32] H. Poth, *Phys. Rep.* 196 (1990) 135.
- [33] A. Wolf, Wechselwirkung zwischen hochgeladenen Ionen und freien Elektronen in einem Ionenspeicherring. MPI-K Heidelberg Report, vol. 15, 1992.
- [34] O. Kester, Entwicklung einer Elektronenstrahlionenquelle mit "schneller" Ionenextraktion zur Anwendung bei der Strahlentherapie mit leichten Ionen (Dissertation Johann-Wolfgang-Goethe Universität, Frankfurt, 1995).

BUSSMANN M., SCHRAMM U. AND HABS D.

Preparing a laser cooled plasma for stopping highly charged ions.

European Physical Journal D **45(1)** (2007) 129–132

Springer Berlin Heidelberg New York

Reprinted with kind permission from Springer Science and Business Media.

License Number 1845960187565

Preparing a laser cooled plasma for stopping highly charged ions

M. Bussmann^a, U. Schramm, and D. Habs

Ludwig-Maximilians-Universität München, Department für Physik, Am Coulombwall 1, 85748 Garching, Germany

Received 25 January 2007

Published online 11 May 2007 – © EDP Sciences, Società Italiana di Fisica, Springer-Verlag 2007

Abstract. We present a new cooling scheme for the preparation of highly charged ions for future in-trap precision experiments. A plasma of laser cooled $^{24}\text{Mg}^+$ ions trapped in a 3D harmonic confinement potential is used as a stopping medium for the highly charged ions. We focus on the dynamic evolution of the plasma, determining suitable cooling conditions for fast recooling of the $^{24}\text{Mg}^+$ ions. The results of a realistic parallel simulation of the complete stopping process presented here indicate that a small, constant detuning of the laser frequency is sufficient for subsequent recooling of the plasma, thus maintaining the stability of the plasma.

PACS. 02.70.Ns Molecular dynamics and particle methods – 32.80.Pj Optical cooling of atoms; trapping – 34.50.Bw Energy loss and stopping power – 52.27.Gr Strongly-coupled plasmas

1 Introduction

The preparation of cold highly charged ions is a vital prerequisite for future in-trap precision experiments [1–4]. High charge states allow to gain precision for example in determining nuclear masses or measuring QED effects with tightly bound electrons.

2 Using a laser cooled plasma as a stopping medium

We present a new scheme for in-trap preparation of ultra cold highly charged ions using a laser cooled one component plasma of $^{24}\text{Mg}^+$ ions as a stopping medium. In the following we focus on the cooling conditions necessary to maintain a stable $^{24}\text{Mg}^+$ plasma and investigate possible charge exchange processes which could reduce the high charge state of the ion of interest.

Laser cooling is a common tool to create ultra cold atomic or ionic ensembles in a very short time [5]. Here we concentrate on in-trap laser cooling of ions, which at present can provide large ensembles of 10^5 to 10^6 ions at temperatures of only a few mK. Laser cooling exploits the strong force a laser beams exerts on the ion when the laser frequency is in resonance with the cooling transition of interest. Only a few ion species provide a closed ground transition suitable for cooling and thus the majority of ion species cannot be directly laser cooled. This limitation can be overcome when considering the Coulomb interaction of the ion of interest with laser cooled ions.

In a laser cooled plasma the mutual Coulomb interaction transfers energy from the hot, highly charged ion which is not laser cooled to the laser cooled ions. If the velocity of the laser cooled ions is kept in the acceptance range of the laser force during this heating process, fast recooling is possible — thus maintaining the plasma characteristics during the cooling.

It is important to note that the transfer of energy per interaction increases linearly with the charge state of the ion of interest. Thus the cooling rate increases with the ion charge state. In modern trap setups such as Penning or Paul traps an ensemble of laser cooled ions of charge state Q can undergo a phase transition into a crystalline state [5–7]. In this state the ion positions are frozen out, because the mutual Coulomb repulsion has overcome the kinetic energy of the ions by orders of magnitude. The plasma of density n and temperature T is strongly coupled, meaning that the plasma parameter $\Gamma = (Q^2 e^2)/(4\pi\epsilon_0 k_B T a_{\text{WS}})$ exceeds unity.

External confinement forces counteract the mutual repulsion of the ions, thereby determining the form and structure of the Coulomb crystal. In a harmonic trap potential the ion crystal resembles a prolate ellipsoid of length L_{axial} and width L_{radial} while the ions are ordered at an equal spacing of $a_{\text{WS}} = (3/4\pi n_{\text{Mg}})^{1/3}$, the Wigner-Seitz radius. In the simulation presented a single highly charged ion is placed near the brim of the ellipsoid, its velocity vector pointing towards the plasma's center, see Figure 1. The axial confinement Ψ_{axial} is much weaker than the radial confinement Ψ_{radial} . In such a configuration the density of the plasma is mainly determined by the radial confinement, while the large axial extent of

^a e-mail: michael.bussmann@physik.uni-muenchen.de

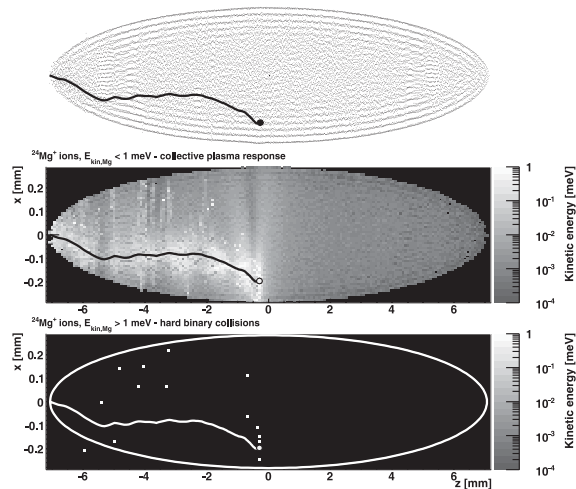


Fig. 1. Three different views of a $^{24}\text{Mg}^+$ plasma ellipsoid of density $n_{\text{Mg}} = 4.23 \times 10^{13} \text{ m}^{-3}$, 11.1 μs after a highly charged ion with an initial energy $E_{\text{kin,HCI}} = 400 \text{ meV}$ and charge state $Q_{\text{HCI}} = 40$ has entered the plasma. At this point in time all the kinetic energy of the heavy ion has been deposited in the plasma. The upper part shows a real space image of a vertical slice through the center of the plasma ellipsoid, including the path of the heavy ion and its current position marked by a circle. The two lower parts show an intensity-coded distribution of the kinetic energies of the $^{24}\text{Mg}^+$ ions, integrated in y -direction.

the plasma allows for many subsequent interactions of the highly charged ion with the plasma ions.

3 Characterizing the stopping process. A realistic molecular dynamics simulation of the plasma-plasma and plasma-HCI interaction

Although standard stopping theory [8] can provide an estimate of the overall stopping power for a highly charged ion of given charge state Q_{HCI} and initial energy $E_{\text{kin,HCI}}$, it does not provide insight into the dynamics of the stopping process.

In the special case of the strongly coupled plasma studied here, the response of the ions when interacting with the highly charged ion cannot be treated assuming a simple binary collision model. Instead, the evolution of the plasma during the stopping process must include a realistic description of the coupling between the ions.

We introduce a newly developed simulation which completely integrates strong coupling into the stopping process by computing the Coulomb interaction between all particles involved. This ansatz requires efficient parallel algorithms since the computation effort essentially scales with the square of the number N of interacting particles considered.

The equation of motion

$$m_i \frac{d^2 \mathbf{r}_i}{dt^2} = \left(\sum_{j \neq i}^{N+1} \frac{q_i q_j}{4\pi\epsilon_0 |\mathbf{r}_i - \mathbf{r}_j|^3} (\mathbf{r}_i - \mathbf{r}_j) \right) - q_i (\Psi_{\text{radial}}, \Psi_{\text{radial}}, \Psi_{\text{axial}}) \begin{pmatrix} x_i \\ y_i \\ z_i \end{pmatrix} + F_{\text{laser}} \left(\frac{d\mathbf{r}_i}{dt} \right) \quad (1)$$

is solved for each particle i of the $N+1$ simulated particles at position $\mathbf{r}_i = (x_i, y_i, z_i)$.

With this high number of particles a realistic model of the real stopping process can be studied without relying on quasi-particle models. In the equation of motion the laser force can be approximated by an effective force depending only on the ion velocity \mathbf{v}_i :

$$F_{\text{laser}}(\mathbf{v}_i) = \frac{\hbar}{8} \frac{S \Gamma_{\text{laser}}^3 \mathbf{k}_{\text{laser}}}{(\delta - \mathbf{v}_i \cdot \mathbf{k}_{\text{laser}})^2 + (\Gamma_{\text{trans}}/2)^2 (1 + S)} \quad (2)$$

where the laser beam is characterized by the saturation parameter S and the wave vector $\mathbf{k}_{\text{laser}} = (0, 0, \pm 2\pi/\lambda_{\text{laser}})$. Cooling $^{24}\text{Mg}^+$ ions requires a laser wavelength of $\lambda_{\text{laser}} = 280 \text{ nm}$.

In a typical cooling setup two laser beams are applied from opposite directions along the axial direction at a small detuning δ of the laser frequency relative to the frequency of the cooling transition. In such a set-up the momentum acceptance of the laser force is on the order of the transition line width Γ_{trans} ($\Gamma_{\text{trans}} = 2\pi \times 42.7 \text{ MHz}$ for $^{24}\text{Mg}^+$). Fast recoiling is only possible if the majority of the ions can be addressed by the laser force choosing a fixed detuning δ .

In the study presented here the laser force is deliberately set to $F_{\text{laser}} \equiv 0$ in order to study the unperturbed evolution of the velocity distribution of the plasma during the passage of the HCI through the plasma. The simulation thus allows to study the plasma dynamics of the precooled crystalline ensemble of ions during the stopping process in order to optimize the final laser parameters for efficient recoiling of the laser ions.

In the special case considered, $N = 10^5$ laser cooled $^{24}\text{Mg}^+$ ions are introduced as a stopping medium for one highly charged ion (HCI) of mass $m_{\text{HCI}} = 100 \text{ a.m.u.}$ The initial kinetic energy $E_{\text{kin,HCI}}$ and the charge state Q_{HCI} of the HCI as well as the density n_{Mg} of the plasma have been varied to study their influence on the stopping process. All the relevant simulation parameters are found in Table 1.

4 Binary collisions vs. collective plasma response

The interaction of the HCI and the plasma ions can be separated in two parts: at small impact parameters b the interaction is governed by close binary collisions, while at large impact parameters the energy is transferred into a collective response of a major part of the plasma, each

Table 1. Parameters for the simulation.

| Simulation input parameters | | |
|---|-----------------------|-----------------------|
| integration time $\Delta\tau_{\text{step}}$ [s] | 10^{-9} | |
| Ψ_{radial} [V/m ²] | 2.5×10^5 | 3.5×10^5 |
| Ψ_{axial} [V/m ²] | 2.5×10^3 | 3.5×10^3 |
| Plasma input parameters | | |
| Number of Mg ⁺ ions | 10^5 | |
| $A_{\text{Mg}}, Q_{\text{Mg}}$ | 24, 1 | |
| T_{Mg} [K] | 10^{-3} | |
| HCl input parameters | | |
| Number of highly charged ions | 1 | |
| A_{HCl} | 100 | |
| Q_{HCl} | 10, 20, 30, 40 | |
| $E_{\text{kin,HCl}}$ [meV] | 100, 200, 300, 400 | |
| Plasma properties derived from the simulation | | |
| Γ_{Mg} | 814 | 911 |
| $a_{\text{WS}}(n_{\text{Mg}})$ [m] | 19.9×10^{-6} | 17.8×10^{-6} |
| L_{radial} [m] | 632×10^{-6} | 565×10^{-6} |
| L_{axial} [m] | 15.8×10^{-3} | 14.1×10^{-3} |
| n_{Mg} [m ⁻³] | 3.02×10^{13} | 4.23×10^{13} |

of the plasma ions carrying only a small fraction of the energy.

Following the argument given in [9] one can estimate that those $^{24}\text{Mg}^+$ ions with a kinetic energy $E_{\text{kin,Mg}} > 1$ meV took part in a close binary collision with the HCl. Figure 1 shows three views of the HCl's trajectory inside the plasma to illustrate this differentiation. At the start of the simulation the HCl is placed on axis near the brim of the plasma ellipsoid and is then given its initial kinetic energy, its velocity vector pointing to the center of the plasma ellipsoid.

The upper part of Figure 1 shows a slice through the center of the $^{24}\text{Mg}^+$ ensemble revealing the crystalline shell structure with the solid line following the trajectory of the HCl and the filled circle marking its position. For the same set of simulation parameters the middle part and lower part show the spatial distribution of the kinetic energy of the $^{24}\text{Mg}^+$ ions, again including the HCl trajectory and position. The middle part shows the distribution of the kinetic energy for all $^{24}\text{Mg}^+$ ions with $E_{\text{kin,Mg}} < 1$ meV while in the lower part only those few ions with $E_{\text{kin,Mg}} > 1$ meV enter the plotted distribution. The logarithmic scale chosen for the intensity-encoded kinetic energy reveals the large extent of the plasma region affected by the passage of the HCl. The corresponding simulation parameters are $n_{\text{Mg}} = 4.23 \times 10^{13} \text{ m}^{-3}$, $E_{\text{kin,HCl}} = 400$ meV and $Q_{\text{HCl}} = 40$.

5 Charge exchange, plasma stability and fast recoiling

As can be deduced from Figure 1 the number of $^{24}\text{Mg}^+$ ions carrying a large kinetic energy after a close collision with the HCl is minute compared to the total number of ions in the plasma. Furthermore, the crystalline structure is not destroyed by the HCl. Nevertheless, the amount of energy carried away by those few ions is of the same

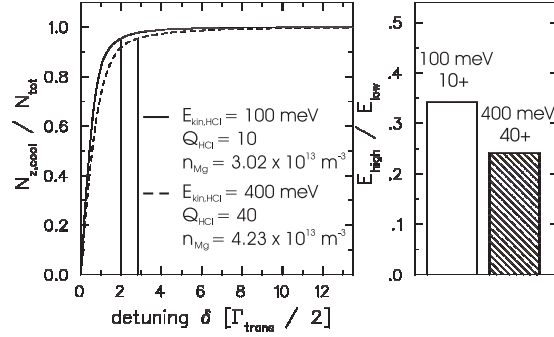


Fig. 2. Left: ratio of the number $N_{z,\text{cool}}$ of ions with $v_{z,\text{Mg}} \leq v_\delta$ and the total number $N_{\text{tot}} = 10^5$ of $^{24}\text{Mg}^+$ ions versus the laser detuning in units of transition line width $\Gamma_{\text{trans}}/2$. The vertical lines mark the detuning value at which 95.4% of the ions are within the acceptance of the laser force. Right: sum E_{high} of the kinetic energy for all ions with $E_{\text{kin,Mg}} > 1$ meV over the sum E_{low} of the kinetic energy for all ions with $E_{\text{kin,Mg}} < 1$ meV. The hollow box corresponds to the same data set as the solid line in the left part, the hatched box to the dashed line.

order as the energy deposited in the bulk of the plasma, as shown in the right part of Figure 2, where the total kinetic energy E_{high} of all ions with $E_{\text{kin,Mg}} > 1$ meV is compared to the total kinetic energy E_{low} of all ions with $E_{\text{kin,Mg}} < 1$ meV.

Following equation (2) one can choose a fixed detuning δ matched to the range of $^{24}\text{Mg}^+$ ion velocities in order to recool almost all $^{24}\text{Mg}^+$ ions without scanning the laser frequency. The choice for δ also depends on the individual trap characteristics which manifest in a heating rate intrinsic to the trap system which must be counteracted by the cooling laser force [10]. This heating rate becomes more important for large crystals which ultimately limits the value of the detuning δ to a few times the natural transition line width.

Fortunately, the simulation results show that this constraint can be met without significant ion loss. Depending on the desired percentage of ions which should be directly addressed by the laser force one can reduce the detuning, thus increasing the cooling rate for the majority of the $^{24}\text{Mg}^+$ ions. This is illustrated in Figure 2 where the percentage of ions with $v_{z,\text{Mg}} \leq v_\delta$ is plotted versus the detuning $\delta = \mathbf{v}_\delta \cdot \mathbf{k}_{\text{laser}}$. Here, two different scenarios are compared, one in which the total energy deposited in the plasma and the energy loss $dE_{\text{kin,HCl}}/ds$ are small (solid line) and one case for which both values are higher in comparison (dashed line). For both curves the majority of the ions can be easily cooled using only a small laser detuning. Thus we conclude that small detuning values are feasible for recoiling. It is therefore not necessary to constantly detune the laser frequency, which must be performed on the order of seconds to efficiently reduce a large momentum spread of the ion ensemble. Instead, a laser beam with a moderate saturation parameter S on the order of unity and a fixed laser frequency are sufficient to recool the ensemble on a time scale of few ms [5] comparable

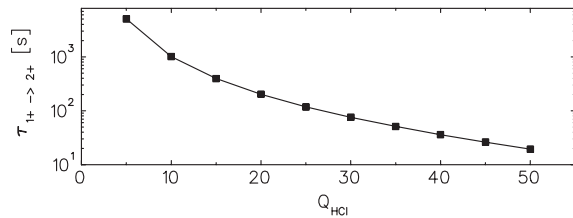


Fig. 3. Average time $\tau_{1+ \rightarrow 2+}$ for the charge exchange process $^{100}\text{X}^{Q+} + ^{24}\text{Mg}^{1+} \rightarrow ^{100}\text{X}^{(Q-1)+} + ^{24}\text{Mg}^{2+}$ for a HCl X with energy $E_{\text{kin,HCl}} = 400$ eV at a plasma density of $n_{\text{Mg}} = 4.23 \times 10^{13} \text{ m}^{-3}$.

to the total stopping time [9], reaching repetition rates of kHz.

Charge exchange becomes important especially for the high charge states demanded by future precision experiments. Experimental data [11, 12] still is rare for charge exchange processes with highly charged ions at small relative velocities. Thus one has to rely on theoretical models of charge exchange [13] to give an estimate on the cross sections and exchange rates expected in a typical cooling setup as shown in Figure 3. The figure shows an estimate for an initial kinetic energy of $E_{\text{kin,HCl}} = 400$ eV, a factor 1000 higher than the energies used in the simulation, thereby clearly showing that charge exchange can be neglected in the cooling scheme proposed here.

6 Summary

We have introduced a new cooling scheme using laser cooled ions to efficiently cool highly charged ions. Ion losses due to charge exchange are negligible while fast re-cooling is possible. Highly charged ions can be cooled to mK temperatures, either for later extraction or integration into the Coulomb crystal lattice after recooling. After the stopping of the highly charged ion the plasma can be recooled fast, without detuning of the laser frequency or reloading of ions to the trap.

References

1. J. Dilling et al., *Int. J. Mass Spectrom.* **251**, 198 (2006)
2. F. Herfurth et al., *Int. J. Mass Spectrom.* **251**, 266 (2006)
3. R. Ringle et al., *Int. J. Mass Spectrom.* **251**, 300 (2006)
4. D. Habs et al., *Eur. Phys. J. A* **25**, 57 (2005)
5. U. Schramm, D. Habs, *Prog. Part. Nucl. Phys.* **53**, 583 (2004), and references therein
6. D.J. Wineland et al., *Phys. Rev. Lett.* **59**, 2935 (1987)
7. H. Walther, *Adv. At. Mol. Opt. Phys.* **31**, 137 (1993)
8. G. Zwicknagel et al., *Phys. Rep.* **309**, 117 (1999)
9. M. Bussmann et al., *Proceedings of the International Workshop on Non-Neutral Plasmas NNP06, Aarhus, 2006*, edited by M. Drewsen (*AIP Conf. Proceedings* **862**, Melville, 2006), p. 221
10. U. Schramm et al., *J. Phys. B* **36**, 561 (2003)
11. H. Cederquist et al., *Phys. Rev. A* **51**, 2191 (1995)
12. B.R. Beck et al., *Phys. Rev. Lett.* **77**, 1735 (1996)
13. R.E. Olson et al., *Phys. Rev. A* **14**, 579 (1976)

BUSSMANN M., SCHRAMM U. AND HABS D.

Simulating the stopping dynamics of highly charged ions in an ultra-cold, strongly coupled plasma.

Hyperfine Interactions **173(1-3)** (2007) 27–34

Springer Berlin Heidelberg New York

Reprinted with kind permission from Springer Science and Business Media.

License Number 1845951403592

Hyperfine Interact (2006) 173:27–34
DOI 10.1007/s10751-007-9538-z

Simulating the stopping dynamics of highly charged ions in an ultra-cold, strongly coupled plasma

M. Bussmann · U. Schramm · D. Habs

Published online: 21 June 2007
© Springer Science + Business Media B.V. 2007

Abstract We introduce a method for stopping highly charged ions (HCIs) in a laser-cooled one-component plasma (OCP) of $^{24}\text{Mg}^+$ ions and present results on stopping times derived from realistic molecular dynamics simulations of the complete stopping process. This stopping scheme can provide ultra-cold highly charged ions for future in-trap precision mass measurements. The choice of an ultra-cold ion plasma as a stopping medium is governed by the almost negligible charge exchange of the HCI with the laser-cooled ions and the very low temperatures which can be reached. In our analysis we focus on the stability and fast recooling of the plasma – two features essential for the experimental realization of this stopping scheme.

Keywords Stopping · Highly charged ions · Laser cooling · Plasma · Strong coupling · Molecular dynamics simulation

PACS 02.70.Ns · 34.50.Bw · 32.80.Pj · 21.10.Dr · 52.27.Gr · 52.27.Jt

M. Bussmann (✉) · D. Habs
Ludwig-Maximilians-University Munich, Am Coulombwall 1, 85748 Garching, Germany
e-mail: michael.bussmann@physik.uni-muenchen.de

D. Habs
e-mail: dietrich.habs@physik.uni-muenchen.de

U. Schramm
Forschungszentrum Dresden-Rossendorf, Bautzener Landstrasse 128,
Dresden 01328, Germany
e-mail: u.schramm@fzd.de

 Springer

1 Introduction

Future in-trap precision measurements of nuclear masses m_{HCl} [1–5] will exploit the increase in resolution Δm_{HCl} provided by ions with high charge state Q_{HCl} :

$$\frac{\Delta m_{\text{HCl}}}{m_{\text{HCl}}} \propto \frac{m_{\text{HCl}}}{t_{\text{RF}} B N_{\text{counts}}^{1/2}} \times \frac{1}{Q_{\text{HCl}}} \tag{1}$$

where t_{RF} is the measurement time, B the magnetic field, and N_{counts} the number of measurements with individual ions.

These high charge states are typically produced by charge breeding (see [6] and references therein) which provides bunched ion beams with a momentum spread larger than the acceptance of the precision traps with which the masses are measured. Several cooling schemes exist [7–10] which match the momentum spread of the highly charged ions to the trap acceptance. These schemes will be challenged by the increase in both precision and the range of nuclear masses measured, while some of them are canceled out due to fast degeneration of high charge states during the cooling.

The nuclei of interest in future experiments include rare, unstable nuclei with a lifetime below 100 ms. Measuring their masses precisely requires a fast, efficient cooling method. In particular losses due to charge exchange must be minimized if only low production rates are expected. Furthermore, in-trap precision measurements such as optical spectroscopy or tests of fundamental theories (see [11] and references therein) require ultra-cold ions.

2 Using laser-cooled ions as a stopping medium

Laser-cooled ions provide a unique stopping medium for which charge exchange with the HCl is negligible [12–14] while temperatures T_{Mg} in the mK range are accessible [15–17]. In our simulation we study both the stopping power at low HCl velocities as well as the plasma dynamics during the stopping. For decreasing HCl velocities v_{HCl} the energy loss dE_{HCl} per length ds increases as can be derived from linear response stopping theory (see [18] and references therein):

$$\frac{dE_{\text{kin,HCl}}}{ds} = -\frac{Q_{\text{HCl}}^2 e^2}{4\pi\epsilon_0} \frac{\omega_p^2}{v_{\text{HCl}}^2} \int_{b_{\text{min}}}^{b_{\text{max}}} \frac{db}{b} = \frac{Q_{\text{HCl}}^2 e^2}{4\pi\epsilon_0} \frac{\omega_p^2}{v_{\text{HCl}}^2} \Lambda_C(E_{\text{kin,HCl}}), \tag{2}$$

where $v_{\text{HCl}} > v_{\text{th}}$, the thermal velocity of the $^{24}\text{Mg}^+$ ions of mass m_{Mg} , defined by $v_{\text{th}} = (3k_B T_{\text{Mg}}/m_{\text{Mg}})^{1/2}$.

The Coulomb-logarithm $\Lambda_C \equiv \int_{b_{\text{min}}}^{b_{\text{max}}} db/b = \ln(b_{\text{max}}/b_{\text{min}})$ depends on the ratio of the minimum impact parameter $b_{\text{min}} = Q_{\text{HCl}} Q_{\text{Mg}} e^2 / (4\pi\epsilon_0 \mu v_{\text{HCl}}^2)$, where μ is the reduced mass of the HCl and the $^{24}\text{Mg}^+$ ion, to the maximum impact parameter $b_{\text{max}} = v_{\text{HCl}}/\omega_p$, the ratio of the HCl’s velocity to the plasma frequency $\omega_p = ((Q_{\text{Mg}}^2 e^2 n_{\text{Mg}})/(\epsilon_0 m_{\text{Mg}}))^{1/2}$. In this approach no strong coupling between the plasma ions of charge state Q_{Mg} and only a linear coupling between the HCl and the plasma ions is assumed [18]. Moreover, it is not possible to deduce the spatial distribution of the energy deposited in the plasma or the velocity distribution of the plasma ions as long as no equilibrium state is reached.

Table 1 Plasma parameters derived from the simulation

| Properties of the $^{24}\text{Mg}^+$ plasma | | |
|--|-----------------------|-----------------------|
| L_{radial} [m] | 632×10^{-6} | 565×10^{-6} |
| L_{axial} [m] | 15.8×10^{-3} | 14.1×10^{-3} |
| α | 25 | 25 |
| n_{Mg} [m^{-3}] | 3.02×10^{13} | 4.23×10^{13} |
| $a_{\text{WS}}(n_{\text{Mg}})$ [m] | 19.9×10^{-6} | 17.8×10^{-6} |
| ω_{p} [$2\pi \times \text{MHz}$] | 1.482 | 1.754 |
| Γ_{Mg} | 814 | 911 |

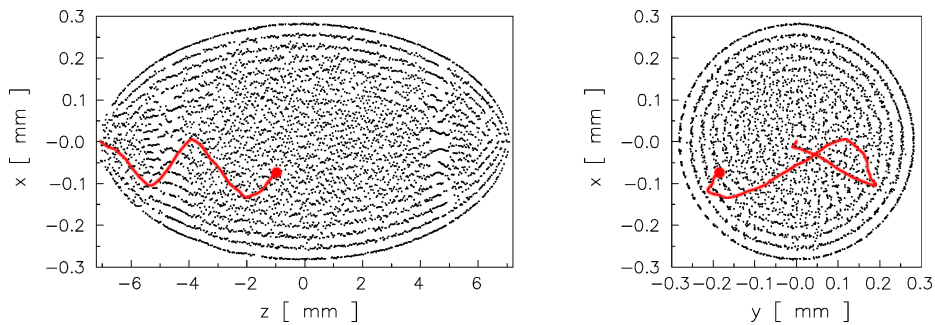


Fig. 1 HCl trajectory through the crystalline $^{24}\text{Mg}^+$ plasma in side view (*left*) and front view (*right*). The ion path points from *left* to *right* while only some $^{24}\text{Mg}^+$ ions are displayed to reveal the crystalline structure. Plasma density: $n_{\text{Mg}} = 4.23 \times 10^{13} \text{ m}^{-3}$, initial energy: $E_{\text{kin,HCl}} = 300 \text{ meV}$, charge state: $Q_{\text{HCl}} = 30$

3 Simulating the stopping dynamics

We use a complete molecular dynamics simulation [12] of the stopping dynamics including the mutual Coulomb interaction of $N_{\text{Mg}} = 10^5$ ions and the interaction with the HCl to study energy deposition and plasma reaction to the HCl. Both the HCl and the plasma ions are confined in a three dimensional harmonic potential, for which the radial confinement Ψ_{radial} is greater than the axial confinement Ψ_{axial} . This confinement is typical of Penning or Paul traps.

In a laser-cooled plasma of density n_{Mg} the coupling increases with decreasing temperature until the mutual Coulomb interaction overcomes the kinetic energy of the ions. At this point the plasma parameter which is given by $\Gamma = (Q_{\text{Mg}}^2 e^2) / (4\pi \epsilon_0 k_B T_{\text{Mg}} a_{\text{WS}})$ is of the order of unity and the coupling between the ions becomes strong. The motion of the strongly coupled ions is then governed by the mutual Coulomb repulsion and the external confining fields. The plasma forms a prolate ellipsoid of length L_{axial} and width L_{radial} (see Table 1) while a clear crystalline structure with a spacing of $a_{\text{WS}} = (3/4\pi n_{\text{Mg}})^{1/3}$, the Wigner–Seitz radius, becomes visible (see [19] and references therein). In the simulation the HCl is placed on axis near the brim of this plasma ellipsoid describing a complicated path through the plasma as seen in Fig. 1.

A realistic simulation of the stopping dynamics which describes the full plasma dynamics must include the long range correlations between the ions of the strongly coupled plasma. In molecular dynamics simulations this requires the computation

Table 2 Input parameters to the molecular dynamics simulation

| | | |
|---|----------------------|-----------------------|
| Common input parameters | | |
| Integration time $\Delta\tau_{\text{step}}$ [s] | 10^{-9} | |
| | Lower plasma density | Higher plasma density |
| Ψ_{radial} [V/m ²] | 2.5×10^5 | 3.5×10^5 |
| Ψ_{axial} [V/m ²] | 2.5×10^3 | 3.5×10^3 |
| Plasma input parameters | | |
| Number N of Mg ⁺ ions | 10^5 | |
| $A_{\text{Mg}}, Q_{\text{Mg}}$ | 124, 1 | |
| T_{Mg} [K] | 10^{-3} | |
| Input parameters for the highly charged ion (HCI) | | |
| Number of highly charged ions | 1 | |
| A_{HCI} | 100 | |
| Q_{HCI} | 10, 20, 30, 40 | |
| $E_{\text{kin,HCI}}$ [meV] | 100, 200, 300, 400 | |

of the mutual interaction of all particles at each time step. For large numbers of ions this requires a large amount of computational power only available in a parallel computing environment.

We use a newly developed, parallel molecular dynamics simulation [20, 21] which solves the equation of motion

$$\begin{aligned}
 m_i \frac{d^2 r_i}{dt^2} &= F_{\text{Coulomb}} + F_{\text{trap}} \\
 &= \left(\sum_{j \neq i}^{N_{\text{Mg}}+1} \frac{q_i q_j}{4\pi \epsilon_0 |r_i - r_j|^3} (r_i - r_j) \right) - q_i \Psi^T(t) r_i
 \end{aligned} \tag{3}$$

for each of the $N_{\text{Mg}} = 10^5$ ions of charge q_i at positions r_i and one HCI for various confinement strengths $\Psi^T = (\Psi_{\text{radial}}, \Psi_{\text{radial}}, \Psi_{\text{axial}})$, HCI charge q_i and initial energies. The parameters used in the simulation can be found in Table 2.

Note that we do not introduce a cooling force, since we want to follow the undisturbed phase space evolution of the plasma to identify the constraints on the external cooling force necessary to maintain plasma stability and low temperature.

4 Results

4.1 Stopping times

The stopping times given in Fig. 2 serve as an upper limit to the stopping times expected for this cooling scheme. They only include those contributions to the energy loss given by collective plasma response, therefore neglecting all hard binary hits which carry away more kinetic energy than $\Delta E_{\text{kin,trans}} = 2Q_{\text{Mg}}^2 Q_{\text{HCI}}^2 e^4 / ((4\pi \epsilon_0)^2 m_{\text{Mg}} b_{\text{trans}}^2 v_{\text{rel}}^2)$. This energy loss corresponds to a certain impact parameter b_{trans} which marks the transition between the regime at which hard binary

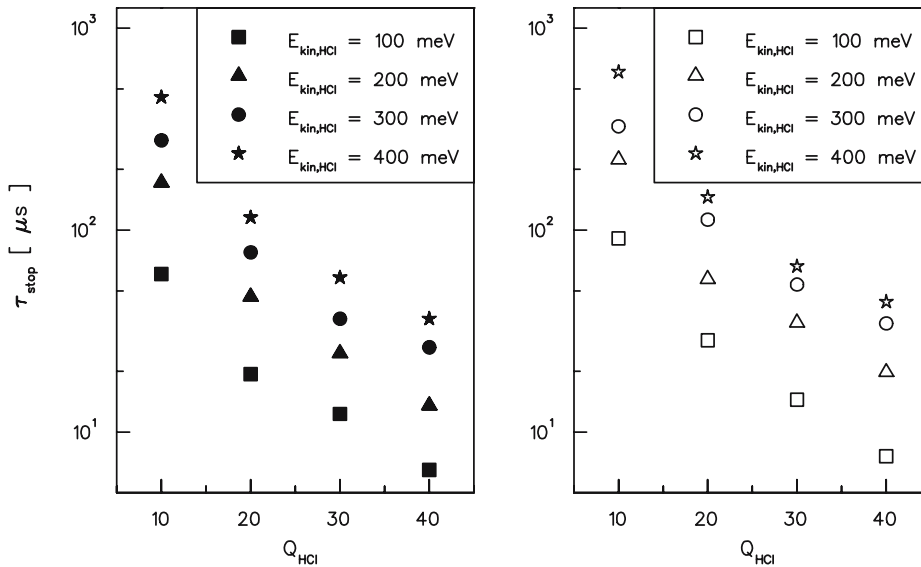


Fig. 2 Stopping times vs. HCI charge state. The *solid symbols* correspond to $n_{Mg} = 4.23 \times 10^{13} m^{-3}$, the *open symbols* to $n_{Mg} = 3.02 \times 10^{13} m^{-3}$

collisions dominate the energy loss to the regime where collective plasma response is dominant (see [12] for details):

$$\begin{aligned} \frac{dE_{kin,HCI}}{ds} &= \left. \frac{dE_{kin,HCI}}{ds} \right|_{bin.} + \left. \frac{dE_{kin,HCI}}{ds} \right|_{coll.} \\ &= \int_{b_{min}}^{b_{trans}} \frac{dE_{kin,HCI}}{dsdb} db + \int_{b_{trans}}^{b_{max}} \frac{dE_{kin,HCI}}{dsdb} db. \end{aligned}$$

For the case of $E_{kin,HCI} = 100 \text{ meV}$, $n_{Mg} = 4.23 \times 10^{13} m^{-3}$ and $Q_{HCI} = 40$ one finds $b_{trans} = 0.64 \times a_{WS}$ and $\Delta E_{kin,trans} \approx 1 \text{ meV}$.

Though the transition impact parameter depends on the properties of the HCI and the plasma, the figures listed here give a good estimate of its magnitude which is comparable to the inter-ion spacing. This suggests that for any interaction at a distance longer than a_{WS} several plasma ions carry away the HCI energy, which is finally dissipated over the whole plasma as shown in Fig. 3.

The energy loss due to hard binary collisions can only be estimated if improved statistics are available. Simulation results suggest that it can contribute as much to the total energy loss as collective plasma response (see Fig. 4).

4.2 Plasma stability and fast recoiling

Two key aspects studied in the simulation are the stability of the plasma during the stopping process and the prospects for fast recoiling. While Fig. 3 shows that a great amount of the energy deposited in the plasma by the HCI is distributed over

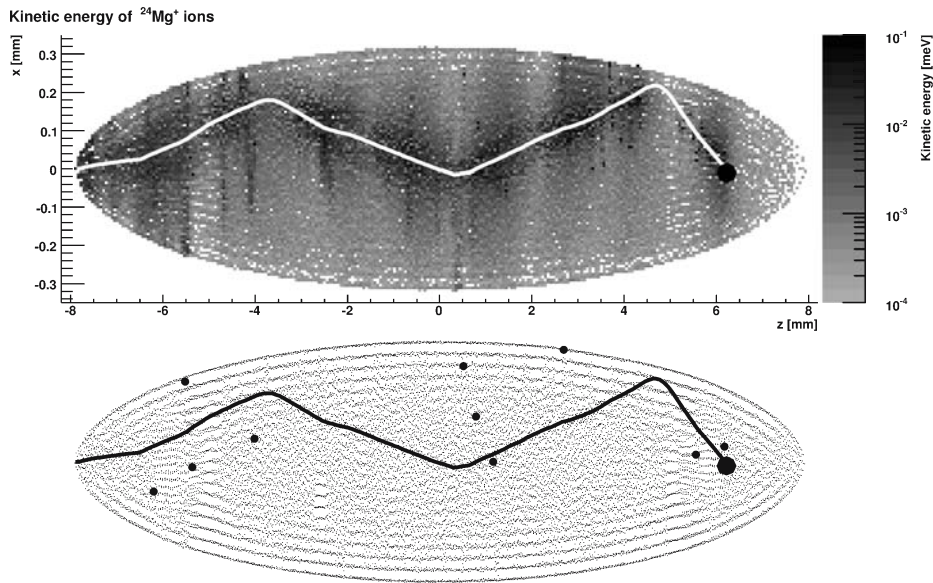


Fig. 3 *Upper part:* Energy deposition by the HCl during its passage through the $^{24}\text{Mg}^+$ plasma. The energy values (intensity encoded) result from a projection of the kinetic energy of the $^{24}\text{Mg}^+$ ions along the y -axis. The trajectory of the HCl (black circle) is drawn in white. *Lower Part:* Real space view of the HCl and the plasma ions. The medium sized black circles represent those $^{24}\text{Mg}^+$ ions which reached $E_{\text{kin,Mg}} > 1 \text{ meV}$ during the simulation. Simulation parameters: $n_{\text{Mg}} = 3.02 \times 10^{13} \text{ m}^{-3}$, $E_{\text{kin,HCl}} = 400 \text{ meV}$, $Q_{\text{HCl}} = 20$

the whole plasma bulk, Fig. 4 shows that the velocity distribution of the majority of the $^{24}\text{Mg}^+$ scarcely changes due to the stopping: In the upper left part of Fig. 4 the two non-hatched histograms show the velocity distribution of the $^{24}\text{Mg}^+$ ions before and after the stopping of a HCl with $Q_{\text{HCl}} = 10$, $E_{\text{kin,HCl}} = 100 \text{ meV}$, while the hatched histogram shows the velocity distribution after stopping a HCl with $Q_{\text{HCl}} = 40$, $E_{\text{kin,HCl}} = 400 \text{ meV}$.

We conclude that most of the ions remain at their lattice positions and only a minute number of ions gain enough energy to freely propagate through the plasma. These ions either hit the trap wall or are finally recooled by their interaction with the other ions. Ion loss therefore is negligible. Moreover, the velocities of the majority of the ions lie well in the acceptance range of the laser force $F_{\text{L}}(\mathbf{v}_{\text{Mg}}) = (\hbar/8) \times |\mathbf{k}_{\text{L}}| \Sigma \Gamma_{\text{L}}^3 / ((\delta - \mathbf{v}_{\text{Mg}} \cdot \mathbf{k}_{\text{L}})^2 + (\Gamma_{\text{L}}/2)^2 (1 + S))$ of two counterpropagating laser beams with saturation parameter S and detuning δ . The plasma can thus be recooled fast without changing the laser frequency – see the lower part of Fig. 4 for an example of a set of laser parameters suitable for cooling all $^{24}\text{Mg}^+$ ions with $E_{\text{kin,Mg}} < 1 \text{ meV}$.

5 Summary and Outlook

We have shown that it is feasible to stop highly charged ions in a plasma of laser-cooled $^{24}\text{Mg}^+$ ions. Compared to other stopping schemes there is virtually no loss of HCl due to charge exchange. The $^{24}\text{Mg}^+$ plasma stays stable and recooling is fast and

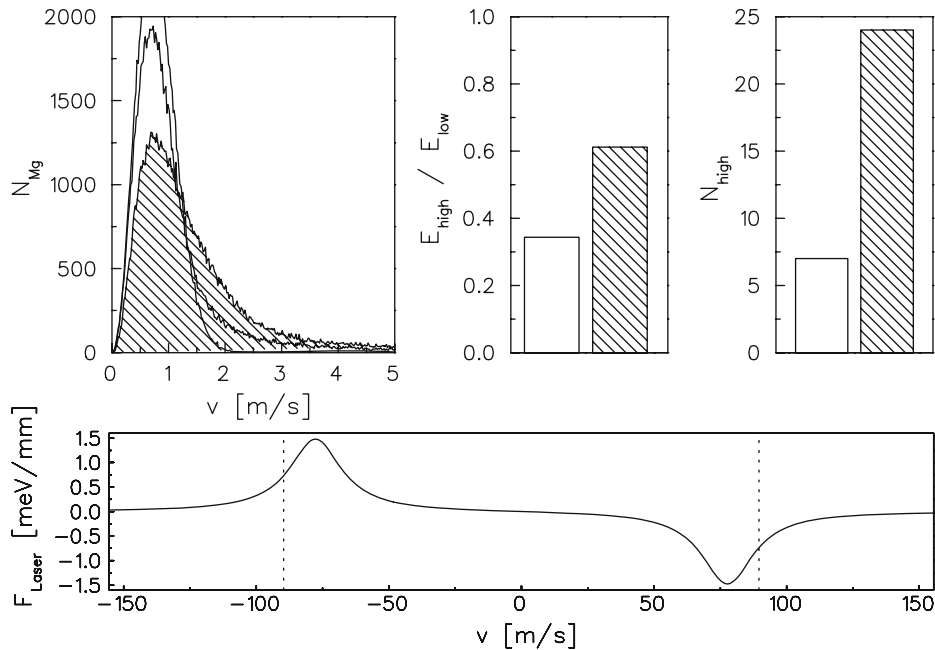


Fig. 4 Upper left: Velocity distribution of the $^{24}\text{Mg}^+$ before and after the HCI has stopped ($n_{\text{Mg}} = 3.02 \times 10^{13} \text{ m}^{-3}$, see text for details). Upper middle: Ratio of the total kinetic energy E_{high} of all $^{24}\text{Mg}^+$ with $E_{\text{kin,Mg}} > 1 \text{ meV}$ and the total kinetic energy E_{low} of all $^{24}\text{Mg}^+$ with $E_{\text{kin,Mg}} < 1 \text{ meV}$. Upper right: Number of ions with $E_{\text{kin,Mg}} > 1 \text{ meV}$. The hatched area corresponds to $Q_{\text{HCI}} = 40$, $E_{\text{kin,HCI}} = 400 \text{ meV}$, the other to $Q_{\text{HCI}} = 10$, $E_{\text{kin,HCI}} = 100 \text{ meV}$. Lower part: Combined force of two counterpropagating laser beams ($\delta = 6.5 \times \Gamma_L$, $S = 3$, transition wavelength $\lambda_L = 2\pi/|\mathbf{k}_L| = 280 \text{ nm}$, natural line width $\Gamma_L = 2\pi \times 42.7 \text{ MHz}$). The dashed lines at $v = \pm 90 \text{ m/s}$ correspond to an ion energy of $E_{\text{kin,Mg}} = 1 \text{ meV}$

efficient. Stopping times for the HCI at low initial energies are found to be as low as few ten μs .

We are currently investigating efficient extraction schemes while gathering more statistics to finally give results on the total stopping power. The simulation code used in this work can be easily adopted to simulate various extraction methods as well as to investigate other problems involving the dynamics of strongly coupled many-particle systems.

Acknowledgements This work was partially supported by the BMBF, project 06ML183, and Leibniz-Rechenzentrum, project UH351AE. M. Bussmann would like to thank M. Schubert for providing the Matrix cluster for computation.

References

- Dilling, J., Bricault, P., Smith, M., Kluge, H.-J., TITAN collaboration: The proposed TITAN facility at ISAC for very precise mass measurements on highly charged short-lived isotopes. Nucl. Instrum. Methods Phys. Res., Sect. B **204**, 492–496 (2003)

2. Schwarz, S., Bollen, G., Lawton, D., Lofy, P., Morrissey, D.J., Ottarson, J., Ringle, R., Schury, P., Sun, T., Varentsov, V., Weissman, L.: The low-energy-beam and ion-trap facility at NSCL/MSU. *Nucl. Instrum. Methods Phys. Res., Sect. B* **204**, 507–511 (2003)
3. Quint, W., Dilling, J., Djekić, S., Häffner, H., Hermanspahn, N., Kluge, H.-J., Marx, G., Moore, R., Rodriguez, D., Schönfelder, J., Sikler, G., Valenzuela, T., Verdú, J., Weber, C., Werth, G., HITRAP: A facility for experiments with trapped highly charged ions. *Hyperfine Interact.* **132**, 457–461 (2001)
4. Szerypo, J., Habs, D., Heinz, S., Neumayr, J., Thierolf, P., Wilfart, A., Voit, F.: MAFFTRAP: ion trap system for MAFF. *Nucl. Instrum. Methods Phys. Res., Sect. B* **204** 512–516 (2003)
5. Blaum, K., MATS collaboration: MATS technical proposal, FAIR/NUSTAR LOI Identification No. 8 (2005)
6. Kester, O.: Entwicklung einer Elektronenstrahlionenquelle mit “schneller” Ionenextraktion zur Anwendung bei der Strahlentherapie mit leichten Ionen, Dissertation Johann-Wolfgang-Goethe Universität, Frankfurt (1995)
7. Savard, G., Becker, St., Bollen, G., Kluge, H.-J., Moore, R.B., Otto, Th., Schweikhard, L., Stolzenberg, H., Wiess, U.: A new cooling technique for heavy ions in a Penning trap. *Phys. Lett. A* **158**, 247–252 (1991)
8. Herfurth, F., Dilling, J., Kellerbauer, A., Bollen, G., Henry, S., Kluge, H.-J., Lamour, E., Lunney, D., Moore, R.B., Scheidenberger, C., Schwarz, S., Sikler, G., Szerypo, J.: A linear radiofrequency ion trap for accumulation, bunching, and emittance improvement of radioactive ion beams. *Nucl. Instrum. Methods Phys. Res., Sect. A* **469**, 254–275 (2001)
9. Häffner, H., Beier, T., Djekić, S., Hermanspahn, N., Kluge, H.-J., Quint, W., Stahl, S., Verdú, J., Valenzuela, T., Werth, G.: Double Penning trap technique for precise g factor determinations in highly charged ions. *Eur. Phys. J. D* **22**, 163–182 (2003)
10. Gabrielse, G., Fei, X., Orozco, L.A., Tjoelker, R.L., Haas, J., Kalinowsky, H., Trainor, T.A., Kells, W.: Cooling and slowing of trapped antiprotons below 100 meV. *Phys. Rev. Lett.* **63**, 1360–1363 (1989)
11. Werth, G., Beier, Th., Djekic, S., Kluge, H.-J., Quint, W., Valenzuela, T., Verdú, J., Vogel, M.: Precision studies in traps: measurement of fundamental constants and tests of fundamental theories. *Nucl. Instrum. Methods Phys. Res., Sect. B* **205**, 1–8 (2003)
12. Bussmann, M., Schramm, U., Habs, D., Kolhinen, V.S., Szerypo, J.: Stopping highly charged ions in a laser-cooled one component plasma of $^{24}\text{Mg}^+$ ions. *Int. J. Mass Spectrom.* **251**, 179–189 (2006)
13. Beck, B.R., Steiger, J., Weinberg, G., Church, D.A., McDonald, J., Schneider, D.: Measurement of charge exchange between H_2 and low-energy ions with charge states $35 \leq q \leq 80$. *Phys. Rev. Lett.* **77**, 1735–1738 (1996)
14. Olson, R.E., Salop, A.: Electron transfer between multicharged ions and neutral species. *Phys. Rev. A: At., Mol., Opt. Phys.* **14**, 579–585 (1976)
15. Larson, D.J., Bergquist, J.C., Bollinger, J.J., Itano, W.M., Wineland, D.J.: Sympathetic cooling of trapped ions: a laser-cooled two-species nonneutral ion plasma. *Phys. Rev. Lett.* **57**, 70–73 (1986)
16. Bove, P., Hornekær, L., Brodersen, C., Drewsen, M., Hangst, J.S.: Sympathetic crystallization of trapped ions. *Phys. Rev. Lett.* **82**, 2071–2074 (1999)
17. Roth, B., Fröhlich, U., Schiller, S.: Sympathetic cooling of $^4\text{He}^+$ ions in a radio-frequency trap. *Phys. Rev. Lett.* **94**, 053001-1–053001-4 (2005)
18. Zwicknagel, G., Toepffer, C., Reinhard, P.-G.: Stopping of heavy ions in plasmas at strong coupling. *Phys. Rep.* **309**, 117–208 (1999)
19. Schramm, U., Habs, D.: Crystalline ion beams. *Prog. Part. Nucl. Phys.* **53**, 583–677 (2004)
20. Sutmann, G.: Classical molecular dynamics. In: Grotendorst, J., Marx, D., Muramatsu, M. (eds.) *Quantum Simulations of Complex Many-Body Systems*, NIC Series, vol. 10, pp. 211–254. John von Neumann Institute for Computing, Jülich (2002)
21. Plimpton, S., Hendrickson, B.: A new parallel method for molecular dynamics simulation of macromolecular systems. *J. Comput. Chem.* **17**, 326–337 (1996)

CONFERENCE PRESENTATIONS

Poster Presentations

Structure of Bunched Crystalline Ion Beams in PALLAS

Poster presented at the

Third International Conference and 292nd W.E.-Heraeus-Seminar on Trapped Charged Particles and Fundamental Interactions TCPFI

on August 27th 2002 in Wildbad-Kreuth, Germany

Form and Structure of Bunched Crystalline Ion Beams

Poster presented at the

International Workshop on Beam Cooling and Related Topics COOL03

on May 22nd 2003 in Lake Yamanaka near Mt. Fuji, Japan

Sympathetic Cooling of Highly Charged Ions in Laser-Cooled Plasmas for Precision Mass Measurements

Poster presented at the

DPG Frühjahrstagung 2005 "Physik seit Einstein"

on March 4th 2005 in Berlin, Germany

Probing the Structure of Crystalline Ion Beams

Poster presented at the

DPG Frühjahrstagung 2005 "Physik seit Einstein"

on March 5th 2005 in Berlin, Germany

Laser Cooling of Relativistic C^{3+} Ion Beams at the ESR

Poster presented at the

DPG Frühjahrstagung 2005 "Physik seit Einstein"

on March 7th 2005 in Berlin, Germany

Simulating the Particle Dynamics in Strongly Coupled Plasmas for Systems with Large Particle Number

Poster presented at the

International Workshop on Atomic Physics

on November 28th 2006 in Dresden, Germany

Laser Cooling of Relativistic C^{3+} Ion Beams and Precision Laser Spectroscopy at the Experimental Storage Ring at GSI

Poster presented at the

XXV International Conference on Photonic, Electronic and Atomic Collisions ICPEAC07

on July 31st 2007 in Freiburg, Germany

Oral Presentations

Form und Struktur gebunchter kristalliner Ionenstrahlen im Speicherring PALLAS

Talk given at the
DPG Frühjahrstagung 2003 AMOP
on March 27th 2003 in Hannover, Germany

Untersuchungen zur Form und Struktur gebunchter kristalliner Ionenstrahlen

Talk given at the
DPG Frühjahrstagung 2004 AMOP
on March 25th 2004 in Munich, Germany

Laser Cooling and Spectroscopy of Relativistic C^{3+} Beams at the ESR

Talk given at the
6th International Conference on Nuclear Physics at Storage Rings STORI'05
on May 24th 2005 in Bonn, Germany

Laser Cooling of Heavy Ion Beams

Talk given at the
Forum for the Centenary of the Scientific Breakthroughs by Albert Einstein
on October 13th 2005 in Lanzhou, China

Simulating Strongly Coupled One Component Plasmas at Low Temperatures

Talk given at the
Workshop on Non-Neutral Plasmas NNP06
on June 28th 2006 in Aarhus, Denmark

Laser Cooling of Relativistic Bunched C^{3+} Ion Beams at the Storage Ring ESR

Talk given at the
International Conference on Trapped Charged Particles and Fundamental Physics TCP06
on September 5th 2006 in Parksville BC, Canada

Simulating the Dynamics of Strongly Coupled Many-Particle Plasmas at Low Temperatures.

Talk given at the
DPG Frühjahrstagung 2007 AMOP
on March 20th 2007 in Düsseldorf, Germany

Laser Cooling of Relativistic C^{3+} Beams at the ESR

Talk given at the
DPG Frühjahrstagung 2007 AMOP
on March 23rd 2007 in Düsseldorf, Germany

Oral Presentations (continued)

Laser Cooling of Relativistic Ion Beams and Precision Laser Spectroscopy of Lithium-like Ions at GSI

Talk given at the

3rd Topical Workshop of the SPARC Collaboration SPARC07

on April 29th 2007 in Paris, France

Laser Cooling of Relativistic C^{3+} Ion Beams and Precision Laser Spectroscopy at the Experimental Storage Ring at GSI

Talk given at the

XXV International Conference on Photonic, Electronic and Atomic Collisions ICPEAC07

on July 31st 2007 in Freiburg, Germany

Laser Cooling of Relativistic Ion Beams: Summary of Experimental Results and Prospects for FAIR experiments

Talk given at the

Workshop on Beam Cooling and Related Topics COOL07

on September 14th 2007 in Bad Kreuznach, Germany

CURRICULUM VITAE

Hans Michael Bussmann

born on **February 16th 1976** in **Bielefeld**, Germany

Academic Education

- since June 2002** **PHD student in Physics**
at the LMU Munich, Germany in the group of Prof. Habs
subject BEAM COOLING WITH LASERS
- February 2002** **Diploma in Physics**
at the LMU Munich, Germany
grade WITH DISTINCTION (1.0)
- February 2001 – February 2002** **Diploma Thesis**
at the LMU Munich, Germany in the group of Prof. Schaile
subject ASSOCIATED HIGGS PRODUCTION AT TEVATRON AND LHC
- April 1998** **German "Vordiplom" in Physics**
at the LMU Munich, Germany
grade 1.0
- October 1996** **Begin of Studies in Physics**
at the LMU Munich, Germany
Subsidiary Subjects COMPUTER SCIENCES, MATHEMATICS
- June 1995** **German "Abitur"**
at the Cecilien-Gymnasium Bielefeld, Germany
grade 1.0
- 1986–1995** **Secondary School**
Cecilien-Gymnasium Bielefeld, Germany
Main Courses MATHEMATICS, PHYSICS, ENGLISH, PHILOSOPHY
- 1982–1986** **Elementary School**
Sudbrackschule Bielefeld, Germany

Practical Education

- July 25th 2000 – November 29th 2000** **Summer Student**
CERN Geneva, Switzerland in the group of Luis Hervas
subject TESTING THE ELECTRONICS OF THE ATLAS EB-CALORIMETER
- April 1st 2000 – May 31st 2000** **Student Trainee**
LMU Munich, Germany in the group of Prof. Schaile
subject TESTING THE ATLAS MUON DRIFT TUBES
- March 6th 2000 – March 31st 2000** **Student Trainee**
MPI for Quantum Optics Garching, Germany in the group of Prof. Walther
subject DETERMINING THE PROPERTIES OF A RUBIDIUM BEAM
- September 27th 1999 – November 5th 1999** **Student Trainee**
Institut Laue-Langevin Grenoble, France in the group of Roland Gähler
subject SIMULATION AND TESTS OF MAGNET COILS FOR A NRSE SETUP
- August 2nd 1999 – September 24th 1999** **Summer Student**
DESY Hamburg, Germany in the group of Prof. Klanner
subject TESTING THE ZEUS MICRO-VERTEX DETECTORS
- March 8th 1999 – April 30th 1999** **Student Trainee**
MPI for Quantum Optics Garching, Germany in the group of Prof. Walther
subject STABILIZING THE FREQUENCY OF A DIODE LASER
- August 10th 1998 – September 11th 1998** **Student Trainee**
MPI for Quantum Optics Garching, Germany in the group of Prof. Walther
subject BUILDING A RUBIDIUM POLARIZATION SPECTROSCOPY SETUP
- October 1995 – October 1996** **Community Service**
at the Dietrich Bonhoeffer Haus Bielefeld, Germany

Teaching Experience

- 2007** **Instructor**
F1-Praktikum: Versuch M12 Paulfalle
ADVANCED PRACTICAL TRAINING FOR PHYSICS STUDENTS
- 2006** **Course Assistant**
Experimentalphysik 1 EP1
INTRODUCTORY COURSE ON PHYSICS FOR NON-PHYSICS STUDENTS
- 2005** **Course Assistant**
Experimentalphysik 2 EP2
ADVANCED COURSE ON PHYSICS FOR NON-PHYSICS STUDENTS
- 2004** **Course Assistant**
Experimentalphysik 1 EP1
INTRODUCTORY COURSE ON PHYSICS FOR NON-PHYSICS STUDENTS
- 2003** **Course Assistant**
Experimentalphysik 1 EP1
INTRODUCTORY COURSE ON PHYSICS FOR NON-PHYSICS STUDENTS
- 2002** **Course Assistant**
Physik 1 P1
INTRODUCTORY COURSE ON PHYSICS FOR PHYSICS STUDENTS
- 1997** **Course Assistant**
Mathematik für Erstsemester
INTRODUCTORY COURSE ON MATHEMATICS FOR PHYSICS STUDENTS

München, den

Michael Bussmann

DANKSAGUNG

Es hält sich hartnäckig die Mär, eine Doktorarbeit sei das Werk einer einzelnen Person. Zwar ist für den Inhalt und die Ergebnisse dieser Arbeit einzig der Autor verantwortlich – insbesondere für jeden im Text zu findenden Fehler. Dennoch wäre diese Arbeit ohne die Unterstützung vieler Kollegen und Freunde, deren Beiträge dem Leser meist verborgen bleiben [219], nicht in dieser Form veröffentlicht worden. All diesen Menschen möchte ich hiermit danken und hoffe, dass ich Ihnen mit der vorliegenden Arbeit zeigen kann, dass ihre Mühe Früchte getragen hat.

Zuvorderst und besonders möchte ich meinem Doktorvater Professor Dr. Dietrich Habs danken. Es ist selten, einen Lehrstuhlinhaber zu treffen, der aktiv an den Projekten seiner Mitarbeiter teilnimmt, immer ein offenes Ohr hat, sich Zeit für oft leidenschaftliche Diskussionen nimmt und mitreissende Begeisterung für neue Ideen zeigt. Stets konnte ich mir sicher sein, in Dietrich Habs einen Gesprächspartner zu finden, der bei offenen Fragen selbst zu Bleistift und Papier griff, um nach einem arbeitsreichen Wochenende die Lösung auch kniffliger Probleme mit wenigen einfachen Formeln zu präsentieren – meist in Form einer handgeschriebenen Notiz auf meinem Bürostuhl, rechtzeitig zum Arbeitsbeginn am Montagmorgen. Für diese enge Zusammenarbeit möchte ich mich hier bedanken. Ebenfalls möchte ich mich bei Professor Gregor Morfill für die Übernahme der Zweitkorrektur sowie bei Alexei Ivlev für seine Hilfe beim Verständnis komplexer Plasmadynamik bedanken.

Besonders danken möchte ich Ulrich Schramm. Niemandem verdanke ich mehr Einsicht in die Themen dieser Arbeit als ihm. Ich hatte das Glück, in Ulrich Schramm einen Kollegen zu finden, dem ich im physikalischen wie menschlichen Urteil immer vertrauen kann, der mir Mut zuspricht, wenn ich ihn brauche und der jede meiner Fragen geduldig und verständlich beantworten kann. Selbst nach Fertigstellung dieser Arbeit habe ich in jedem Gespräch mit ihm das Gefühl, einen Blick in eine Schatzkiste an physikalischem Wissen, wissenschaftlicher Intuition und tiefem Naturverständnis werfen und dabei auch noch so unverschämt sein zu dürfen, alles mitzunehmen was ich tragen kann. Ich kann hier noch zehn Seiten anfügen, aber ich denke es ist in Ordnung wenn ich mich etwas beschränke: DANKE, ULI!

Immer wenn ich etwas nicht verstehe, was im Allgemeinen mehrmals pro Tag der Fall ist, brauche ich geduldige Ansprechpartner, um im Gespräch meine Gedanken zu ordnen. Mein grosses Glück ist, immer ein offenes Ohr zu finden. In meiner Anfangszeit war es vor allem mein Vorgänger Tobias Schätz, ohne dessen Hilfe ich niemals so schnell soviel Neues gelernt hätte. Danken möchte ich auch Peter Thirolf, den ich irgendwann mal zu einer Wette herausfordern möchte, wer von uns beiden am längsten konzentriert arbeiten kann. Ebenfalls

danken möchte ich Jürgen Neumayr, besonders für die Rückendeckung. Martin Gross, für die Äpfel. Michael Sewtz, für Korrekturlesen und Diskussionen. Jerzy Szerypo, für den Tee. Oliver Kester, für die Feiern. Sophie Heinz, für gemeinsame Rechtsbrüche. Florian Grüner, für's Rechnenlassen. Veli Kolhinen, for hiking discussions - Powerpuffgirls forever. Walter Assmann, für die morgendlichen U-Bahn-Diskussionen. Sicherlich ebenso wichtig für das Gelingen dieser Arbeit waren alle Mitstreiter auf dem Weg zur Promotion: Tom, I don't know what to say, except: Thank you, for everything. Stefan, bei der nächsten Diskussion hast Du auch mal recht, ganz bestimmt. Wolfgang, für Genf und München. Mario, für die rote Pille. Mustapha, für die Zellteilung. Nicht zu vergessen Jörg, Andreas, Matthias, Raphael und alle anderen MPQler. Last but not least danke ich allen Diplomanden und Werkstudenten, Katrin, Thomas, Christian (die Tür muss immer geschlossen bleiben!) sowie meinen zwei unermüdlichen Helfern Florian und Stephan.

Es ist sehr schwierig, eine Reihenfolge festzulegen, wem man zuerst dankt und wer danach genannt werden soll. Deshalb sei in willkürlicher Reihenfolge gedankt: Rolf Oehm und dem besten Werkstatt-Team der Welt – danke für die hervorragende Arbeit, für die Geduld mit meinem technischen Unverständnis und für die tollen Feste. Otto Schaile, Klaus Steinberger und Rudi Lutter, deren Arbeit viel zu selten gewürdigt wird, weil die Computer immer laufen – danke für jede Datenrettung und dafür, dass ich mich breitmachen durfte. Ich danke Johann Krapfl und der Elektronikwerkstatt, ohne die kein Experiment je Daten genommen hätte, ebenso allen am technologischen Labor, insbesondere Hans-Jörg Maier für den gemeinsamen Kampf ums Kühlwasser, Ulrich Friebe und Dagmar Frischke für jede Hilfe. Andrea Leinthal danke ich für die Kekse, die ich geklaut habe. Reinhardt Satzkowksi danke ich für die Seentour, gemeinsame Fahrten und das Gespräch auf dem Gang. Meike Dlaboha und Alexandra Herrmann danke ich, dass sie dafür gesorgt haben, dass ich nicht immer nur gearbeitet habe. Michael Schumann, Christian Hübsch, Elisabeth Krönauer und Nicoletta Groff danke ich dafür, meine Ideen zur technischen Realisierung gebracht zu haben. Ludwig Beck, Walter Carli und allen am MLL danke ich für Strahlenschutz und Teamgeist.

Nicht nur in München habe ich Hilfe erfahren, auch die Darmstädter Experimente konnten nur gelingen, weil viele grossartige Physiker geholfen haben: Markus Steck und das ganze ESR-Team, Sergei Karpuk, Guido Saathoff, Sascha Reinhardt, Christian Novotny, Wilfried Nörtershäuser und Christopher Geppert samt Team, Thomas Stöhlker, Hans-Jürgen Kluge, Christophor Kozhuharov, Thomas Kühl und alle anderen die ich hier unerwähnt gelassen habe. Danken möchte ich allen, mit denen ich das Glück hatte zusammenarbeiten und diskutieren zu dürfen.

Zuletzt möchte ich allen danken, die den Weg meiner Promotion begleitet haben und ohne die ich es nicht geschafft hätte: Meiner Familie und meinen Freunden.

Merci!